UNCLASSIFIED

CENTRAL RESEARCH LIBRARY
DOCUMENT COLLECTION
cy. 8

MARTIN MARIETTA ENERGY SYSTEMS LIBRARIES
3 4456 0049745 1

ORNL-2331
Progress

HOMOGENEOUS REACTOR PROJECT

QUARTERLY PROGRESS REPORT

FOR PERIOD ENDING APRIL 30, 1957

CENTRAL RESEARCH LIBRARY
DOCUMENT COLLECTION
LIBRARY LOAN COPY
DO NOT TRANSFER TO ANOTHER PERSON
If you wish someone else to see this document, send in name with document and the library will arrange a loan.

OAK RIDGE NATIONAL LABORATORY
OPERATED BY
UNION CARBIDE NUCLEAR COMPANY
A Division of Union Carbide and Carbon Corporation
UCC
POST OFFICE BOX X · OAK RIDGE, TENNESSEE

UNCLASSIFIED

Printed in USA. Price 1.00 cents. Available from the

Office of Technical Services
U. S. Department of Commerce
Washington 25, D. C.

LEGAL NOTICE

This report was prepared as an account of Government sponsored work. Neither the United States, nor the Commission, nor any person acting on behalf of the Commission:

A. Makes any warranty or representation, express or implied, with respect to the accuracy, completeness, or usefulness of the information contained in this report, or that the use of any information, apparatus, method, or process disclosed in this report may not infringe privately owned rights; or

B. Assumes any liabilities with respect to the use of, or for damages resulting from the use of any information, apparatus, method, or process disclosed in this report.

As used in the above, "person acting on behalf of the Commission" includes any employee or contractor of the Commission to the extent that such employee or contractor prepares, handles or distributes, or provides access to, any information pursuant to his employment or contract with the Commission.

UNCLASSIFIED

ORNL-2331

Contract No. W-7405-eng-26

HOMOGENEOUS REACTOR PROJECT

QUARTERLY PROGRESS REPORT

For Period Ending April 30, 1957

Project Director – R. B. Briggs
Associate Director – C. E. Winters

Homogeneous Reactor Test – S. E. Beall
Reactor Design and Analysis – J. A. Lane
Engineering Development – J. A. Lane
Reactor Materials Research – E. G. Bohlmann
Chemical Engineering Development – D. E. Ferguson
Supporting Chemical Research – E. H. Taylor

DATE ISSUED

AUG 14 1957

OAK RIDGE NATIONAL LABORATORY
Operated by
UNION CARBIDE NUCLEAR COMPANY
A Division of Union Carbide and Carbon Corporation
Post Office Box X
Oak Ridge, Tennessee

UNCLASSIFIED

MARTIN MARIETTA ENERGY SYSTEMS LIBRARIES

3 4456 0049745 1

ORNL-2331
Progress

INTERNAL DISTRIBUTION

1. C. E. Center
2. Biology Library
3. Health Physics Library
4. Metallurgy Library
5-6. Reactor Experimental Engineering Library
7-9. Central Research Library
10-14. Laboratory Records Department
15. Laboratory Records, ORNL R.C.
16. G. M. Adamson
17. J. E. Baker
18. S. E. Beall
19. A. M. Billings
20. D. S. Billington
21. E. P. Blizard
22. E. G. Bohlmann
23. C. J. Borkowski
24. G. E. Boyd
25. J. C. Bresee
26. F. R. Bruce
27. W. D. Burch
28. C. A. Burchsted
29. A. D. Callihan
30. D. W. Cardwell
31. W. L. Carter
32. G. H. Cartledge
33. R. A. Charpie
34. R. D. Cheverton
35. H. C. Claiborne
36. W. E. Clark
37. T. E. Cole
38. E. L. Compere
39. D. D. Cowen
40. S. Cromer
41. F. L. Culler
42. J. S. Culver
43. J. S. Drury
44. W. K. Eister
45. L. B. Emlet (K-25)
46. D. E. Ferguson
47. J. H. Frye, Jr.
48. C. H. Gabbard
49. J. L. Gabbard
50. W. R. Gall
51. H. E. Goeller
52. A. T. Gresky
53. J. C. Griess
54. E. Guth
55. P. A. Haas
56. P. H. Harley
57. P. N. Haubenreich
58. J. W. Hill
59. C. J. Hochanadel
60. A. Hollaender
61. A. S. Householder
62. G. H. Jenks
63. W. H. Jordan
64. S. I. Kaplan
65. P. R. Kasten
66. C. P. Keim
67. M. T. Kelley
68. R. B. Korsmeyer
69. K. A. Kraus
70. J. A. Lane
71. W. J. Leonard
72. R. E. Leuze
73. S. C. Lind
74. R. B. Lindauer
75. R. S. Livingston
76. M. I. Lundin
77. R. N. Lyon
78. J. L. Marsh (C&CCC, South Charleston)
79. H. F. McDuffie
80. J. P. McBride
81. H. A. McLain
82. R. A. McNees
83. J. R. McWherter
84. O. Menis
85. E. C. Miller
86. C. S. Morgan
87. K. Z. Morgan
88. E. J. Murphy
89. M. L. Nelson
90. J. P. Murray (Y-12)
91. L. F. Parsly
92. Sigfred Peterson
93. M. L. Picklesimer
94. L. R. Quarles
95. W. D. Reel
96. P. M. Reyling
97. R. C. Robertson
98. A. M. Rom
99. M. W. Rosenthal
100. H. C. Savage

101. C. H. Secoy
102. C. L. Segaser
103. E. D. Shipley
104. M. J. Skinner
105. R. W. Stoughton
106. A. H. Snell
107. I. Spiewak
108. C. D. Susano
109. J. A. Swartout
110. E. H. Taylor
111. D. G. Thomas
112. P. F. Thomason
113. M. Tobias
114. D. S. Toomb
115. W. E. Unger
116. R. Van Winkle
117. B. Weaver
118. A. M. Weinberg
119. E. P. Wigner (consultant)
120. G. C. Williams
121. J. C. Wilson
122. C. E. Winters
123. F. C. Zapp
124. ORNL – Y-12 Technical Library, Document Reference Section
125. HRP Director's Office, Y-12

EXTERNAL DISTRIBUTION

126. F. C. Moesel, AEC, Washington
127. Houdry Corporation (Attn: G. A. Mills)
128. Division of Research and Development, AEC, ORO
129-135. TISE for P.A.R.P.
136-686. Given distribution as shown in TID-4500 (13th ed.) under Reactors–Power category (100 copies – OTS)

Reports previously issued in this series are as follows:

ORNL-527	Date Issued, December 28, 1949
ORNL-630	Period Ending February 28, 1950
ORNL-730	Feasibility Report – Date Issued, July 6, 1950
ORNL-826	Period Ending August 31, 1950
ORNL-925	Period Ending November 30, 1950
ORNL-990	Period Ending February 28, 1951
ORNL-1057	Period Ending May 15, 1951
ORNL-1121	Period Ending August 15, 1951
ORNL-1221	Period Ending November 15, 1951
ORNL-1280	Period Ending March 15, 1952
ORNL-1318	Period Ending July 1, 1952
ORNL-1424	Period Ending October 1, 1952
ORNL-1478	Period Ending January 1, 1953
ORNL-1554	Period Ending March 31, 1953
ORNL-1605	Period Ending July 31, 1953
ORNL-1658	Period Ending October 31, 1953
ORNL-1678	Period Ending January 31, 1954
ORNL-1753	Period Ending April 30, 1954
ORNL-1772	Period Ending July 31, 1954
ORNL-1813	Period Ending October 31, 1954
ORNL-1853	Period Ending January 31, 1955
ORNL-1895	Period Ending April 30, 1955
ORNL-1943	Period Ending July 31, 1955
ORNL-2004	Period Ending October 31, 1955
ORNL-2057	Period Ending January 31, 1956
ORNL-2096	Period Ending April 30, 1956
ORNL-2148	Period Ending July 31, 1956
ORNL-2222	Period Ending October 31, 1956
ORNL-2272	Period Ending January 31, 1957

HRP QUARTERLY PROGRESS REPORT

SUMMARY

PART I. HOMOGENEOUS REACTOR TEST

1. HRT Operations

Run 5, with distilled water at 1500 psi and 270 to 280°C, commenced on February 4, after replacement of the blanket dump and letdown valves and substitution of ±100-psi differential-pressure cells for core-blanket differential-pressure control. Operations were hampered by gas binding of the feed pumps; however, changes were developed to remove the sources of difficulty. Total time at run conditions was 72 hr; total flange leakage (as indicated by the leak-detector system) was less than 2 cc/day.

Run 6 was made at 1700 psi operating pressure and was interrupted once to replace a blanket feed-pump head which had ruptured a diaphragm. The run was concluded during the last week in February, after accumulating 164 hr at operating conditions.

After the fuel feed-pump heads and the letdown valve were replaced, run 7 was commenced, at 1700 psi and 270 to 280°C. Sufficient UO_2SO_4, plus 50% excess H_2SO_4, was added on March 4 to yield a fuel concentration of 5 g of uranium per kilogram of H_2O; and a second, like charge was added one week later. Repeated tie-ins with the chemical processing plant were made without difficulty. The run was interrupted briefly to replace the bellows in the core-blanket equalizing valve and was then resumed until 527 hr was logged at operating conditions with uranium in the system. Weighing and analysis of the reactor contents after the run showed better than 98% uranium recovery.

The third series of simulated remote-maintenance operations was carried out following run 7. For a portion of the activities the shield tank was flooded with condensate, and valve and pressurizer-heater replacements were conducted from above through the water layer. Attempts to freeze plugs in 3½-in. lines under water were unsuccessful; further efforts await the revision of the refrigeration system to increase its capacity to design specifications.

After the period of hot operation, the reactor was shut down and all flanges were examined by a fluorescent penetrant method to determine the extent of the chloride stress-cracking previously found. In this examination almost two-thirds of the high-temperature flanges but less than one-fourth of the low-temperature flanges were rejected or designated as questionable. Representative flanges were then removed and examined metallographically. Some cracks were found in hot flanges that had not been found by the penetrants, and many low-temperature flanges were shown to have been rejected in the penetrant examination for defects other than cracks. Replacement was recommended for flanges in the high-temperature system and for those in the low-temperature system that had been rejected in the penetrant examination.

Sixteen leak-detector lines were removed from the system and examined metallographically. Chloride cracks were found in tubing sections that had been located within a few inches of high-temperature flanges but were not found in any other sections. Carburization, loose grains, shallow cracks, deep pitting, and poor welds were found to be present in all the tubes in sufficient amounts to warrant replacing of the lines to hot flanges.

2. HRT Design

The installation of a CO_2 fire-extinguishing system and an exhaust system in the lower control room was recommended because of the fire hazard which would be present if the hydrocarbon (Amsco) leaked from the refrigeration system.

Calculations were made which indicated that cell pressure might increase to 34 psig in the event of a catastrophic failure of the high-pressure systems after the replacement (spare) fuel heat exchanger is installed. If the spare heat exchanger is ever installed, the liquid inventory of the system will be reduced by 1000 lb to limit the pressure rise to 32 psig.

A 1-in.-thick carbon-steel blast shield was recommended for the replacement heat exchanger.

Radiation decomposition of the insulation of the stator windings of the fuel circulating pump can result in a stator-can pressure of 2 atm absolute in a year of reactor operation.

A long-range program was initiated for the development of tools and procedures for remote maintenance on the core and blanket corrosion specimen holders and the rupture-disk assembly of the pressure balancing system.

The data obtained from the flange thermal-cycling test loop indicate that leak rates within the tolerances specified for the HRT can be obtained in a flanged joint if flanges and rings are made to close tolerances and if adequate care is taken to prevent damage to the seating surfaces of the flange grooves and rings.

3. HRT Component Development

The 400A-1 pump continued to circulate 0.04 *m* UO_2SO_4 solution without difficulty, and a recent inspection showed negligible wear. The 400A-2 pump experienced two failures in mechanical seal components during the report period.

Diaphragm-pump development loops continued to operate. Three failures occurred during the quarter: one feed-pump diaphragm at 6757 hr and two purge-pump diaphragms at 4031 and 7403 hr. Use of 100-mesh screens to protect diaphragms from dirt particles promises to prolong pump life. A contract with Ohio State University to determine fatigue properties of diaphragm sheet in UO_2SO_4 is under way. Preliminary runs with Stellite trim in the check-valve material test indicated very short life in pumped distilled water.

Shop drawing and materials procurement are under way for the HRT spare heat exchanger.

During the report period the HRT mockup completed a run circulating 1.3 *m* UO_2SO_4 solution, and following inspection another run was started to study the behavior of iodine in the system when operating with 0.04 *m* UO_2SO_4.

4. HRT Controls and Instrumentation

The vertically mounted letdown valve was removed from the HRT mockup after 6500 hr of operation. It was still in excellent condition but was replaced with a new valve to evaluate the effects of horizontal operation. The valves in the HRT are also mounted horizontally. One of the two fuel-blanket differential-pressure transmitters installed in the HRT exhibits an 11% linear "zero" shift with a static pressure change of 2000 psi. This transmitter will be zero-adjusted at pressure and used for standby operation.

The protective waterproof housing for the HRT cell microphones was redesigned, primarily to facilitate remote removal. A new fission-chamber pulse preamplifier was developed to provide a better signal-to-noise ratio at the pulse counters. New oxygen-metering and stop valves were developed to provide better flow control and positive shutoff in the oxygen-addition lines.

A report was issued covering revisions and additions to the control circuit to provide a time delay to permit radiolytic-gas recombination before dumping and to provide for the new demineralized-cooling-water loop and for miscellaneous revisions. The thermocouple tabulation was brought up to date, and the material costs for the temperature-measurement systems were listed. The temperature effects on liquid-level control in the replacement heat exchanger were studied, and it was recommended that two level indicators be installed.

5. HRT Processing Plant

The HRT chemical plant was operated for about 200 hr in conjunction with the reactor during the natural-uranium test runs. Startups and shutdowns were carried out successfully without disturbing the reactor operation. Corrosion in the reactor was not sufficient to produce suspended solids of any consequence, and the underflow receiver collected only 0.25 g of solids, which may have been left from preceding tests.

Various remote-maintenance operations were carried out successfully, and semipermanent freeze plugs, required to seal off lines only during maintenance, were tested.

A check of the off-gas adsorber beds, based on recent adsorption data, indicates that the beds are adequate for the design flow rate, but oxygen purge rates in excess of the 500 cc/min for which the beds were designed would result in the release of substantial amounts of radioactive materials to the stack. The principal contributor would be Xe^{133}.

The dissolving-equipment checkout has been delayed by difficulties in sealing the tantalum dissolver nozzles to connecting lines of Carpenter-20 and by leaks from cracked welds in the junction of the tantalum nozzles to the tantalum liner. Early dissolving tests in a mockup of the

dissolving equipment yielded inconsistent results. Apparently, keeping boiling rates low to minimize sulfuric acid entrainment and thus to minimize corrosion of the Carpenter-20 connecting lines does not provide sufficient agitation for complete dissolution.

PART II. REACTOR DESIGN AND ANALYSIS

6. HRE-3 (Thorium Breeder Reactor)

A program has been initiated for the conceptual design of HRE-3, which will be a two-region, solution-core, slurry-blanket, thorium breeder reactor of 60 Mw thermal capacity. The initial reference design is based on parameters chosen to permit demonstration of breeding and to provide a technology which may be readily extrapolated to full-size power reactors.

7. Reactor Analysis

Fuel costs have been obtained for two-region aqueous homogeneous reactors containing U^{233}-ThO_2-D_2O slurry in both the core and the blanket regions. For comparison, costs were also computed for one-region slurry reactors and for two-region systems having no thorium in the core. In the computations isotope concentrations were established by means of equilibrium isotope equations. The major design variables were core diameter, blanket thickness, thorium concentrations in core and blanket, U^{233} concentration in blanket, and poison fraction in core. The critical fuel concentration was obtained by using a two-group two-region reactor model. Charges for chemical processing by a Thorex plant were estimated with the aid of a simplified cost equation. A 4% inventory charge was used, and η^{23} was taken as 2.25. Over a wide range, fuel costs were found to be surprisingly insensitive to variations in the design and operating conditions. There appeared to be no decisive difference in fuel costs between solution-core and slurry-core systems; breeding gain, however, was improved by the use of slurry in the core. For two-region systems fuel costs were as low as 1.2 mills/kwhr; for one-region systems they were about 0.5 mill/kwhr higher.

Fuel costs were obtained for single-region reactors operating under non-steady-state conditions. Reactor fluids studied were UO_2SO_4-water, UO_2SO_4-Li_2SO_4-water, and UO_3-ThO_2-water systems; both D_2O and H_2O were considered. Power level, core diameter, fertile material concentration, inventory charge, cross section of fission products, fuel-processing charge, and fuel-processing cycle time were considered as parameters. Increasing the power from 100 to 1000 thermal megawatts decreased fuel cost by about 1 mill/kwhr for the D_2O systems, while increasing inventory charge from 4 to 12% increased fuel costs by about 0.5 mill/kwhr. The optimum reactor diameter increased and fuel cycle time decreased as the power level was increased. Doubling the fuel-processing charges or the fission-product poisoning increased fuel costs by about 0.1 mill/kwhr.

Thermal fluxes and power densities were calculated with the use of a two-group, one-dimensional, multiregion model for several multiregion research reactors. The reactors were all variations of a basic type, namely, a three-region machine containing a central sphere of D_2O, an annulus containing U^{233} and D_2O, and an outer D_2O reflector. For all reactors considered, thermal fluxes of the order of 10^{15} neutrons/cm^2·sec would be available in the central region, assuming that 100 thermal megawatts was generated in the fuel annulus. The power density at the inner wall of this annulus was about 180 kw/liter, for a 40-cm-radius central sphere, a 20-cm-thick fuel annulus, and a 90-cm-thick outer reflector.

An Oracle code was written for calculating the fuel costs in a one-region, thorium breeder reactor operating under steady-state conditions. An Oracle code was written for obtaining the critical mass and flux distributions in an n-region reactor, using a two-group, one-dimensional model. A general code was written for the Oracle Curve Plotter which makes it possible to obtain the results of computations directly from the Oracle in graphic form.

PART III. ENGINEERING DEVELOPMENT

8. Development of Fuel-System Components

The 20-cfm canned motor blower operated for 282 hr at pressures from 15 to 1000 psi with negligible bearing wear. Specifications were issued to vendors for a 4000-gpm top-maintenance circulating pump, which will serve as a prototype for large homogeneous reactor pumps. A Stellite-piston feed pump has been operated in water for 167 hr, during which time piston leakage has quadrupled. A diaphragm oxygen compressor

which delivers 0.9 scfm at 2500 psi has been tested successfully and is being used to supply gas to the HRT mockup. Design of the test facility for thermal cycling of reactor components between 380 and 580°F was completed during the report period, and material orders were placed.

9. Development of Reactor Slurry Systems

Methods other than high-temperature circulation of thorium oxide slurries for achieving particle-size reduction below about 1 μ are being investigated. Of the methods examined so far, multiple passes of the dry powder through a Mikro-Pulverizer appear to be the most satisfactory.

A method of comparing thorium oxide cakes has been developed in which the ease of resuspension of cake is measured by the weight fraction of cake remaining on a 10-mesh screen after agitation in water.

A circulating loop containing several 10-ft sections of glass pipe has been constructed for the determination of resuspension velocities of settled beds for different slurries and oxide concentrations.

A vertical-tube viscometer has been designed to determine the rheological properties of thorium oxide slurries at temperatures up to 200°C and at pressures up to 300 psig. The tubes are positioned vertically to overcome difficulties due to settling of solids at low flows.

Run 200A-11 was started in the 200-gpm loop to determine the handling characteristics of a thorium–½% uranium oxide slurry containing 3000-ppm sulfate at 300°C and to establish the maximum slurry concentration capable of being circulated. It was found that the maximum concentration which could be circulated without difficulty was about 1400 to 1500 g of thorium per kilogram of H_2O. During the initial 2100 hr of circulation, the handling characteristics and generalized attack rate at 300°C for the sulfated mixed-oxide slurry were similar to those for the sulfated thorium oxide slurry with no uranium. Two forced shutdowns at concentrations of about 1000 g of thorium per kilogram of H_2O occurred during the run as a result of rupture-disk failures. Even though these failures resulted in violent boiling and loss of water, the loop was restarted without trouble.

The first slurry run with the blanket mockup was terminated after a total of 1730 hr of operation. After the system was shut down and drained, a bed of thoria about 13 in. deep was found in the bottom of the blanket vessel. Refilling with water and subsequent circulation failed to remove all of the bed, largely because the streams from the inlet nozzles did not reach all parts of the lower hemisphere, and oxide had to be raked in front of the nozzles before removal was complete.

The pump impeller and flow nozzle were badly eroded, a condition which may have been aggravated by low oxygen concentration during the run and by cavitation in the impeller that was due to the relatively low overpressure used. From the appearance of the nozzle it is estimated that light attack occurred at a velocity of 35 fps and that severe pitting began at a velocity of 40 fps.

Since conditions favorable for the promotion of stress-corrosion cracking occurred in the pressurizer (high chloride concentration), an examination was made by a dye-penetrant method. Several apparently deep cracks were revealed in the pipe wall located in the vapor phase; however, the defects were shown by metallographic examination to be shallow grooves which probably originated as tiny bubbles in the ingot at the time that the pipe was formed.

10. Instrument and Valve Development

The design of the seal-weldable differential-pressure transmitters to be used in the development programs was modified to eliminate a threaded strength joint, which is subject to galling.

A valve incorporating an integral tap for flushing the valve sealing surfaces was designed to provide developmental information. The valve will be used for slurry drain service on a test facility. Several hardenable platinum-alloy caps on stainless steel valve plugs being tested in the valve test loop have loosened in service, and thus the performance results are inconclusive.

PART IV. REACTOR MATERIALS RESEARCH

11. Solution Corrosion

A third test of the mockup of the Zircaloy-2–stainless steel transition joint used in the HRT reactor vessel was completed. No additional mechanical deflections of the bellows were made, but 12 additional thermal cycles of the unit were carried out. The joint and bellows functioned properly and were leak-tight.

Corrosion of stainless steel in 0.04 *m* UO_2SO_4 containing equimolal beryllium sulfate was no greater at 10 to 15 fps and was much less at 15 to 75 fps than in the HRT solution at 200 and 225°C. Increasing the beryllium sulfate concentration to 0.08 *m* increased corrosion at 225°C and resulted in an unstable solution at 300°C.

Corrosion of a variety of materials in boiler water at 250°C was determined at several oxygen concentrations. Carbon steels showed a minimum corrosion rate at 250 to 300 ppm oxygen, but pitting attack occurred. Corrosion of stainless steels increased with increasing oxygen concentration. Zircaloy-2, titanium RC-55, and niobium showed low corrosion rates in all cases.

Loop history was found to have a great effect on corrosion of stainless steel specimens in 0.17 *m* UO_2SO_4 containing 0.04 *m* H_2SO_4 and 0.03 *m* $CuSO_4$. The differences previously observed between 100A loop results and in-pile loop results can be explained by this effect.

The addition of 50 ppm chloride ion to 0.17 *m* UO_2SO_4 produced pitting at 250°C and stress-corrosion cracking at 200°C on type 347 stainless steel when oxygen exhaustion was allowed to occur. No pitting or cracking occurred if the stainless steel surface was in contact with oxygen-containing solution.

Bromide concentrations of 100 and 200 ppm in boiling and aerated 0.04 *m* UO_2SO_4 solution containing 0.02 *m* H_2SO_4 and 0.005 *m* $CuSO_4$ were found to produce cracking in stressed type 347 stainless steel. Cracking occurred during the 2000- to 2500-hr period in the 100-ppm bromide test and during the 1000- to 1500-hr exposure period in the 200-ppm bromide test. Cracking was also observed on stressed type 347 stainless steel exposed in a similar boiling and aerated uranyl sulfate solution containing 100 ppm chloride; the cracking took place during the exposure interval between 2000 and 2500 hr.

Pertechnetate concentrations of 60 ppm and less in oxygenated distilled water at 300°C containing 100 ppm chloride were completely ineffective in preventing stress-corrosion cracking of solution-exposed type 347 stainless steel U-bends during exposure periods up to 250 hr. A significant loss in the initial pertechnetate ion concentration was observed in the tests. At pertechnetate concentrations of 510 and 825 ppm, cracking was prevented during 100- and 350-hr runs, respectively. Some technetium was lost from solution during these tests.

Zirconium-base alloys with silicon, chromium, molybdenum, nickel, niobium, and vanadium were exposed for 1000 hr at 300°C in oxygenated 0.04 *m* UO_2SO_4 solution containing 0.02 *m* H_2SO_4 and 0.005 *m* $CuSO_4$. Alloys of 0.7% Cr–99.3% Zr and 7% Mo–20% Nb–73% Zr exhibited corrosion behavior very comparable with that for Zircaloy-2.

The rate of attack by boiling 5 wt % HNO_3 solution on deposits of Stellite 6 was reduced markedly by pre-exposure in boiling 3 wt % Na_3PO_4 solution. In a number of tests, distilled water at 80°C with an oxygen overpressure of 150 psi caused localized attack of Stellite 6 specimens; in other similar tests, the specimens remained unaffected by the environment. Hard-chrome-plated stainless steel specimens exhibited satisfactory corrosion resistance in distilled water and in simulated HRT core solution at 80°C.

Tests to detect porosity of gold plate on type 347 stainless steel bellows by exposure in boiling 10 wt % HCl solution showed that 0.2- and 2.0-mil-thick gold plates were highly unsatisfactory. In both cases severe blistering and cracking of the plate were encountered.

AlSiMags 192 (TiO_2) and 652 (96 wt % Al_2O_3) exhibited corrosion resistance superior to that of high-purity Kearfott aluminum oxide in oxygenated 1.33 *m* UO_2SO_4 solution at 250°C. The apparent corrosion rates for the former materials were 15 to 17 mpy, as compared with rates of 28 to 30 mpy for the Kearfott alumina after 1000-hr tests.

12. Slurry Corrosion

The assembly and checkout operation of a second thorium oxide slurry corrosion test facility, loop BS, have been completed, with 2010 hr of operation on slurry having been logged. This second test loop has proved satisfactory from an operational standpoint.

Dynamic slurry-corrosion loop CS has been modified by replacing the three annular-flow corrosion sample barrels with standard-type sample barrels like those used in the solution-corrosion test loops (this type of sample barrel is also used in loop BS). This revision eliminated the small annular-flow channel in which plugging had occurred. A calibrated venturi was also installed in loop CS as an aid in following the changes in density and/or flow rate of the circulating slurry.

A new letdown-type sample device to facilitate removal of samples of the circulating thorium oxide slurry has been installed on both loops BS and CS.

Corrosion data and operational observations are given for six thorium oxide slurry runs made at 300°C in 100A pump loops BS and CS.

Four of the tests in loop BS were made to complete a study of the effect of sulfate on the corrosivity of slurries at approximate concentrations of 500 g of thorium per kilogram of water. Neither the sulfate additives nor the presence of spheroids, which formed during circulation, appeared to affect the rate of attack.

The fifth test in loop BS circulated slurry prepared from 650°C-calcined thoria at an average concentration of 478 g of thorium per kilogram of water for 500 hr at 300°C. Generally, corrosion rates paralleled those obtained in previous tests with slurries prepared from thoria calcined at 800°C.

In a 500-hr run in loop CS, slurry prepared from a different batch of 800°C-calcined thoria was circulated at 300°C at an average concentration of 516 g of thorium per kilogram of water. Specimen corrosion rates were moderate, but severe erosive attack occurred in the circulating pump.

Low attack rates were generally observed in toroid tests with slurries prepared from thoria calcined at either high or low temperatures. Slurries of thoria of 1.2 μ average size fired at 1200, 1400, and 1600°C underwent little degradation during circulation, whereas those prepared from 550- and 650°C-calcined thoria of 2.6 to 4.6 μ average size were degraded to approximately 0.7 μ during 300 hr of circulation at 250°C.

A new development-model rotator for an in-pile slurry toroid is described.

13. Radiation Corrosion

The construction and operational testing of in-pile loop L-2-17 were completed, and the loop is presently in operation in beam hole HB-2 of the LITR. Loop L-4-18 is now being constructed.

Design and development work for a dynamic-loop radiation-corrosion facility in the ORR has continued. An experimental model, designated 0-1-20, is being constructed so that operating characteristics can be determined. The loop cooler is capable of removing 14 kw, and the core cooler, 4 kw. The loop heater, which is integral with the loop cooler, will supply 8 kw.

A retraction mechanism for the ORR loop package has been designed. Retraction of the loop 18 in. will reduce the neutron flux by a factor of about 100 and the gamma-ray intensity by a factor of about 35.

The ninth in-pile loop experiment, L-4-13, has been completed. This loop and the core and line sample holders were fabricated from type 347 stainless steel. The solution was 0.17 *M* UO_2SO_4 and for the first time was made up by use of heavy water. The main-stream operating temperature was 250°C. The effect of power density on corrosion rates of crystal-bar-zirconium specimens was in reasonably good agreement with that observed in the only other experiment containing crystal-bar zirconium and that observed on Zircaloy-2 in all previous 250°C experiments. The type 309 SCb and type 347 stainless steel specimens exhibited somewhat lower corrosion rates than those in previous experiments. However, this is the first experiment at 250°C with steel coupon holders and in which the excess acid was maintained near 0.02 *m*.

Exposure of in-pile loops L-4-16 (stainless steel) and L-2-14 (titanium) has been completed. Experiment L-4-16 was conducted with 0.17 *m* UO_2SO_4 solution at 280°C in the main stream. The over-all steel corrosion rate was 0.5 mpy. Experiment L-2-14 was the first all-titanium loop and the first in which the 0.17 *m* UO_2SO_4 solution contained 0.4 *m* excess acid. The objective of the experiment was to establish the effect of the high excess acid on the titanium- and zirconium-alloy corrosion rates. The over-all titanium corrosion rate based on oxygen consumption was 2.7 mpy.

Operational testing of the new in-pile autoclave mockup test facility has been completed. A number of minor modifications were made to the autoclave equipment to facilitate assembly and eliminate operational difficulties encountered during the initial tests. The first experiment for operation in the new multibomb radiation-corrosion facility has been assembled and pretreated at the Y-12 site and is ready for in-pile operation.

Four autoclave experiments were completed. A pressure phenomenon, in which the pressure increased appreciably, reached a maximum, and then decreased to somewhat less than the original

pressure, was observed in the initial portion of Z-22, a Zircaloy-2 experiment containing depleted 0.17 *m* UO_2SO_4 and 0.02 *m* $CuSO_4$. A similar pressure excursion was observed in an earlier, similar experiment. A lack of a gross effect on corrosion by a small amount of atmospheric nitrogen in the depleted system was indicated.

A very-high-power-density Zircaloy-2 experiment, Z-23 (1.3 *m* UO_2SO_4, 93% U^{235}; 0.04 *m* $CuSO_4$; 0.04 *m* H_2SO_4), is discussed. The corrosion rate (23 mpy at 280°C and 109 w/ml) agrees very well with the equation

$$CR = 0.318PD\left(1 - e^{-95/CR^{1.5}}\right) ,$$

the constants of which were evaluated by data from experiments at much lower power densities.

A low-power-density Zircaloy-2 experiment, L6Z-102 (0.17 *m* UO_2SO_4, 0.04 *m* $CuSO_4$), along with preliminary in-pile loop data (L-2-15, L-4-16), indicates that the constants in the equation for corrosion rate vs power density for this system at 280°C should be revised to read as follows:

$$CR = 2.45PD\left(1 - e^{-95/CR^{1.5}}\right) .$$

A type 347 stainless steel experiment, L6S-103, is discussed. This experiment (0.17 *m* UO_2SO_4, 0.01 *m* $CuSO_4$) was similar to three earlier experiments except that the small amount of atmospheric nitrogen formerly included was excluded from L6S-103. During the initial 380 hr the observed corrosion was considerably less in this system than in previous systems which contained nitrogen.

14. Metallurgy

Hardness-time-temperature curves have been determined for Zr–15% Nb, sponge Zr–15% Nb, Zr–15% Nb–1% Fe, and Zr–15% Nb–2% Pd by aging quenched and reheated specimens in the isothermal transformation machine, where specimens reach the desired temperature within 5 sec. The hardness curves agree reasonably well with those determined for the longer times by aging in capsules in tube furnaces. However, the microstructures are entirely different. Photomicrographs are shown. A third "transition" transformation product in the decomposition of the retained beta of the Zr–15% Nb–2% Pd alloy may have been found.

A 25-lb ingot of sponge Zr–15% Nb has been successfully extruded to a $1\frac{1}{8}$-in. round bar for fabrication into in-pile corrosion bombs. The conditions of extrusion are given, and macrographs of the surface extrusion defects are shown.

Cold-worked iodide Zr and Ti have been observed to absorb large amounts of H_2 and to undergo extensive recrystallization at an ambient temperature of 230 to 240°C in a recombiner loop. Control experiments have been performed in a modified Sievert's apparatus in an attempt to reproduce the H_2 absorption and recrystallization. All results are, so far, negative.

The mechanical-property study of zirconium-base alloys, being performed at Armour Research Institute under contract, is now being concentrated on a series of Zr–15% Nb base alloys whose compositions and heat treatments have been specified from the time-temperature-hardness data obtained and published in the last two reports. The alloys have been cast and are now being fabricated into specimens.

Considerable anisotropy has been found in the impact properties of Zircaloy-2. These differences are not found at low temperatures or in the nil ductility temperature as determined by drop-weight testing. Both titanium and zirconium show a surprising ability to arrest a moving crack, as shown by the very low nil ductility temperatures.

Widespread brittle failures occurred to bolts, nuts, and ferrules which had seen four-month service in the HRP flange test loop. This intergranular cracking was ascribed to cadmium embrittlement which stemmed from the cadmium-plated nuts and ferrules.

Development of an internal-probe eddy-current testing device for tubing inspection shows possibilities but, as yet, has not been completely successful for type 347 stainless steel. Immersed ultrasonic methods are being used for the replacement leak-detector tubing and have been shown to be capable of picking up a 3% defect, provided the surface has been polished.

Welding techniques have been developed for making the root pass in stainless steel and titanium weldments by using preplaced inserts. Of the various shapes of inserts investigated, the round inserts appear in most cases to be the most satisfactory; however, for small-diameter tubing, washer-type inserts with a square cross section are recommended.

An elevated-temperature irradiation of metal specimens in the MTR was completed, and an ambient-temperature experiment was shipped to the MTR for irradiation. A study was started, in cooperation with the Naval Research Laboratory, to correlate results from several brittle-fracture test methods.

PART V. CHEMICAL ENGINEERING DEVELOPMENT

15. Uranyl Sulfate Fuel Processing

Particles of simulated reactor solids containing more than 40% Fe_2O_3 showed a marked tendency to increase in size when heated to 275 to 300°C in uranyl sulfate solution. Growth was rapid at 300°C; at 275°C an initiation period of about 3 hr, during which little growth occurred, was followed by a short period of very rapid growth. Particles containing 85% ZrO_2 did not grow appreciably even at 300°C.

In simulated fuel solution at 100°C in the presence of Co^{60} radiation, the stability of iodate was measured as a function of the H_2/O_2 ratio in the gas phase above such solutions. For a given temperature, increasing the H_2/O_2 ratio decreased the iodate stability; increasing the uranium concentration increased iodate stability. Increasing the temperature to 120°C markedly lowered the iodate stability, as also did the presence of metallic ions, which catalyze the decomposition of radiation-induced peroxides.

Uranyl sulfate solution processing by UO_4 precipitation gave a decontamination factor of 8.7 from cesium, with a 0.3% uranium loss from a starting solution containing 50 g of uranium per liter. Dissolution and decomposition of UO_4 in dilute sulfuric acid solutions were complete in 30 min at 80°C.

Krypton solubility measurements in 0.02 *m* UO_2SO_4 solutions and in water at 100 to 300°C showed no deviations from predicted values as a result of low partial pressures of krypton and the presence of solute at low (5 g of uranium per liter) concentrations.

No significant effect of temperature, flow rate, and ZrO_2 concentration was observed on the rate of ZrO_2 deposition in a circulating loop. However, in all tests the concentration of solids in suspension appears to reach an equilibrium value in about 10 hr. This concentration varied only slightly with flow rate and temperature but was markedly dependent on the amount of ZrO_2 added to the loop.

16. Uranyl Sulfate Blanket Processing

Plutonium solubility in 1.4 *m* UO_2SO_4 and specific adsorption on stainless steel were essentially the same for surface-area/volume ratios of 0.2, 0.4, and 0.6 cm^2/ml. As the plutonium concentration was increased to 45 mg per kilogram of H_2O, essentially all the plutonium remained in solution as Pu(VI). There was a small amount of adsorption, but no plutonium was precipitated. As more plutonium was added, the soluble plutonium decreased to 5 mg per kilogram of H_2O, and plutonium adsorption and precipitation increased rapidly.

When 1.4 *m* UO_2SO_4 containing more than 300 mg of Pu(VI) per kilogram of H_2O was heated to 250°C in pyrex tubes under 200 psi of O_2, approximately 215 mg of Pu(VI) per kilogram of H_2O remained in solution.

About 80% of the plutonium was present as Pu(IV) when 1.6 *m* UO_2SO_4 containing chromium was heated to 250°C under 200 psi of O_2 in a Co^{60} gamma flux of 2 w/liter. This is in contrast with measurements made in the absence of radiation in which Pu(VI) is formed when 1.4 *m* UO_2SO_4 solutions containing plutonium are heated under stoichiometric hydrogen and oxygen.

Fifty-seven per cent of the plutonium formed by LITR irradiation of 1.4 *m* UO_2SO_4 in a titanium bomb under oxygen was in solution at a concentration of 26 mg per kilogram of H_2O, 42% was adsorbed on the titanium, and only 1% was in the precipitate. Neptunium distribution was similar – 56% in solution, 43% adsorbed, and 1% in the precipitate. Analysis showed that less than 0.1% of the plutonium in solution was in the reduced valence state.

Loop P-1, for plutonium studies, has been operated with dilute UO_2SO_4 solution and oxygen. Some leaks occurred during thermal cycling around valve glands and fittings.

17. Thorium Oxide Blanket Processing

The adsorption of uranium from dilute uranyl sulfate solution on thorium oxide in aqueous slurries at 250°C was investigated. In tests with ThO_2 pretreated with sulfur-saturated alcohol, dilute H_2SO_4, or dilute $Th(SO_4)_2$, the uranium adsorption was decreased by a factor of about 10.

The lowest uranium adsorption on ThO_2 (600°C calcined) slurries in 0.01 *m* UO_2SO_4 at 250°C was 2000 ppm.

Uranium adsorption decreased as the ThO_2 calcination temperature increased. Thorium oxide calcined at 650°C adsorbed 3300 to 4400 ppm uranium from 0.05 *m* UO_2SO_4 containing 0.05 *m* H_2SO_4 at 250°C, but thorium oxide calcined at 1100°C adsorbed only 80 to 190 ppm.

18. Thorium Oxide Slurry Development

Chemical and radiochemical analyses were obtained on nine thorium oxide slurries – seven containing enriched uranium at a U/Th ratio of 0.005 – which had been irradiated at 300°C in the LITR. Uranium-to-thorium ratios agreed with data of the original slurries, and the corrosion-product pickup agreed with out-of-pile results. The bulk of the radioactive materials was associated with the slurry solids, only cesium appearing in the supernatant in significant amounts.

In out-of-pile tests on the catalytic combination of hydrogen and oxygen by aqueous thorium-uranium oxide slurries containing molybdenum oxide catalyst, the addition of thorium sulfate up to 10,000 ppm sulfate did not appear to deactivate the catalyst. Combination rates were negligible with slurries of thorium-uranium mixed oxides fired at 650 and 800°C and containing MoO_3, but the rate was satisfactory with 1000°C-fired material even without previous activation by hydrogen.

The properties of a thorium-uranium oxide (250 g of thorium per liter) prepared by thermal decomposition of the 10°C coprecipitated oxalates resembled those of a pure oxide fired similarly. The hindered-settling rates and the critical concentration increased with increasing slurry temperature and increasing oxide calcination temperature to 1170°C. There was some evidence of gelation or foaming at 300°C.

Marked dispersion effects at room temperature were noted in a slurry of 800°C-fired oxide containing 250 g of thorium per kilogram of H_2O which had been heated overnight at 300°C with 13,000 ppm hydrogen bentonite. Dispersion was also obtained with similar slurries heated with 5000 ppm SiO_2, based on ThO_2, added as $Na_2O{\cdot}SiO_2$ or H_2SiO_3. Dispersion with this concentration of silicate appeared relatively insensitive to pH over the range 6 to 12.

With slurries of 800°C-fired pilot-plant oxide containing 250 g of thorium per kilogram of H_2O, addition of $Na_2O{\cdot}SiO_2$ up to 20,000 ppm SiO_2, based on ThO_2, decreased the settling rates of thorium oxide slurries up to slurry temperatures of 275°C. Above this temperature little change was observed as the result of the silicate addition. With slurries of the oxide which had been micropulverized, settling rates were much slower at all temperatures, even at 300°C, and at all silica concentrations. The effect was more pronounced below 225°C.

Studies at 100°C with a slurry of 800°C-fired oxide containing 250 g of thorium per kilogram of H_2O and 10,000 ppm SiO_2, based on ThO_2, as $Na_2O{\cdot}SiO_2$ indicated that equilibrium is apparently attained in less than 1 hr, the time depending somewhat on the previous heat treatment of the slurry.

Marked dispersion effects were noted in slurries of thorium-silicon oxide (0.5 and 1 mole % SiO_2 based on ThO_2) autoclaved with Na_2SiO_3 and H_2SiO_3 at additive concentrations of 1000 to 10,000 ppm SiO_2, based on ThO_2. The thorium-silicon oxide was prepared by firing ThO_2 and H_2SiO_3 at 1000°C for 24 hr.

Local concentrations of ThO_2 at the bottom of the blanket in the slurry blanket mockup were considerably higher (1100 g of thorium per kilogram of H_2O) than would be expected from the x-ray settling data (700 g of thorium per kilogram of H_2O). Settling studies with a 40-in.-dia column of slurry to determine the effect of bed height on slurry concentration at the bottom of a slurry column indicated that bed height alone does not explain the discrepancy and that the settling time, bed cross section, and the dynamics all have a bearing.

Thoria sols stabilized with nitrate ion were not stable under reactor conditions. Thoria beads in the 100-μ range (wet) prepared from nitrate sols, gelled by hexamethylenetetramine solution, retained their spherical shape on firing at 1400°C.

PART VI. SUPPORTING CHEMICAL RESEARCH

19. Aqueous Systems at Elevated Temperatures

Studies of the homogeneous reaction of hydrogen with oxygen, catalyzed by dissolved copper salts in aqueous solutions, were continued. Tests performed at 200 and 175°C are reported in which the effects of copper concentration and acidity upon catalytic activity were determined for the sulfate system (copper sulfate plus sulfuric acid). The results were shown to be inconsistent with the mechanism proposed by Halpern for the perchlorate system at 110°C. A two-parameter kinetic equation has been derived which agrees well with the 175°C data above 0.04 *M* acidity.

20. Radiation Chemistry

The initial product yields of the Co^{60} radiation-induced decomposition of heavy water containing 0.4 *M* sulfuric acid have been determined to be $G_{D_2} = 0.39$, $G_{D_2O_2} = 0.83$, $G_D = 3.95$, and $G_{OD} = 3.08$. The acid systems used to define these yields were D_2 formation in degassed dilute bromide solution, peroxide formation in an aerated solution, and ferrous oxidation in an aerated solution.

CONTENTS

SUMMARY v

PART I. HOMOGENEOUS REACTOR TEST

1. HRT OPERATIONS 3
   - 1.1 Reactor Operations 3
     - 1.1.1 Leak-Detector System 4
     - 1.1.2 Water Inventory 6
     - 1.1.3 Corrosion and Fuel Stability 6
   - 1.2 Maintenance of Radioactive Components 7
   - 1.3 Flange Inspection 8
   - 1.4 HRT Leak-Detector Tubing 10
2. HRT DESIGN 19
   - 2.1 Refrigeration System 19
   - 2.2 Water Treatment 19
   - 2.3 Replacement Heat Exchanger 20
   - 2.4 Radiation Damage to the Motor of the Fuel Circulating Pump 21
   - 2.5 Remote Maintenance 22
   - 2.6 Flange Development Program 22
3. HRT COMPONENT DEVELOPMENT 26
   - 3.1 Pump Development 26
     - 3.1.1 400A-1 Pump and Loop 26
     - 3.1.2 400A-2 Pump and Loop 26
     - 3.1.3 300A-1 Pump 26
   - 3.2 Feed Pumps 26
     - 3.2.1 Feed-Pump Test Loops 26
     - 3.2.2 Purge Pumps 27
     - 3.2.3 Corrosion Fatigue Tests of Diaphragms 27
     - 3.2.4 Check-Valve Material Test 27
   - 3.3 HRT Replacement (Spare) Heat Exchanger 28
   - 3.4 HRT Mockup 28
4. HRT CONTROLS AND INSTRUMENTATION 31
   - 4.1 Component and System Testing 31
     - 4.1.1 Letdown Valves 31
     - 4.1.2 Fuel-Blanket Differential-Pressure Transmitters 31
   - 4.2 Development 32
     - 4.2.1 Sound Transmitters 32
     - 4.2.2 Fission-Chamber Pulse Preamplifier 32
     - 4.2.3 Oxygen-Injection System 32
   - 4.3 Design 32
     - 4.3.1 Control Circuits 32
     - 4.3.2 Temperature Measurement Systems 34
     - 4.3.3 Replacement Heat Exchanger Instrumentation 34
5. HRT PROCESSING PLANT 35
   - 5.1 High-Pressure-System Operation with Reactor 35

5.1.1 Practice Startup and Shutdown 35
5.1.2 Solids Removal 35
5.1.3 Operation with 0.56-in.-dia Hydroclone 35
5.2 Dissolver-System Installation 36
5.2.1 Chloride-Contaminated Leak-Detector Tubing 36
5.2.2 Carpenter-20 Material Defects 36
5.2.3 Dissolver Installation 36
5.2.4 High-Pressure-System Flange Tests 36
5.3 Remote-Maintenance Practice 36
5.3.1 Compact Right-Angle Wrench 36
5.3.2 Circulating-Pump Installation 36
5.3.3 Semipermanent-Freeze-Plug Test 37
5.4 Closed-Cycle Cooling Water 37
5.5 Waste Disposal 37
5.5.1 Charcoal Beds 37
5.5.2 Storage Tanks 38
5.6 Solids-Dissolving Studies 38

PART II. REACTOR DESIGN AND ANALYSIS

6. HRE-3 (THORIUM BREEDER REACTOR) 43

7. REACTOR ANALYSIS 45
7.1 Fuel Costs in Spherical Thorium Slurry Reactors 45
7.1.1 Two-Region Reactors 46
7.1.2 One-Region Reactors 47
7.1.3 Comparison of Reactor Types 49
7.2 Fuel Costs in Single-Region Power Reactors 50
7.3 Flux Peaking in Homogeneous Reactors 52
7.4 Mathematics and Computation 57

PART III. ENGINEERING DEVELOPMENT

8. DEVELOPMENT OF FUEL-SYSTEM COMPONENTS 61
8.1 20-cfm Canned-Motor Blower 61
8.2 Large Circulating Pump 61
8.3 Stellite Reciprocating Feed Pump 61
8.4 Oxygen Compressor 61
8.5 Titanium Program 63
8.6 High-Pressure Steam Boiler Facility 63
8.7 Remote Maintenance 63
8.8 Heat-Exchanger Tube-Joint Test 63

9. DEVELOPMENT OF REACTOR SLURRY SYSTEMS 64
9.1 Thorium Oxide Particle-Size Reduction 64
9.2 Disintegration of Thorium Oxide Cakes 64
9.3 Slurry Resuspension Velocity 64
9.4 Slurry Rheology 66
9.5 Circulating-Slurry Behavior 70
9.6 HRT Blanket System Development 71

10. INSTRUMENT AND VALVE DEVELOPMENT 79

10.1 Instrument Development 79
10.1.1 Differential-Pressure Transmitters 79
10.2 Valve Development 79
10.2.1 Slurry Valves 79
10.2.2 Valve Trim 80

PART IV. REACTOR MATERIALS RESEARCH

11. SOLUTION CORROSION 83
11.1 Dynamic Corrosion Studies 83
11.1.1 Third Operating Test of the HRT Core–Pressure-Vessel Flange and Transition-Joint Mockup 83
11.1.2 Corrosion of Stainless Steel in Dilute Uranyl Sulfate Solutions Containing Beryllium Sulfate 84
11.1.3 Corrosion in Water at 250°C 87
11.1.4 Effect of Loop History on the Corrosion of Stainless Steel 89
11.1.5 Effect of Adding Chloride Ions to Uranyl Sulfate Solutions 89
11.2 Laboratory Corrosion Studies 90
11.2.1 Stress-Corrosion Cracking 90
11.2.2 Corrosion Tests with Zirconium Alloys 93
11.2.3 Miscellaneous Tests 93

12. SLURRY CORROSION 96
12.1 Pump Loops 96
12.1.1 Loop Engineering 96
12.1.2 100A Pump-Loop Tests 100
12.1.3 Tests with Sulfate Additives 101
12.1.4 Circulation of 650°C-calcined Thoria Slurry 103
12.1.5 Wear of Pump Components 103
12.1.6 Circulation Test in Revised Loop CS 107
12.2 Toroids 109
12.2.1 Effect of Calcination Temperature 109
12.3 In-Pile Slurry Toroid Development 110

13. RADIATION CORROSION 112
13.1 In-Pile Loops 112
13.1.1 Development and Construction 112
13.1.2 General Description of In-Pile Loop Experiment L-4-13 113
13.1.3 Qualitative Results of Inspection and Evaluation of Loop L-4-13 115
13.1.4 Quantitative Results of Inspection and Evaluation of Loop L-4-13 116
13.1.5 Discussion of Results from Loop L-4-13 116
13.1.6 In-Pile Loop L-4-16 118
13.1.7 In-Pile Loop L-2-14 118
13.1.8 In-Pile Loop L-2-17 118
13.2 In-Pile Autoclave Tests, LITR 119
13.2.1 Development and Construction 119
13.2.2 In-Pile Tests 120

14. METALLURGY 124
14.1 Physical Metallurgy 124
14.1.1 Zirconium-Alloy Development 124

14.1.2 Zirconium-Hydrogen System 127
14.1.3 Special Zirconium Alloys – Mechanical Properties 132
14.2 Mechanical Metallurgy 132
14.2.1 Zirconium Alloys 132
14.2.2 Titanium Alloys 132
14.3 Metallurgical Development and Service 134
14.3.1 Bolt Failures in HRP Flange Test Loop 134
14.4 Inspection Development 136
14.4.1 Eddy-Current Testing of ¼-in. Type 347 Stainless Steel Tubing 136
14.5 Welding Development 136
14.6 Effects of Radiation on Structural Metals and Alloys 138

PART V. CHEMICAL ENGINEERING DEVELOPMENT

15. URANYL SULFATE FUEL PROCESSING 141
15.1 Properties of Simulated Reactor Solids 141
15.2 Iodine Chemistry 142
15.3 Volatility of Iodine Under Reactor Conditions 147
15.4 Rare-Gas Solubility 149
15.5 Uranium Processing 149
15.6 Behavior of Dilute ZrO_2 Suspensions in Circulating Fuel Solution 150

16. URANYL SULFATE BLANKET PROCESSING 151
16.1 Solubility of Pu(VI) in Uranyl Sulfate Solutions 151
16.2 Plutonium Valence in Uranyl Sulfate Solutions 151
16.3 Plutonium Behavior in 1.4 *m* UO_2SO_4 Contained in Stainless Steel 151
16.4 In-Pile Experiment 152
16.5 Uranyl Sulfate Solution from the HRT Mockup 153
16.6 Laboratory Support for Loop P-1 Program 153
16.7 Loop P-1 Studies 153

17. THORIUM OXIDE BLANKET PROCESSING 156
17.1 Cation Adsorption on ThO_2 156

18. THORIUM OXIDE SLURRY DEVELOPMENT 157
18.1 Slurry Irradiation Studies 157
18.1.1 Slurry Irradiations in the LITR 157
18.1.2 Postirradiation Examination of Slurries 157
18.2 Gas Recombination Studies 159
18.2.1 Effect of Sulfate 159
18.2.2 Effect of Calcination Temperature 160
18.3 Thorium-Uranium Mixed Oxide Studies 161
18.3.1 Effect of Firing Temperature on Characteristic Properties 161
18.3.2 Hindered-settling Rates at Elevated Temperatures 162
18.4 Silicate Addition Studies 164
18.4.1 Room-Temperature Sedimentation Studies 164
18.4.2 Settling Rates at Elevated Temperatures 164
18.4.3 Equilibrium Studies 166
18.4.4 Studies with Mixed Thorium-Silicon Oxide 167
18.5 Deep-Bed Settling Experiments 168
18.6 Preparation of Thoria Sols and Gels 169

PART VI. SUPPORTING CHEMICAL RESEARCH

19. AQUEOUS SYSTEMS AT ELEVATED TEMPERATURES 173

19.1 Characterization of Slurry Flocculation of pH 173

19.2 Homogeneous Catalysis of the Hydrogen-Oxygen Reaction in Aqueous Solutions 173

20. RADIATION CHEMISTRY 176

20.1 Fundamental Processes in the Radiation Chemistry of Heavy Water 176

Part I

HOMOGENEOUS REACTOR TEST

S. E. Beall

1. HRT OPERATIONS

S. E. Beall

H. F. Bauman
N. A. Brown[1]
J. R. Buchanan
N. W. Curtis[2]
J. R. Engel
J. D. Flynn
D. F. Frech
T. H. Gladney[1]
R. H. Guymon
R. J. Harvey
P. N. Haubenreich
J. W. Hill, Jr.
R. W. Jurgensen[3]
S. I. Kaplan
J. O. Kolb
H. M. McLeod
G. W. Rivenbark
H. K. Search[1]
R. Van Winkle
R. R. Wiethaup

1.1 REACTOR OPERATIONS

Additional simulated operating tests with externally supplied heat were conducted during the quarter to evaluate procedure and equipment changes suggested by the runs during the previous quarter. After replacement of the blanket dump and letdown valves and substitution of ±100-psi differential-pressure cells for the existing ±50-psi core-blanket differential-pressure control cells, the reactor was charged with distilled water and restarted. Run 5 extended from February 4 to February 14, 1957, and included 72 hr at 1500 psi and 270 to 280°C. Severe gas-binding of the fuel feed pumps occurred during the run; oxygen had leaked back through the check valves and into the pumps from the discharge lines when the pumps were operating at low pumping rates, and an improper valve switching sequence had blocked the inlet flow long enough to starve the pumps. These difficulties were eliminated by revisions in operating procedure and wiring arrangement. With the exception of the core dome connection, flange leakage was acceptably low during the run, depleting the water in the leak-detector system by less than 2 cc/day.

The operating pressure was raised to 1700 psi for run 6. One scheduled shutdown was made during the run, to replace a blanket feed-pump head which had leaking check valves and a ruptured diaphragm. At the conclusion of the run, after 164 hr had been logged at operating conditions, it was necessary to replace both fuel feed-pump heads and the fuel letdown valve because of excessive corrosion of the Stellite surfaces in these components.

Uranyl sulfate, prepared from depleted uranium, and sulfuric acid were added during run 7, on March 4, in sufficient amounts to yield a fuel concentration of 5 g of uranium per kilogram of H_2O with 50% excess acid. A second, equal addition was made after one week of continuous operation. The reactor was maintained steadily at 1700 psi and 270 to 280°C for 260 hr, during which time flow from the reactor to the chemical processing system was repeatedly started and stopped for test purposes. No difficulties were encountered in connecting the two systems or in operating the systems jointly.

From March 18 to March 22, a loss of water amounting to 20 lb/day was indicated by the reactor-inventory weighing devices. On March 22, a search for the source of water leakage revealed a cracked bellows in the fuel-blanket differential-pressure equalizing valve. The reactor was shut down, the equalizing valve replaced, and normal operation resumed within 30 hr. The run was finally terminated on March 28 after 625 operating hours at full temperature and pressure, of which 527 hr was with uranium in the system.

During the dump on March 22, the pressure-balancing control system was in normal operation and performed satisfactorily. Core and blanket pressure-time curves were similar to those for earlier dump tests.[4] The core-blanket differential pressure, as indicated by the permanent pneumatic differential-pressure cell, is shown in Fig. 1.1. An electric differential-pressure cell connected between flanges on the top of the core and blanket did not show the sharp initial peak. The pressure-equalizing valve opened very briefly at the beginning of the dump; thereafter it remained closed.

[1]On loan from TVA.

[2]On loan from Pennsylvania Power and Light Co.

[3]On loan from American Gas and Electric Co.

[4]S. E. Beall *et al.*, *HRP Quar. Prog. Rep. Jan. 31, 1957*, ORNL-2272, Fig. 1.2, p 6.

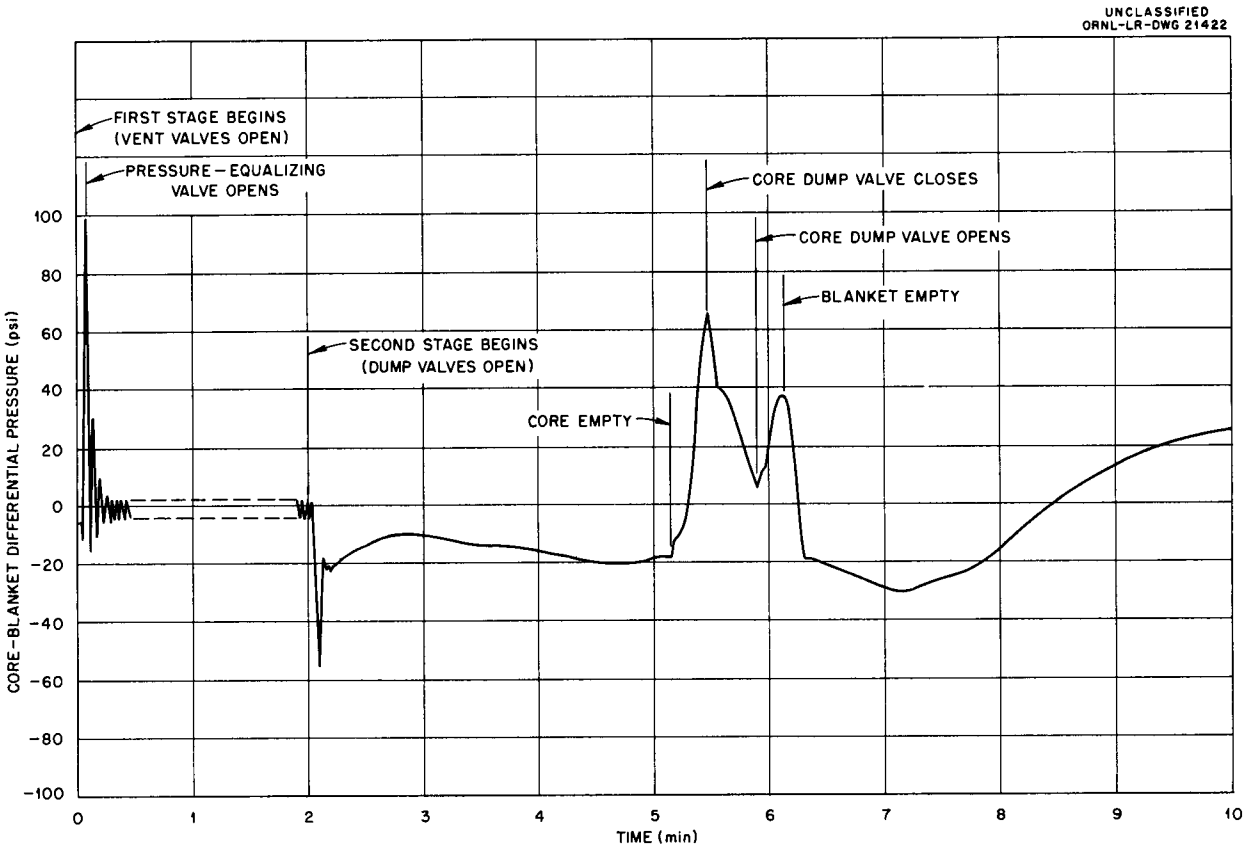

Fig. 1.1. Core-Blanket Differential Pressure During Dump Test No. 7. Initial conditions: 1700 psig, 277°C.

The dump at the termination of the run was made with the pressure-equalizing valve intentionally held open. The indicated differential pressures during the first 10 sec of this dump were almost identical with those obtained during the previous dump with the pressure-equalizing valve closed. Again the pneumatic cell showed a sharp peak of about 90 psi, while the electric cell showed practically no pressure differential. Apparently the indication of a sharp initial peak is due to the physical arrangement of the pipes connecting the pneumatic cell to the pressurizer vent lines, and possibly to the characteristics of the pneumatic system.

Inventory of the contents of the core and blanket systems before and after each dump showed no detectable transfer between the two systems, and analysis of the blanket contents showed no uranium at any time. After the run was terminated, the reactor was rinsed and the contents were weighed and analyzed. Recovered uranium matched the amount charged to within 60 g.

The balance of the quarter was devoted to remote-maintenance practice (Sec 1.2) and to metallurgical inspection of the system flanges and leak-detector tubing.

1.1.1 Leak-Detector System

The HRT leak-detector system serves three functions: to detect leaks in flanged joints which have oval-ring gaskets, to prevent the leakage of reactor solutions into the space between the gasket and the bottom of the flange groove, and to indicate quickly whether a flanged joint has been made up and tightened properly after being opened.

Although initially designed to be operated under hydraulic pressurization,[5] the leak-detector system was later operated more satisfactorily by maintaining a gas pressure (helium) on the vertical water-supply tank. Leakage of water from the leak-detector system was measured as a decrease

[5] J. E. Kuster, *HRT Leak Detection System*, ORNL CF-56-4-105 (April 20, 1956).

in the liquid level of the 6-in.-long sight glass attached to the tank. The unit volume of the sight glass and supply tank is $41\frac{1}{4}$ cc/in.; the liquid level can be read to the nearest $\frac{1}{16}$ in.

Changes in cell air temperature, control-room air temperature, flange temperatures, and total pressure on the leak-detector system cause volume changes in the leak-detector water which tend to obscure the leakage indication; however, at steady operation these conditions approach constant values, and corrections have been determined for each. In the total high-pressure leak-detector system, a volume of about 15 liters, the maximum change in volume occurs during heatup of the reactor system from room temperature to 280°C. This change is about 100 cc, corresponding to a level change of $2\frac{1}{2}$ in. in the sight glass.

It is felt that leakage of water from the system can be tolerated, as long as the pressure of the leak-detector system can be maintained higher than that in the primary system. The nominal operating pressure of the leak-detector system is 2000 ± 100 psi when the primary system is at 1700 psi. When the new leak-detector tubing is installed, revisions will be made to reduce further any likelihood that the leak-detector pressure will drop below system pressure.

The steady-state leak rates observed during operations are summarized in Table 1.1. Leakage from individual flanges was not located upon shutdown, because remote-maintenance practice did not permit uninterrupted operation of the leak-detector system.

It was found that the worst leakage occurs when a flange is cooled rapidly but that the leakage stops when equilibrium temperature is reached. One such temperature excursion occurred in run 5, when the blanket circulating pump was started in preparation for heating the system following a period of pressurizing. Hot water from the pressurizer had spilled over into the circulating system and heated the blanket outlet pipe to about 110°C, while the bulk of the water was at about 70°C. The temperature of the blanket outlet pipe dropped approximately 40°C in 2 min, resulting in the loss of some 700 cc of water from the leak-detector system. Table 1.2 presents the leak-detector fluid losses for 11 occasions on which the system was cooled from operating temperature, including nine dumps. Due to the transient nature of the leakage, it was not possible to pin down its source.

Except for one processing-plant tie-line flange (Table 1.1, entry No. 10) and those flanges involved in component replacement, no flanges had to be tightened. Of the 100 high-pressure and 49

Table 1.1. Leak-Detector Water Losses During Steady Operation

Run No.	Period	Leakage Rate	Remarks
5	Last 56 hr	28 cc/day	No flanges tightened before start of run 6
6	First 90 hr	2 cc/day	
	Next 71 hr	4.5 cc/day	
7	First 60 hr	8 cc/day	
	18 hr following new startup	10 cc/day	Just prior to first uranium addition
	280 hr following uranium addition	3 cc/day	Prior to chemical-plant tie-in
	Following first chemical-plant tie-in	34 cc/5 hr	Severe thermal shock to chemical-plant tie-line flanges
	Following second chemical-plant tie-in	14 cc/5 hr	Same as above
	Following third chemical-plant tie-in	20 cc/5 hr	Same as above
	Following fourth chemical-plant tie-in	0 cc/5 hr	One tie-line flange with subnormal bolt torque found and retightened
	Last 94 hr; after replacement of pressure balancing valve	24 cc/day	

Table 1.2. HRT Leak-Detector Behavior During Thermal Cycles

Run No.	Date	Cooling Before Dumping		Conditions at Start of Dump		Approximate Measured Leakage from Leak-Detector Volume (cc)
		Initial Temperature (°C)	Rate (°C/hr)	Temperature (°C)	Pressure (psig)	
5	2-6-57	276	20	265	700	<10
	2-8-57	270	~50	230	500	40
	2-12-57	276	20	No dump		80
6	2-15-57	240	~50	180	300	0
	2-19-57	275	~42	170	500	40
	2-26-57	279	43	148	700	1200 est
7	3-2-57	278	23	154	550	0
	3-4-57	280	30	No dump		24
	3-14-57	277	23	No dump		0
	3-22-57	274	No cooling	274	1700	120
	3-28-57	274	No cooling	274	1700	50

low-pressure flanges attached to the leak-detector system, about 40% now have higher bolt torques than the originally suggested maximum, although most of them exceed it by less than 20%. The bolt stresses in all cases are within permissible limits.

1.1.2 Water Inventory

During the past quarter, operations successfully demonstrated methods of computing the inventory of water in the fuel and blanket systems. Isolated determinations were sometimes in error for various reasons, but a series of computed inventories proved to be a reliable indication of trends, permitting the detection of leaks from the reactor or transfers between the two systems.

Throughout the operations with oxygenated water and with depleted-uranium solution, all water additions or removals were recorded. Routinely, during each shift, instrument readings were used to compute the quantities of water in the fuel and blanket systems. The computed inventories were compared with the ledger balances to detect losses or transfers. Computed values were checked on three occasions when the reactor was drained at the conclusion of runs, and the quantity removed from each system was always within 30 lb of the value predicted by prior calculations.

Physical inventory is taken by a combination of directly observed weight indications and weights computed from temperature, pressure, and volume of fluid: Weigh-cell readings are used to compute weights in the dump and condensate tanks, and weights in the high-pressure systems are computed from volumes established by calibrations[6,7] and the density of the fluids at the observed temperature and pressure. Holdup in unweighed portions of the low-pressure system is calculated for certain standard liquid levels, while the system is operated so that the liquid stands at these levels during the recording of inventory data.

1.1.3 Corrosion and Fuel Stability

Careful inventory of fuel-solution solute was maintained during the depleted-uranium run (No. 7); the uncertainty in the book inventory of solute at the end of the run is believed to be less than 2%. The book inventory of nickel was obtained by multiplying the analytical weight ratio (Ni/SO_4) by the book inventory of sulfate ion at the time

[6] C. C. Cardwell and P. N. Haubenreich, *Results of HRT Test I B 5a, Volume Calibration of Fuel High-Pressure System*, ORNL CF-56-7-116 (July 30, 1956).

[7] N. W. Curtis and P. N. Haubenreich, *Results of HRT Test III B 5a, Volume Calibration of Blanket High-Pressure System*, ORNL CF-56-7-117 (July 30, 1956).

of sampling. If attributed entirely to the type 347 stainless steel of the fuel high-pressure system, the rate of increase of nickel inventory corresponds to an average corrosion rate of 0.43 ± 0.03 mpy. No significant indication of Zircaloy-2 corrosion was found by solution analyses.

Within the limits of analytical uncertainty, there was no evidence for solution instability in the 115 samples of fuel solution taken during the course of the run. No solids were found in these samples. Small amounts of solids found in the solutions drained from the hydroclone in the chemical processing system (about 70 ppm) are probably residues from early experiments in which synthetic solids were used. The only observed instance of solution instability occurred at the return line from the fuel pressurizer, where fuel solution was diluted by steam condensate at temperatures between 280 and 325°C. Approximately 20 g of black or brown solids, consisting of uranium oxide with small amounts of nickel, copper, and iron oxides, was recovered from this location at the end of run 7. The x-ray pattern and composition of this material are similar to those of material recovered from the same location in the HRT mockup.[8]

1.2 MAINTENANCE OF RADIOACTIVE COMPONENTS

The third remote-maintenance practice period was held from April 2 through April 8. This practice period, like the two previous ones, has afforded the opportunity (1) to test the proper functioning of the various maintenance devices, (2) to test the feasibility of the contemplated job procedures, and (3) to familiarize HRT personnel with the tools and procedures required to perform remote-maintenance jobs.

During the two and one-half days required to flood the cell with condensate, several jobs were performed remotely in air. One was the removal and replacement of the rupture-disk assembly, in which a wooden mockup of a special shield plug which contains the necessary tools and viewing equipment to perform the work remotely was utilized. A pressurizer liquid-level-indicator assembly and the two gas bleed valves on the fuel pressurizer were also removed and replaced remotely in air.

All eight of the fuel and blanket pressurizer heaters were removed and replaced remotely. Two of the heaters were handled while submerged. The fuel feed block valve, which lies 23 ft below the top of the cell, was removed and replaced under water. Visibility through the cell flood water was extremely poor initially but improved sufficiently to permit work after the flood water was circulated through a pair of filters for approximately 24 hr. Other underwater jobs performed were the removal and replacement of the fuel dump valve, the fuel high-pressure-sampler inlet valve, and the microformer head of the liquid-level indicator on the fuel storage tank.

During the replacement of the dump valve, an attempt was made to remove the flood water trapped in the valve piping between freeze plugs. The method employed involved the attachment of a rubber ring gasket, $\frac{1}{8}$ in. thick and $\frac{9}{16}$ in. high, around the outside diameter of the stainless steel oval-ring gasket in the lower flange of the valve assembly. Two pieces of hypodermic tubing, one 6 in. long and one $\frac{1}{2}$ in. long, were inserted through the rubber gasket flush with the inside diameter. An external air supply was attached to the 6-in. tube; the other tube remained open to the cell flood water. After the valve assembly was set on its fixture and the upper flange made up, the bolts were inserted and started in the lower flange. The upper flange bolts were then torqued and the joint was made leak-tight. With the lower flange bolts engaged just enough to seat the rubber gasket, and the valve in the open position, air was then admitted to the assembly through the longer tube. When air bubbled through the other tube, the flange bolts were tightened to seat the stainless steel ring gasket. Although the leak-detector system indicated a tight joint after the bolts were torqued, subsequent examination of the joint after the cell was emptied showed that the rubber gasket was torn and that one piece of rubber was trapped in the flange groove over the leak-detector hole. The stainless steel gasket and the bottom flange groove suffered indentation damage, apparently caused by the discharge hypodermic tubing.

An unsuccessful attempt was made to handle the pressure-balancing valve between the core and blanket systems. Consideration is being given to the piping and location of this valve to facilitate its remote replacement.

---

[8] D. M. Richardson, *Composition of Solids from HRT Mockup Pressurizer*, ORNL CF-56-6-56 (June 8, 1956).

Efforts to form freeze plugs in the main loop piping were unfruitful; however, changes planned in the HRT refrigeration system should correct this difficulty.

1.3 FLANGE INSPECTION[9]

When the chloride cracking was first discovered in the HRT leak-detector system and flanges,[10,11] it was decided to continue the program of engineering test operation while replacement flanges and tubing were being obtained. At the conclusion of this period of operation, the reactor was shut down and a complete examination made to determine the extent of the cracking problem.

Before the inspection a study was made of all nondestructive test methods that could possibly be used for in-place examination of the ring-groove area of the flanges. Among the methods examined were radiography, ultrasonic reflectoscope and Immerscope, ultrasonic surface shear wave, eddy-current testing, acid macroetching, and various penetrant inspection methods. It was obvious that all methods contained serious disadvantages and that none could give complete assurance of success in such an inspection. The only two that showed any promise were penetrant inspection and eddy-current testing, and sufficient time was not available for the development of the very small special coils and accompanying electronic circuits that would be required for eddy-current testing. Of the various methods of penetrant inspection, the postemulsification fluorescent penetrant method was selected as having the most advantages.

Every flange in the HRT system was penetrant inspected. The inspection was carried out in a manner which was designed for maximum sensitivity to cracks but low sensitivity to pits. The procedure was as follows:

1. Steam-clean the surface.
2. Rinse with acetone.
3. Dry the flange, using a high-output hair drier, and then cool below 100°F.
4. Brush-apply Super Pentrex ZL-22 and allow it to remain on the surface for 10 to 15 min.
5. Brush-apply emulsifier ZE-3 and scrub in with a stiff brush (emulsification time, 12 min).
6. Wash with a brisk water spray.
7. Develop, using dry-powder developer ZP-4.
8. If any suspected areas are noted, wipe them with a rag dampened with acetone and if necessary apply new developer.

The results of the penetrant inspection are summarized in Table 1.3. In the columns headed "Final" are listed the recommendations after they were revised as a result of the metallographic

[9] This work was supervised by G. M. Adamson, R. S. Crouse, and J. K. White of the HRP Metallurgy Group; the actual inspection was done by Inspection Engineering.

[10] E. G. Bohlmann and G. M. Adamson, "Stress-Corrosion Cracking Problems in the Homogeneous Reactor Test," Paper 57-NESC-111, *2nd Nuclear Engineering and Science Conference, March 11–14, 1957.*

[11] G. M. Adamson *et al.*, *Metallurgical Examination of HRT Leak Detector Tubing and Flanges*, ORNL CF-57-1-109 (Jan. 31, 1957).

Table 1.3. Summary of Preliminary and Final Recommendations for HRT Flanges

	Acceptable		Reject		Questionable		Total Number Examined
	Final	Original	Final	Original	Final	Original	
High temperature, 2500 lb	14	21	16	6	19	22	49
1500 lb	7	8	8	1	3	9	18
300 lb	9	8	6	1	1	7	16
	30	37	30	8	23	38	83
Low temperature, 2500 lb	23	20	7	5	2	7	32
1500 lb	58	32	15	6		35	73
300 lb	56	43	15	4	—	24	71
	137	95	37	15	2	66	176

study, and in the "Original" columns are the tentative recommendations made at the time of penetrant inspection. The separation as to temperature is arbitrary, with the flanges that were continually at 100°C or higher being considered as at high temperature. The pressure rating was based entirely on the size of flange. The 1500-lb flanges were actually used in both the high-pressure and low-pressure system.

As expected, considerable difficulty was encountered in interpreting the penetrant indications. Short narrow cracks were difficult to distinguish from other defects. Photomicrographs of several defects which would give penetrant indications are shown in Fig. 1.2. In Fig. 1.3 are black-light photographs of two of the flanges. Flange A-271X (Fig. 1.3*b*) was one of two flanges that were clearly rejectable and shows the largest and most concentrated cracked area found. The other photograph (Fig. 1.3*a*) is more typical. The curved arrow points to what was considered a scratch or machining mark, and the straight arrow to a probable crack, which was considered grounds for rejection. The other spots are small pits or excess developer left on the surface. Near the right side of the photograph is a pit with wings that could indicate a crack; however, after the developer was removed and the area rechecked it was called a pit.

As a check on the inspection method some questionable and some rejected flanges were removed (12 from the high-pressure system and 21 from the low-pressure system) and sectioned for metallographic examination. These flanges were first sectioned through areas designated as suspicious by the dye penetrant, and the remaining cuts, to a total of eight, were made in a random manner. The results of this examination are given in Tables 1.4 to 1.6, and typical photomicrographs are shown in Fig. 1.4. The comparison between these two inspection methods was disappointing. Of the nine flanges rejected by metallography, five were shown to be cracked in seven or more sections, but the penetrant inspection had indicated no more than four suspicious areas in any of the flanges. Only two were shown by the penetrant inspection to be heavily cracked. In two metallographic sections, with thicknesses at the bottom of the groove of 0.10 and 0.25 in., cracks were found extending through the entire

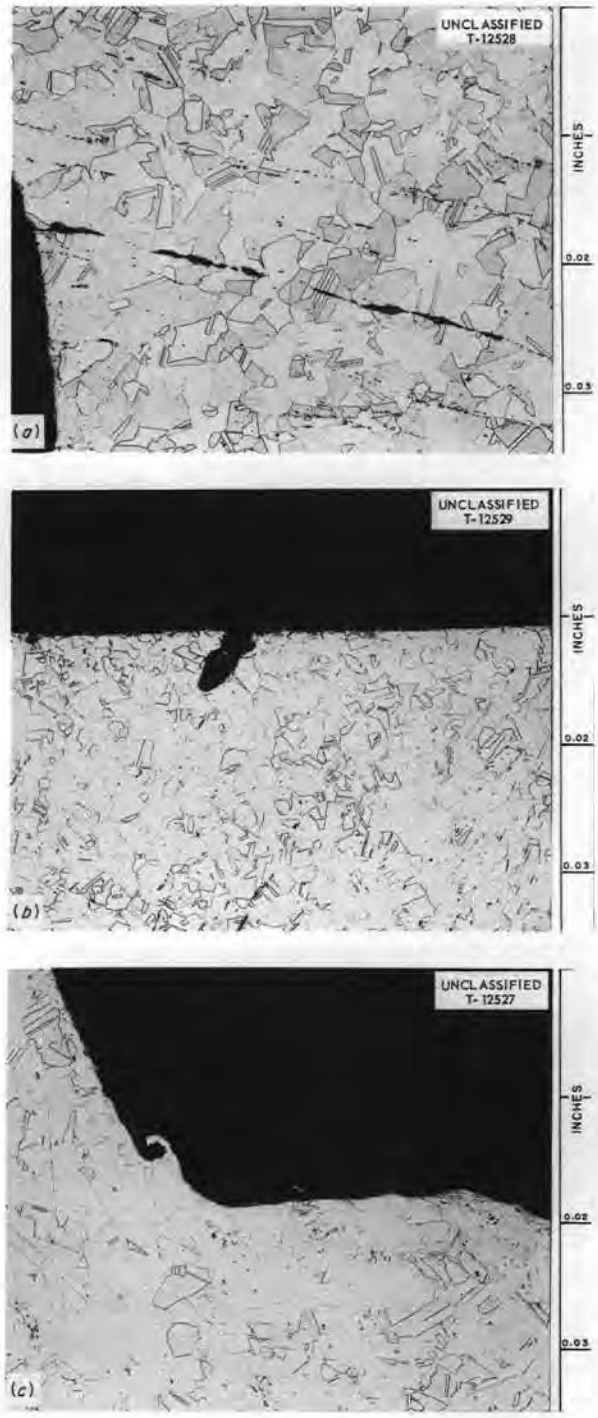

Fig. 1.2. Photomicrographs of Defects in Flange Grooves That Would Give False Indications in Penetrant Inspection. 100X. (*a*) Stringer; (*b*) surface pit; (*c*) machining burr. Over-all reduction 32%.

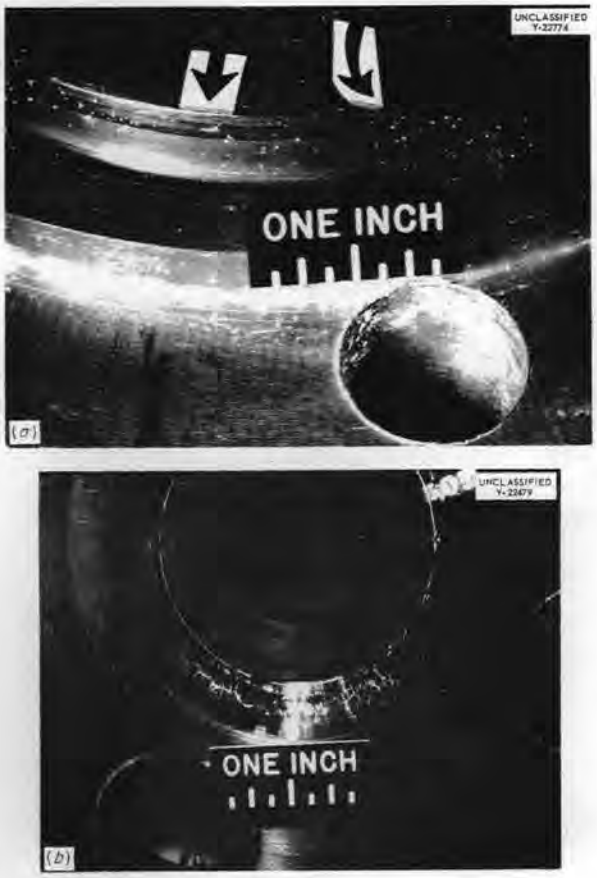

Fig. 1.3. Black-Light Photographs of Penetrant Indications in Flange Grooves. (*a*) Flange B-215X; (*b*) flange A-271X.

section. The most common depth of crack was about 0.01 in., although many as shallow as 0.002 in. or as deep as 0.03 in. were found. While cracks were located on both flange faces and the bottom of the groove, they were most common near the corner, where stress had been highest.

More favorable results were obtained with the low-temperature flanges. Of the 21 examined, cracks were found in only 3, and all cracks were very shallow (Fig. 1.5). Two of the three cracked flanges had been heated for short intervals during such operations as sampling or dumping. Metallographically, defects were found in areas indicated by the penetrant, but they were usually small pits or burrs, which in many cases required several polishing operations to locate.

From a consideration of these results, it was recommended that all high-temperature flanges be replaced. Complete replacement appears to be warranted because (1) it cannot be assumed that the inspection technique located all the cracks, (2) the majority of the high-temperature flanges were already either rejected or questionable, and (3) after the system has become radioactive, replacement would be probably impossible. For the low-temperature system, in which cracking is not so likely, the results of the penetrant inspection were recommended for acceptance. This will cause the removal of some flanges with pits and burrs but will allow a considerable number to remain in the system. These recommendations were accepted, with the modification that any low-temperature flanges that would be extremely difficult to replace after the system is radioactive should be replaced now.

1.4 HRT LEAK-DETECTOR TUBING[12]

Sixteen lengths of leak-detector tubing were removed from the system and examined to confirm the belief that chlorides from the type 304 stainless steel leak-detector tubing were responsible for the cracking described in Sec 1.3 and to better determine the general condition of the tubing. These lengths were completely sectioned in the 6 in. nearest the flange, with random sections, plus a section in any bend or weld, in the remaining lengths. Five tubes were examined by Inspection Engineering with the Immerscope, and additional sections were taken through any suspicious areas. Because of the shape of the tubing, poor sensitivity was obtained with the Immerscope. Five of these lines had been connected to high-temperature flanges, seven to low-temperature flanges, and three to intermittently heated flanges; one was a spare and had not been used.

Figure 1.6 shows branching transgranular cracks, typical of chloride-induced stress corrosion, which were found in two of the tubes examined. In each case the lines had been connected to high-temperature flanges, and the chloride cracks were found only in a short length that had been adjacent to the flange. These cracks varied in depth from a few mils to complete penetration of the 0.065-in. wall.

---

[12]This work was performed by G. M. Adamson, T. M. Kegley, Jr., and W. J. Leonard of the HRP Metallurgy Group.

Table 1.4. Summary of Results of Metallographic Examination of HRT Flanges

	Acceptable	Rejected	Questionable	Total
High temperature	3	9		12
Low temperature	11	4	6	21

Table 1.5. Results of Penetrant Inspection and Subsequent Metallographic Examination of High-Temperature Flanges

Flange No.	Size (in.)	Temperature (°C)	Original Rating	Penetrant Indication	Metallographic Results	Metallographic Rating
A-100	4	270	Rejected	Pitting; two possible cracks	Inclusions; one pit 2 mils deep, with 3-mil crack	Rejected
B-100	3½	270	Questionable	Pitted; two crack indications	Large cracks in seven sections	Rejected
B-100X	3½	270	Rejected	Pitted; several crack indications	Cracks in every section	Rejected
A-113X	½	270	Rejected	Many possible cracks	Small-to-medium crack in seven sections	Rejected
LE-147	3	290	Questionable	Small but cracklike indication	Several small closed pits	Acceptable
B-167	½	147*	Acceptable	Few pits	One deep crack	Rejected
B-167X	½	147*	Questionable	Deep pits	One small crack	Rejected
A-171X	1	300	Questionable	Several possible cracks	Cracks in all sections	Rejected
A-200	3½	270	Questionable	One deep and two shallow cracks	Cracks in three sections	Rejected
B-211	½	241	Questionable	Pitted; three possible cracks	Some rough surface	Acceptable
A-230	½	268	Questionable	Pitted; three possible cracks	Nothing	Acceptable
A-271X	1	300	Rejected	Many deep cracks	Seven sections cracked	Rejected

*Heated to higher temperatures for short period during special operations.

Table 1.6. Results of Penetrant Inspection and Subsequent Metallographic Examination of Low-Temperature Flanges

Flange No.	Size (in.)	Temperature (°C)	Original Rating	Penetrant Indication	Metallographic Results	Metallographic Rating
B-106X	½	44	Rejected	Large dent; no cracks	Two large deep pits	Questionable
A-109X	¾	39	Rejected	Several possible cracks	Few shallow pits and laps	Acceptable
B-109X	¾	39	Rejected	Crack in bolt hole; groove acceptable	Nothing	Acceptable
B-110X	½	40	Rejected	Few pits; two small crack indications	One deep and several shallow pits	Questionable
A-114X	½	43	Rejected	Four possible cracks	Shallow pits; rough surface	Questionable
A-117X	1	44	Questionable	Two possible cracks	Small crack, 1 mil	Rejected
B-127X	½	44*	Questionable	Pitted; two deep crack indications	Three small cracks	Rejected
D-127X	½	44*	Questionable	Pitted; three possible cracks	Several deep pits	Rejected
A-162X	1	44	Rejected	Pitted; two possible cracks	One deep and several shallow pits	Questionable
B-209X	¾	40	Rejected	Long marks; two possible cracks	Small pits and burr	Acceptable
A-214X	½	47	Acceptable	Good flange	Rough surface	Acceptable
A-219X	1	43	Questionable	Pitting; two possible cracks	Deep pits, one section	Questionable
B-224X	½	34	Rejected	Three possible cracks	Small pits; one stringer to surface	Acceptable
A-229-1	½	44*	Questionable	Pitted; one possible crack	One 2-mil crack; few pits	Rejected
B-229	½	44	Rejected	One pit; three possible cracks	Deep pit; no cracks	Questionable
A-270	1	44	Questionable	Considerable pitting	Little pitting	Acceptable
A-657X	¾	40	Rejected	Row of cracks	Small burr	Acceptable
A-658X	¾	40	Rejected	Row possible on side; two in corner	Few shallow pits in one section	Acceptable
794A-1	½	40	Questionable	Pitted; one possible crack	No cracks; few small pits and inclusions	Acceptable
796A-1	½	40	Acceptable	Generally porous	Inclusions; no cracks	Acceptable
797A-1	½	40	Acceptable	Pitted; one possible crack	Small shallow pits	Acceptable

*Heated to higher temperatures for short period during special operations.

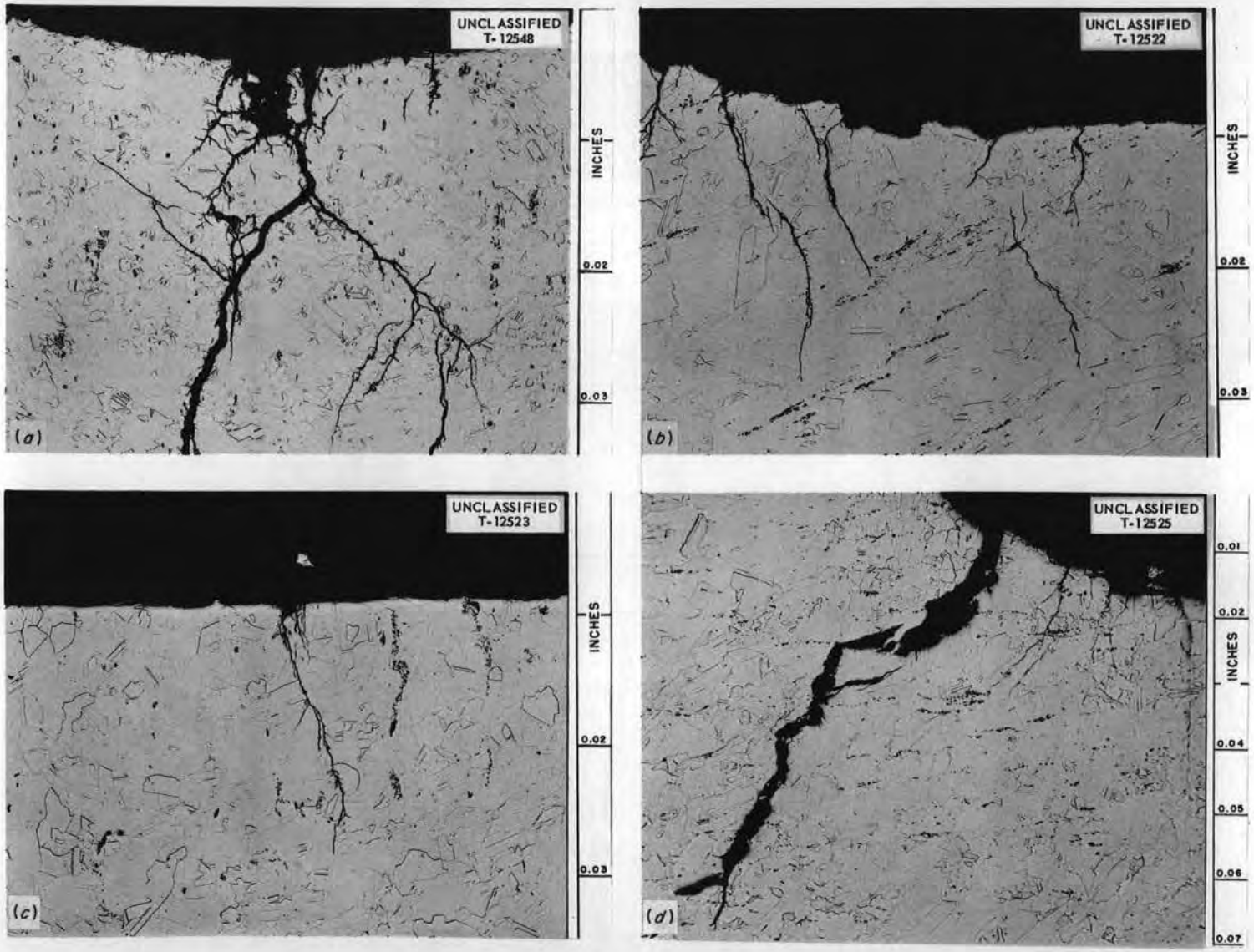

Fig. 1.4. Typical Cracks Found in High-Temperature Flanges. (*a*) Bottom of flange A-271X; (*b*) corner of flange A-100X; (*c*) side of flange B-100X; (*d*) corner of flange B-100. Magnification: (*a*), (*b*), and (*c*), 100X; (*d*) 50X. Over-all reduction 16%.

Fig. 1.5. Deepest Crack Found in Low-Temperature Flanges; Flange B-127X. 100X.

Serious defects which would not meet HRP specifications were found in 15 of the tubes. The good tube was a spare, and it appeared to have been constructed from a different lot of tubing, apparently type 347 stainless steel. Six of the tubes, in all temperature ranges, contained crack-like defects which started at the surface, penetrated a few mils, turned, and ran parallel to it (Fig. 1.7). These defects were found in all sections of the tubes and usually terminated in a row of aligned inclusions. While they may have been accentuated by the operation of the reactor, they are thought to have been present in the original tubing. Another type of defect found in all areas of 11 tubes is shown in Fig. 1.8. These defects probably occurred during the reactor operation, but their source is not understood.

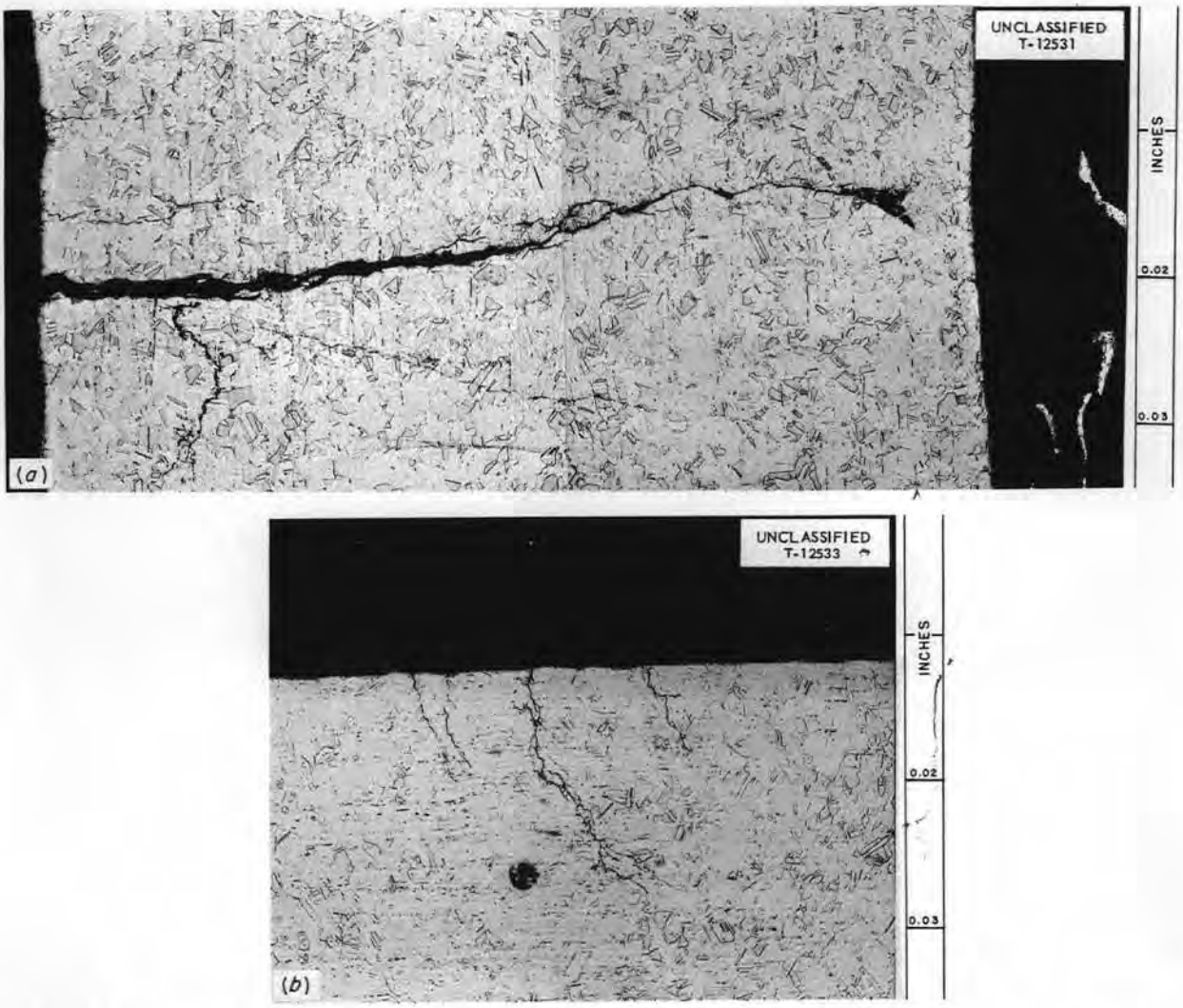

Fig. 1.6. Chloride Stress Cracks Found in Leak-Detector Tubing. 100X. (*a*) Line A-171; (*b*) line LE-145. Over-all reduction 18%.

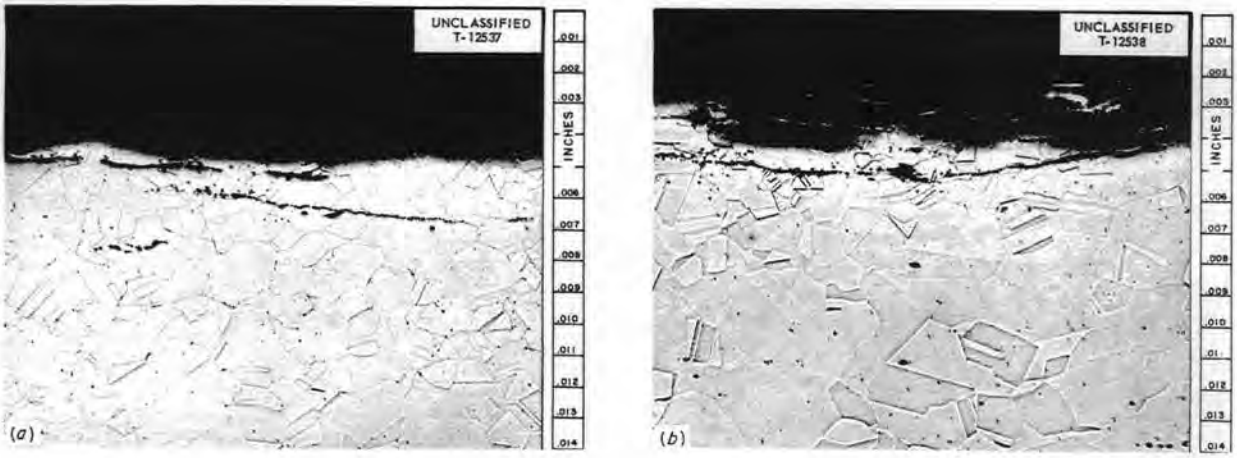

Fig. 1.7. Crack-like Defects Found Under the Surface in Many Leak-Detector Lines. 250X. (*a*) Line B-214; (*b*) line B-245. Over-all reduction 33%.

Fig. 1.8. "Worm Hole" Type of Defects Found in Leak-Detector Lines. 250X. Reduced 33%.

Although they may be incipient chloride cracks, they do not branch enough and are too wide to be typical of chloride-induced cracking. Inclusions at the fusion line of the seam welds, lack of penetration of the welds, carburized surfaces which in some cases contained loose grains, etched and roughened surfaces which may contain incipient chloride cracks, and sleeve welds with deep crevices were also found (Figs. 1.9 and 1.10).

To prove the speculated cause for tubing and flange cracking,[10,11] samples of the drawing compound used by the tubing manufacturer were requested. The manufacturer sent three samples and stated that any of the three or a mixture could have been used. Samples of each lubricant were placed on the outside or on the inside of lengths of type 304 stainless steel tubing. The tubing surfaces had been first machined to remove any prior defects from the manufacturing. After the lubricant had been placed in the inside, the ends of these tubes were plugged with fire clay. All tubes were held for 30 min at 1900°F in a hydrogen atmosphere. A metallographic examination revealed that no carburization of the outside and, in two cases, none of the inside had occurred. However, with compound B on the inside, a carburized surface very similar to that of the bad tubing was found (Fig. 1.11). By ORNL analyses, this compound was shown to contain 49% chlorine. This test proves conclusively that the source of the HRT chloride difficulties was the lubricating compound used in the tube-drawing operation.

A recommendation was made that all high-temperature lines be replaced, since (1) two out of five lines to hot flanges showed cracks, (2) portions were found in almost all tubes which would not meet HRP standards, (3) cleaning of the tubes in place could not be depended upon to remove the chlorides, and (4) welds which are not of HRP quality were used in joining the tubes. Similar conditions were found in the low-temperature lines, although no cracks were found. It was decided that the chance of a failure occurring simultaneously in a low-temperature flange and in the corresponding leak-detector line was not sufficient to justify replacement of these lines.

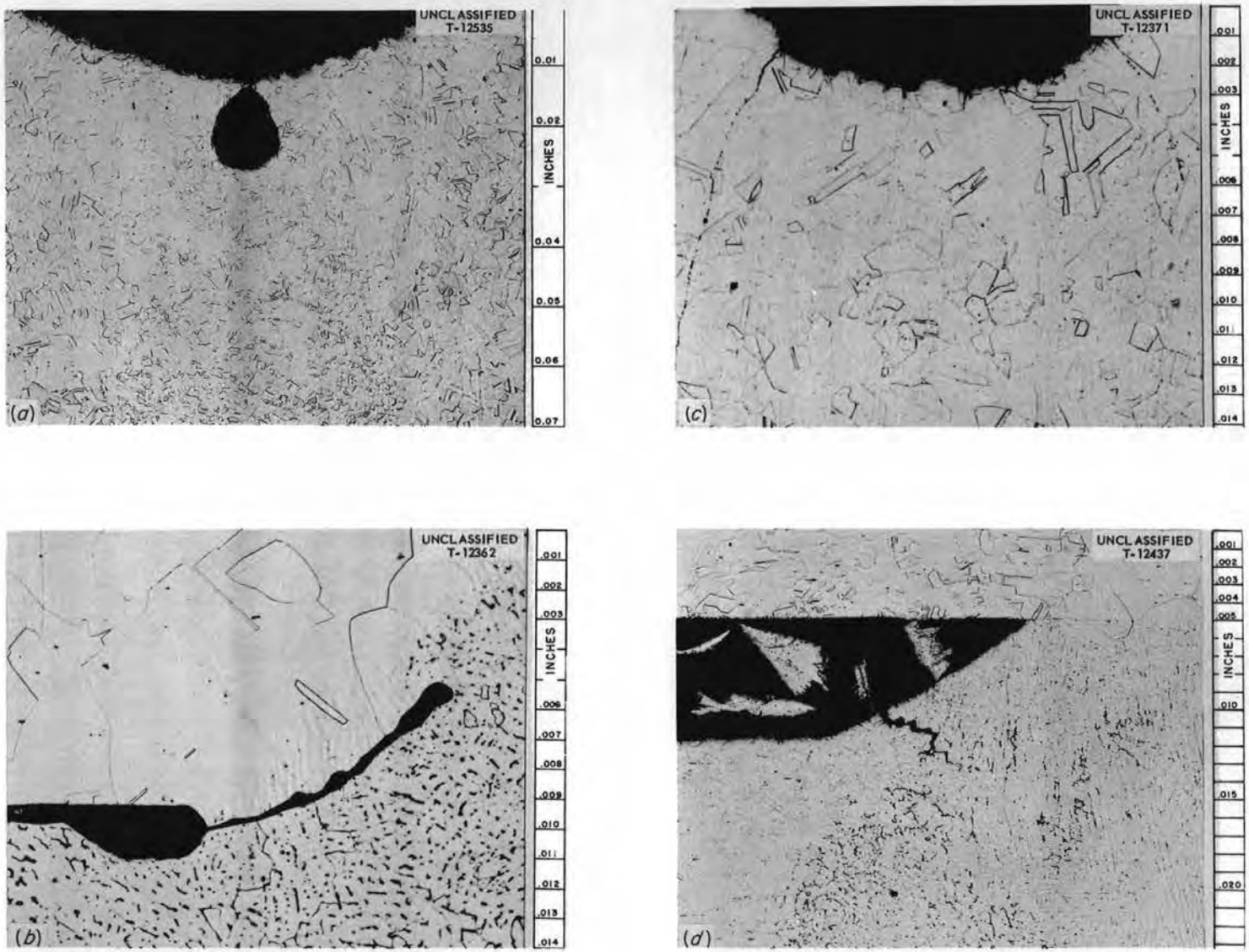

Fig. 1.9. Miscellaneous Defects Found in Leak-Detector Lines. (*a*) Closed pit; 50X; (*b*) lack of penetration in weld; 250X; (*c*) line of inclusions; 250X; (*d*) weld crack; 150X. Over-all reduction 23.5%.

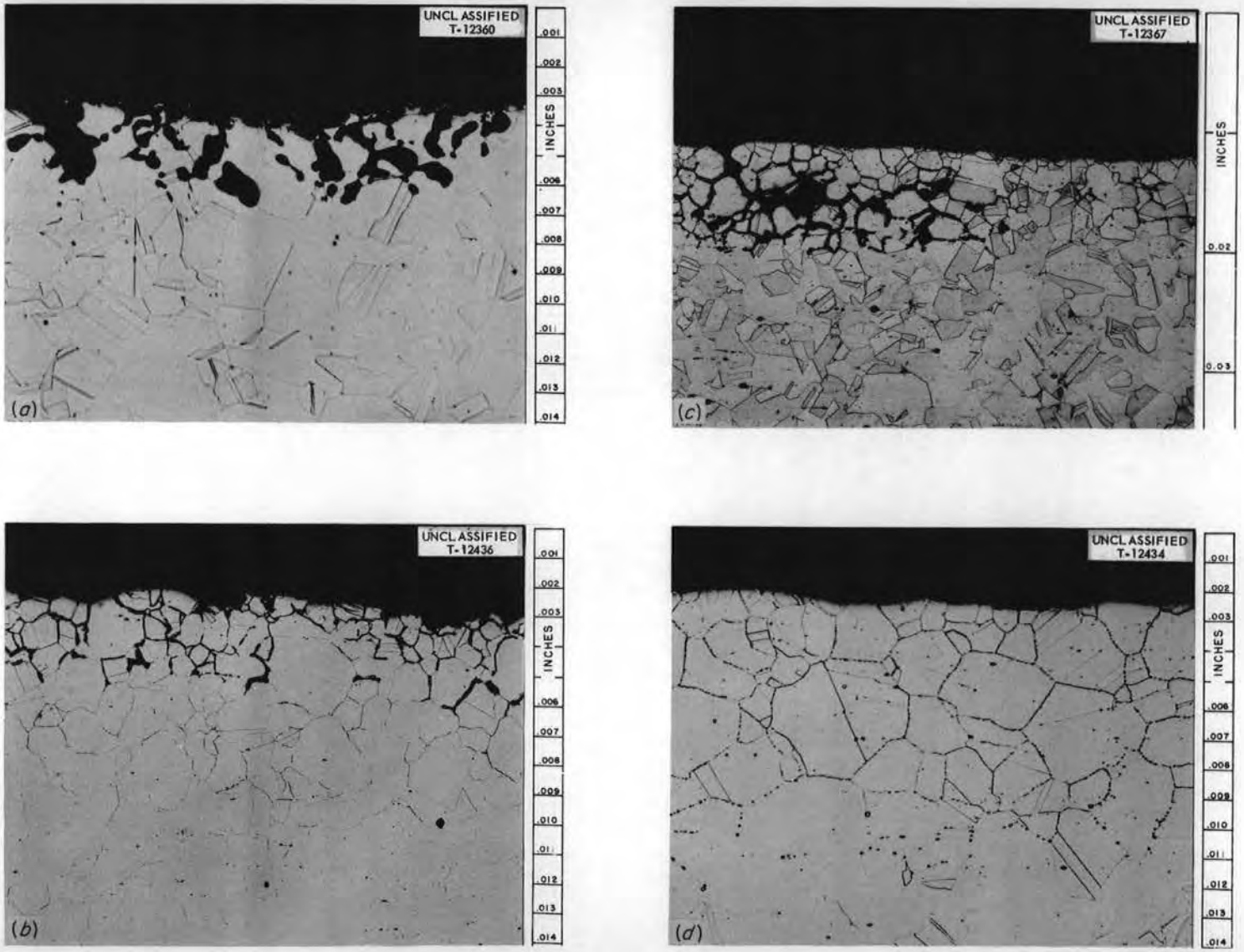

Fig. 1.10. Structure of Carburized Surfaces in Leak-Detector Lines. (*a*) Line LE-145; 250X; (*b*) line A-100; 250X; (*c*) line A-216; 100X; (*d*) line A-211; 250X. Over-all reduction 23.5%.

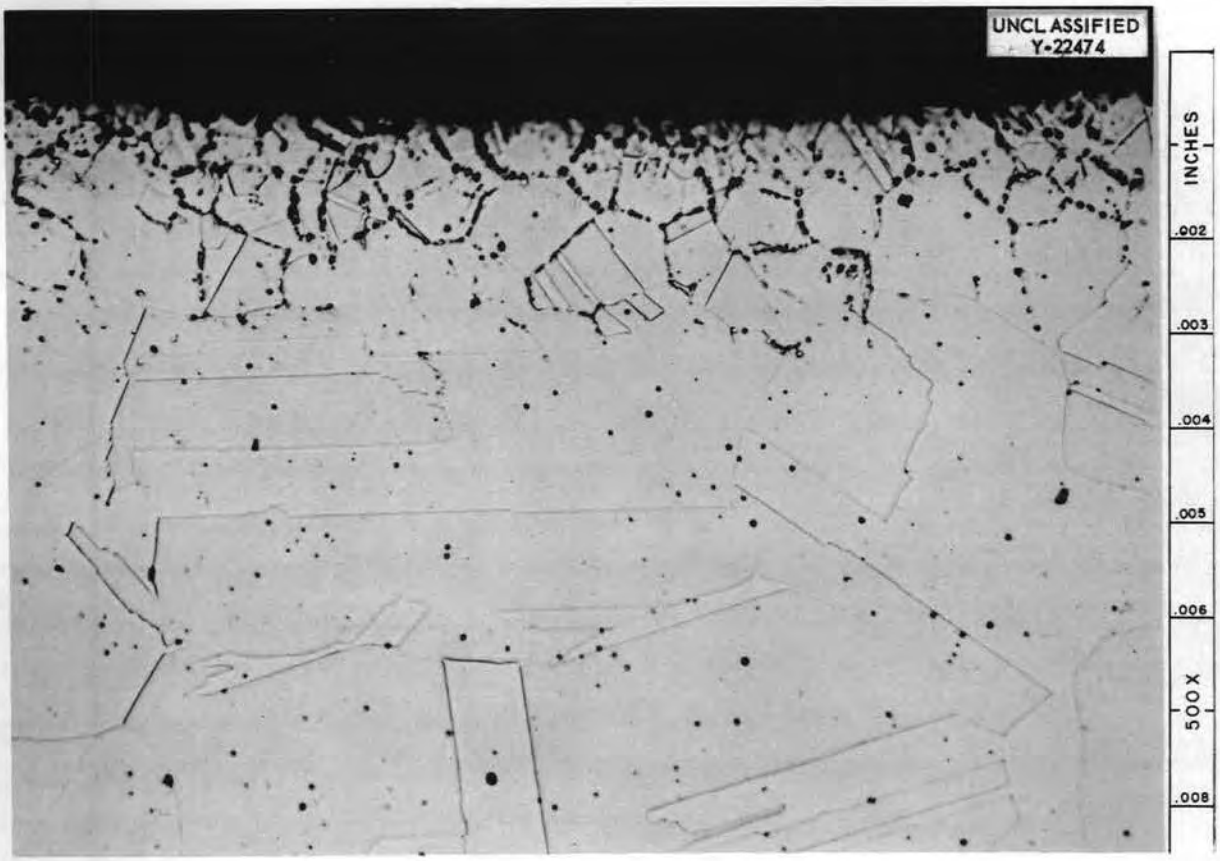

Fig. 1.11. Structure of Type 304 Stainless Steel Tubing Carburized with Drawing Compound. 500X.

2. HRT DESIGN

W. R. Gall M. I. Lundin

J. C. Bolger
F. C. Bowen[1]
C. A. Burchsted
R. D. Cheverton
C. J. Claffey
C. W. Collins
E. H. Gift
E. M. Guglielmo[1]
P. H. Harley
R. O. Maak[2]
E. A. Mason
H. A. McLain
R. C. Moren[3]
R. G. Pitkin[1]
R. C. Robertson
J. N. Robinson
W. Robinson
H. C. Roller
R. E. Schappel
C. L. Segaser
I. Spiewak
D. O. Tarr[1]
W. L. Wright
F. C. Zapp

2.1 REFRIGERATION SYSTEM

The substitution of Amsco for Freon-11 as the secondary refrigerant for the HRT[4] has created a possible fire hazard in the lower control-room area because of the probability of leakage of Amsco (a flammable hydrocarbon) from the circulating system. Although the possibility of fire is considered relatively remote because of the very low vapor pressure of Amsco, a permanently installed CO_2 fire-extinguishing system was recommended as a precautionary measure. The system would consist of three 100-lb CO_2 bottles manifolded to discharge through four strategically located nozzles in the lower control area. The valves would be actuated automatically through temperature-sensing devices, or could be operated manually from the third-level control area. The installation of a 2000-cfm fan, exhausting to the atmosphere outside the building, was also recommended for the removal of accumulated Amsco fumes from the lower control area. This fan would be operated only intermittently to remove potentially dangerous concentrations of the fumes. Interlocks on the fan and on the Amsco circulating pumps would stop these units in the event of actuation of the fire-extinguishing system.

2.2 WATER TREATMENT

The investigation of chemical treatment of water for service in reactor cooling and steam systems continues. The use of hydrazine and a coordinated phosphate treatment was recommended[4] for the control of oxygen concentration and pH in the HRT steam-system feed water. Operation of the steam and cooling-water systems during the past few months without treatment will necessitate chemical cleaning of these systems prior to further extensive operation. Citric acid, inhibited sulfuric acid, and inhibited phosphoric acid are being investigated as agents for this purpose; the last agent appears the most promising at this time.

Potassium chromate, in concentrations of from 500 to 1000 ppm, appears to be the most promising agent for the control of corrosion in the primary circulating cooling-water system. However, as this water circulates from the reactor cell to the control room, further study of its behavior under radiation is necessary. A chromate and phosphate di-anodic treatment is being considered for the cooling-tower water system, which is external to the reactor cell. Control of algae in this system is made difficult by the fact that chlorine, one of the more effective agents against most bacteriological growths, is not suitable because the water might be flushed through the primary system under emergency conditions, exposing the stainless steel components of the reactor to chloride contamination.

The design of the storage, mixing, and pumping facility was completed for the chemical treatment of feed water to the steam system. Duplicate facilities, each consisting of a tank, a proportioning pump, and associated piping, were provided for the preparation and injection of oxygen-scavenging (hydrazine or sulfite) and pH-control (phosphate) chemicals. Although hydrazine and tri-, di-, or monosodium phosphate may be mixed in the same tank, separate facilities will be required if it becomes necessary to use a sulfite treatment for oxygen control.[5] The feed nozzles

[1]Contract with Vitro Corporation.

[2]On loan from Foster Wheeler Corp.

[3]On loan from Westinghouse Electric Corp.

[4]W. R. Gall *et al.*, *HRP Quar. Prog. Rep. Jan. 31, 1957*, ORNL-2272, p 22.

[5]H. A. McLain, *Treatment of the HRT Steam System Water*, ORNL CF-56-11-132 (Nov. 29, 1956).

are located 18 in. apart in the steam-system feed water pump inlet.

2.3 REPLACEMENT HEAT EXCHANGER

Calculations were made to determine the maximum pressure rise which would occur in the cell in the event of instantaneous rupture of the entire high-pressure system, followed by the immediate release of steam from the core and blanket systems through the 6- and 4-in. nozzles, respectively. The pressure rise was determined as a function of heat-exchanger fluid inventory. Previous calculations indicated that such an occurrence in the present system, which contains a heat exchanger with a capacity of 2020 lb of water, would result in a pressure rise to 29.2 psig.[6] Assuming that the replacement heat exchanger is to be 43 in. in inside diameter and is to have a capacity of 3400 lb of water, it was estimated that such a rupture of the system would result in a pressure rise to 34 psig. To assure that any pressure rise due to such a catastrophe does not exceed the cell test pressure of 32 psig, it was recommended that the water volume of the steam system be reduced by 1000 lb, the reduction preferably being made from the blanket exchanger.

The effect of a spray system in reducing cell pressure was also investigated. Although such a system would not be effective in reducing the peak cell pressure, it would be very effective in reducing the time required for the cell pressure to return to atmospheric. Figure 2.1 shows the change in cell pressure with time, following a catastrophic failure of the high-pressure systems.

Figure 2.2 shows the replacement heat exchanger for the HRT with its proposed blast shield. The complex configuration of the tube headers prevented consideration of a close-fitting shield such as was used on the present HRT main heat exchangers. However, calculations made to determine the blast-shield requirements of the replacement exchanger indicated that a 1-in.-thick mild-carbon-steel shell would be adequate.

Assuming pessimistic conditions in the event of an explosion of the heat exchanger, maximum

[6] P. M. Wood, *A Further Study of Pressure Rise in HRT Shield*, ORNL CF-55-1-3 (Jan. 3, 1955).

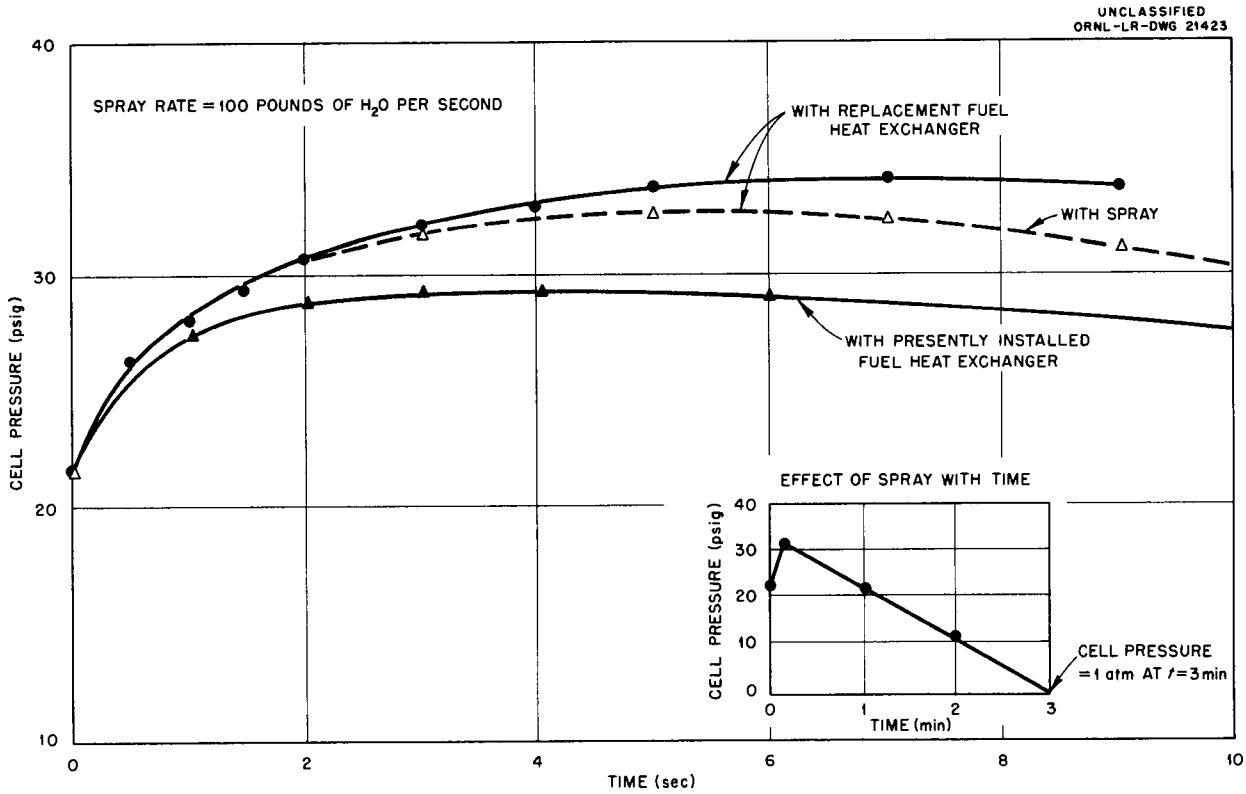

Fig. 2.1. Variation of Cell Pressure with Time Following a Catastrophic Failure of the High-Pressure Systems.

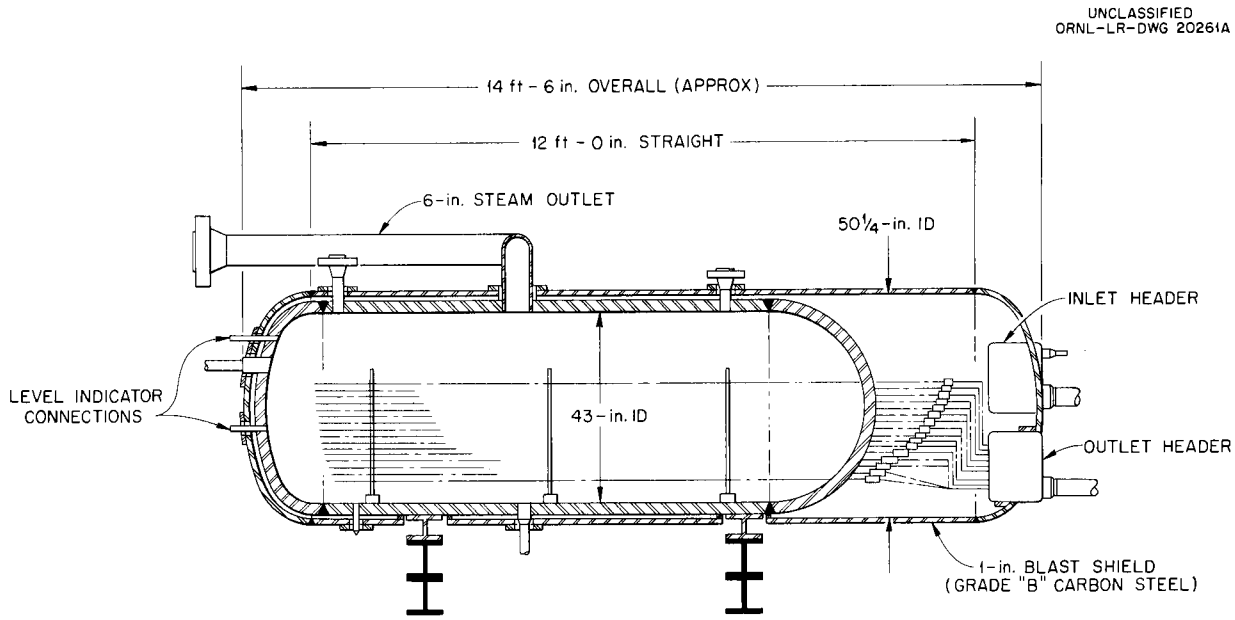

Fig. 2.2. Blast Shield for Replacement Heat Exchanger.

missile velocities of fragments of the heat exchanger shell were calculated to be less than 220 fps. This figure was supported by evidence published on several boiler explosions and test data describing the explosions of hot-water heaters.[7,8] Assuming a "worst case" condition of a fragment of the heat-exchanger shell 12 × 12 in. striking the blast shield edgewise, a calculated missile velocity of 357 fps would be required to penetrate a 1-in.-thick shield.

Because the blast shield would be subjected to a momentary pressure buildup following a rupture of the heat exchanger, calculations were made in order to determine the possibility of the blast shield failing as a result of this pressure. It was found that for an unpierced cylindrical vessel a shell 0.835 in. thick would be required. Actually the blast shield would have openings in several places for the headers, steam nozzle, supports, and so on; so this compares very favorably with the 1-in.-thick shell recommended. However, it was recommended that steel collars be welded to the shield about each hole to prevent possible tearing at the hole.

[7]Watts Regulator Co., *Official Report on the Doylestown Hot Water Heater Demonstration*, Lawrence, Mass., Oct. 1948.

[8]C. S. Robinson, *Explosions, Their Anatomy and Destructiveness*, McGraw-Hill, New York, 1944.

2.4 RADIATION DAMAGE TO THE MOTOR OF THE FUEL CIRCULATING PUMP

Calculations for determining the possible radiation damage to the windings of the HRT fuel circulating pump indicate that, under normal reactor operating conditions and a calculated exposure of the windings to a gamma flux of 6×10^{10} gammas/cm^2·sec, the stator windings will have a life expectancy of about one year. Should fuel solution leak into the motor chamber, as a result of a leak in the thermal barrier or flow past the shaft seal, the gamma flux at the windings could increase to as much as 1.4×10^{12} photons/cm^2·sec and result in pump failure because of insulation breakdown in as little as one month.

The 0.040-in.-dia stator windings of the HRT fuel circulating pump are insulated with two layers of Fiberglas tape with a triple dip of silicone resin. Under normal reactor operating conditions, the rate of decomposition of this insulation would be such that, at the end of one year, hydrogen gas pressure within the stator can would be approximately 2 atm absolute. As indicated in Fig. 2.3, showing a cross section of the pump at the motor windings, the inner wall of the stator can is a thin-walled cylinder; during reactor shutdown, when the internal pressure in this cylinder would be atmospheric, the 30-psi external pressure of gas from the decomposed insulation would

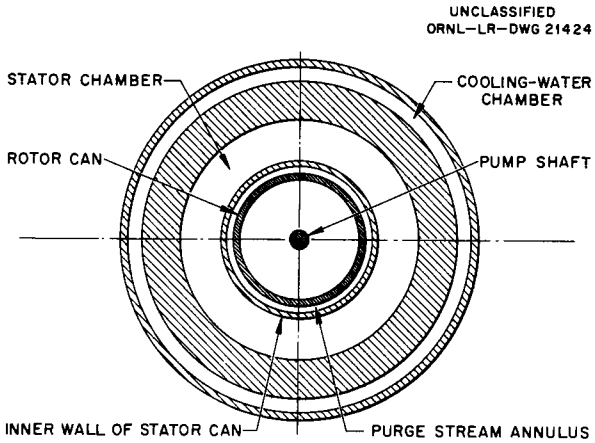

Fig. 2.3. Cross Section of Fuel Circulating Pump.

probably collapse the can, being five times as great as the 6 psig allowed by Code[9] type of calculations.

2.5 REMOTE MAINTENANCE

A long-range program was established for the development of tools and methods for remote maintenance in the HRT, with immediate emphasis given to the facilities for the removal and replacement of core and blanket corrosion-specimen holders and the rupture-disk assembly in the pressure-balancing system. Completion of the design phase of the program is scheduled for June 15, 1957, and fabrication is to be completed by November 1, 1957. Earlier studies indicated that the radiation levels to be expected at the fuel and blanket corrosion-specimen ports are 2900 and 2300 r/hr, respectively, and 4000 r/hr at the rupture-disk assembly port. These levels are for dry operation without flooding. Flooding the cell only to the depth of the equipment flanges to be opened attenuates the radiation by a small factor in most cases. Additional shielding must be employed unless the cell is completely flooded, and a small increase in shielding thickness will compensate for the attenuation contributed by flooding to the flange levels.

Figure 2.4 shows a typical tool and shield assembly for performing those operations which must be carried out within the reactor cell (e.g., unbolting or bolting flanges, etc.). Special roof plugs, having removable inserts, permit access to the rupture-disk assembly and the corrosion-specimen holders.[10] Several tool-assembly carriers, tailored to fit the particular applications, will be required.

Replaceable tool assemblies, which will consist of a lead cylinder with eccentric plug inserts, will be utilized. Both the cylinder and the plugs can be rotated to align the tools which will be mounted in the plugs and be passed through them. The tool assembly will rest on a hollow cylindrical lead-shield section, which will in turn rest on a support ring positioned on a drip pan placed over the reactor shield opening. The lead-shield section will double as a transfer shield for removing flanges and the rupture-disk assembly.

2.6 FLANGE DEVELOPMENT PROGRAM

Analysis of data obtained from the flange thermal-cycling facility indicated that leak rates within the tolerances specified for the HRT can be obtained in a bolted ring-joint flange assembly if properly prepared flanges and rings are used and if proper care is taken in the assembly of the joint. (The maximum leak rate observed at elevated temperature and pressure was 1 cc of water per day.) The seating surfaces and dimensions of the flanges and rings used in the facility were prepared to the close tolerances specified in HRP specification HRP-202a, and extreme care was taken in all stages, from machining through installation, to prevent scratching of those surfaces. During the series of tests from which the conclusion was drawn, each joint was broken four times. The gasket of each joint was rotated each time to prevent reseating at the same point. The joints were thermally cycled between atmospheric pressure and 2000 psi at a rate of 55°C/hr for both heating and cooling. Table 2.1 lists the flanges in the facility.

It was also concluded that by initially tightening the bolts to a bolt stress of 45,000 psi following several thermal cycles, an asymptotic bolt loading of 30,000 psi could be obtained. Figure 2.5 indicates that bolt loading drops off exponentially, closely approaching the 30,000-psi value after only three cycles. This method of initially overstressing is recommended for reactor service in

[9] ASME Boiler and Pressure Vessel Code, Section VIII, *Unfired Pressure Vessels*, 1956.

[10] S. E. Beall *et al.*, *HRP Quar. Prog. Rep. Oct. 1, 1956*, ORNL-2222, pp 7, 9.

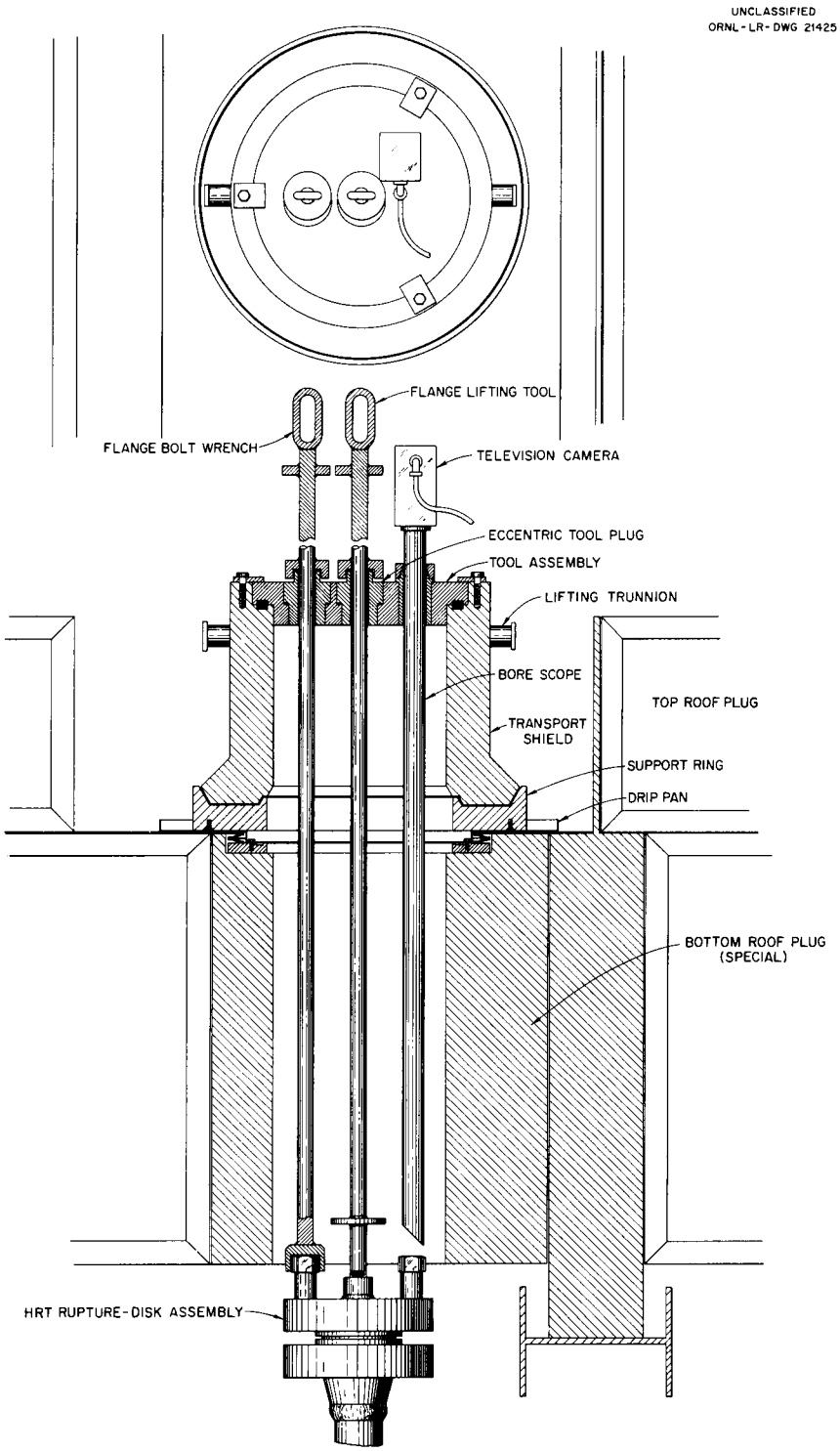

Fig. 2.4. Typical Tool and Shield Assembly.

place of the previously recommended method of initially tightening to a stress of 30,000 psi with subsequent retightening of the bolts following several successive thermal cycles. Not only is the latter method considered impractical once the reactor is radioactive, but it is also felt that the high asymptotic bolt loading of the recommended method will have greater chance of retaining the integrity of the joint following the many thousands of hours of operation under the loads imposed by the piping during thermal cycling and operation at temperature. In the tests made in the thermal-cycling facility no accounting could be made for the piping loads on the flanges that would be found in operation of the reactor.

No difference in leak rate was observed to be due to the type of ring-joint gasket used; both oval- and octagonal-cross-section rings gave essentially equivalent results as long as tolerances and care of handling were maintained. The flange grooves showed slight, but essentially equal, deformation regardless of the type of ring used. The observed deformation of the oval rings was such as to produce an essentially octagonal ring after several thermal cycles; no apparent deformation of the octagonal rings was noticed. Further tests will be conducted in which a new ring of the same type will be installed each time that the flanged joint is opened (i.e., at the end of nine cycles).

It was tentatively concluded that, for large flanges particularly, stresses in the bolts of a flanged joint should be maintained uniform, to

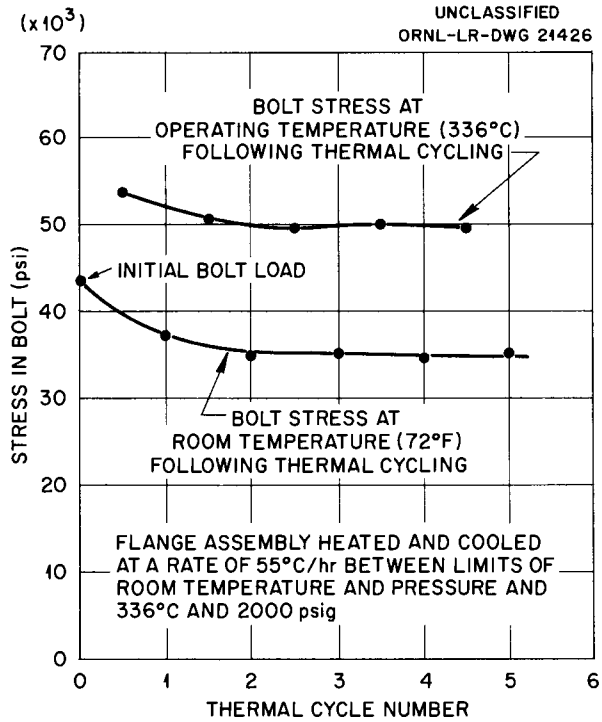

Fig. 2.5. Variation of Bolt Loading in a Flange as a Function of Thermal Cycling.

Table 2.1. Thermal-Cycling Facility

Station	Nominal Size of Flange (in.)	Rating of Flange (lb)	Size of Ring	Type of Ring
1	2	2500	R-26	Oval
2	1	2500	R-18	Octagonal
3	1	2500	R-18	Octagonal
4	2	2500	R-26	Oval
5	3½	2500	R-38	Octagonal
6	½	1500	R-12	Oval
7	½	1500	R-12	Oval
8	3½	2500	R-38	Octagonal

within ±10% of the specified bolt loading for the flange. It was indicated that bolt loading of this degree of uniformity can be obtained with torque wrenches if the bolts are carefully cleaned, lubricated, and calibrated prior to assembly.

It must be re-emphasized that protection of the seating surfaces of flange grooves and ring-joint gaskets is essential at every stage from manufacture through installation if a leak-tight joint is to be obtained.

3. HRT COMPONENT DEVELOPMENT

I. Spiewak

J. M. Baker
R. Blumberg
J. S. Culver
C. H. Gabbard
B. A. Hannaford
P. H. Harley
P. G. Herndon
E. C. Hise
J. C. Moyers
I. K. Nambo
D. E. Willis

3.1 PUMP DEVELOPMENT

3.1.1 400A-1 Pump and Loop

The 400A-1 Westinghouse pump, which contains a titanium impeller and a stainless steel thermal barrier with a titanium wear-ring insert, was dismantled for inspection after operating for 7460 hr after the thermal barrier was welded to the stator flange. For 7217 hr, a solution of 0.04 *m* UO_2SO_4, 0.005 *m* $CuSO_4$, and 50 mole % excess H_2SO_4 had been circulated at 255°C. The only measurable wear noted during the inspection was a change of 0.004 in. in the Graphitar thrust bearing. No localized corrosion was observed. The pump was reassembled and has since operated for 1200 hr with the same solution at 255°C.

3.1.2 400A-2 Pump and Loop

The 400A-2 Westinghouse pump, while fitted with a $\frac{1}{16}$-in.-wide gold-plated stainless steel thermal-barrier gasket, circulated a solution of 0.04 *m* UO_2SO_4, 0.005 *m* $CuSO_4$, and 50 mole % excess H_2SO_4 for 1226 hr at 250°C. At that time the pump was dismantled for inspection because heat-balance checks on the pump cooling water indicated leakage around the thermal-barrier seal. The gold-to-stainless-steel bond on the thermal-barrier gasket had failed, resulting in a leak of approximately 650 ml/min through the seal.

The pump was then fitted with a modified thermal barrier combining the thermal-barrier and the main flange seal (see Fig. 3.1). The pump operated for 758 hr on 0.04 *m* UO_2SO_4 solution at 250°C with the modified thermal barrier. This run was interrupted when excessive mixing between the hot loop and the motor cavity was again noted. The trouble was traced to an improperly installed shaft sleeve, which was corrected prior to resuming operation.

3.1.3 300A-1 Pump

The 300A-1 pump has operated in the HRT mockup for a total of 1009 hr since the revised thermal-barrier seal weld was made.[1] Of this total, 142 hr was with 0.13 *m* UO_2SO_4 solution at 260°C, 376 hr with 1.3 *m* UO_2SO_4 solution at 260°C, and 491 hr with 0.04 *m* UO_2SO_4 solution at 280 to 300°C.

3.2 FEED PUMPS

3.2.1 Feed-Pump Test Loops

A variety of diaphragm materials (Table 3.1) are currently being tested. Operation with water is being continued on test loop No. 1.

Two new all-welded heads with 0.031-in.-thick diaphragms and 100-mesh screens, to protect the

[1] I. Spiewak *et al.*, *HRP Quar. Prog. Rep. Jan. 31, 1957*, ORNL-2272, p 28.

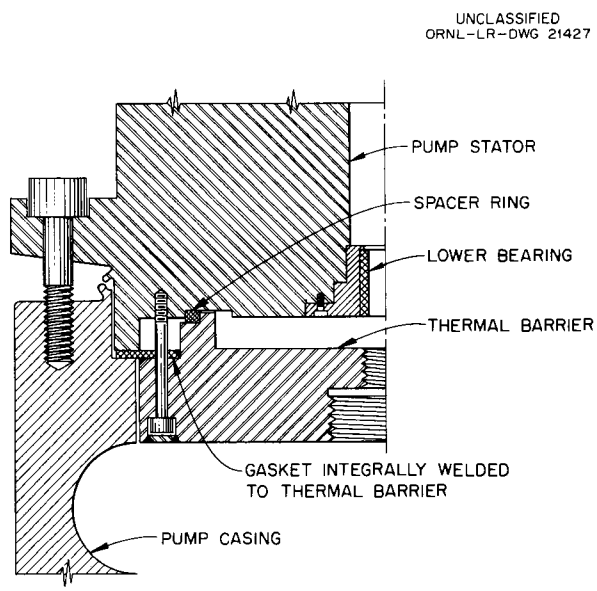

Fig. 3.1. Modified Thermal Barrier.

Table 3.1. Duration of Current Life Tests of Feed- and Purge-Pump Heads

Head Location	Diaphragm	Time (hr)
Feed Pumps		
Feed-pump loop No. 1 (water)		
East	0.031-in., annealed, liquid-blasted finish	300
West	0.019-in., annealed, No. 4 finish (standard HRT head)	3900
Feed-pump loop No. 2 (UO_2SO_4)		
South	0.031-in., annealed, mirror finish	600
North	0.031-in., $\frac{1}{4}$ hard, as-rolled finish	600
HRT mockup (UO_2SO_4)		
South	0.022-in., $\frac{1}{4}$ hard, polished	3040
North	0.031-in., $\frac{1}{2}$ hard, as-rolled finish	450
Purge Pumps		
Purge-pump loop No. 1	Standard, 0.019-in., annealed	700
HRT mockup	Standard, 0.019-in., annealed	400

diaphragms from foreign particles, were installed on loop No. 2. One of the heads has an annealed and mirror-polished diaphragm, and the other has a $\frac{1}{2}$-hard diaphragm with an as-rolled finish. The heads were given a brief check on water and then began pumping 1.5 gpm of 0.04 *m* UO_2SO_4 for an endurance run.

The north-head diaphragm of the HRT mockup feed pump was found cracked after 6757 hr of operation. The crack seemed to originate at a small dent and to follow the general direction of the finish marks, which were nearly vertical. The fact that the crack was aligned with the finish marks rather than with the direction of maximum stress is evidence that the diaphragm finish is an important consideration in service life (see Fig. 3.2).

3.2.2 Purge Pumps

During the past quarter there were two purge-pump diaphragm failures: one in the HRT mockup at 4031 hr and the other on purge-pump loop No. 1 at 7043 hr. There were also several failures at the reactor site in considerably less time than is normally expected. All these failures seem to have resulted from scratches made by polishing the diaphragm, from dents caused by dirt particles, or from a combination of the two.

The purge-pump heads were redesigned to include 100-mesh screens, which should eliminate the particle problem. Diaphragm stock with better surface finish was ordered.

3.2.3 Corrosion Fatigue Tests of Diaphragms

A contract has been placed with Ohio State University to determine the effect of cold work and surface finish on the fatigue properties of type 347 stainless steel in the presence of uranyl sulfate solution. Preparation of equipment and samples was completed, and testing was begun to determine the endurance limit of standard diaphragm material (0.019-in., annealed, No. 4 finish) in 0.04 *m* uranyl sulfate solution.

3.2.4 Check-Valve Material Test

Recent experience with check-valve trim operating in pumped distilled water in the HRT has indicated much poorer life expectancy than had previously been experienced in pumped uranyl sulfate solutions in development equipment. Accordingly, a valve-trim test facility consisting of three small hydropulse pumps was built and put into operation.

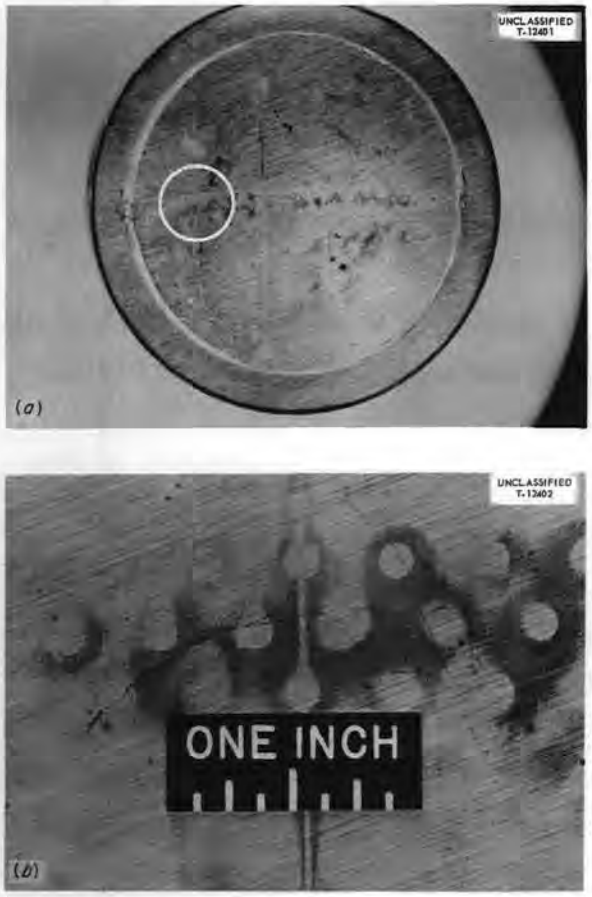

Fig. 3.2. Cracked Diaphragm from HRT Mockup. (*a*) Encircled area shows location of crack; (*b*) enlarged view of cracked area.

Two sets of standard trim (Stellite No. 6 seats vs Star J balls) failed in distilled water after 130 and 160 hr. This establishes a base line for comparing other materials. The materials to be tested are as follows:

Ball		Seats
Star J	vs	17-4 PH stainless steel
Star J	vs	Frogaloy
Al_2O_3	vs	Carpenter-20
Kennametal K501	vs	Kennametal K501
Al_2O_3	vs	Al_2O_3
Star J	vs	Type 347 stainless steel
Other Stellites		

3.3 HRT REPLACEMENT (SPARE) HEAT EXCHANGER

All essential features of the HRT replacement heat exchanger were agreed upon, and Babcock & Wilcox is proceeding with shop drawings and material procurement. The 40-ft-long $^5/_8$-in. tubes are to be made at the Babcock & Wilcox Beaver Falls Tube Works. Fig. 3.3 shows the final design.

3.4 HRT MOCKUP

During the report period the HRT mockup completed a run circulating 1.3 *m* UO_2SO_4 solution, and following inspection another run was started to study the behavior of iodine in the system when operating with 0.04 *m* UO_2SO_4. Total operating time was 1009 hr.

The high-concentration run begun in the previous quarter was interrupted by circulating-pump malfunction after 200 hr.[2] Following repair, 0.13 *m* UO_2SO_4 was circulated for 142 hr, and then the concentration was raised to 1.3 *m*. Temperature and pressure were 260°C and 1400 psi. The generalized corrosion rate experienced during the latter portion of the run (376 hr at 1.3 *m*) was 12 mpy. The run was terminated as the result of a feed-pump diaphragm failure (see Sec 3.2.1).

Inspection of the circulating-loop corrosion specimens indicated the corrosion rates listed below:

Specimen	Corrosion Rate (mpy)
Ti-75A	0.20, 0.53
Zircaloy-2	0.91, 1.14
Type 309 stainless steel	0.05, 0.05
Type 347 stainless steel	0.29, 0.38

The type 347 stainless steel coupons in the vertical leg to the pressurizer indicated 0.12 mpy in the vapor phase and a variation of from 0.11 to 1.48 mpy in the liquid phase. The type 347 stainless steel coupons in the pressurizer-heater leg showed a corrosion rate of only 0.06 mpy after 5376 hr.

The high-pressure loop was in good condition as inspected from the tee between the pressurizer and

[2] *Ibid.*, 30–31.

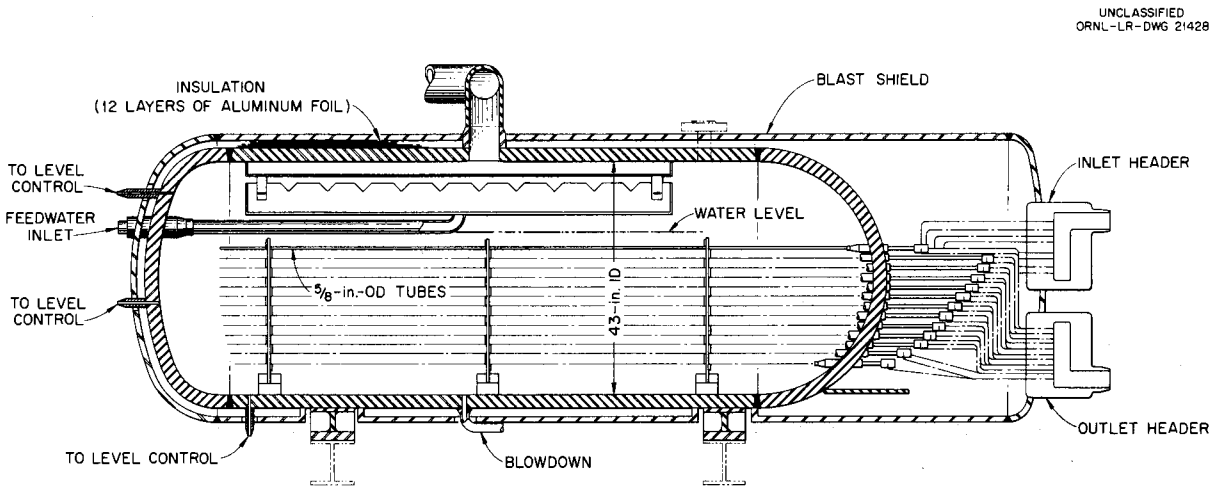

Fig. 3.3. Replacement Heat Exchanger.

the main loop. The horizontal line going to the pressurizer had a deposit of 150 g of black solids, largely Fe_2O_3. On the wall of the pipe at the bottom of the vertical leg to the pressurizer, there were some yellow solids, essentially $UO_3 \cdot \frac{1}{2}H_2O$.

The inside of the stainless steel ring at the orifice flange and the flange face between the O-ring and the pipe opening were badly corroded. This corrosion was caused by leakage of liquid around the titanium orifice plate. The O-ring had lost 43 g of an original weight of 650 g. The weight loss of the flange face was estimated to be 80 g.

Inspection of the high-pressure loop and of a wire specimen from the letdown heat exchanger failed to account for the amount of corrosion predicted on the basis of soluble nickel in the two portions of the high-concentration run.

In preparation for the next run a catalytic recombiner was added to the low-pressure system, and a diaphragm oxygen compressor, instead of gas bottles, was installed as a high-pressure oxygen supply. The north feed-pump head was replaced, and a combination valve and check valve to relieve feed-pump gas binding was installed (Fig. 3.4). A capillary flowmeter was added to the flange leak-detector system.

The mockup was started up once again with 0.04 *m* UO_2SO_4, 0.02 *m* H_2SO_4, 0.005 *m* $CuSO_4$, and 500 ppm of O_2. Conditions were 280 to 300°C and 1700 psi. As of this writing, the run is still in progress after 491 hr; the corrosion rate is

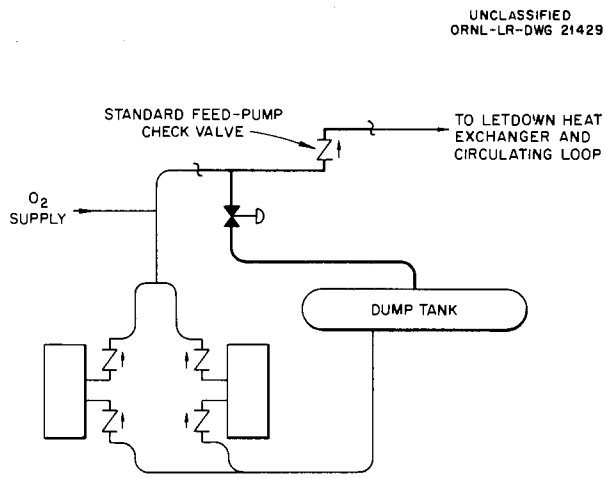

Fig. 3.4. Feed-Pump Venting Arrangement.

0.75 mpy. Some special tests that have been conducted are described below:

1. Feed-pump gas binding. – The feed pump was gas-bound several times by injecting oxygen into the suction line. The bypass valve at the pump discharge was then opened into the dump tank. In each attempt normal flow was restored in 4 min or less.

2. Flange leak rate. – The pressure drop across a capillary tube[3] 6 ft long was calibrated for flows from 0 to 5 cc/hr, and the capillary tube was

[3]E. C. Hise, *Capillary Flowmeter*, ORNL CF-57-2-144 (Feb. 20, 1957).

installed in the leak-detector lines between the pressurized-water header and four flanges. With the flanges uninsulated, the temperature fluctuations caused an apparent leak rate of ±0.2 cc/hr while the loop was at equilibrium. A true leak of 1 cc/hr was easily detected and located within about 5 min.

3. Heat-transfer coefficient for main heat exchanger. – The over-all heat-transfer coefficient in the shell-and-tube heat exchanger, which heats the high-pressure loop by condensing steam, was 460 Btu/hr·ft^2·°F when the heat exchanger was new but has now dropped to 260 Btu/hr·ft^2·°F. This decrease is attributed to fouling of the inside of the tubes during solid-injection tests and possibly during the 1.3 *m* UO_2SO_4 run.

4. Iodine injection. – Tracer iodine was injected into the high-pressure system in two increments to bring the loop concentration to 10 ppm. The high-pressure samples showed a rapid depletion of iodine. Low-pressure samples showed only a trace of iodine. The condensate built up to about 2 ppm of iodine and then gradually decreased. All liquid samples had less than 0.1 ppm of iodine 6 hr after the addition.

The majority of the iodine was apparently adsorbed on the platinized alumina recombiner, which built up an activity of 80 mr/hr, which was reduced to 50 mr/hr after operating for 6 hr at 425°C. Iodine removed in the oxygen off-gas varied from 5 μg/hr when the recombiner was off to 12 μg/hr when it was operating.

5. Iodine poisoning of recombiner catalyst. – The mockup recombiner was a 2-in.-deep bed mounted in a 12-in. pipe. Gas and steam flow and pellet area were about 40% of HRT scale. The iodine addition reduced the bed efficiency from 99.97% to 98.89%. Also, temperature measurements in the bed showed that part of the bed was poisoned.

4. HRT CONTROLS AND INSTRUMENTATION

D. S. Toomb

E. H. Bell
A. M. Billings
J. D. Grimes[1]
J. C. Gundlach
R. L. Moore
R. M. Pierce[1]
L. R. Quarles[2]
W. P. Walker[2]
K. W. West
H. D. Wills

4.1 COMPONENT AND SYSTEM TESTING

4.1.1 Letdown Valves

The HRT-model letdown valve installed on the HRT mockup was taken out of service after 6500 hr of operation. Ten hours of this time was with 5% HNO_3, about 400 hr with water, about 5500 hr with HRT fuel solution, and the last 576 hr with 300-g/liter uranyl sulfate. The valve, which was mounted vertically with the operator down, was in excellent condition, as is shown in Fig. 4.1, a photograph of the Stellite No. 6 plug. A new valve was installed in a horizontal position and was leak-tight in a 15-min test after 700 hr of service in fuel solution. This valve will remain in the HRT mockup to determine whether horizontal mounting affects the performance of the valve.

One of the letdown valves which failed during operation of the HRT was examined metallurgically.[3] The valve had operated for 3 hr in 3% Na_3PO_4 at 100°C, for 48 hr in 5% HNO_3 at 85°C, and for approximately 100 hr in oxygenated water. A photograph of the Stellite No. 6 plug which was badly eroded on the seating cone was shown in the last quarterly report.[4]

4.1.2 Fuel-Blanket Differential-Pressure Transmitters

Tests were performed on the two installed differential-pressure transmitters of the HRT which produce pneumatic signals proportional to the difference in pressure between the fuel and blanket systems. The results indicate that one cell shifts "zero" 11% linearly with applied static pressure to 2000 psi and that the other shifts 2% over the same range.

The transmitters exhibited excellent stability with cycling. Errors of less than 1% in range and $1\frac{1}{4}$% in "zero" were observed after 500 cycles with a ±75-psi differential signal. To indicate "zero" stability with time, the transmitters were adjusted at 2000 psi and held at this pressure. No change in output signal was observed in 12 hr. As a result of these tests, the transmitters will be "zero" adjusted at operating pressure. The more stable instrument will be used for control, and the other will be kept on standby.

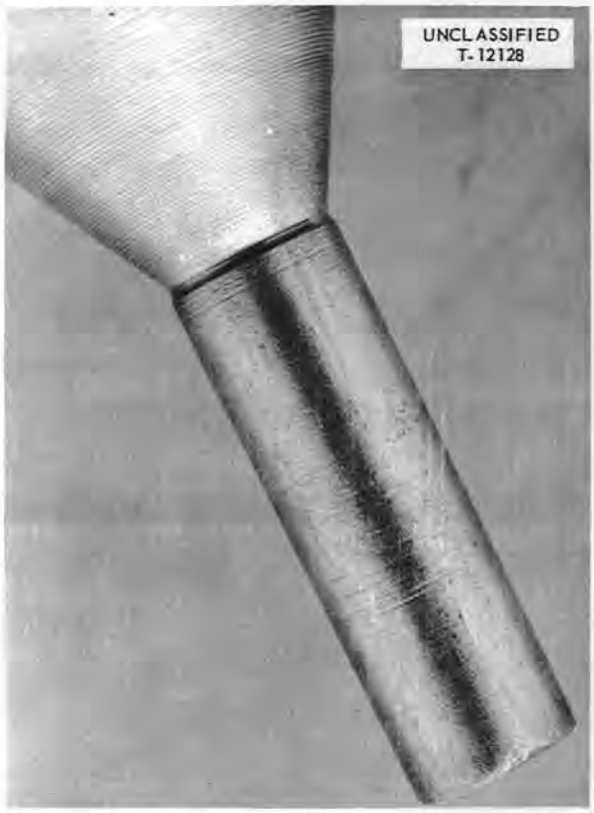

Fig. 4.1. Stellite-6 Letdown Valve Plug After 6500 hr of Service.

[1]On loan from TVA.

[2]Consultant from University of Virginia.

[3]J. P. Hammond and T. M. Kegley, Jr., *Corrosive Attack to Stellite 6 HRT Let Down Valve HCV-245*, ORNL CF-57-3-94 (March 20, 1957).

[4]D. S. Toomb *et al.*, *HRP Quar. Prog. Rep. Jan. 31, 1957*, ORNL-2272, p 35.

4.2 DEVELOPMENT

4.2.1 Sound Transmitters

The protective waterproof housing for the microphones used to monitor check-valve and pump-bearing noises was redesigned to facilitate remote removal and to permit easier replacement of the microphone. The new unit, which is also simpler to fabricate, is shown in Fig. 4.2.

4.2.2 Fission-Chamber Pulse Preamplifier

A new preamplifier has been developed to amplify the output voltage pulses from the two Westinghouse type WL-6376 fission chambers used to monitor neutron flux in the HRT. The new model, designated ORNL Q-1857, will replace ORNL A1-A, which was previously used in such applications, and will give a much higher signal-to-noise ratio at the receiving end of the connecting cable.

Features of the new amplifier include: (1) a self-contained power supply capable of providing up to 290 v to the fission chamber, (2) improved pulse resolution, (3) gain of 150 when driving a 100-ohm load, (4) pulse differention in the preamplifier to avoid "piling up" of pulses in the connecting cable, (5) the acceptance of either positive or negative pulses by the circuit, and (6) no significant deterioration of the output pulse in 500 ft of cable properly terminated.

4.2.3 Oxygen-Injection System

The HRT oxygen-metering valves for controlling the gas flow from a storage tank into the reactor high-pressure systems have been redesigned to utilize commercially available replaceable trim (needle and seat) which is available in a variety of sizes and materials. A tungsten carbide set ground to a clearance of 0.0005 in. will be tested initially in the valve shown in Fig. 4.3. The flow coefficient may be adjusted by varying the cross-sectional area of a small spline ground in the needle. The first size to be tested will have a capacity of 3.78 standard cubic centimeters per minute with a 1-psi differential.

To prevent the back flow of liquid from the reactor system to the oxygen control valve and metering capillary in case oxygen pressure is lost, a 2000-psi bellows-sealed valve incorporating a gold gasket has been designed. This valve is shown in Fig. 4.4.

4.3 DESIGN

4.3.1 Control Circuits

A design report was issued[5] covering the following wiring revisions and additions to the HRT

[5] R. L. Moore, *Electrical Revision to HRT Control System*, ORNL CF-57-2-48 (Feb. 13, 1957).

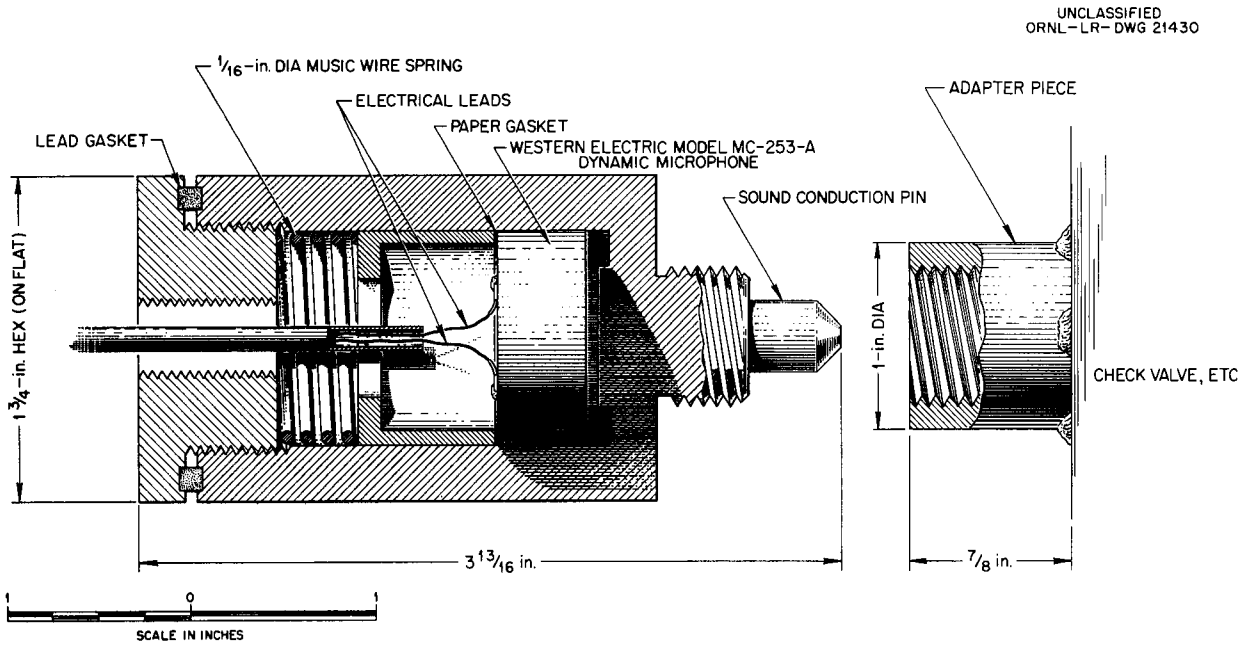

Fig. 4.2. Microphone Assembly for Underwater Service.

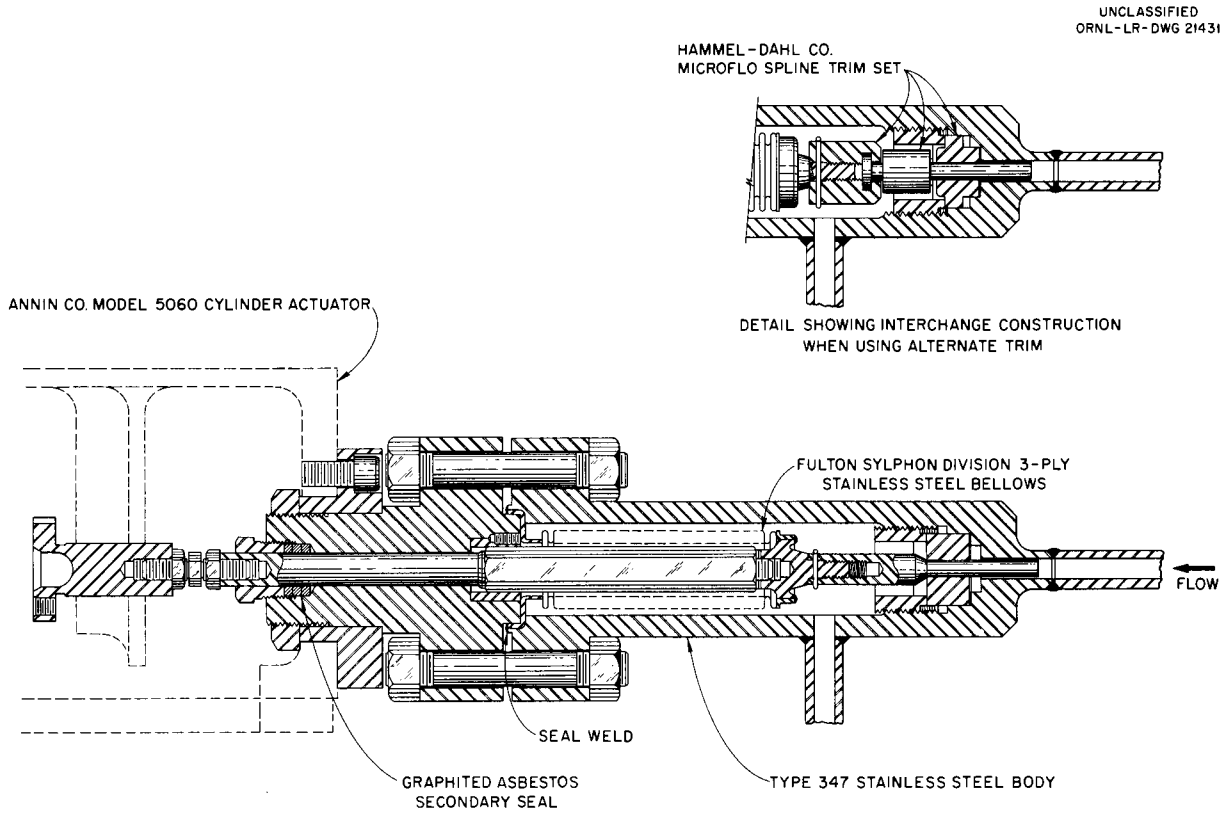

Fig. 4.3. Oxygen Metering Valve.

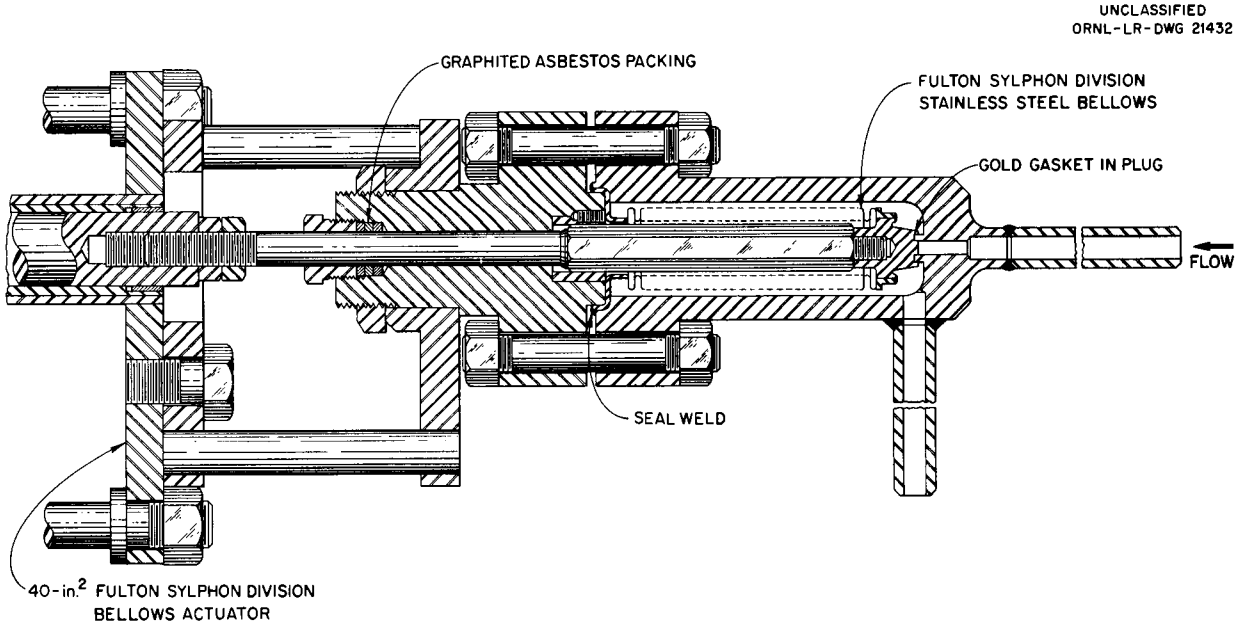

Fig. 4.4. Oxygen Shutoff Valve.

control circuits: (1) the addition of a time delay to allow for radiolytic-gas recombination before dumping, (2) the rearrangement of control wiring to provide parallel connections in critical circuitry, (3) the revision of the circuit to provide for the addition of oxygen to the high-pressure system, (4) the addition of circuits to provide controls for the new demineralized-cooling-water loop, and (5) the addition of waste-disposal-system alarms to the annuciator system of the main control room. Also, drawings for the addition of block valves to the lines from the instrument cubicles and for the addition of a manual emergency override of automatic block-valve actuation were prepared.

4.3.2 Temperature Measurement Systems

A report listing all HRT thermocouples, their locations, junction box connections, and instrument terminations was issued.[6] The report also describes the method of attachment of thermocouples to process piping and vessels, the means for remote disconnection, the wire type, and the cost of materials used in the systems.

[6] J. D. Grimes, *HRT Temperature Measurement Systems — Issue No. 3*, ORNL CF-57-1-159 (Jan. 17, 1957).

4.3.3 Replacement Heat Exchanger Instrumentation

The control of liquid level in pressurized vessels by differential-pressure measurements is complicated by the fluid-density changes due to temperature, power removal, and convection-current effects. The location of the pressure-measuring taps must be optimized to gain maximum indication of level in the vessel, and yet the liquid level usually must be held to narrow limits despite the density changes. A report was prepared[7] describing these temperature effects, with particular application to the replacement HRT heat exchanger, which requires critical control to avoid uncovering the tubes with low level and to avoid entrainment with high water level. It was recommended that two level transmitters be installed, one to be connected to pressure taps 20 in. apart spanning the control range and utilizing a steam-traced reference leg, and the other to span the entire water range of the heat exchanger to indicate levels below the control range.

[7] R. L. Moore, *Temperature Effects on the Measurement of Aqueous Liquid Level by the Differential Pressure Method and Recommendations for Placement of Taps on the HRT Replacement Heat Exchanger*, ORNL CF-57-4-64 (April 26, 1957).

5. HRT PROCESSING PLANT

W. D. Burch E. O. Nurmi W. E. Unger
W. L. Albrecht P. A. Haas
T. A. Arehart C. C. Haws
G. B. Berry R. W. Horton
B. F. Bottenfield J. Lee
N. C. Bradley C. S. Lisser
N. A. Brown F. C. McCullough
S. D. Clinton A. M. Rom
W. J. Clossey W. F. Schaffer
J. L. Gory H. O. Weeren
R. H. Winget

Operation of the high-pressure system of the HRT chemical plant as an integral part of the reactor complex was successfully demonstrated during the 500-hr natural-uranium run of the reactor. Startup and shutdown procedures were practiced and perfected. The dissolver-system installation was completed, and flushing and cleaning of the equipment were started. Remote-maintenance practice included installation of the circulating pump, checks to see that all removable components of the high-pressure system were accessible, and an underwater test of simulated semipermanent freeze plugs.

5.1 HIGH-PRESSURE-SYSTEM OPERATION WITH REACTOR

During the quarter the high-pressure system of the chemical plant was again hydrostatically tested at 2500 psi and was operated on water as a separate unit to demonstrate the integrity and operability of all components. Then, during the 500-hr natural-uranium run of the HRT, the system was operated as an integral part of the reactor system for the first time.

5.1.1 Practice Startup and Shutdown

The main purposes of the integral operation were to determine the over-all operability of the system and to perfect proposed startup and shutdown procedures, which, if done improperly, might adversely affect reactor operation. Constant inventories are maintained in the chemical plant from week to week by starting with that quantity of solution which, when heated to 280°C, exactly fills the system. The solution is heated by bleeding-in a small flow of hot solution from the reactor after first raising the chemical plant to reactor pressure by opening one isolation valve to the reactor. Since the solution is cold prior to the pressurization, the solution volume is less (by 3 liters) than the system volume, and this quantity is transferred from the reactor to the chemical plant in a few seconds when the valve is opened. The resulting small momentary loss of reactor pressure is recovered in 2 to 3 min without upsetting reactor operations. The chemical plant is shut down by closing the isolation valves, the effect of which cannot be detected in reactor operations.

The chemical plant was started up and shut down four times to perfect these procedures and to give all operating shifts an opportunity to practice the operations. Continuous periods of operation with the reactor varied from 8 to 48 hr, with the total operating time, including startup and shutdown, being more than 200 hr. All components performed normally, and the operation was considered a complete success.

5.1.2 Solids Removal

Following the third shutdown the underflow receiver was drained and sampled. The receiver contained 0.23 g of solids, but this quantity is insignificant and probably had remained from the operation last fall, when over 2000 g of solids was added to the system. Approximately the same quantity (0.23 g) was again drained from the system after the last run.

5.1.3 Operation with 0.56-in.-dia Hydroclone

Prior to the final run the 0.4-in.-dia hydroclone was replaced with a 0.56-in. clone to determine its operating characteristics. Flows of 1.45 gpm were attainable, compared with about 0.85 gpm

with the smaller clone. The pressure drop across the clone was ~45 psi at this flow, and the total drop across the entire system was more than 80 psi. The remaining pressure loss was chiefly across the isolation valves between the reactor and the chemical plant.

5.2 DISSOLVER-SYSTEM INSTALLATION

Prior to the high-pressure-system operation, installation of the dissolver system was nearly completed, and subsequently the last details of the construction were concluded. Flushing and cleaning operations were initiated.

5.2.1 Chloride-Contaminated Leak-Detector Tubing

Another batch of chloride-contaminated leak-detector tubing was discovered *prior* to installation of the 14 new leak-detector lines in the dissolver system. Apparently all the last 400 ft of chemical plant leak-detector tubing supplies was contaminated with the same chloride-bearing material found previously in the reactor cell, although the chemical plant tubing was from a different manufacturer. Since some tubing from this same batch had been installed previously, all low-pressure leak-detector lines were filled with water and allowed to stand for 24 hr, and then the water was drained and sampled. Fortunately, there was no serious contamination, although two samples were reported above 3 ppm. Previously all high-pressure leak-detector lines had been checked and found uncontaminated.

5.2.2 Carpenter-20 Material Defects

When x rays of a 4-ft length of Carpenter-20 seam-welded pipe showed indications of porosity and a crack in the seam weld, the decision was made to radiograph all the pipe installed in the dissolver system. One defective section was found and replaced. A reducer machined from bar stock was also found to be cracked, with the crack completely penetrating the pipe wall.

Radiographs of an 8-in.-dia tank end cap of Carpenter-20 showed a large void where the vendor had plug-welded a centering-pin hole. Further checks of two more 8-in.-dia caps and four 14-in.-dia caps from this vendor showed nearly all the plug welds to be defective. In addition, some of the holes had been plugged with a stainless steel other than Carpenter-20. All seven plugs were cut out and replaced.

5.2.3 Dissolver Installation

Because of a cracked weld in the dissolver-flange tantalum liner, the flange assembly was returned to the vendor for repair. Difficulties were also experienced with sealing the tantalum tube to Carpenter-20 pipe joint above the dissolver. The Swagelok fittings crimped the 15-mil-wall tubing without effecting a seal. Inserts of Carpenter-20 were machined to increase the effective wall thickness to about 75 mils, but this modification cannot be tested until the repaired flange assembly has been received.

5.2.4 High-Pressure-System Flange Tests

The pitch diameters of all 0.5-in. 2500-psi flanges installed in the high-pressure system were measured with the new gage recently obtained, and all except two were within 0.002 in. of standard dimensions. Of these two, one was approximately 0.003 in. and the other 0.0035 in. over standard. Significantly, the two leaks that occurred during shakedown operation were from these flanges.

5.3 REMOTE-MAINTENANCE PRACTICE

Several proposed remote-maintenance procedures were practiced. Although water will be used later for shielding purposes, this practice was performed with the cell empty.

5.3.1 Compact Right-Angle Wrench

The small, compact right-angle wrench (Fig. 5.1) was shown to be better adapted to remote operation than the bulky, pneumatic right-angle wrench previously tested. All six pairs of flanges mounted in horizontal lines can be broken and remade with this wrench, including the three that had proved inaccessible with the pneumatic wrench. Torques up to 200 ft-lb were transmitted through the right-angle drive, which is adequate for the small flanges in the chemical plant.

5.3.2 Circulating-Pump Installation

What appears to be the most difficult maintenance procedure, installation of the circulating pump, was partially performed by remote methods. The pump was lowered into place with the overhead crane, flanges were aligned with the aligning tool, and bolts were installed by means of a magnet. The suction flange, mounted in a rigid horizontal line, was in perfect alignment and, when torqued, was found to be leak-tight.

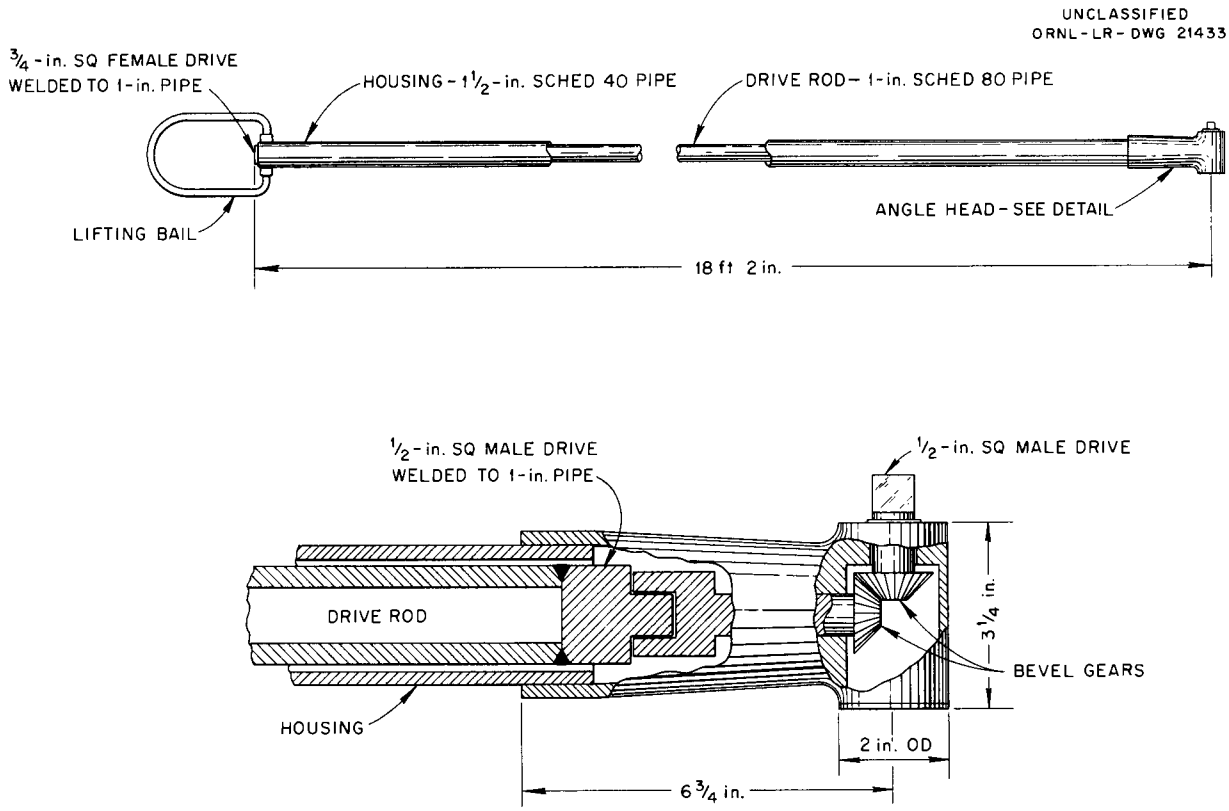

Fig. 5.1. Compact Right-Angle Wrench for Remote Maintenance.

5.3.3 Semipermanent-Freeze-Plug Test

A test with simulated semipermanent freeze plugs[1] on ½-in. pipe demonstrated that five series-connected plugs can be frozen under water. In the test, 12 ft of freeze-coil tubing was exposed under water. Freon flows of 1.85 gpm at a temperature of −40°F were required to freeze the plugs. Approximately 30 freeze coils will be required for maintenance purposes, and series connections will simplify the installation. Of significance is the fact that when this type of coil (six turns of ⅜-in.-dia stainless steel tubing, wound around the ½-in. pipe) is exposed under water, refrigerant temperatures must be below −10°F in order to freeze the plug.

5.4 CLOSED-CYCLE COOLING WATER

A closed-cycle cooling-water system is being designed to reduce the risk of chloride corrosion from potable water on process equipment. Design is 75% complete for altering the present once-through cooling-water system to a closed-cycle system. The calculated cooling load for the chemical plant is 140,000 Btu/hr at a flow rate of 18 gpm. A 5-hp pump with a 250-psi working pressure was ordered for use with a 325-gal stainless steel tank and a stainless steel shell-and-tube heat exchanger from the surplus-equipment yard.

5.5 WASTE DISPOSAL

5.5.1 Charcoal Beds

The performance to be expected of the charcoal beds that will be used in the HRT for adsorbing radioactive gases from the exit gas stream has been recalculated on the basis of the experimental data of Browning and Bolta.[2] The calculations show that the performance is very strongly dependent on the flow rate of the oxygen sweep

[1] R. H. Winget, *Semipermanent Freeze Plug Tests for HRT-CP*, ORNL CF-57-3-44 (March 11, 1957).

[2] W. E. Browning and C. C. Bolta, *Measurement and Analysis of the Holdup of Gas Mixtures by Charcoal Adsorption Traps*, ORNL-2116 (April 15, 1957).

gas and that a flow rate of 250 cc/min per bed is near the maximum feasible flow rate. Figure 5.2 shows the variation in exit-gas activity with flow rate for two levels of reactor power output.

These activity levels may be substantially larger if there is any significant short-circuiting within the carbon bed, resulting in a shorter holdup time. Preliminary calculations indicate that at low flow rates the exit-gas activities may be higher by a factor of 3; at high flow rates the effect would be less.

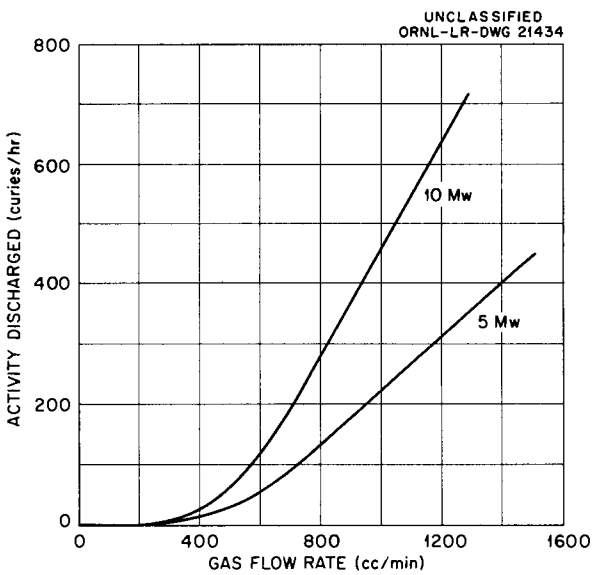

Fig. 5.2. Variation in Exit-Gas Activity for Two Power Levels.

Most of the activity that will be discharged from the carbon beds will be from the xenon isotopes, particularly Xe^{133}. There is no experimental value for the adsorption coefficient of xenon in the presence of a sweep gas. For this study, therefore, it was assumed that the adsorption coefficient for xenon is affected by the sweep gas to the same extent as the adsorption coefficient for krypton. The xenon adsorption coefficient must be experimentally determined before the carbon-bed performance can be accurately calculated.

5.5.2 Storage Tanks

The decay storage tanks in the chemical processing cell will hold six months' production of waste solution. This capacity is adequate if the present reactor schedule is not altered. If the reactor should be started up earlier than scheduled, however, more storage capacity will be needed. A preliminary design for an underground storage facility has been made, and a detailed design is being prepared. It is proposed to install a 500-gal underground storage tank south of Building 7500 and adjacent to the loading pit. Facilities are included for sampling, cooling, and venting the tank. Carrier handling equipment will be available in the loading pit, and an air lift will be provided for solution transfer to the carrier. The loading pit would be flooded during transfer operations to minimize radiation exposure. A 40-gal 7.5-ton carrier will be used to transport waste solutions from the reactor area to the Thorex Pilot Plant.

5.6 SOLIDS-DISSOLVING STUDIES

The HRT-CP solids-dissolution equipment has been mocked up to test the procedures and equipment installed for dissolving the corrosion-product solids which will be removed from the reactor core fuel. The recommended procedure[3] calls for dissolving in boiling 10.8 *M* H_2SO_4 and concentrating by evaporation. At least three such cycles are required to dissolve more than 97% of the solids.

The solids used to simulate corrosion products were oxides of zirconium, iron, and chromium produced by autoclaving the hydroxides of these metals with oxygen overpressure at 300°C in uranyl sulfate (10 g of uranium per kilogram of H_2O). The solids were then charged to the plant-scale dissolver, treated with 15 ml of 10.8 *M* H_2SO_4 per gram of solid, and evaporated. After the third cycle the dissolver contents were withdrawn and filtered to collect the solids. The results are in Table 5.1.

The corrosion of the Carpenter-20 reflux condensers was computed to be at a rate of 120 to 150 mpy, based on the copper and nickel analysis of the dissolver solution. It has not been determined whether the corrosion is caused by concentrated dissolver solution carried into the condenser as entrainment or by SO_2 formed by decomposition of the sulfuric acid.

---

[3]W. E. Unger *et al.*, *HRP Quar. Prog. Rep. Oct. 31, 1956*, ORNL-2222, p 26.

Table 5.1. Dissolution of Simulated Corrosion Products

Test	Number of Cycles	Milliliters of H_2SO_4 per Gram of Solid	Solids Charged (g)	Undissolved Solids Remaining (g)
1	2	15	400	10.0161
2	2	15	400	0.00
3	2	10	400	0.0052
4[a]	2	15	400	80.77
5[b]	3	15	400	12.31
6[b]	3	15	400	28.84
7[c]	3	15	400	33.17

[a]5 ft of Carpenter-20 0.5-in.-OD pipe, horizontal reflux condenser.
[b]2.5 ft of Carpenter-20 0.5-in.-OD pipe, horizontal reflux condenser.
[c]2.5 ft of Carpenter-20 0.5-in.-OD pipe, vertical reflux condenser.

Part II

REACTOR DESIGN AND ANALYSIS

J. A. Lane

6. HRE-3 (THORIUM BREEDER REACTOR)

W. R. Gall
J. C. Bolger
E. H. Gift
R. O. Moak[1]
M. I. Lundin
E. A. Mason
H. A. McLain
R. C. Robertson

The conceptual design of HRE-3 has been started. This reactor is to be of a type and of sufficient size to demonstrate breeding and to develop technology to gain experience in the operation of components which may be readily extrapolated to full-size power reactors.

Design work on the HRE-3 has begun on the basis of a two-region solution-core, slurry-blanket system. The normal power level of 60 Mw has been distributed as follows: core power, 50 Mw; blanket power, 10 Mw.

The parameters given in Table 6.1 have been set as a basis for design studies. Based on the temperatures and pressures shown in Table 6.1, the following preliminary design data have been calculated:

Core volume, liters	950
Blanket volume, liters	6500
Average power densities at 60 Mw	
Core, kw/liter	52.6
Blanket, kw/liter	1.54
Critical concentration in core (T_{av} = 270°C), g/liter	
Initial (with 93% U^{235})	5.0
Equilibrium (U^{235} and higher isotopes)	10.6
Uranium concentration in blanket (for 10 Mw operation), g/liter	3
Fuel flow rate, lb/hr	2.547×10^6
Fuel pumping rate, gpm	5700
Blanket flow rate, lb/hr	1.845×10^6
Blanket pumping rate, gpm	1940
Blanket temperatures, °C	
Blanket inlet	260
Blanket outlet	280
Steam conditions at 60 Mw	
Generation rate, lb/hr	2×10^5
Steam-drum pressure, psi	450
Steam-drum temperature, °F	457
Feed temperature, °F	212
Fuel high-pressure piping	14-in. OD sched 140
Fuel velocity in pipe, fps	19.4
Pressure drop per 100 ft of pipe, psi	3

The 4-ft core-vessel diameter was selected in preference to a larger sized vessel in order to demonstrate a core power density comparable to that expected in a large-scale power reactor. Within the range of core diameters considered there is little incentive to increase core diameter from the standpoint of Zircaloy wall corrosion and breeding ratio. Following is a comparison of some data for 4- and 5-ft-dia spherical cores:

Core diameter, ft	4	5
Core power, Mw	50	50
Power density at wall, kw/liter	41	25
Estimated corrosion rate, mpy	25	20
Estimated breeding ratio (with 2-ft, 1000-g/liter ThO_2 blanket)	1.07	1.08

The tentative choice of 1000 g of ThO_2 per liter as the blanket concentration has been made on the basis of the higher breeding gain obtainable as compared with that for a 500-g/liter blanket. It is realized, however, that the higher concentration may introduce more difficult handling problems. Breeding ratios of 0.96 and 1.07 are obtainable, respectively, for slurry concentrations of 500 and 1000 g of thorium per liter of D_2O.

In addition, it was assumed that increased blanket flow rates would aid in maintaining slurry suspension. For this reason the temperature rise across the blanket was set at 20°C, as compared with 30°C across the core.

The first layout of the reactor complex will be governed by the following considerations:

1. All components will be arranged to facilitate

[1]On loan from Foster Wheeler Corp.

maintenance. The maintenance philosophy to be adopted in the design will be based on all operations being done dry. However, provision will be made so that the shield can be flooded if extreme conditions make it necessary.

2. All high-pressure radioactive components must be located inside a containment vessel which is surrounded entirely by a shield sufficient to protect personnel against radioactivity of reactor fluids in event of a drastic failure of the system.

Table 6.1. Parameters Established as a Basis for Design Studies

	Design	Maximum Conditions
Core power level, Mw	50	
Core inlet temperature, °C	250	
Core outlet temperature, °C	280	300
Operating pressure, psia	1500	2000
Core inside diameter, ft	4	
Blanket thickness, ft	2	
Core solution	UO_2SO_4-$CuSO_4$-H_2SO_4 in D_2O	
Blanket composition	1000-g/liter $ThO_2 + UO_2$ in D_2O	

7. REACTOR ANALYSIS

P. R. Kasten

T. B. Fowler C. W. Nestor, Jr.
M. P. Lietzke M. W. Rosenthal
M. Tobias

7.1 FUEL COSTS IN SPHERICAL THORIUM SLURRY REACTORS

Studies of fuel costs in homogeneous reactors are important in establishing the optimum fuel-processing cycle (i.e., batch vs continuous) for a given reactor system and in comparing the merits of different fuel systems and reactor types. Such studies include a determination of the effect of design variables such as reactor size, power level, geometry, fixed charge rates on inventories, and processing costs important for the selection of future homogeneous reactors. As part of the over-all effort, fuel costs have been calculated for two-region spherical thorium-slurry reactors at steady state and for single-region solution and slurry reactors operating under batch as well as steady-state conditions. Further calculations of batch operation of two-region reactors will be carried out to complete the studies.

Previous results[1-3] pertaining to the nuclear and economic characteristics of spherical thorium-slurry reactors operating under equilibrium conditions have been extended.[4] Fuel cost, breeding gain, and core-wall power densities have been computed for two-region reactors with D_2O-ThO_2-$U^{233}O_3$ slurry in both the core and the blanket, for two-region reactors with a slurry blanket but with no thorium in the core, and for one-region reactors containing D_2O-ThO_2-$U^{233}O_3$ slurry. The major parameters were varied over the ranges indicated in Table 7.1. In addition, reactor power was varied for some cases. The influence that η (U^{233}) and resonance escape probability for thorium oxide slurries have upon the fuel cost was also investigated. Other values used (except where specifically noted) are given in Table 7.2.

[1] P. R. Kasten *et al.*, *HRP Quar. Prog. Rep. Jan. 31, 1957*, ORNL-2272, p 49–51.

[2] M. W. Rosenthal and M. Tobias, *Nuclear Characteristics of Two-Region Slurry Reactors*, ORNL CF-56-12-82 (Dec. 20, 1956).

[3] P. R. Kasten *et al.*, *HRP Quar. Prog. Rep. Oct. 31, 1956*, ORNL-2222, p 41–44.

[4] M. W. Rosenthal, M. Tobias, and T. B. Fowler, *Fuel Costs in Spherical Slurry Reactors*, ORNL-2313 (to be issued).

Table 7.2. Other Values Used in Fuel-Cost Study

Item	Value
η (U^{233})	2.25
Net electrical power per reactor, Mw	125
Inventory charge (D_2O and fuel), %	4
Heavy-water makeup, %/year	5
Fuel value, \$/g of U^{233} or U^{235}	16
Fixed charges on Thorex plant, \$/day	5500
Uranium processing cost, ¢/g	50
Thorium processing cost, \$/kg	3.00
Heavy-water recovery, ¢/liter	35

Table 7.1. Parameter Values Used in Slurry Reactor Studies

	Two-Region Reactors	One-Region Reactors
Core diameter, ft	8–15	8–20
Blanket thickness, ft	$1\frac{1}{2}$–3	
Core thorium concentration, g/liter	0–300	0–400
Core poison fraction, %	3–20	4–12
Blanket thorium concentration, g/liter	500–2000	
Blanket U^{233} concentration, g per kg of thorium	1–7	

The computational techniques and general procedures were similar to those used in earlier investigations.[5] In the following sections the influence of specific parameters upon fuel cost is discussed.

7.1.1 Two-Region Reactors

(a) Concentration of U^{233} in Blanket and Core Poison Fraction. – These variables were determined by the blanket- and core-processing rates. The optimum values (from a fuel-cost standpoint) were found to be largely independent of other parameters; moreover, there was little change in fuel cost with changes in either blanket U^{233} concentration or core poison fraction. For all slurry-core systems the optimum poison fraction was about 0.08, independent of the other design parameters. The optimum poison fraction for the solution core was about 0.07. The lowest fuel cost occurred at a blanket U^{233} concentration of about 4.0 g per kilogram of thorium.

(b) Blanket Thickness and Blanket Thorium Concentration. – An example of the effects of these parameters on fuel cost and breeding gain is presented in Fig. 7.1. The optimum thorium concentration in the blanket generally was between 1000 and 2000 g/liter; however, with the more heavily loaded cores and thicker blankets, the fuel costs obtained for a blanket thorium concentration of 750 g/liter were little different from those for the more heavily loaded blankets. For blanket thorium concentrations between 1000 and 2000 g/liter, the blanket thickness giving the lowest fuel cost generally was between 1½ and 2½ ft. As would be expected, higher thorium loadings would be desirable if thin blankets were used. Systems having low thorium concentrations in the core required more heavily loaded blankets to minimize fuel costs. For solution cores, still heavier and thicker blankets would be desirable, particularly if the core diameters were small.

(c) Core Thorium and Core Diameter. – The effects of these variables upon fuel costs are shown in Fig. 7.2. These results indicate (on

[5] H. C. Claiborne and M. Tobias, *Some Economic Aspects of Thorium Breeder Reactors*, ORNL-1810 (Oct. 12, 1955).

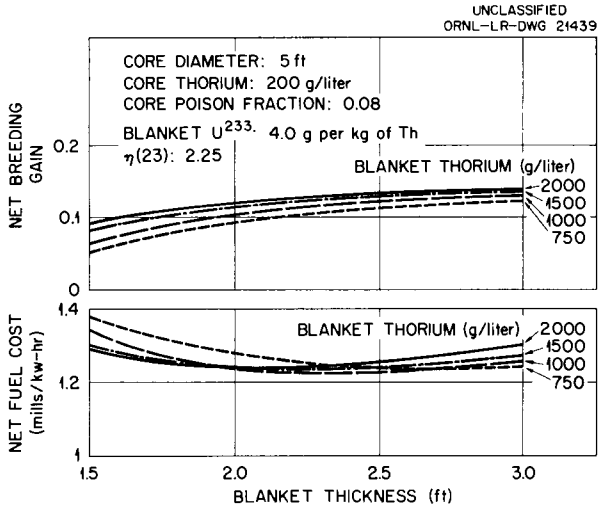

Fig. 7.1. Breeding Gain and Fuel Cost as Functions of Blanket Thickness for Various Blanket Thorium Concentrations.

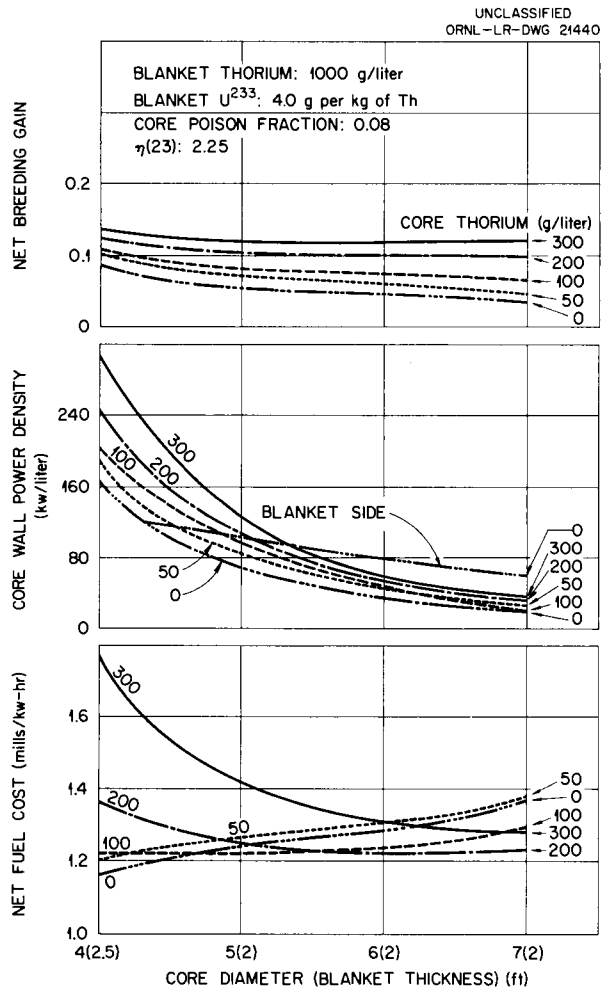

Fig. 7.2. Breeding Gain, Power Density at the Core Wall, and Fuel Cost as Functions of Core Diameter and Core Thorium Concentration.

the basis of fuel cost alone) that the small, solution-core reactors would have a slight advantage over the slurry reactors. However, the power density at the core wall would be very high for such reactors. If larger cores are required because of power-density limitations, the fuel-cost advantage moves to the slurry core. The slurry-core systems would yield higher outputs of fuel, although all the reactors shown had positive breeding gains. As illustrated in Fig. 7.2, the optimum fuel cost was about 1.2 mills/kwhr, independent of core diameter. The decrease in fuel cost associated with going from a core thorium concentration of 50 g/liter to zero resulted from assuming hydroclone separation of fission products from the core solution. The hydroclone installation added only 0.03 mill/kwhr investment cost to the system, while the variable Thorex processing cost was reduced by two-thirds. The relative flatness of the optimum net-fuel-cost curve in Fig. 7.2 results because changes in processing charges and yield of product were offset by accompanying changes in the fuel inventory charge. Similar compensating effects account for the insensitiveness of fuel costs to changes in other design parameters.

Table 7.3 presents a breakdown of costs and neutron balances for some reactors having low fuel costs. The changes which occurred on addition of slurry can be seen by comparison of the two 6-ft-core-diameter reactors. Neutron balances are normalized to 100 absorptions in U^{233} and U^{235}.

(*d*) Reactor Power. – Most of the computations in this study were based upon the concept of a three-reactor station, each reactor producing 125 Mw of electricity. However, the effect of varying power alone was also investigated for several cases. As shown in Table 7.4, the fuel cost was found to be a strong function of power capability. The greater part of the change was due to variation in the fixed chemical-processing charge. Since the total fixed processing costs ($5500/day) were assumed to be independent of throughput, this charge on a mills/kwhr basis was inversely proportional to the reactor power.

(e) Nuclear Parameters. – The values of η (U^{233}) and the resonance escape probability of thorium oxide slurries are not known with certainty. Therefore the effects of changes in these parameters on the results were computed in order to examine the reliability of the nuclear calculations. The fuel cost increased by about 0.2 mill/kwhr when η was lowered to 2.18, and was reduced by about the same amount when η was changed to 2.32.

The importance of resonance escape probability (p^{02}) upon fuel cost was studied by using values for ($1 - p^{02}$) 20% higher or lower than a standard value. In the neighborhood of a core thorium concentration of 200 g/liter, the changes in p^{02} were found to have a negligible effect upon fuel costs.

(*f*) Xenon Removal. – For most of the cases studied the contribution of xenon to the poison fraction was assumed to be 0.01. To achieve this condition, about 80% of the xenon must be removed before neutron capture occurs. Since xenon-removal systems for slurries have not been demonstrated, the effect of operating without xenon removal was studied by increasing the xenon poison fraction to 0.05 (the samarium contribution was held at 0.008). In the systems examined, when the xenon poison fraction was increased by 0.04, the total poison fraction yielding the lowest fuel cost also increased by approximately the same amount. The values in Table 7.5 illustrate this effect by comparing two cases at optimum total poison fraction but at different xenon poison levels. Thus the variable part of the core poison fraction was unchanged and the core processing rate remained about the same. The larger fuel cost at the higher xenon level appears to be almost entirely a result of the reduction in breeding gain.

7.1.2 One-Region Reactors

(*a*) Poison Fraction. – The poison fraction producing the minimum fuel cost for a given system was found to be in the range from 0.06 to 0.10, the exact value depending on the specific diameter and thorium concentration. However, a value of 0.08 gave costs which were close to the minimum for all cases.

(*b*) Diameter and Thorium Concentration. – The breeding gain and fuel cost for some of the reactors studied are shown in Fig. 7.3. Detailed information for a typical one-region reactor is given in the last column in Table 7.3. In general, for thorium concentrations less than 400 g/liter, the reactor diameter had to be greater than 10 ft in order to have positive breeding gains; the

Table 7.3. Cost Breakdown and Neutron Balances for Some Typical Reactors

Core diameter, ft	6	5	4	6	14
Blanket thickness, ft	2	2	2½	2	
Core thorium concentration, g/liter	200	100	0	0	250
Blanket thorium concentration, g/liter	1000	1000	1000	1000	
Blanket U^{233} concentration, g per kg of thorium	4	4	4	4	
Core poison fraction	0.08	0.08	0.08	0.08	0.08
Critical concentration, g of U^{233} per liter	9.4	6.4	4.1	1.4	6.8
Net breeding gain	0.102	0.081	0.089	0.045	0.012
Core wall power density, kw/liter	53	91	170	80	
Core cycle time, days	637	418	884	342	1094
Blanket cycle time, days	295	205	176	210	
Inventory of U^{233} and U^{235}, kg	368	272	200	148	522
Inventory of heavy water, lb	96,100	87,400	89,600	99,500	157,000
Net U^{233} and U^{235} production, g/day	49	39	43	21	6
Grams of U^{233} per g of U produced	0.67	0.65	0.77	0.72	0.41
Estimated cost, mills/kwhr					
Uranium inventory	0.27	0.20	0.15	0.11	0.38
D_2O inventory and losses	0.27	0.25	0.25	0.29	0.45
Thorium inventory and feed	0.01	0.01	0.01	0.01	0.01
Fixed chemical processing	0.76	0.76	0.76	0.76	0.76
Core processing	0.13	0.13	0.07	0.08	0.19
Blanket processing	0.09	0.12	0.18	0.18	
Uranium sale, credit	0.33	0.26	0.29	0.15	0.04
Net fuel cost	1.22	1.22	1.16	1.29	1.76
Net absorptions per 100 absorptions in fuel					
Absorptions in core by					
$U^{233} + U^{235}$	92.6	88.6	80.4	78.9	100
$U^{234} + U^{236}$	7.4	8.3	9.4	10.1	10.1
Th	60.1	38.2	0	0	92.9
Pa^{233}	1.2	1.1	0	0	1.1
Poisons	6.6	6.4	5.8	5.6	7.2
Heavy water	0.4	0.6	0.8	2.2	0.6
Absorptions in core tank	0.7	1.0	1.4	2.9	
Absorptions in blanket by					
U^{233}	7.4	11.4	19.6	21.1	
$U^{234} + U^{235} + U^{236}$	0.04	0.1	0.2	0.2	
Th	44.4	63.6	101.4	96.5	
Pa^{233}	0.3	0.7	1.5	1.4	
Poisons	0.2	0.3	0.6	0.6	
Heavy water	0.1	0.1	0.2	0.2	
Fast leakage	1.9	2.7	1.9	3.0	8.4
Slow leakage	0.4	0.6	0.4	0.7	3.1

Table 7.4. Effect of Power Level on Fuel Costs

Electric Power (Mw)	Net Fuel Cost (mills/kwhr)	Fixed Chemical-Processing Charge (mills/kwhr)
80	1.75	1.19
125	1.22	0.76
200	0.88	0.48

Table 7.5. Effect of Xenon Poison Fraction on Fuel Costs

Xenon poison fraction	0.01	0.05
Optimum total poison fraction	0.08	0.12
Core cycle time, days	637	718
Breeding gain	0.102	0.070
Fuel inventory charge, mill/kwhr	0.27	0.29
Core processing charge, mill/kwhr	0.13	0.14
Fuel product (credit), mill/kwhr	0.33	0.22
Net fuel cost, mills/kwhr	1.22	1.35

12-ft-dia reactor was a breeder at a thorium concentration of 350 g/liter, while at 250 g of thorium per liter the 14-ft-dia reactor was a breeder. For reactors between 10 and 16 ft in diameter, the thorium concentration yielding the lowest fuel costs was between 200 and 250 g/liter. The lowest fuel cost computed was 1.76 mills/kwhr, for a 14-ft-dia reactor containing 250 g of thorium per liter. In the curve for the 14-ft reactor, the inflection in the neighborhood of 225 g of thorium per liter was a result of the reactor changing from a breeder to a nonbreeder. This inflection was associated with a marked increase in U^{236} concentration, which produced an increase in fuel processing charges.

(c) Power and Nuclear Parameters. – The effect of reactor power on the fuel costs of one-region reactors was similar to that mentioned earlier for two-region systems. For example, the fuel cost for one reactor was 1.78 mills/kwhr at 125 Mw of electric capability, but only 0.96 mill/kwhr when the output per reactor was increased to 375 Mw.

The importance of changes in nuclear parameters was generally the same for the one-region reactors as for the two-region systems, although the effect of a reduction in η (U^{233}) was somewhat greater for the one-region cores.

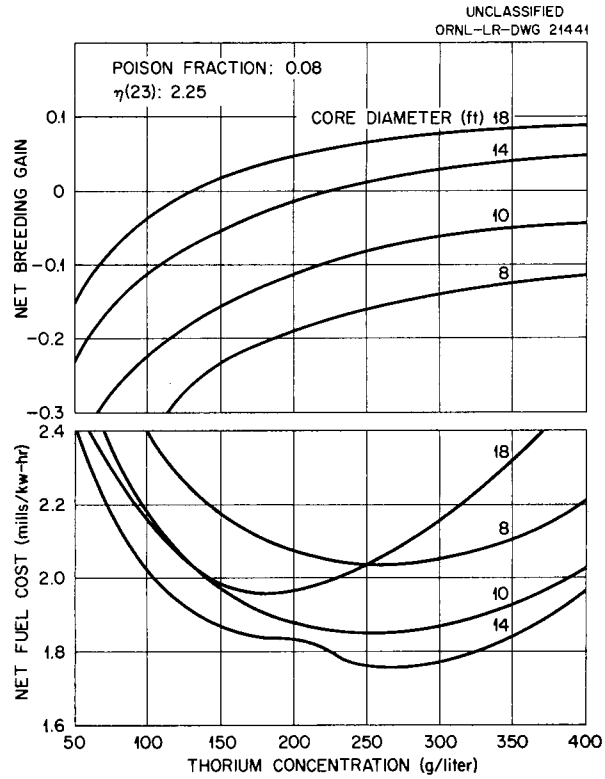

Fig. 7.3. Breeding Gain and Fuel Cost as Functions of Thorium Concentration in One-Region Reactors.

7.1.3 Comparison of Reactor Types

There appears to be no decisive difference in fuel costs between solution-core and slurry-core systems. For small core diameters (4 to 4½ ft) the solution core had a slight cost advantage (gained from the use of hydroclone separation), but the core-wall power densities were high (~200 kw/liter). For larger core reactors the cost advantage shifted to the slurry-core systems, which also had higher breeding gains.

Comparing the lowest fuel costs for each reactor type, the two-region system produced power with a fuel cost that was about 0.5 mill/kwhr less than that of the one-region reactor. Breeding gains were generally higher for two-region reactors in the range of interest, particularly for systems with small pressure vessels.

7.2 FUEL COSTS IN SINGLE-REGION POWER REACTORS

The fuel costs associated with electrical power produced from nuclear reactors will be a function of feed cost, inventory charge, fuel processing cost, and operating conditions. In order to better understand the relative importance of these costs under specified conditions, a parameter study was undertaken. The total fuel cost as used here was defined as the cost of electrical power other than that associated with capital investment charges (reactor plant plus turbogenerator unit), fixed charges for fuel processing, and operation and maintenance charges. Included in the total fuel cost was the cost of nuclear-fuel feed, inventory charge based on the initial fuel loading, and variable fuel-processing charges. Spherical single-region homogeneous aqueous reactors were studied, moderated with either H_2O or D_2O and fueled with enriched UO_3 plus ThO_2 or fueled with UO_2SO_4 of varying enrichments. The effect of adding Li_2SO_4 to the UO_2SO_4 was also considered. In the UO_3 + ThO_2 system it was assumed that the initial fuel was U^{235} and that sufficient U^{233} was available as subsequent feed material if required. The effect of fueling with U^{235} in cases where the reactors did not produce sufficient U^{233} was also considered in a qualitative way and was found to add about 0.1 mill/kwhr to the fuel cost. The reactors were considered to operate at a temperature of 280°C and a pressure of 2000 psia. An 80% load factor and a net thermal-to-electrical efficiency of 25% were assumed. The thermal power level was considered to be 500 Mw for nearly all cases.

For the systems and operating conditions given above, the fuel power costs were obtained[6] for cases in which inventory charge, cost of nuclear fuel, fuel process-cycle time, fuel-processing charge, absorption cross section of fission products, reactor diameter, and concentration of fertile material were considered as parameters. In more restricted parameter studies the effects of power level, value of η^{23}, value of η^{49}, and poison removal upon fuel cost were also determined. For all cases, non-steady-state conditions were considered; fuel costs were calculated for 10- and 25-year periods. The parameter values used in this study are given in Table 7.6.

Cost factors which were considered but which made a negligible contribution to the total fuel cost were fuel processing losses (0.1% of fuel processed was considered lost), D_2O losses (5% of D_2O inventory per year), hydroclone costs ($70/day), 30-day inventory supplies, and shipping charges (it was assumed that the amortization charges for shipping costs would be negligible). In all cases the inventory charges were based on the volume of the reactor vessel plus the volume of the external system. This latter volume was calculated on the basis of an average heat-removal capability of 20 kw per liter of external volume. The enrichment of the heavy water was assumed to be 99.75% D_2O, and the D_2O cost was taken as $28/lb.

Only the optimum or near-optimum reactor conditions were selected in plotting results. These optimum conditions refer to the diameter, fuel-processing cycle time, and fertile-material concentration which gave the minimum fuel cost of all the diameters, cycle times, and fertile-material concentrations studied for that particular case. Fuel costs were calculated for both 10 and 25 years of reactor operation; these costs were usually slightly lower after 25 years than after 10 years, but the differences were small, usually being between zero and 0.1 mill/kwhr. Therefore only results for 10-year operation are given here.

Of the parameter values considered, the reactor system, power level, inventory charge, effective value of η, and cost of fissionable fuel had the greatest influence on the fuel cost. Changing the power level affected optimum reactor conditions significantly. The variations in relative poisons and relative chemical processing considered here did not change fuel costs to a large degree, the individual effects usually being about 0.1 mill/kwhr.

Results based on feed costs of $15/g for 90% enriched material and $40/kg for natural uranium are given in Figs. 7.4 to 7.6. Figures 7.4 and 7.5 show the effects of power level, inventory charge, and reactor composition upon fuel cost. The influence of reactor composition is due to the different values of η and fraction poisons associated with the different systems. Increasing the inventory charge from 4 to 12% increased fuel cost by about 0.5 mill/kwhr for the D_2O systems. Although not shown, the effect of Li_2SO_4 addition

[6] P. R. Kasten, T. B. Fowler, and M. P. Lietzke, *Fuel Power-Costs in Single-Region Homogeneous Reactors*, ORNL-2341 (to be issued).

Table 7.6. Range of Parometer Values Used in Fuel-Cost Study

Reactor systems	D_2O-UO_3-ThO_2, H_2O-UO_3-ThO_2, D_2O-UO_2SO_4, H_2O-UO_2SO_4, D_2O-UO_2SO_4-Li_2SO_4, H_2O-UO_2SO_4-Li_2SO_4
Reactor diameter, ft	3 to 14
Fertile-material concentration, g of U^{238} or of Th^{232} per liter	100 to 1000
Cost of 90% enriched fuel,[a] \$/g	15, 22.5, 30, 60
Relative processing charge[b]	1, 2
Inventory charge, 1%	4, 12
Fuel process cycle time, days	100, 300, 500, ∞
Relative fission-product poisoning[c]	¼, ½, 1
Power level, thermal Mw	100, 500, 1000
η^{49}	1.93, 2.00, 2.05
η^{23}	2.15, 2.25

[a]Value of material of lower enrichments was calculated relative to these costs, and a natural-uranium cost of \$40/kg.

[b]A value of 1 for relative fuel processing implies a charge of \$0.54 per gram of $U^{233} + U^{234} + U^{235} + U^{236}$ processed, \$1 per gram of Pu processed, and \$3.50 per kilogram of fertile material processed. A value of 2 implies processing charges twice the above values.

[c]A relative poisoning of 1 implies representation of the fission-product poisons by two effective nuclei having yields of 0.11 and 1.81 atoms/fission, and thermal absorption cross sections of 132 and 13.9 barns, respectively [based on values of W. L. Robb *et al.*, *Nucleonics* 13(12), 30 (1955)]. A value of ½ or ¼ implies cross sections ½ or ¼ the above values.

to the UO_2SO_4-H_2O system had negligible effect upon fuel cost, since a high poison fraction was present initially. The addition in equimolar proportions of Li_2SO_4 to the UO_2SO_4-D_2O system increased fuel costs by about 0.1 mill/kwhr.

The influences of fuel-processing cycle time, fuel-processing charge, and fission-product poisoning upon fuel cost are shown in Fig. 7.6 for the UO_3-ThO_2-D_2O system. It is seen that doubling the fission-product poisoning increased the fuel cost about 0.1 mill/kwhr throughout the range of θ considered and that doubling the processing charge increased the fuel cost about 0.1 mill/kwhr at optimum conditions.

Throughout this study the fixed charges for fuel processing were neglected (although the results obtained for different fuel-processing charges could in a sense be considered to show the effect of adding fixed charges). In all cases studied, increasing the fuel-processing charges increased the optimum fuel-processing cycle time. Clearly, if processing charges were high enough, the optimum reactor conditions would correspond to zero fuel processing. Although fuel would undoubtedly be processed at the end of reactor operation, the permissible unit cost for processing at that time would be high compared with the permissible unit cost for a short fuel-processing cycle time. If the fixed charges for processing correspond only to that period required to process the fuel, then the optimum cycle time would be greater than the value obtained for fixed charges independent of θ.

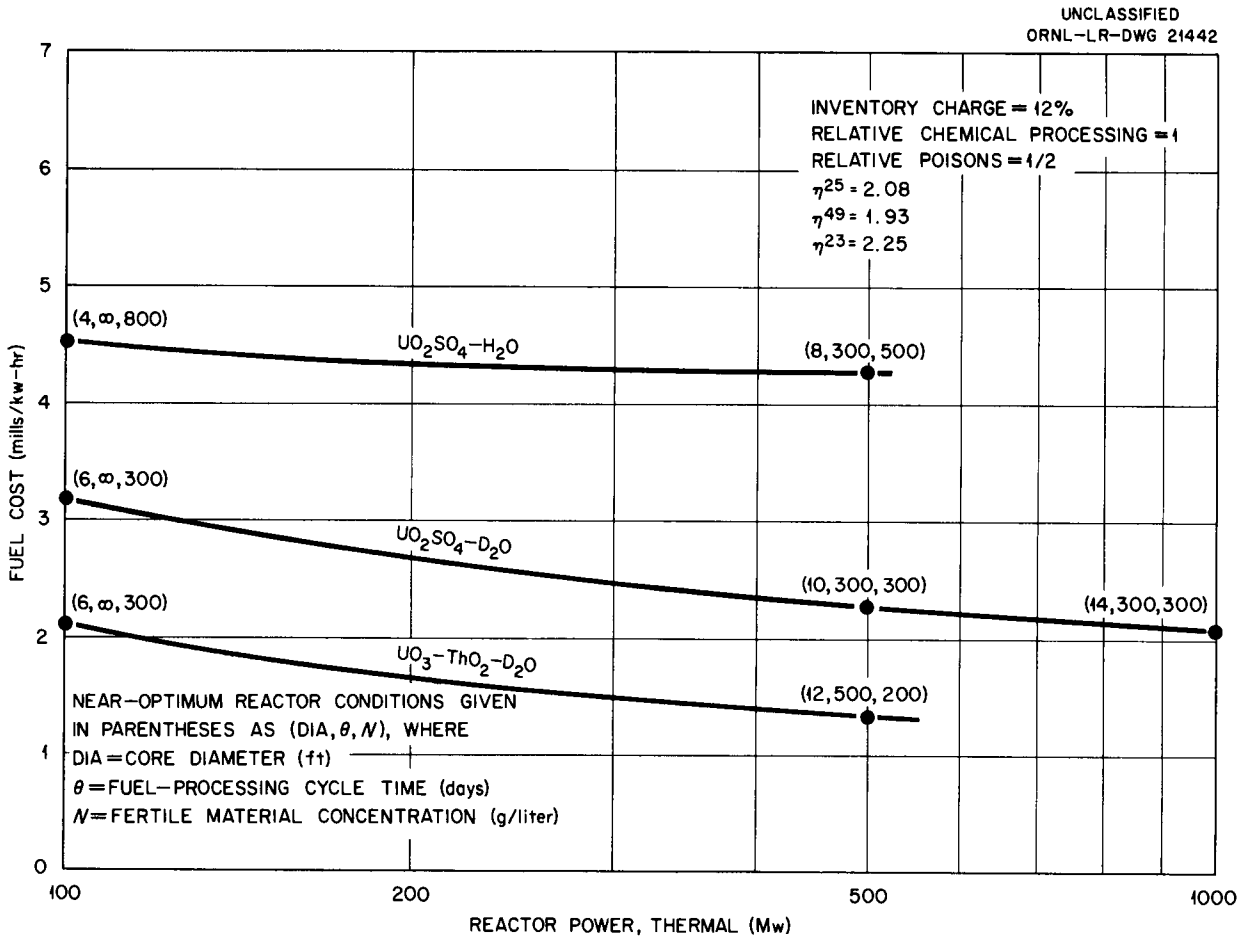

Fig. 7.4. Fuel Costs in Single-Region Reactors as a Function of Power Level.

7.3 FLUX PEAKING IN HOMOGENEOUS REACTORS

Nuclear calculations have been performed with the use of a two-group, multiregion, one-dimensional model for some D_2O-moderated, multiregion homogeneous reactors. The principal purposes of these computations were to determine, for a specified power level, the thermal flux available for experimental purposes and also the wall power densities.

The reactors considered in this study were fueled with U^{233} and moderated by D_2O, had spherical geometry, contained fuel in an annulus region, and were operated at 280°C and a power of 100 thermal megawatts. The reactor systems considered are indicated in Fig. 7.7.

The available thermal fluxes in the central region, the power densities at the inner boundary of the fuel annulus, and the ratios of the maximum thermal flux in the central region to the average thermal flux in the fuel are given in Table 7.7 for the reactor configuration shown in Fig. 7.7*a*. Table 7.8 lists the average thermal flux in the central converter and the power density at the inner wall of the fuel annulus for various converter fuel concentrations, on the basis of the configuration shown in Fig. 7.7*b*. The configuration shown in Fig. 7.7*c* considered the converter fuel in an annulus around a central sphere containing an experimental sample. Results for this case are shown in Table 7.9. The fuel annulus and the experimental sample will require cooling and structural materials; these effects were simulated by the addition of a poison cross section to the central D_2O-filled sphere. The poison fraction referred to in Table 7.9 is the ratio of the poison cross section in the central sphere to the converter-fuel absorption section.

In general, the thermal fluxes available in the central region were high, ranging from 2.7×10^{15}

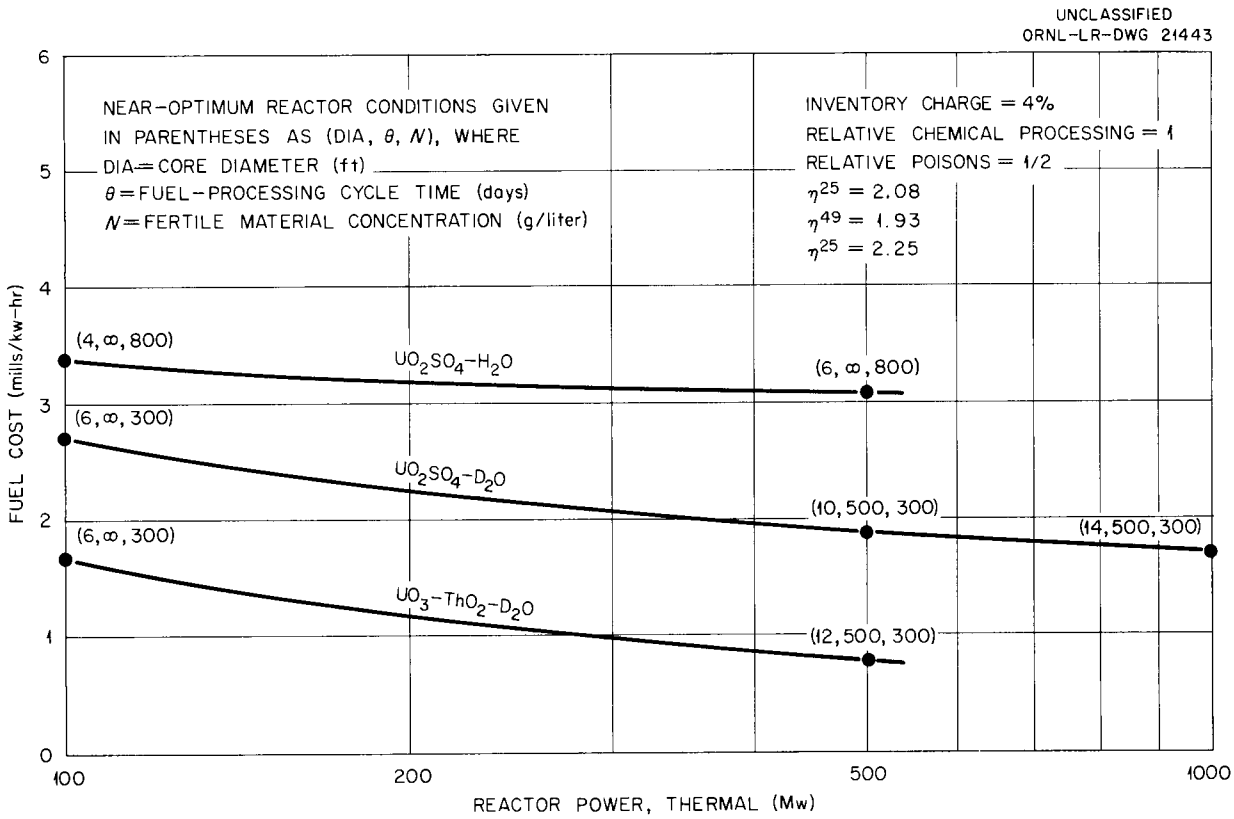

Fig. 7.5. Fuel Costs in Single-Region Reactors as a Function of Power Level.

Table 7.7. Thermal Fluxes and Wall Power Densities for Core Configurations of Fig. 7.7*a* at a Reactor Power of 100 Mw

R_1 (cm)	R_3 (cm)	Average Thermal Flux in Central Region (neutrons/cm^2·sec)	Maximum Thermal Flux in Central Region (neutrons/cm^2·sec)	Central Thermal Flux / Average Thermal Flux in Fuel	Power Density at R_2 (kw/liter)	Average Power Density in Fuel Region (kw/liter)
		$\times 10^{15}$	$\times 10^{15}$			
30	60	2.69	2.96	1.47	156	129
35	60	2.51	2.80	1.49	167	142
40	60	2.33	2.65	1.52	187	164
45	60	2.16	2.50	1.56	226	204
50	60	1.99	2.36	1.61	315	294
40	55	2.45	2.85	1.55	275	249

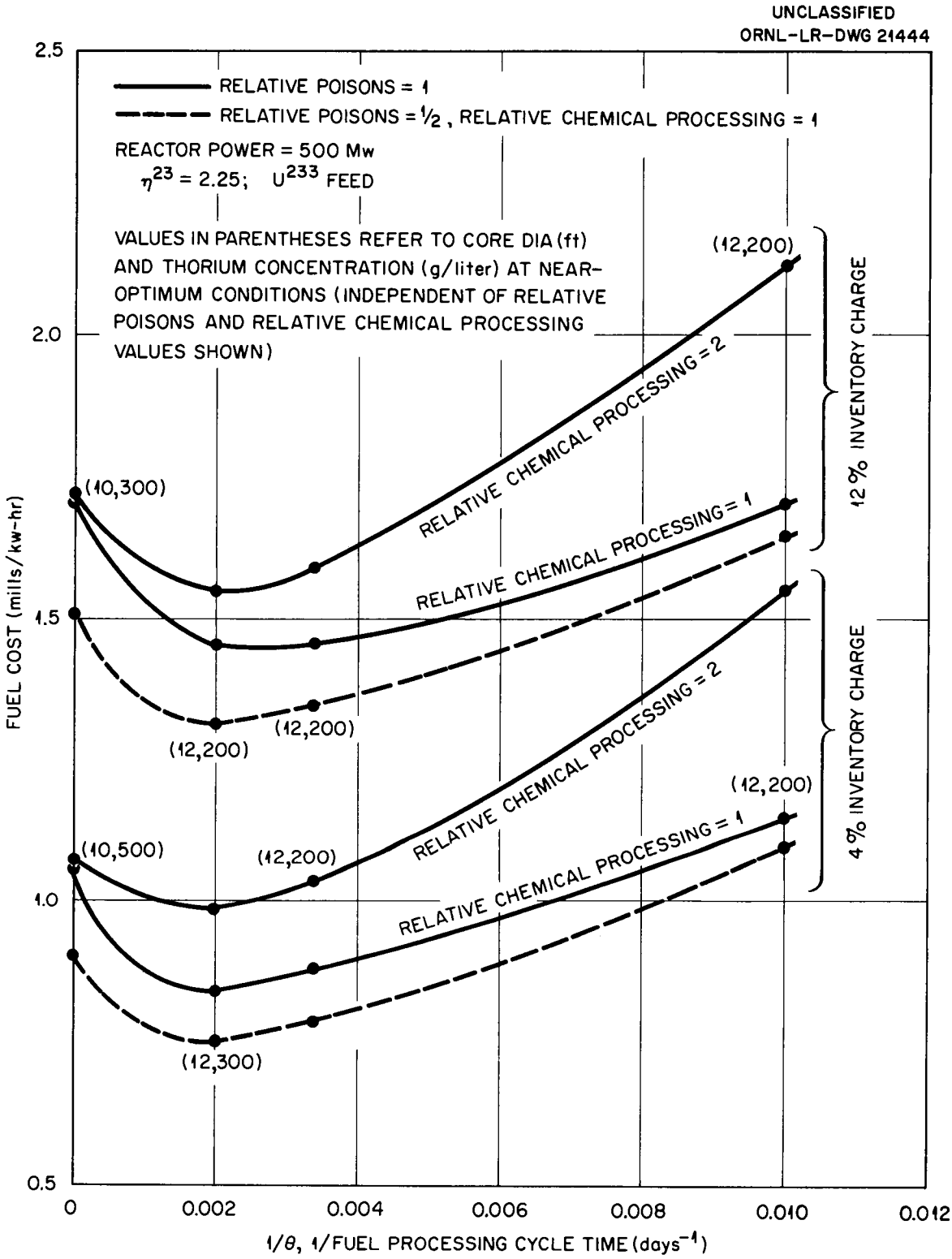

Fig. 7.6. Effects of Fuel-Processing Cycle Time, Fuel-Processing Charge, and Poisoning by Fission Products upon Fuel Cost in UO_3-ThO_2-D_2O Reactors.

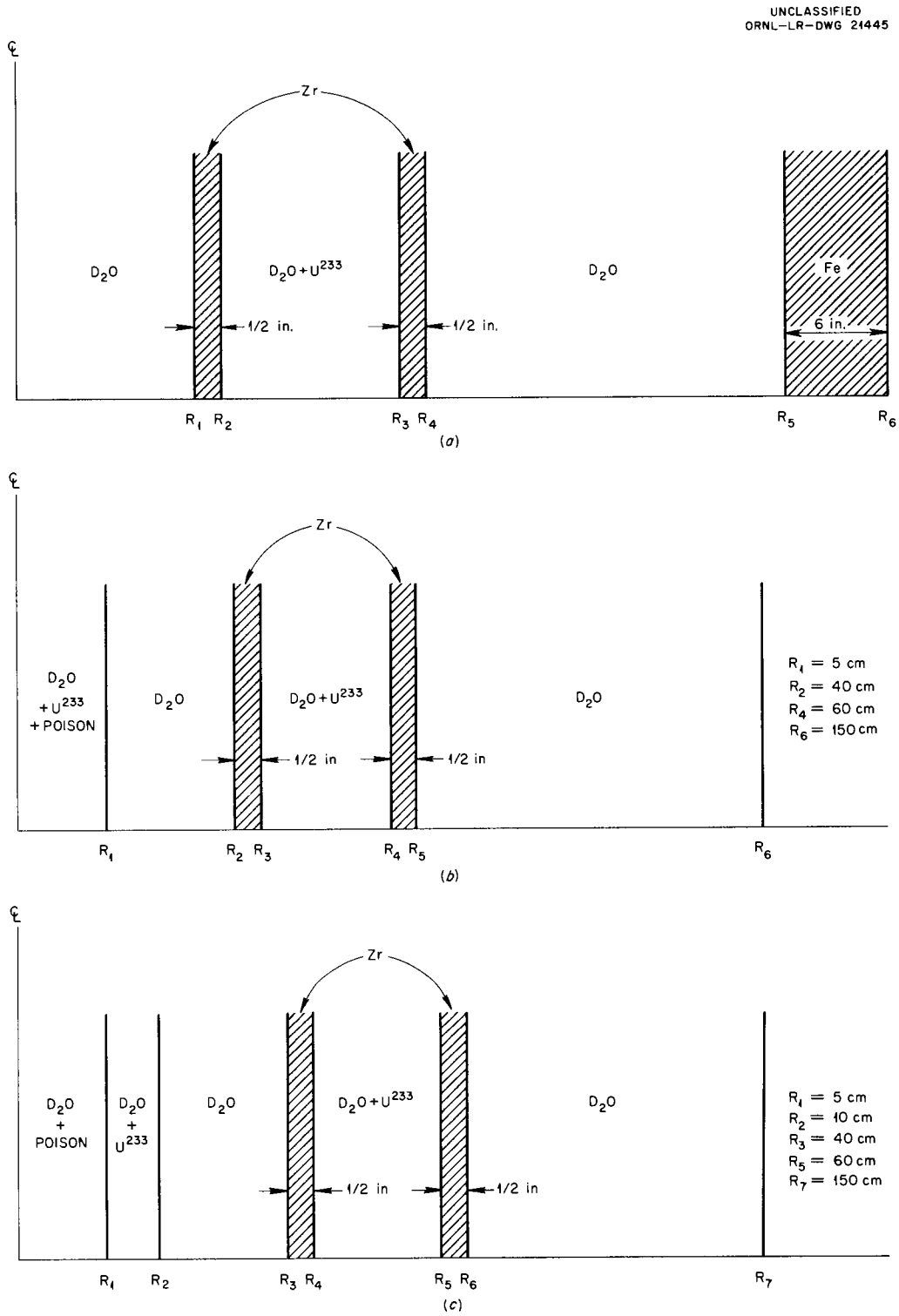

Fig. 7.7. Core Regions Considered in Study of Flux Peaking in Spherical Homogeneous Reactors. (*a*) Annular fuel region; (*b*) annular fuel region plus central-converter region; (*c*) annular fuel region plus annular-converter region.

Table 7.8. Thermal Fluxes and Wall Power Densities for Core Configurations of Fig. 7.7*b* at a Reactor Power of 100 Mw

Converter Fuel Concentration (g of U^{233} per liter)	Average Thermal Flux in Central Region (neutrons/cm^2·sec)	Power Density at R_3 (kw/liter)
	$\times 10^{15}$	
1	2.60	187
2	2.57	187
10	2.35	187
30	1.94	187
60	1.54	187
60*	1.69	184
100	1.22	187

*D_2O regions assumed to be at $T = 150°C$.

Table 7.9. Thermal Fluxes and Wall Power Densities for Core Configurations of Fig. 7.7*c* at a Reactor Power of 100 Mw

	Inner Annulus Fuel Concentration (g of U^{233} per liter)	Average Thermal Flux in Inner Fuel Annulus (neutrons/cm^2·sec)	Power Density at R_4 (kw/liter)	Critical Fuel Concentration (g of U^{233} per liter)
		$\times 10^{15}$		
50% poison	10	2.47	188	3.27
	30	2.23	189	3.09
	60	1.97	191	2.90
	100	1.71	192	2.72
100% poison	10	2.43	188	3.28
	30	2.15	189	3.12
	60	1.85	190	2.94
	100	1.60	192	2.77

down to 1×10^{15} neutrons/cm^2·sec for a reactor power of 100 Mw. Previous calculations indicate that these thermal fluxes should provide virgin-neutron fluxes in the neighborhood of 10^{15} neutrons/cm^2·sec. However, wall power densities were several hundred kilowatts per liter.

7.4 MATHEMATICS AND COMPUTATION

An Oracle code was written for calculating the steady-state fuel costs in one-region thorium breeder reactors, taking into consideration the concentration of U^{233}, U^{234}, U^{235}, U^{236}, Th^{232}, Pa^{233}, and fission-product poisons. The variable parameters which were considered were reactor diameter, thorium concentration, reactor power level, fraction poisons, and nuclear values.

A two-group, multiregion Oracle code for spherical thermal reactors was completed. Reactor composition is arbitrary in that the critical fuel concentration can be obtained in any region of the reactor, given the composition of the other regions. Flux distributions and wall power densities are readily obtained.

An Oracle code was written for converting Oracle numerical results to graphical results. This code effectively normalizes all values and plots them on the Oracle Curve Plotter as discrete points. If enough points are plotted, a smooth curve is obtained.

Part III

ENGINEERING DEVELOPMENT

J. A. Lane

8. DEVELOPMENT OF FUEL-SYSTEM COMPONENTS

I. Spiewak

J. S. Culver
C. H. Gabbard
P. G. Herndon
E. C. Hise
P. P. Holz
J. C. Moyers
D. L. Snyder

8.1 20-cfm CANNED-MOTOR BLOWER

Excessive wear during initial operation of the 20-cfm canned-motor blower was determined as having been caused by improper assembly of the bearing-supply O-ring seals. After the worn bearings were replaced, the blower circulated air at atmospheric pressure for 100 hr and then a nitrogen and steam mixture at 500 psi and 150°C for 116 hr and at 1000 psi and 170°C for 66 hr. Termination of the 1000-psi run was necessitated by a leak in the top plug seal of the blower. No measurable wear occurred during any of the runs after the bearings were replaced. The blower was reassembled and a long run was started; during this run the bearing wear will be measured.

8.2 LARGE CIRCULATING PUMP

Specifications were issued to vendors for a 4000-gpm top-maintenance circulating pump, which will serve as a prototype for large homogeneous reactor pumps. Several satisfactory proposals for this pump were received, and an order will be placed within the next quarter.

The top-maintenance feature permits removal of all working parts from a large top closure, leaving the pressure housing of the pump permanently installed in the piping system. Pump maintenance can be simplified thereby because the radiation level will be much less at the closure than at the lower portion of the pump. Another feature of this pump will be the special measures taken to eliminate entry of process fluid into the motor and bearing regions. The general pump design will be similar to that of pumps used to circulate pressurized-water reactor coolant.

8.3 STELLITE RECIPROCATING FEED PUMP[1]

A test loop has been built and operated to test a controlled-leakage Stellite-piston feed pump (Fig. 8.1). The pump consists of a Stellite No. 3 piston and cylinder with close clearances serving as the high-pressure seal. The piston leakage is collected and is routed back to the low-pressure reservoir by a gas purge, so that there is no fluid leakage to the outside. The pump has been operated for 167 hr on distilled water, pumping 1.2 gpm at 500 psi. During this time the leakage rate has increased steadily from 260 to 960 cc/min. Tests are planned with piston ring seals and with uranyl sulfate as the pumped solution.

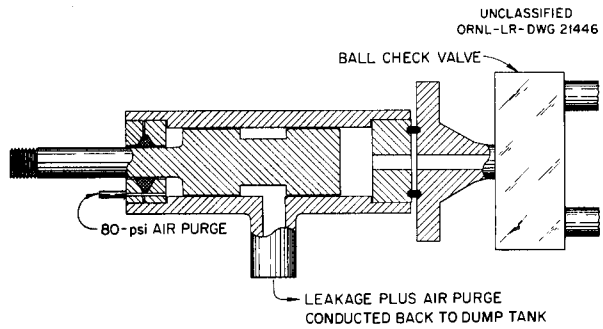

Fig. 8.1. Experimental Stellite Pump (2.5-in. Bore; 1.25-in. Stroke).

8.4 OXYGEN COMPRESSOR

Two high-pressure oxygen compressors have been received and operated. One of these (Fig. 8.2), manufactured by Pressure Products Industries, Inc., of Hatboro, Pennsylvania, has a water-actuated diaphragm and is capable of compressing 0.25 or 0.9 scfm of oxygen to 2500 psi with suction pressures of 250 and 500 psi, respectively. This compressor is presently being used to supply oxygen to the HRT mockup.

The other compressor, manufactured by Harwood Engineering Co., Inc., of Walpole, Massachusetts, uses the hydraulic intensifier principle and compresses the oxygen with water-actuated pistons. This unit was designed for an output of from

[1] C. B. Graham *et al.*, *HRP Quar. Prog. Rep. July 31, 1953*, ORNL-1605, p 60.

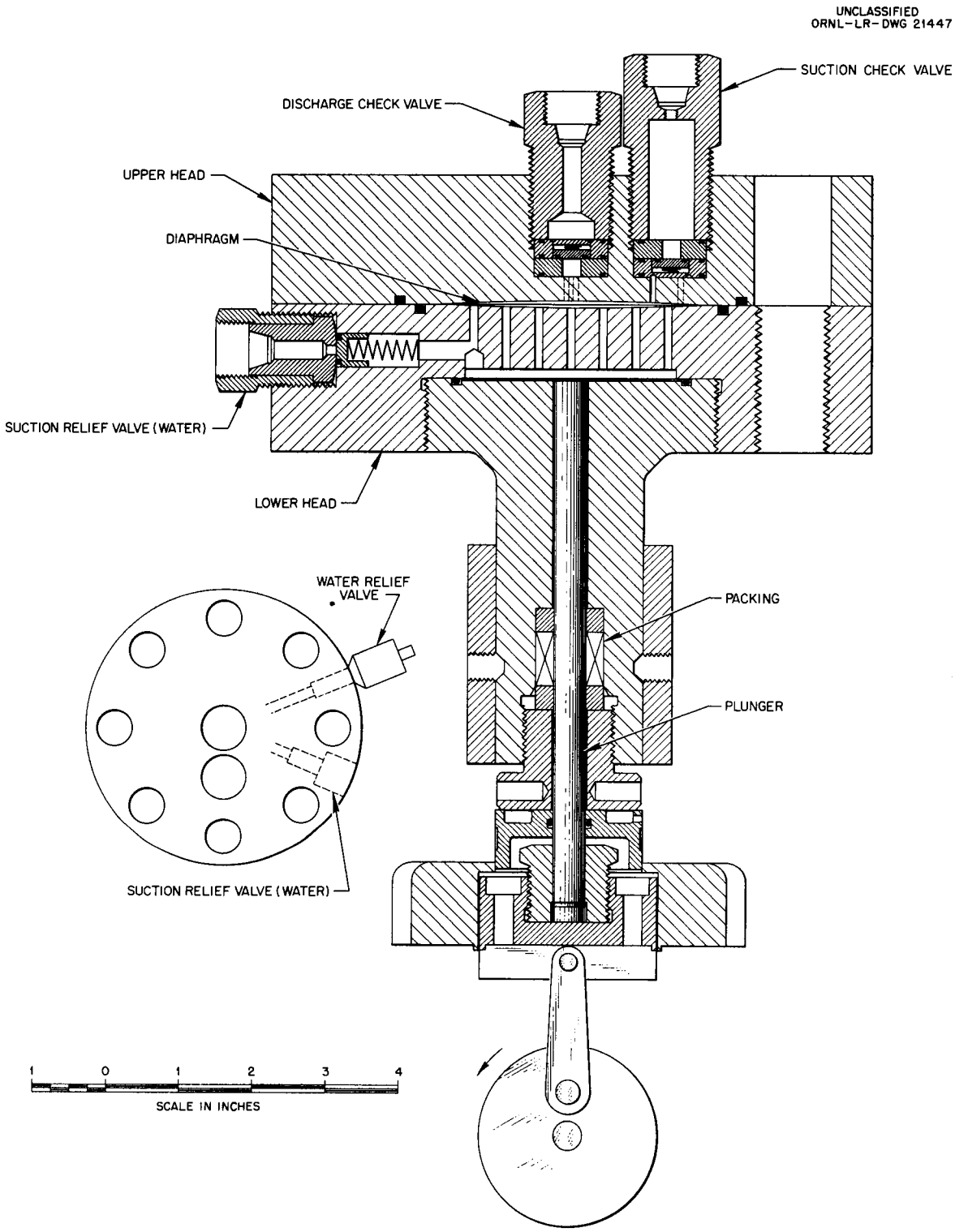

Fig. 8.2. Oxygen Compressor.

6 to 10 scfh, but the operation has been unsatisfactory to date because of faulty check-valve operation and water-component corrosion.

8.5 TITANIUM PROGRAM

The Crane Company received the titanium liners for the 3½- and 20-in. pipe order, but returned them to their supplier for improvement of dimensional tolerances. The Pfaudler Co., after rejecting a second batch of titanium tubing for failing to pass the hydrostatic test, placed another tubing order for the small heat exchanger. Some titanium 110-AT pipe and caps have been ordered for construction of a boiling uranyl sulfate pressurizer for a 400A test loop.

8.6 HIGH-PRESSURE STEAM BOILER FACILITY[2]

Design of the test facility for thermal cycling of reactor components between 380 and 580°F was completed during the report period, and material orders were placed. The Besler high-pressure steam generator, which will supply the needed heat, is undergoing factory tests and should be delivered in May. The feed-water deaerator should be received at about the same time.

8.7 REMOTE MAINTENANCE

A literature survey has been made[3] covering eight different types of power reactors in order to ascertain maintenance philosophies and problems associated with each reactor type. It was emphasized in most designs that a basic maintenance philosophy should be developed early in the plant-layout design stage, since in most cases there are no predecessors upon which the design may be based.

The successful maintenance of most power reactors, especially the circulating-fuel type, depends heavily upon the use of remote tools and techniques for the disassembly and repair of faulty components. Although many of these tools, such as remote automatic-welding and inspection devices and manipulator-operated small tools, are in only the developmental stage, studies by reputable machinery firms have indicated the feasibility of their design and use.

8.8 HEAT-EXCHANGER TUBE-JOINT TESTS[4,5]

Six tube-joint test units were thermally cycled up to 400°F in a boiling shell-side environment containing 100 ppm Cl^- and 50 ppm O_2. Three of the units were exposed for 500 hr and three for 1000 hr. Special features of the tube joints included nickel plating of the tubes and counterbored holes in the tube sheet. No obvious failures resulted during this testing; metallographic examination will be carried out to determine whether any corrosion damage occurred.

[2] C. B. Graham *et al.*, *HRP Quar. Prog. Rep. July 31, 1956*, ORNL-2148, p 50.

[3] B. D. Draper, *Maintenance of Various Reactor Types*, ORNL CF-57-4-92 (April 8, 1957).

[4] I. Spiewak *et al.*, *HRP Quar. Prog. Rep. Oct. 31, 1956*, ORNL-2222, p 52–53.

[5] I. Spiewak *et al.*, *HRP Quar. Prog. Rep. Jan. 31, 1957*, ORNL-2272, p 59–60.

9. DEVELOPMENT OF REACTOR SLURRY SYSTEMS

R. B. Korsmeyer

D. G. Davis
H. L. Falkenberry[1]
R. B. Gallaher
C. H. Gibson
A. S. Kitzes
C. G. Lawson
I. M. Miller
C. S. Morgan
R. H. Nimmo
L. F. Parsly
M. Richardson
A. N. Smith
D. G. Thomas
C. F. VandenBulck[2]
R. P. Wichner

9.1 THORIUM OXIDE PARTICLE-SIZE REDUCTION

Circulation of thorium oxide slurries in test loops brings about a reduction[3] of the mean particle size until it is in the region of 0.3 to 0.5 μ. Reduction to this size is accomplished in times up to the order of hundreds of hours, and reduction below this size is very slight (or slow) in any apparatus which is being used at the present time.[3,4] Loop tests have shown that rapid initial corrosion is eliminated if a pumped slurry is used as a charge material.[5,6]

Since pumping of the thorium oxide for purposes of size reduction is onerous and time-consuming, alternate methods of reducing the particle size of thorium oxide powders prior to their use in experimental equipment are being investigated. The results obtained[7] with several different wet and dry grinders are summarized in Table 9.1. Of the machines listed in the table, the Mikro-Pulverizer is considered to be the most satisfactory from the standpoint of achieving minimum-size particles. The maximum amount of iron pickup with this machine was 25 ppm, based on the ThO_2, with the 1600°C-fired oxide. Further tests are being conducted to determine the most satisfactory method of Mikro-Pulverizer operation. The program is being continued by testing other wet and dry grinding machines.

9.2 DISINTEGRATION OF THORIUM OXIDE CAKES

A method of comparing thorium oxide cakes has been developed in which the ease of resuspension of cake by agitation in water is measured. In the method small pieces of cake (3 to 4.5 g of $\frac{1}{8}$- to $\frac{1}{4}$-in. pieces) plus 35 ml of distilled water are shaken for 2 hr on a mechanical shaker in a 50-ml sample bottle. After shaking, the contents are poured onto a 10-mesh sieve and washed with distilled water. The results can be put on a quantitative basis by measuring the ratio of the weight of cake on the sieve to the initial weight. The cake resuspension index, which increases with increasing resistance to resuspension, is equal to ten times this value. Results were reproduced within $\pm\frac{1}{2}$ unit in duplicate determinations.

Measurements on cakes from the BS, T, S, and 200A loops and the slurry blanket test system are given in Table 9.2. It will be noted that the 200A-3 cake which has been dried at 110°C has a resuspension index of 4, as compared with 9 for similar cake that was never allowed to dry. Cake that had dried completely tended to disintegrate on rewetting. Disintegration was reduced by gradually submerging the cake in water. Cake from the BS-11 return line, which had dried, partially disintegrated on wetting, resulting in an apparent low resuspension index. These tests indicate that the "cake" from the slurry blanket test was essentially an accumulation of soft slurry, which could be relatively easily resuspended.

9.3 SLURRY RESUSPENSION VELOCITY

Analysis of the action of the hydrodynamic forces which can bring about the resuspension of settled beds is complicated because the beds may

[1] On loan from TVA.

[2] On loan from Union Carbide Nuclear Co.

[3] D. E. Ferguson *et al.*, *HRP Quar. Prog. Rep. Jan. 31, 1956*, ORNL-2057, p 116; *Oct. 31, 1955*, ORNL-2004, p 179.

[4] L. F. Parsly, Jr., H. L. Falkenberry, and I. M. Miller, *Report of Slurry Blanket Test Run SM-2*, ORNL CF-57-4-87 (April 29, 1957).

[5] A. S. Kitzes *et al.*, *1. Summary of Runs, S-56, 57, 73, 74, 78, 79, 80, 87, 88, 89 in Which Slurries Circulated at 300°C in 100-A Loops Caked or Accumulated on Pipe Walls. 2. Summary of Runs T-52 Through T-75 in Which a Bypass Line Was Used in Parallel with Main Circulating Loop*, ORNL CF-56-11-131 (Nov. 16, 1956).

[6] E. L. Compere *et al.*, *HRP Quar. Prog. Rep. Oct. 31, 1956*, ORNL-2222, p 88.

[7] R. M. Summers and D. G. Thomas, *Progress Report on Thorium Oxide Particle Size Reduction*, ORNL CF-57-4-76 (April 16, 1957).

Table 9.1. Summary of Thorium Oxide Particle-Size-Reduction Tests

Machine Tested	Oxide Designation	Firing Temperature (°C)	Particle-Size Analysis			
			Before Test		After Test**	
			D_{pmw}* (μ)	Standard Deviation	D_{pmw}* (μ)	Standard Deviation
Waring Blendor	LO-7	800	3.0	3.0	1.6	3.1
Rapasonic homogenizer	LO-7	800	3.0	3.0	1.5	2.5
Colloid mill	LO-7	800	3.0	3.0	1.5	2.7
Mikro-Pulverizer	LO-7	800	3.0	3.0	0.9	2.0
Mikro-Pulverizer	LO-7	1000	2.9	2.7	1.2	2.1
Mikro-Pulverizer	LO-7	1600	4.1	2.2	2.2	2.6

*Mean particle diameter on a weight basis.

**Tests were continued until a doubling of the time of treatment gave less than a 20% reduction in mean particle diameter. The mean diameters reported represent the maximum reduction obtained.

Table 9.2. Cake Resuspension Determinations

Cake Sample	Oxide	Additives During Circulation	Remarks	Cake Resuspension Index
T-86, impeller	LO-5	None	Fresh cake	9
T-86, pump scroll	LO-5	None	Fresh cake	9
200A-3	D-35	800 ppm SO_4	Cake never dried	9
BS-12, suction line	LO-14	3000 ppm SO_4 as $Th(SO_4)_2$	Fresh cake	8
200A-9	LO-12 and 13	800 ppm SO_4	Cake had dried	7
S-96, impeller	LO-5	None	Fresh cake	7
T-85, dischorge line	LO-5	$Al_2(SO_4)_3$ (Al = 300 ppm)	Cake had dried	7
BS-12, discharge line	LO-14	3000 ppm SO_4 as $Th(SO_4)_2$	Fresh cake	6
S-96, discharge line	LO-5	None	Fresh cake	4
200A-3	D-35	800 ppm SO_4	Air-dried at 110°C	4
BS-11, return line	LO-14	3000 ppm SO_4	Cake dried, disintegrated an wetting	2
Slurry blanket	Mixed LO		Cake had dried	½

have formed from either a flocculated or deflocculated suspension. The particles in a bed settled from a deflocculated suspension form a dense closely packed array that is resuspended one particle layer at a time.[8] The particles in a bed settled from a flocculated suspension form a loosely packed array from which clusters of particles are removed by shear forces.[8]

Preliminary data[9] on the resuspension of flocculated thorium oxide slurry are shown in Fig. 9.1. The first three of the five types of flow listed in the literature for deflocculated systems[10] were observed as indicated in the figure.

[8]H. R. Kruyt, *Colloid Science*, vol 1, p 355 ff, Elsevier, New York, 1952.

[9]D. G. Thomas, *Atmospheric Pressure System for Determining Resuspension Velocity of Thorium Oxide Slurries in Round Horizontal Pipes*, ORNL CF-56-10-136 (Oct. 10, 1956).

[10]D. M. Newitt *et al.*, *Trans. Institution Chem. Eng.* 33(2), 93–110 (1955).

A loop containing several 10-ft sections of glass pipe has been constructed (see Fig. 9.2), and resuspension velocities will be determined, together with measurements of the properties of the settled beds for different slurries at different concentrations.

9.4 SLURRY RHEOLOGY

A vertical-tube viscometer has been designed to determine the rheological properties of thorium oxide slurries at temperatures up to 200°C and at pressures up to 300 psig.[11] These conditions were selected to permit fabrication from standard materials (e.g., sched-40 stainless steel pipe fittings and commercially available agitator shaft seals) and to employ common instrumentation and measuring techniques. The tubes are positioned vertically to overcome difficulties due to the settling of solids at low flows.

[11]R. H. Nimmo, *Vertical Tube Viscometer for Slurries*, ORNL CF-57-4-86 (April 29, 1957).

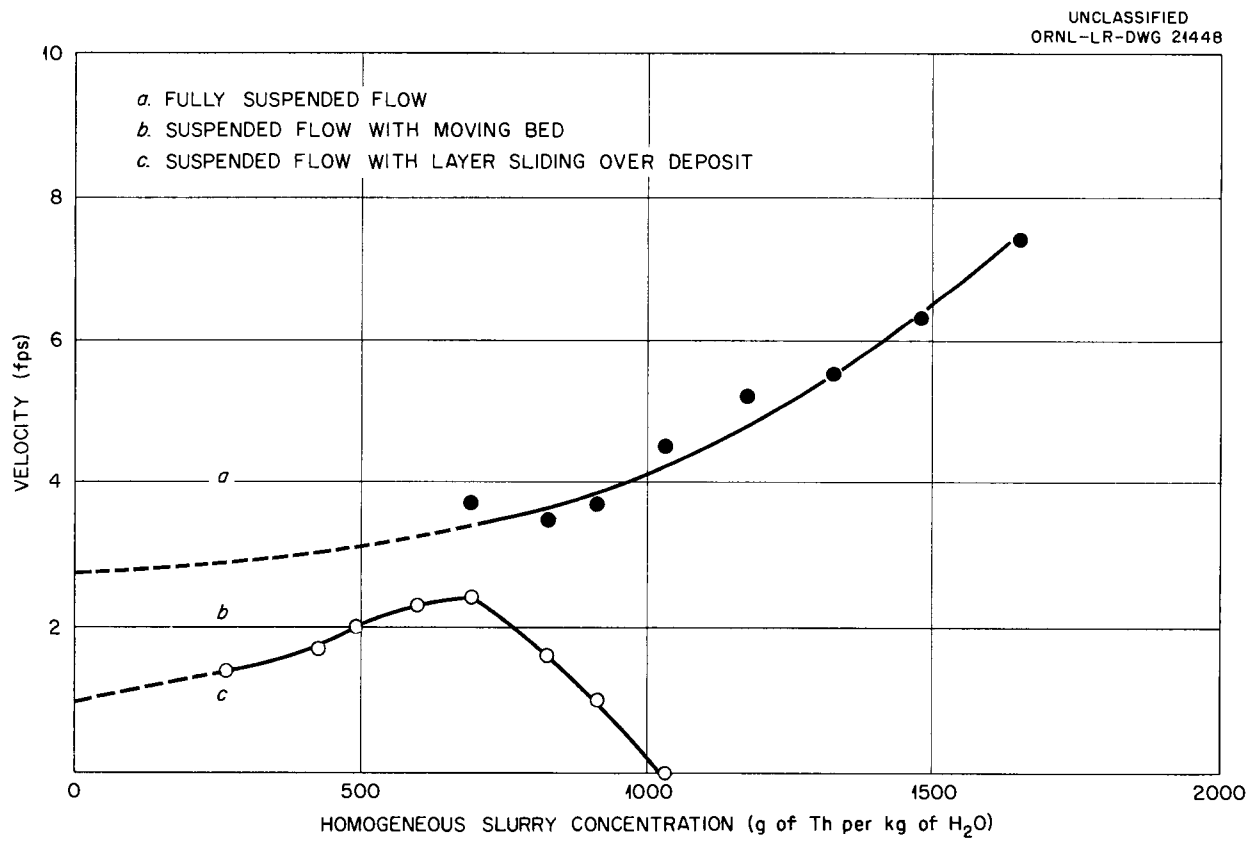

Fig. 9.1. Types of Flow for Aqueous Thorium Oxide Suspensions in ¾-in.-ID Glass Pipe.

Fig. 9.2. Slurry Resuspension Velocity Loop.

Figures 9.3 and 9.4 are schematic flowsheets illustrating two means of determining slurry flow rates and pressure drops at elevated temperatures and pressures, namely: the cooler-sample system and the pressurized receiver system. The cooler-sampler system will be tested first. The jacketed slurry feed tank with its two special drain valves, the two jacketed viscometer tubes of the same internal diameter but of different lengths, and the systems for the two temperature-control media (steam and water) are common to both systems. The slurry feed tank is essentially a blow-case,

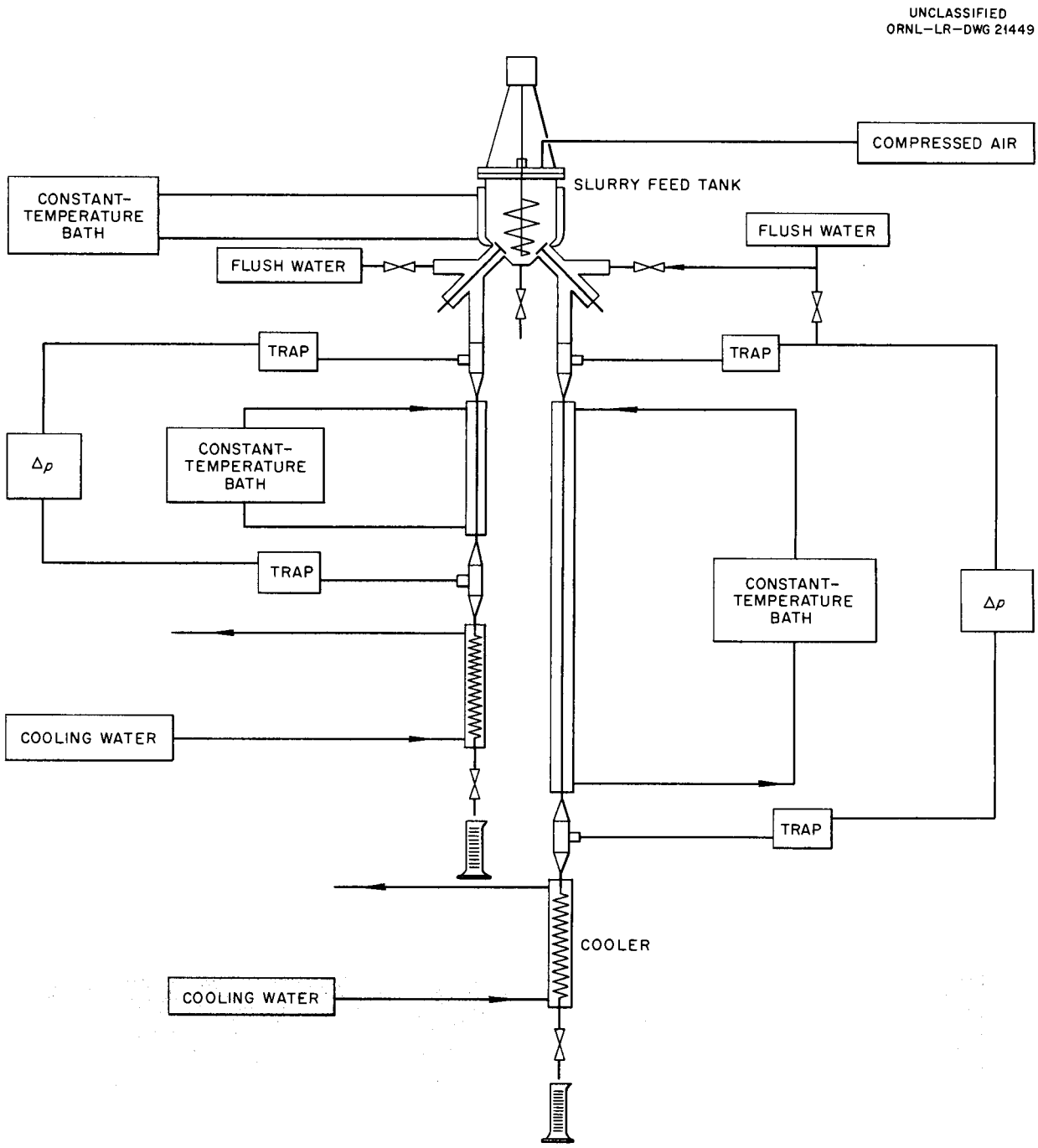

Fig. 9.3. Vertical Tube Viscometer, Cooler-Sampler System.

and in both systems the gas pressure applied above the slurry is automatically controlled.

In the cooler-sampler system hot slurry from the viscometer tube passes through a capillary-tube cooler and a needle valve and is collected in a graduated cylinder at atmospheric pressure. This system is simple, but its accuracy depends upon ability to maintain constant pressure drops across the tubes by needle-valve control.

In the pressurized receiver system, however, the pressure drops are always held constant because the viscometer tubes terminate in receiver vessels which are maintained at a constant gas pressure. Slurry samples are collected for timed

UNCLASSIFIED
ORNL—LR—DWG 21450

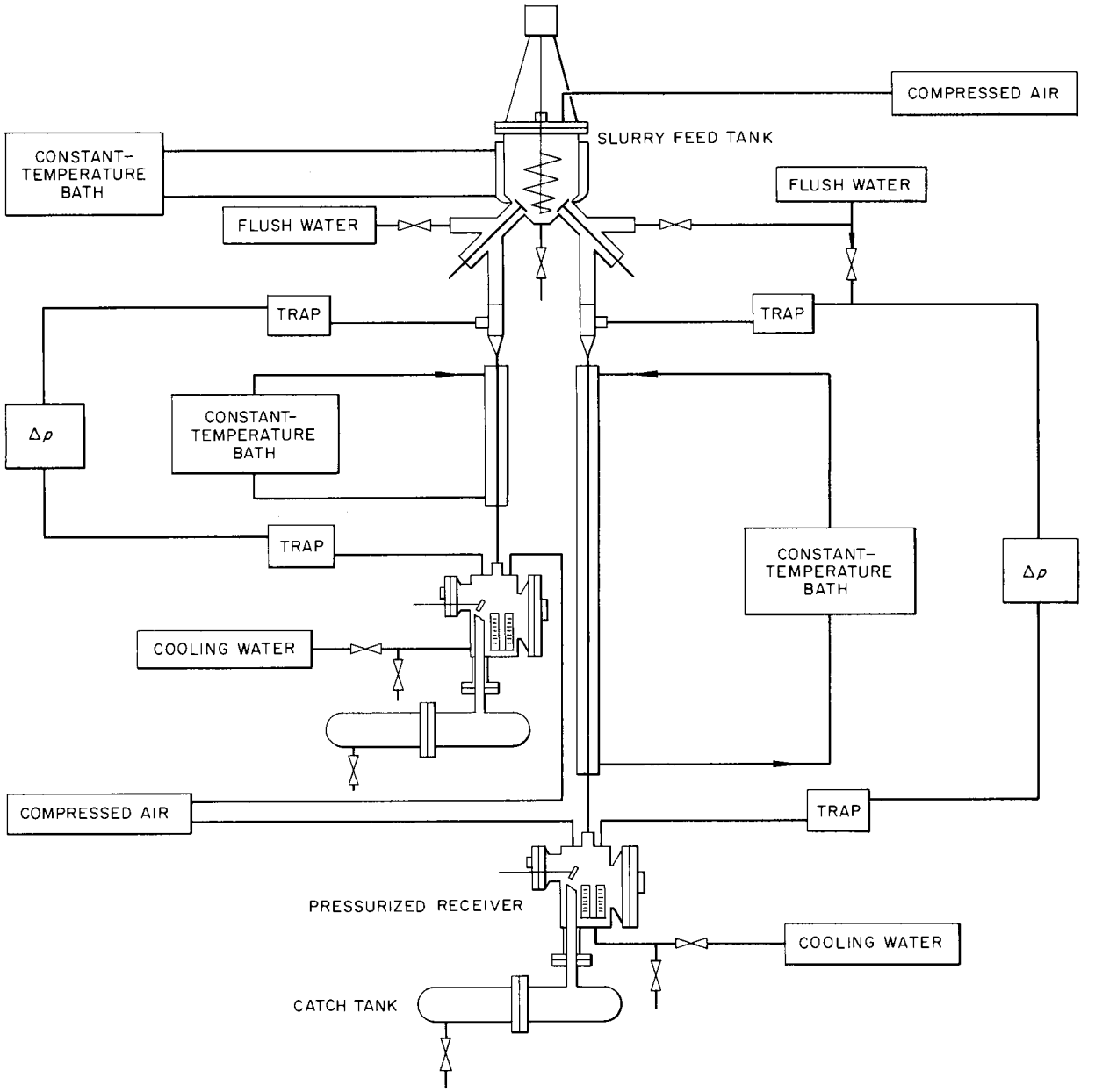

Fig. 9.4. Vertical Tube Viscometer, Pressurizer-Receiver System.

intervals in one of six weigh cylinders, which may be alternately positioned beneath the viscometer tubes. Each receiver is equipped with a movable flow-deflector tube so that all slurry flowing before and after the test period, as well as any flush water, is directed to a standpipe for the catch tanks. Before the samples are removed for external weighing, they are cooled by half-filling the receiver vessel with cold water. These operations may be observed through a sight port in the door of the receiver vessel.

9.5 CIRCULATING-SLURRY BEHAVIOR

During the quarter, run 200A-11 was initiated in the 200-gpm loop to determine the handling characteristics of an admixed thorium-uranium oxide slurry at 300°C and the maximum slurry concentration capable of being circulated in the 200A loop system and to gain experience with improvements in gamma-scanning technique. The loop was initially loaded to give a circulating concentration of 1000 g of thorium per kilogram of water, 0.5% uranium as $UO_3 \cdot H_2O$, 3000 ppm of sulfate as thorium sulfate, and 500 ppm of oxygen. Analyses of samples withdrawn agreed with the calculated concentration. The uranium and sulfate additions were based on the thorium oxide content of the slurry.

The initial charge of slurry was circulated at 300°C and 2000 psig for 890 hr before the first addition of fresh slurry was made. During this period the generalized loop attack averaged 0.8 mpy after the first 100 hr of operation, based on the iron contamination found in the slurry. The solids were examined microscopically for formation of spheres, but none were evident. Particle-size determinations from settling-rate measurements showed that after 37 hr of circulation the particles were degraded so that 50% of them were less than 1 μ.

The concentration was increased over the next 910-hr interval by incremental additions of 7 to 10 kg of unpumped, sulfated thorium oxide, up to a total increase of 55.5 kg, the sulfate content being maintained at the 3000-ppm level. Increasing the concentration did not appear to affect the operation of the loop until the calculated concentration of the circulating stream reached about 2000 g of thorium per kilogram of H_2O. However, samples withdrawn downstream of the pump never exceeded 1600 g of thorium per kilogram of H_2O by analysis. Although some of the inventory unaccounted for was undoubtedly lodged in the pressurizer, a complete accounting is not possible until the loop is shut down.

With each oxide addition the following two events were observed:

1. Fluctuations appeared in the wattmeter trace and then disappeared after 50 hr of continued circulation at 300°C.
2. The slurry-water interface in the pressurizer rose, indicating that some of the slurry had migrated to the pressurizer. The interface could usually be lowered by decreasing the loop and pressurizer temperature.

Within a few hours after the last addition of 10 kg of oxide, the pump power decreased suddenly and the purge-water flow to the back of the pump ceased, indicating that the slurry was not moving through the loop. The sampled concentration at this time was 1600 g of thorium per kilogram of H_2O. Slurry was withdrawn from the loop and replaced with water to regain circulation, and normal operating conditions were re-established except for the large fluctuations in the pump power, which did not disappear until the concentration was further reduced to 1300 g of thorium per kilogram of H_2O (by analysis).

There was no change in the generalized loop attack or the particle-size distribution as a result of the increase in slurry concentration. The attack was still found to be less than 1 mpy, and the particles appeared to be well dispersed when examined microscopically. From sedimentation data about 50% of the particles were less than 1 μ in size. There was no evidence of sphere formation.

During the reduction in slurry concentration from the maximum, some indication of nonhomogeneous flow was picked up with the gamma scanner. In the concentration range of 1400 down to 800 g/kg, there appeared to be a denser region along the bottom ½ in. of the pipe. This region was not detected in the gamma scans made earlier in the run during the concentration buildup.

To date a total of 2100 hr of operation has been accumulated, and the run is still in progress. In general, it can be concluded that the handling characteristics and the generalized attack rate at 300°C for the sulfated thorium–½% uranium oxide slurry are similar to those for the sulfated thorium oxide slurry. No trouble was encountered in

starting up after several forced shutdowns at concentrations of about 1000 g of thorium per kilogram of H_2O. In two instances, when the rupture disk failed, violent boiling and loss of water occurred and the system was vented each time from 2000 psi to atmospheric pressure. The flowmeter readings, corrected for density, agreed with calculated pump performance when the concentration was below 1400 g/kg. Above this concentration the readings were very erratic.

9.6 HRT BLANKET SYSTEM DEVELOPMENT

In the blanket test system the first slurry run with the blanket vessel in the circuit (SM-2) continued for a total of 1730 hr, at which time a leak through a sample flange on the blanket vessel necessitated a shutdown.

Figure 9.5 shows the system temperature, flowmeter reading, pump power, and concentration from 1300 hr to the end of the run. Between 1300 and 1400 hr an experiment was run in which the temperature was increased in three steps from 176 to 200°C. It is evident that a loss of oxide from the circulating stream occurred when the temperature was increased first to 194 and then to 200°C. On cooling to 176°C, the circulating concentration increased to 200 g of thorium per kilogram of H_2O, as compared with the calculated value of 500 g of thorium per kilogram of H_2O, and remained at this value for the remainder of the run.

The pump was stopped twice during the report period, at 1405 hr for 5 min to sample the dense bed in the bottom of the blanket and at 1691 hr for 43 min to observe the change in bed density with time immediately following flow stoppage. Figure 9.6 shows the results of this settling test. The data do not indicate whether a high-density bed existed through which channels were cut by the stream or whether the high-density material resulted from rapid settling after the pump was stopped.

The gamma surveys made during the latter part of the run indicated the presence of high-density material near the top of the blanket as well as in the bottom. When the pump was stopped, the scans indicated that this material settled rapidly.

When the run was terminated, an attempt was made to discharge the inventory through the letdown valve. A small quantity was released, but the valve plugged in a few minutes with concentrated slurry. The dump system was then used, and the dump was finally completed approximately 5 hr after the pump was stopped. During the dump it was necessary to stop temporarily to decant excess water added to cool the slurry.

Inspection ports on the vessel were then opened, and a slurry bed approximately 13 in. deep was found in the bottom of the blanket (Fig. 9.7). Above the bed a thin layer of dried slurry remained on the metal surfaces. Figure 9.8 shows the top of the core. A few large lumps were found in the bottom of the core exit pipe, as seen in the photograph, and also on top of the horizontal section of the exit-pipe assembly. These lumps have been characterized as dried slurry rather than cake, inasmuch as they disintegrated on wetting.

After inspection the loop was refilled with water, run for 5 hr, and dumped. The slurry bed now appeared as shown in Figs. 9.9 and 9.10. Resuspension of the oxide occurred during the wash in the 90-deg sectors in front of the two nozzles, but the slurry in the sectors between 90 and 180 deg from each nozzle (relative to the direction of flow) appeared to be relatively undisturbed. A second rinse again removed a substantial amount of the slurry but left the two high piles still in place. The piled-up slurry was raked into the sectors immediately in front of the nozzles, and a third rinse then removed substantially all the slurry.

After the slurry was cleaned from the pressure vessel, the pump was removed and disassembled. The impeller was badly eroded, as shown in Fig. 9.11. The wear rings also were worn, and all bearing components except the rear journal showed moderate to severe wear. The history of the pump indicates that it was operated for a total of 5578 hr, of which 2114 hr was with slurry. During the total time, wear of the thrust bearing, of the lower radial bearing, and of the upper radial bearing amounted to 0.059, 0.040, and 0.004 in., respectively. Most of the wear occurred in the Graphitar parts of the bearings and during the

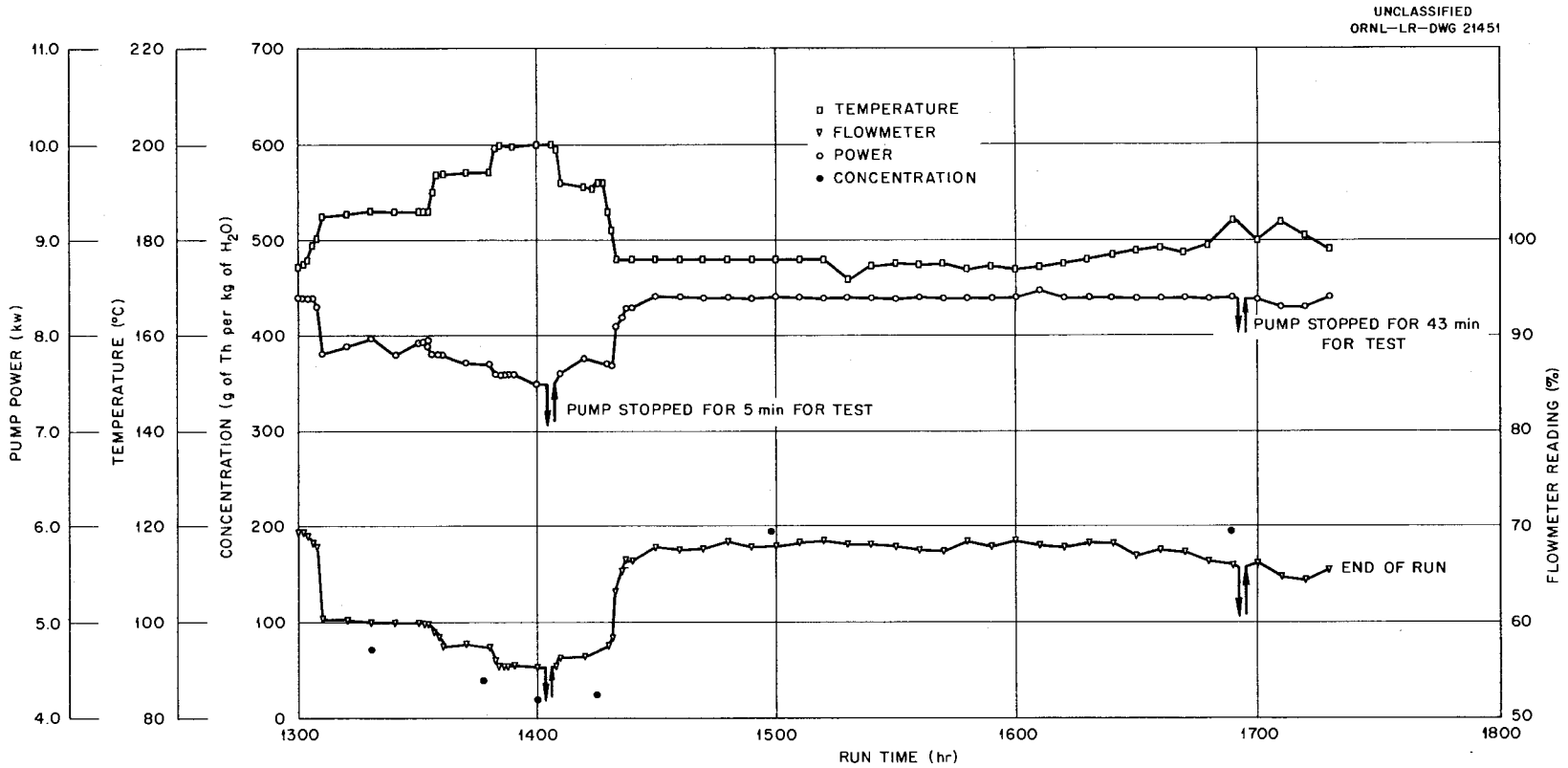

Fig. 9.5. Slurry Blanket Test, Variation of Temperature, Flow, Power, and Concentration with Time.

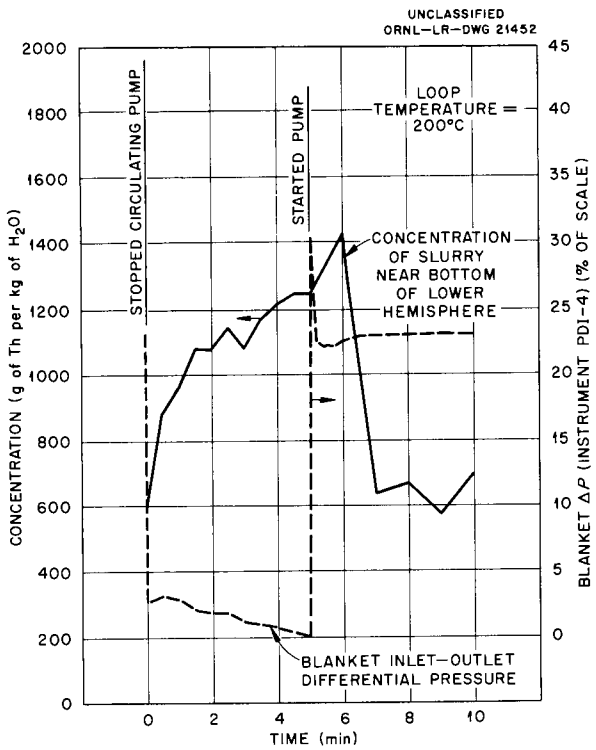

Fig. 9.6. Blanket Sphere Settling Test.

slurry runs. The pump impeller lost 133 g during the last 3385 hr of operation. In addition to the slurry attack, two factors may have contributed to the severe wear and erosion noted: one is generally low dissolved-oxygen concentration during the run, and the second is cavitation due to the relatively low overpressure (50 psi) used.

Attack similar to that on the impeller was found in the flow nozzle. From the attack on the nozzle it is estimated that light attack, characterized by slight ripples on the surface, occurred at 35 fps and that the severe erosive attack started at a velocity of 40 fps.

The rest of the system, except the pressurizer, was found to be in good condition. Since chloride ion was found to have accumulated in the upper part of the pressurizer during the run, an examination was made of the section from just below the vapor-liquid interface to the top to determine whether stress-corrosion cracking had occurred. After the oxide film was removed with grit cloth, apparent deep cracks (by dye-penetrant test) were found in the pipe wall located in the vapor phase, approximately 1 ft below the top. The upper 7-ft section of the pressurizer was cut off for metallographic examination, which showed that the defects were shallow grooves probably formed by tiny bubbles present in the ingot at the time the pipe was formed. There was no evidence of cracking.

A generalized corrosion rate during the final 1150 hr of operation calculated from the iron-to-thorium ratio was 0.95 mpy. The oxygen consumption, however, indicated a rate of at least 5 mpy, if it is assumed that all the oxygen was consumed in converting iron to Fe_2O_3. The discrepancy may be accounted for by assuming that corrosion products from the carbon-steel pressure vessel had remained on its metallized stainless steel surface. The porosity of the stainless steel protective layer was indicated by numerous rust spots.

The system is undergoing extensive repairs and modifications to improve both the circulation of slurry through the blanket vessel and the general operating characteristics of the system. The modifications include changing the inlet nozzles to increase the jet velocity, increasing the pump capacity from 230 to 300 gpm to obtain greater turbulence in the blanket, and installing more extensive sampling and gamma-survey facilities.

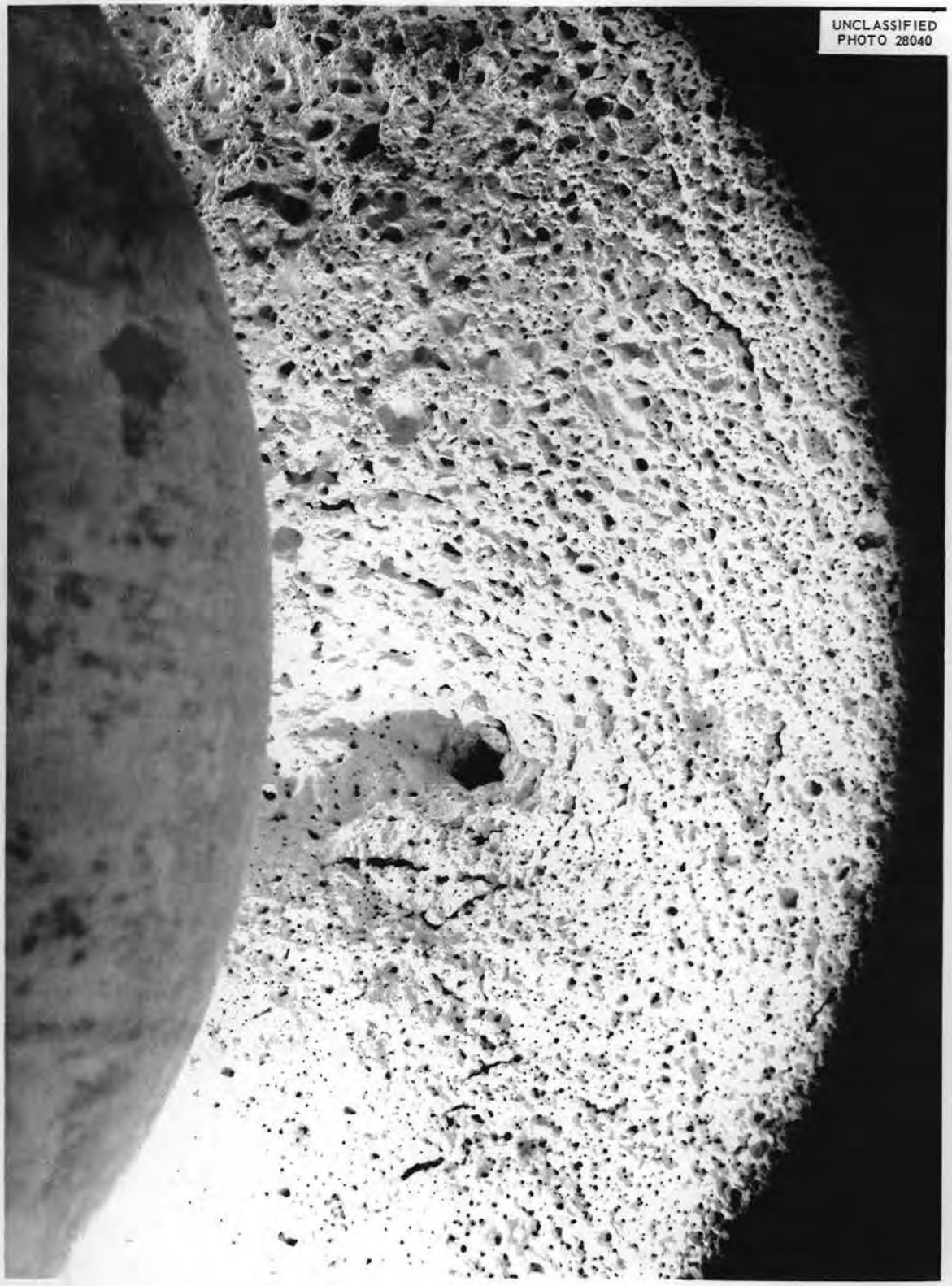

Fig. 9.7. View of Bottom of Blanket After Draining.

Fig. 9.8. Upper Part of Core Vessel and Exit Pipe.

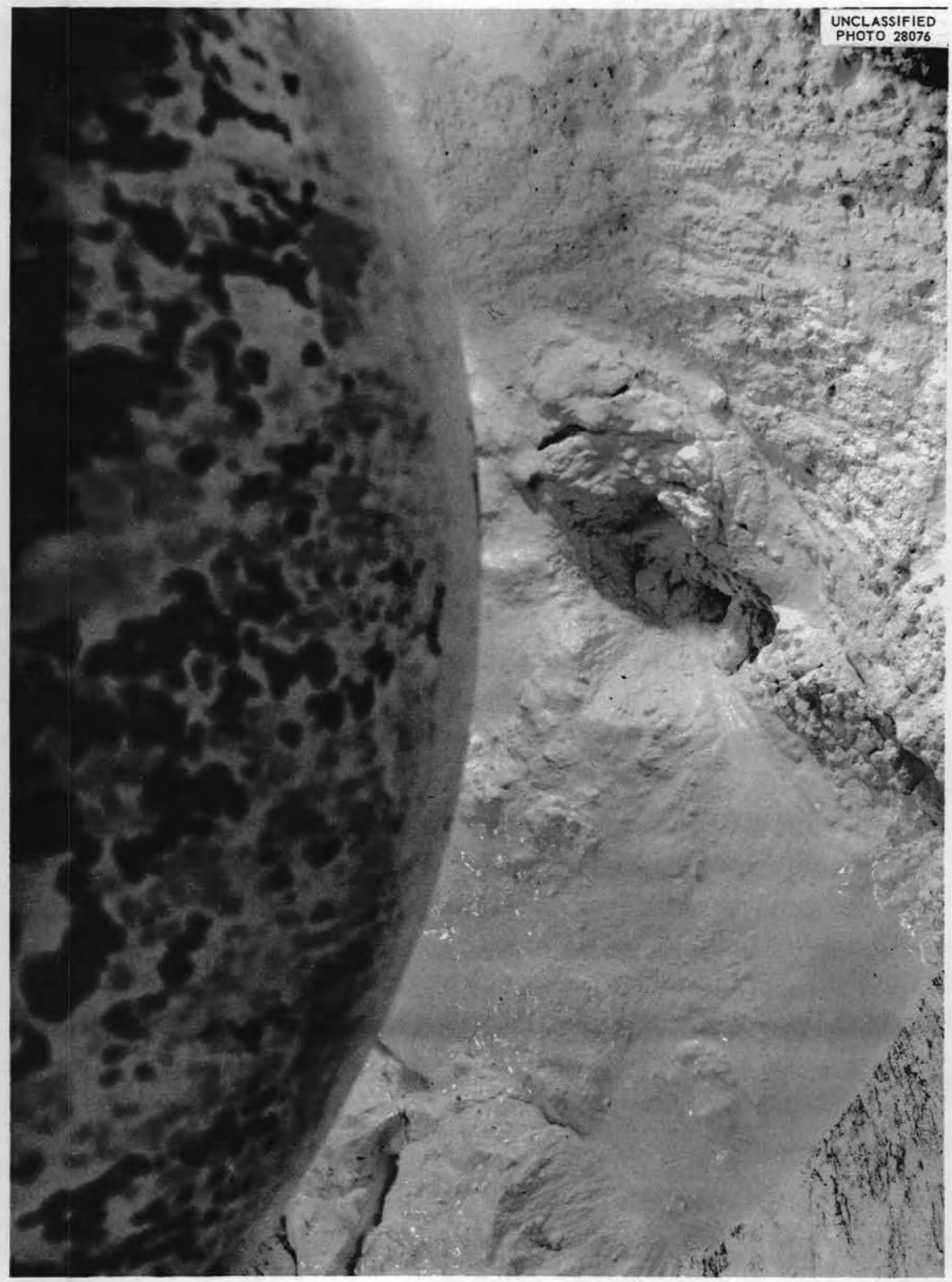

Fig. 9.9. View of Bottom of Blanket After First Wash.

Fig. 9.10. Lower Side of Blanket After First Wash.

UNCLASSIFIED
PHOTO 28223

Fig. 9.11. Slurry Blanket Test, Pump Impeller After Run SM-2.

10. INSTRUMENT AND VALVE DEVELOPMENT

D. S. Toomb

E. H. Bell A. M. Billings

10.1 INSTRUMENT DEVELOPMENT

10.1.1 Differential-Pressure Transmitters

The design of the differential-pressure transmitters used in the HRT[1] was improved for new units to be employed in the component-development programs. The new design (Fig. 10.1), by The Foxboro Company, eliminates the threaded strength joint, which was subject to galling, and the difficult weld which joined the pressure taps to the body block. Differential-pressure ranges from 50 in. of water to 50 psi may be varied by changing range springs. The lower range of approximately 50 in. of water may be further reduced to 25 in. by using a ½-mv/v sensitivity receiver.

[1]D. S. Toomb *et al.*, *HRP Quar. Prog. Rep. Oct. 31, 1955*, ORNL-2004, p 27.

10.2 VALVE DEVELOPMENT

10.2.1 Slurry Valves

A special valve incorporating an integral tap for flushing the valve sealing surfaces was designed for the vertical-tube viscometer facility. The valve, shown in Fig. 10.2, is not suitable for HRP reactor service, because it lacks a bellows seal and utilizes Teflon, which is not radiation resistant. However, the performance of the design will provide valuable developmental information.

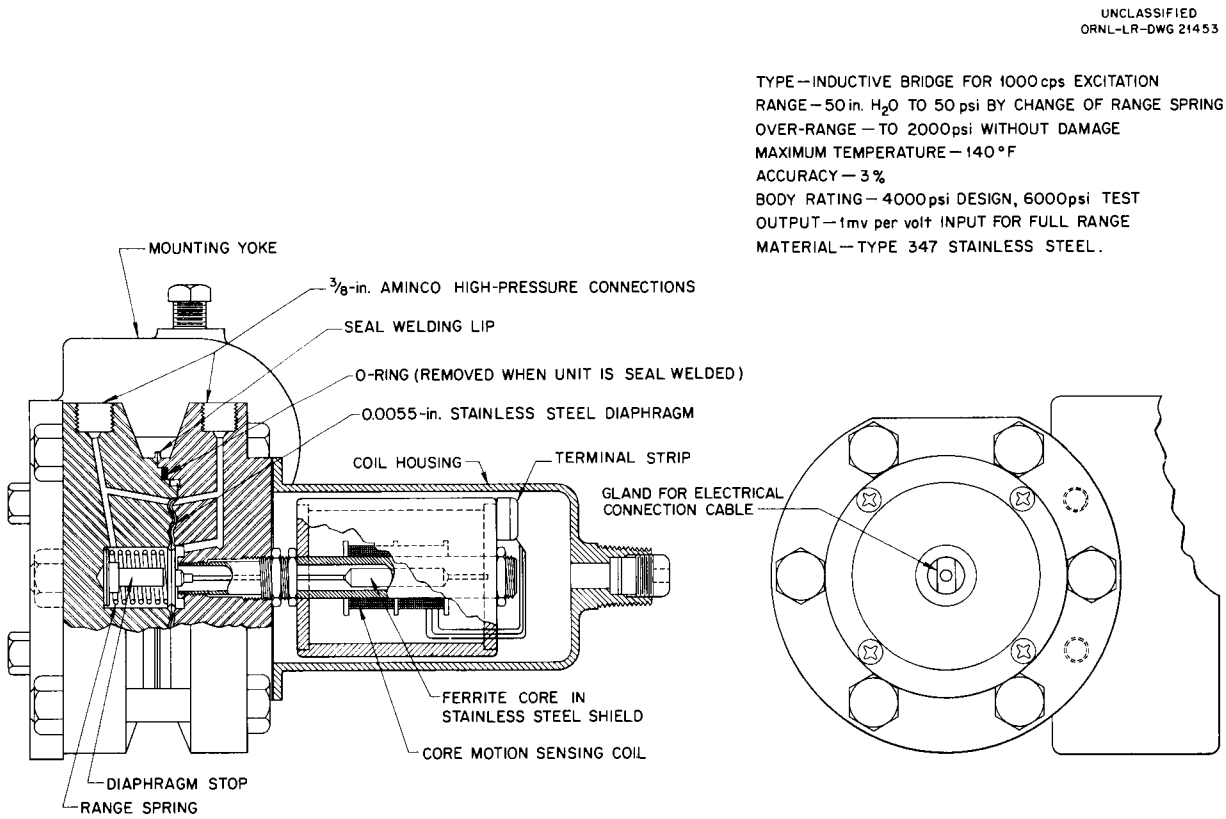

Fig. 10.1. Differential-Pressure Transmitter.

10.2.2 Valve Trim

Platinum-alloy-capped stainless steel valve plugs obtained from Baker and Company, Inc., Newark, New Jersey, are being tested in the valve test loop as part of the valve-trim-materials evaluation program.[2] The alloys available vary in hardness from Rockwell C-20 to C-30. After 400 "dumps" a plug capped with an 80% platinum, 20% iridium alloy hardened to Rockwell C-25 was found to be bubble-tight with 2000 psi of nitrogen gas applied under the seat. In other tests, however, the caps have become loose on the stainless steel bases, and the tests have been inconclusive. The fastening problem will be investigated.

[2] A. M. Billings, *HRP Experimental Valve Program*, ORNL CF-56-2-42 (Feb. 14, 1956).

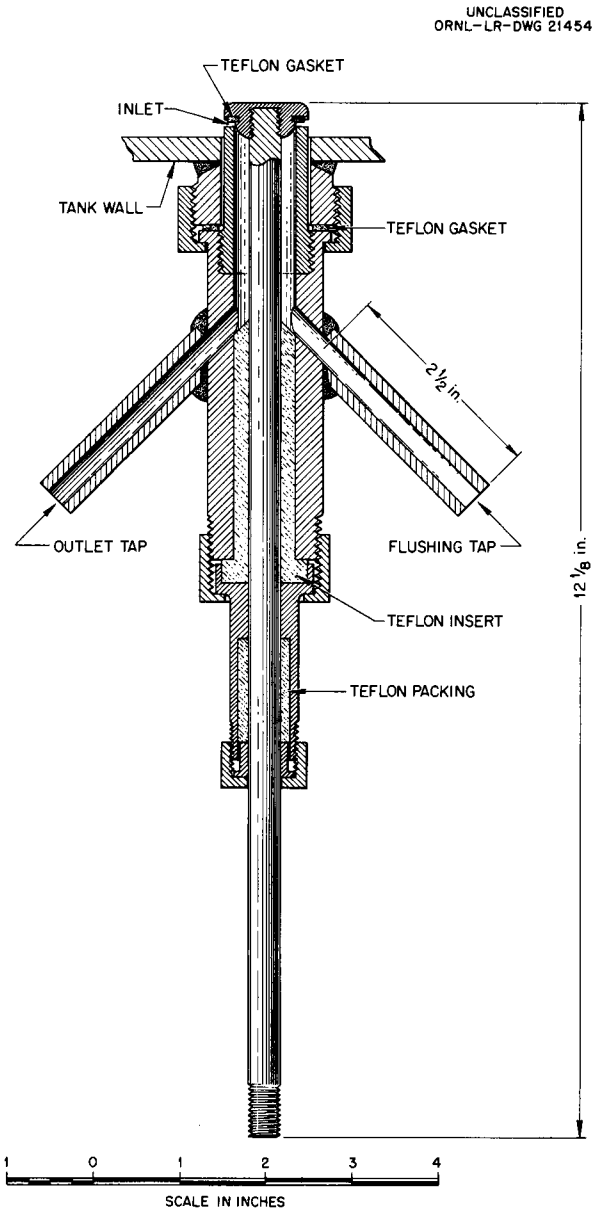

Fig. 10.2. Slurry Drain Valve.

Part IV

REACTOR MATERIALS RESEARCH

E. G. Bohlmann

11. SOLUTION CORROSION[1]

J. C. Griess H. C. Savage
S. R. Buxton D. N. Hess
J. L. English T. H. Mauney
R. S. Greeley P. D. Neumann
W. C. Ulrich

11.1 DYNAMIC CORROSION STUDIES

11.1.1 Third Operating Test of the HRT Core–Pressure-Vessel Flange and Transition-Joint Mockup

A third test of the mockup of the Zircaloy-2–stainless steel transition and expansion joint as used in the HRT reactor vessel has been made in 100A dynamic loop F. The first two tests were mentioned previously,[2,3] and detailed reports have been published elsewhere.[4,5]

Prior to assembly of the flanged joint after the second test, several components were inspected for cracks by the Super Pentrex postemulsified fluorescent-penetrant method. Two cracks or scratches, each about ¼ in. long, were found on the gasket mating surface of the lower 10-in. oval-ring flange. One small pit and two short cracks or scratches were revealed on the 10-in. oval-ring gasket. The gasket cracks or scratches were not related in position to the cracks or scratches on the flange. A 1-in.-long crack was also detected in the bellows–transition-piece circumferential weld. It should be noted that it is not possible to distinguish with certainty between cracks and scratches without metallographic examination, which would entail destruction of the specimen. However, additional inspections by the Super Pentrex method after future tests may show whether the cracks, if they are present, will propagate.

Following the Super Pentrex examination, the test unit was washed thoroughly with water and the flanged joint reassembled. The loop was filled with water to the desired volume and brought to 300°C, and then concentrated fuel solution was added to give a solution containing 0.04 *m* UO_2SO_4, 0.02 *m* H_2SO_4, and 0.005 *m* $CuSO_4$.

In order to determine whether the pitting attack observed in the first two tests[6] was caused by the mechanical action of the bellows, no mechanical deflections were made during the third test. However, thermal cycling was performed as before between 300°C at 1550 psig and 100°C at 100 psig.

The test lasted for only 293 hr, 126 hr on water and 167 hr on fuel solution. Twelve complete thermal cycles were made. The test was terminated when samples of the water from the interior of the bellows were found to contain uranium, which indicated leakage. The interior of the bellows was maintained at 45 to 50 psig below the pressure of the exterior of the bellows so that if leakage occurred through the bellows or past the transition joint, samples of the water from the interior of the bellows would contain uranium. However, after disassembly of the flanged joint, the bellows and transition joint were leak-tested with 50 psig of helium, and no leakage was detected. Therefore it is certain that the uranium in the bellows water came from carry-over of the fuel solution from the pressurizer into the condenser that supplied the bellows water and not from leakage through the bellows or past the transition joint. Another reason for terminating the test was that oxygen depletion occurred, and roughly half the uranium in the fuel solution precipitated. The uranium was redissolved by adding oxygen before the test was terminated.

Prior to disassembly the 10-in.-IPS 1500-lb test-vessel oval-ring joint was leak-tested at

---

[1] Reported in greater detail by J. C. Griess *et al.*, *Quarterly Report of the Solution Corrosion Group for the Period Ending April 30, 1957*, ORNL CF-57-4-55.

[2] H. C. Savage *et al.*, *HRP Quar. Prog. Rep. Oct. 31, 1956*, ORNL-2222, p 75–77.

[3] J. C. Griess *et al.*, *HRP Quar. Prog. Rep. Jan. 31, 1957*, ORNL-2272, p 77–79.

[4] T. H. Mauney *et al.*, *Operating Test of HRT Core Vessel Transition Joint and Expansion Bellows Mockup*, ORNL CF-57-1-68 (Jan. 31, 1957).

[5] R. S. Greeley *et al.*, *Second and Third Operating Test of HRT Core Vessel Transition Joint and Expansion Bellows Mockup*, ORNL CF-57-4-44 (to be issued).

[6] J. C. Griess *et al.*, *HRP Quar. Prog. Rep. Jan. 31, 1957*, ORNL-2272, p 78.

200 psig of helium with a mass-spectrograph-type leak detector. No leakage was observed. After disassembly of the joint and removal of the oval-ring gasket, examination of the flange grooves indicated no leakage of fuel solution into the grooves.

The pitted areas on the bellows[6] were examined closely by moving the reinforcing rings to reveal the entire crevice area between the rings and the bellows. A microscope-dial-gage indicator assembly was used again to measure the pit depths, and the measurements showed no increase in depth. However, the run was too short to allow a conclusion to be drawn as to the effect of mechanical deflections on the pits. Several of the pits broadened slightly, and numerous small new pits (less than 1 mil deep) were observed over much of the transition and bellows area, possibly because of oxygen exhaustion during part of the run.

The corrosion specimens in the loop and test unit were removed, scrubbed, and weighed. They were not defilmed but were replaced in the loop for further testing. All specimens showed zero or relatively low weight losses except the type 347 stainless steel coupon at 50 to 64 fps, which was partially above the critical velocity and corroded at an average rate of 22 mpy. No significant effect of stress, galvanic coupling, or crevice attack was noticed on visual examination of specimens.

For the first time since the test unit was constructed, the weld holding the transition joint in place was cut and the transition joint removed as a unit for examination. The joint itself was not disassembled and is shown in Fig. 11.1. The surfaces shown in the figure had been exposed to oxygen-containing distilled water at 100 to 300°C for 2900 hr and to approximately 0.001 *m* UO_2SO_4 for about 75 hr. The stainless steel surfaces were covered with a rough black film; the Zircaloy-2 surface was covered with a much smoother, more adherent black film; and the titanium surfaces showed bluish-green interference colors. Four type 347 stainless steel coupons exposed inside the bellows gained a slight amount of weight (as scrubbed).

The removal of the transition joint allowed the interior of the bellows to be inspected. Figure 11.2 is a photograph of the interior of the bellows after removal of the transition joint. No pits or cracks were found, although a deposit of a red oxide, identified as Fe_2O_3 by x-ray diffraction, on top of a heavy dark scale prevented detailed examination of the metal surface.

The bellows area between the top convolution and the top circumferential weld was radiographed with a radium source. The crack in the circumferential weld, detected by the Super Pentrex method discussed above, was detected in the radiographs. Also, a small void in the same weld showed up and the pits in the bellows[6] were detected. No other defects were apparent.

Following the above examination the transition joint was replaced and welded. Further testing of the bellows and transition joint to determine the cause of the pitting attack and to test the long-term reliability of the unit is planned.

11.1.2 Corrosion of Stainless Steel in Dilute Uranyl Sulfate Solutions Containing Beryllium Sulfate

The study of uranyl sulfate solutions containing equimolal beryllium sulfate was continued; 200-hr runs were made at 200 and 225°C with the solution used previously,[7] 0.04 *m* UO_2SO_4, 0.04 *m* $BeSO_4$, 0.005 *m* $CuSO_4$. The conditions of these runs are given in Table 11.1 (runs O-12 and O-13). The results showed that corrosion was much less at flow rates above 15 fps and no greater at flow rates less than 15 fps in the beryllium-containing solution than in the HRT solution (0.04 *m* UO_2SO_4, 0.02 *m* H_2SO_4, 0.005 *m* $CuSO_4$) at the same temperatures. Also, corrosion in the beryllium-containing solution was much less at 200 and 225°C than at 250 and 300°C. The lower amount of corrosion was predicted previously on the basis that the beryllium sulfate would be less hydrolyzed at the lower temperatures and therefore that the solution would be less acid and hence less corrosive.[8] Corrosion in the HRT solution, on the other hand, is greater at 200 and 225°C than at 250 and 300°C (ref 9).

The weight losses of type 347 stainless steel coupons are plotted in Fig. 11.3 and are compared with results obtained in the HRT solution. The

[7] J. C. Griess *et al.*, *HRP Quar. Prog. Rep. Jan. 31, 1957*, ORNL-2272, p 83.

[8] *Ibid.*, p 84.

[9] *Ibid.*, p 79–80.

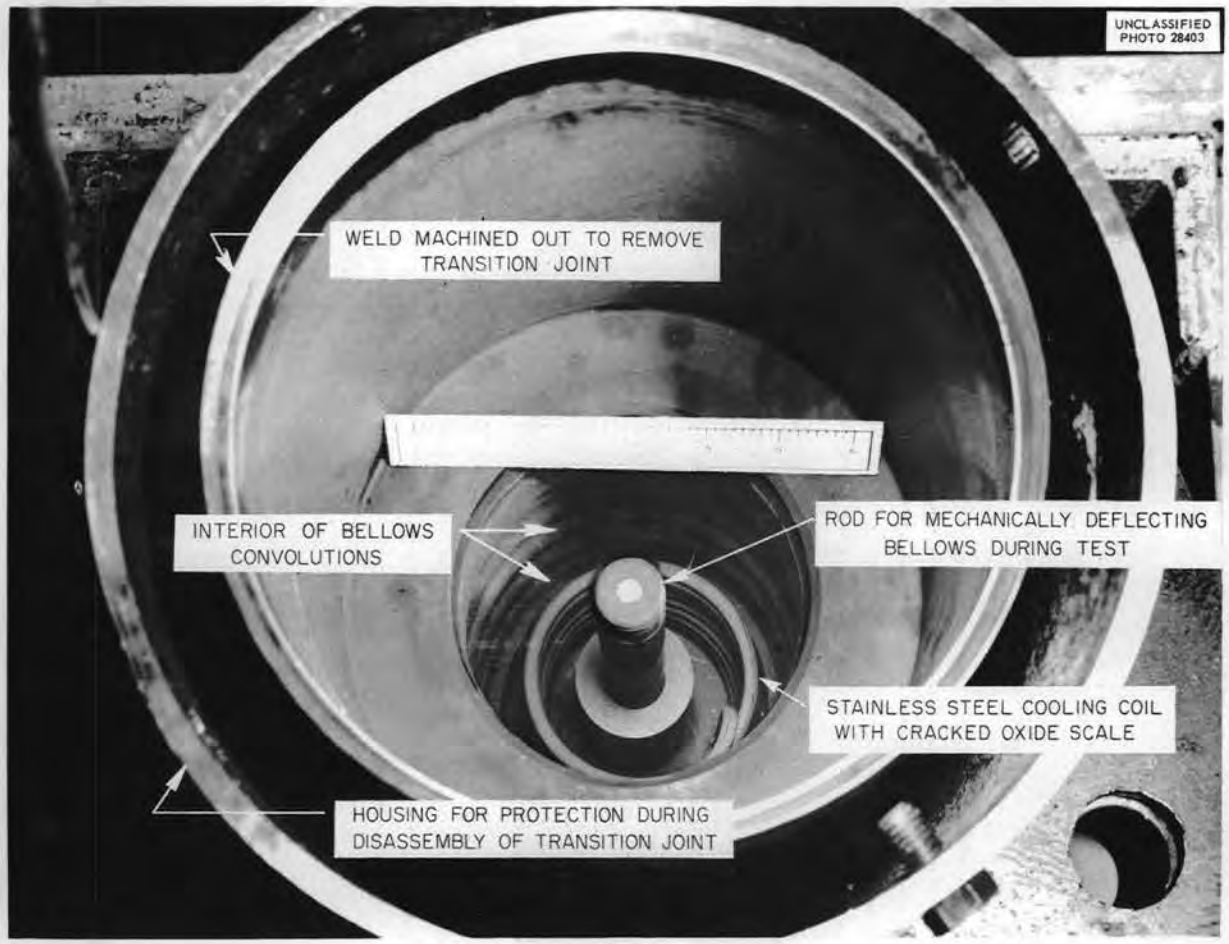

Fig. 11.2. Interior of Bellows After 2920 hr of Exposure to Water at 100 to 300°C.

Table 11.1. Conditions of Uranyl Sulfate–Beryllium Sulfate Runs in Loop O

Run No.	$BeSO_4$ (*m*)	UO_2SO_4 (*m*)	$CuSO_4$ (*m*)	Temperature (°C)	pH at 28°C	Time (hr)	Remarks
12	0.04	0.04	0.005	225	3.2	200	pH decreased slightly
13	0.04	0.04	0.005	200	3.2	199	Solution appeared stable
14	0.03	0.04	0.005	300	3.2	200	pH dropped from 3.2 to 2.2; beryllium concentration decreased by 15% at end of run
15	0.08	0.04	0.005	225	2.7	197	Solution appeared stable
16	0.08	0.04	0.005	300	2.7	200	pH decreased from 2.7 to 2.2; beryllium concentration decreased by 20% at end of run

UNCLASSIFIED
PHOTO 28404

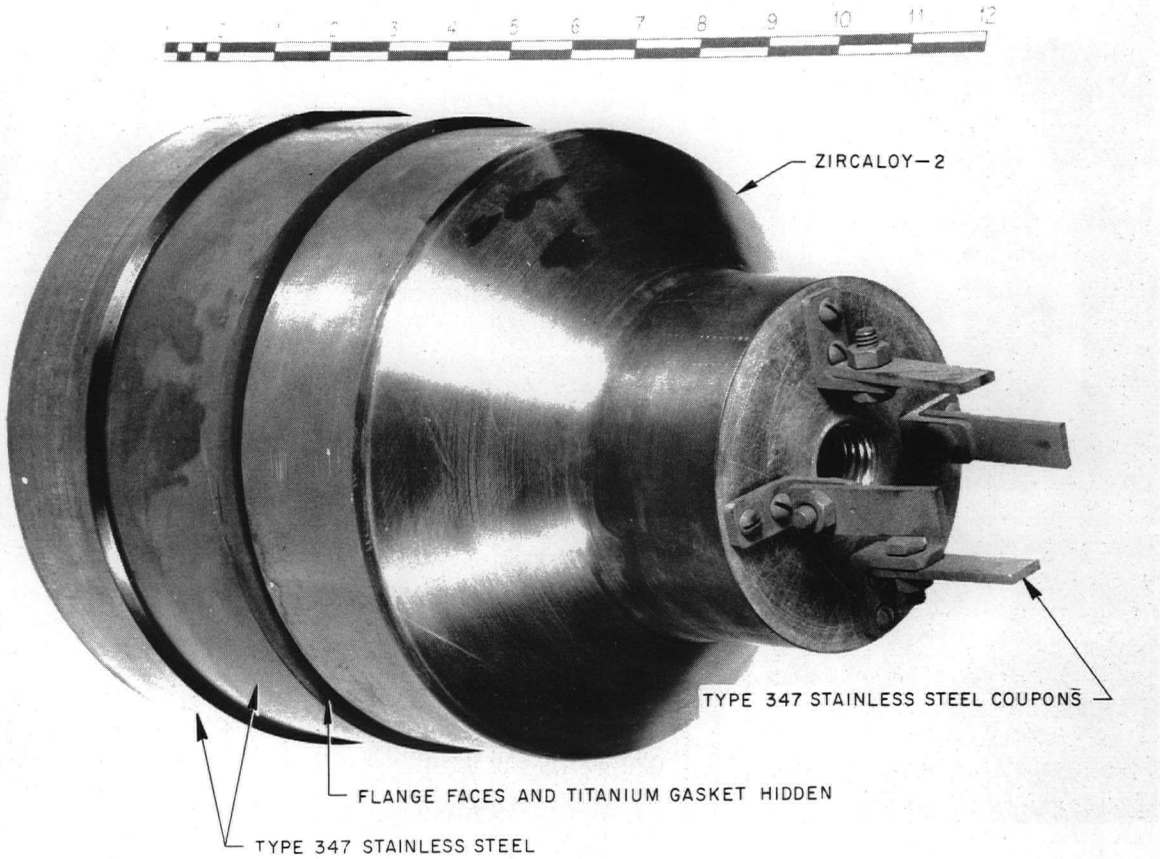

Fig. 11.1. Transition Joint Removed From Bellows Test Unit After 2920 hr of Exposure to Water at 100 to 300°C.

stainless steel specimens in the beryllium-containing solutions at 200 and 225°C were not filmed over at any velocity, in contrast with those exposed in the HRT solution, and their weight losses showed very little velocity dependence. Longer-term runs will be necessary to show whether a protective film will form during a longer exposure.

In order to determine the effect of beryllium sulfate concentration on corrosion in 0.04 *m* UO_2SO_4, two runs were made at 300°C with 0.03 *m* and 0.08 *m* $BeSO_4$, respectively, and one run was made at 225°C with 0.08 *m* $BeSO_4$. The conditions of the runs are given in Table 11.1 (runs O-14, O-15, and O-16). The results showed that corrosion of stainless steel increased with increasing beryllium sulfate concentration, although the difference between 0.03 and 0.04 *m* $BeSO_4$ at 300°C, previously reported,[7] was slight.

In the two runs at 300°C, the final concentration of beryllium gave an indication that these solutions were not entirely stable at that temperature. The concentration of beryllium decreased by 15 to 20% during the runs, although the uranium and copper concentrations remained constant. Also, the pH dropped as much as one unit before the end of the run.

Further tests are in progress to determine the stability of beryllium-containing solutions and to determine the corrosiveness of other solutions over long periods of time.

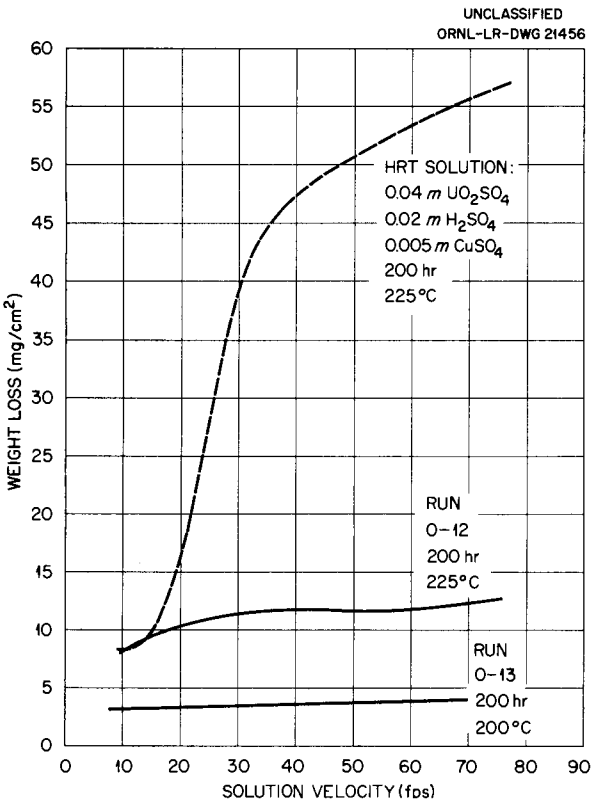

Fig. 11.3. Comparison of the Corrosion of Type 347 Stainless Steel in 0.04 *m* UO_2SO_4 Containing 0.04 *m* $BeSO_4$ and 0.005 *m* $CuSO_4$ with that in HRT solution.

11.1.3 Corrosion in Water at 250°C

A series of tests was made for studying the corrosion of a number of materials in water at 250°C as a function of water treatment and oxygen concentration. The loop was defilmed with chromous sulfate solution[10] prior to the first water run to avoid interference from the scale formed in previous runs with uranyl sulfate solutions. The conditions of the runs are given in Table 11.2.

The first water run was made with deaerated distilled water. In all other runs the water contained 60 ppm phosphate as trisodium phosphate, since this concentration of phosphate will be present in the HRT boiler water.[11] In run I-40, three 10-ml additions of 85% hydrazine hydrate solution were made to the water in the loop to remove completely any residual oxygen. In run I-41 the air dissolved in the water upon loading of the loop was allowed to remain in order to provide a low concentration (20 to 40 ppm) of oxygen in the water during the run. In runs I-42 and I-43, oxygen gas was added to give 300 and 1500 ppm, respectively, at 250°C.

The phosphate concentration remained constant during the runs in which it was added. No attempt was made to maintain a constant pH in the water during a run; and in runs I-42 and I-43 the pH decreased due to the oxidation of some chromium to chromium(VI) with the resulting production of hydrogen ions. Chloride ion was detected in only run I-40, and the concentration was so low, 3 ppm, that it may have been due to contamination of the solution samples during handling or analysis.

Table 11.3 is a condensation of the corrosion results. Pins exposed at flow rates between 18 and 44 fps were averaged, since little velocity effect was observed on any alloy. Generally, the specimens were filmed over, and hence it would be expected that corrosion rates would decrease in longer runs.

It was found that the addition of phosphate to oxygen-free water at 250°C was beneficial to carbon steel and type 414 stainless steel and had little or no effect on the other alloys tested. The effect of oxygen concentrations between zero and 1500 ppm in the phosphate-treated water could not be separated from the effects of chromium(VI) concentration and pH, but the net effect on stainless steel was an increase in corrosion rate with increasing oxygen concentration. Zircaloy-2, titanium RC-55, and niobium were relatively unaffected by oxygen concentration changes. The carbon steels showed a minimum in corrosion rate at 250 to 300 ppm oxygen. However, pitting occurred at that oxygen level and at 1500 ppm oxygen. These pits were shallow (less than 1 mil deep) and appeared to be of the typical oxygen-cell type usually associated with the corrosion of carbon steel in oxygen-containing water. The number and depth of the pits did not seem to be dependent on either flow rate or oxygen concentration.

In each run except the first (I-39), five type 347 stainless steel stressed specimens were exposed at about 3 fps in a special holder inserted in a standard sample barrel. The specimens, having

[10] J. C. Griess *et al.*, *HRP Quar. Prog. Rep. April 30, 1956*, ORNL-2096, p 85.

[11] H. A. McLain, *Treatment of the HRT Steam System Water*, ORNL CF-56-11-132, p 3 (Nov. 29, 1956).

Table 11.2. Conditions of Water Runs at 250°C

All runs were 200 hr

Run No.	Solution Composition	Phosphate Concentration (ppm)	Oxygen Concentration (ppm)	pH	Final Concentration of Ions (ppm)				
					Ni	Cr(III)	Cr(VI)	Fe	Cl
I-39	H_2O	0	0	4–6	<1	<1	<1	<1	<2
I-40	$H_2O + PO_4^{---}$ + hydrazine	60	0	9–10	1	<1	<1	<1	3
I-41	$H_2O + PO_4^{---}$	60	20–40	9–10	<1	<1	<1	2	<2
I-42	$H_2O + PO_4^{---}$	60	300	9 → 6	<1	<1	21	7	<2
I-43	$H_2O + PO_4^{---}$	60	1500	9 → 5	<1	<1	19	<1	<2

Table 11.3. Average Corrosion Rates (mpy) of Alloys in Water Runs at 250°C in 200 hr

Alloy	I-39	I-40	I-41	I-42	I-43
Type 304L SS	0.36	0.23	0.32	0.74	2.0
Type 316L SS	0.36	0.17	0.11	0.54	1.8
Type 318 SS	0.30	0.39	0.20	1.4	2.0
Type 347 SS	0.27	0.26	0.17	0.68	2.6
Type 347 SS stress specimens	*a*	0.73	0.12	0.23	0.64
Carpenter 10 SS	0.13	0.17	0.13	0.38	1.2
Carpenter 20 SS	0.05	0.09	0.05	1.5	0.80
Carpenter 20 Nb SS	0.20	0.21	0.09	1.4	1.4
Type 202 SS	0.22	0.34	0.09	0.56	0.56
Type 414 SS	21	1.1	0.72	1.1	1.3
Croloy 16-1[b]	1.8	0.81	0.22	1.2	1.6
Type 446 SS	0.22	0.22	0.05	1.8	2.2
Type SRF-1132 SS[c]	1.7	0.47	0.39	0.56	2.1
Type A-212 B steel	27	7.5	11	3.1	5.3
Armco iron	34	4.8	7.3	3.7	6.1
Zircaloy-2	0.09	0.0	*d*	*d*	*d*
Titanium RC-55	0.00	0.35	0.01	0.00	0.16
Niobium	*d*	0.34	0.30	0.15	0.85

[a]No stress specimens exposed.

[b]Composition (wt %): 15.9 Cr, 1.42 Ni, 0.018 C, 0.74 Mn, 0.31 Si, 0.90 Cu, bal Fe.

[c]Composition (wt %): 12 Cr, 13.5 Ni, 0.12 C, 0.8 Mn, 0.5 Si, 7.0 Mo, 5.5 Cu, bal Fe.

[d]Specimen gained weight (after defilming).

a No. 32 machine finish, were stressed over a double fulcrum beyond their elastic limit. Microscopic examination of the defilmed specimens after each run indicated no cracks on any specimen. Corrosion rates of the stressed specimens in all runs except I-40 were no greater than the corrosion rates of the type 347 stainless steel pins. It is not known whether the higher corrosion rates of the stressed specimens in run I-40 were due to the 3 ppm chloride that may have been present in solution.

11.1.4 Effect of Loop History on the Corrosion of Stainless Steel

A number of runs in in-pile loops have shown that the in-line corrosion specimens (those not exposed to the reactor neutron flux near the lattice) do not exhibit the same corrosion rates that are observed in 100A loops operated under similar conditions. In another report[12] giving the effects of geometry, steam overpressure, pretreatment, and loop history, it was shown that the last three effects were all possible reasons for the discrepancy between 100A loop and in-pile results but that loop history affected the results to the greatest extent.

Therefore, following the construction of the new 100A type 347 stainless steel loop J, two identical runs were made as nearly like an in-pile loop run as possible (without, of course, the reactor exposure). Prior to each run the loop and corrosion specimens were pretreated successively with 3% trisodium phosphate, 5% nitric acid, and water. Then each run was made with 0.17 *m* UO_2SO_4 containing 0.04 *m* H_2SO_4, 0.03 *m* $CuSO_4$, and about 1000 ppm oxygen at 250°C. The pressurizer was maintained at 280°C to provide roughly a 350-psi steam overpressure. The only difference between the two runs was that the first was made in a new loop and the second in a filmed-over loop. Since every in-pile loop is a new loop, the results from the first run should agree with in-pile in-line results.

The results showed that stainless steel specimens exposed in the new loop had markedly lower weight losses and a substantially higher critical velocity (40 compared with 20 fps) than did the specimens exposed in the filmed-over loop, and that good agreement was obtained between specimens exposed in the new loop and in-line specimens exposed in in-pile loops, for example, L-4-8 (ref 13).

Therefore it appears conclusive that a large area of film-free metal which actively corrodes during a run can inhibit corrosion of stainless steel specimens. This phenomenon has been observed previously,[14] but the mechanism of the inhibition process is not known.

11.1.5 Effect of Adding Chloride Ions to Uranyl Sulfate Solutions

The effects on corrosion of stainless steel caused by chloride ions in uranyl sulfate solutions were investigated in several runs. Previous runs[15,16] have shown pitting attack with 100 and 200 ppm but not with 50 ppm chloride in 0.17 *m* UO_2SO_4 at 250°C. However, the possibility of stress-corrosion cracking was not specifically looked for. Therefore in the present series of runs type 347 stainless steel stress specimens machined from material acceptable by HRP specifications were stressed over a double fulcrum to 75% of room-temperature yield strength (25,600 psi) and exposed in the loop H pressurizer.

Two series of runs were made with 0.17 *m* UO_2SO_4 containing 50 ppm chloride, one at 250°C and one at 200°C. At each temperature the oxygen concentration of the solution was varied from about 1000 ppm to zero. With no oxygen in solution uranium precipitated, and the runs were stopped when the pH decreased from 2.3 to 1.8. The results were as follows:

1. No cracking occurred in 763 hr at 250°C either on specimens exposed only to the chloride-containing solutions or on specimens pretreated for 100 hr at 250°C in chloride-free 0.17 *m* UO_2SO_4 before exposure to the chloride-containing solution.
2. General pitting attack occurred at 250°C during a 111-hr period in which oxygen exhaustion occurred. Metallographic examination indicated no

[12] J. C. Griess *et al.*, ORNL CF-56-7-52, p 13–18 (July 31, 1956) (classified).

[13] J. E. Baker *et al.*, *HRP Radiation Corrosion Studies (In-Pile Loop L-4-8)*, ORNL-2042, p 24 (Aug. 8, 1956).

[14] J. C. Griess and R. E. Wacker, *HRP Quar. Prog. Rep. March 31, 1953*, ORNL-1554, p 64.

[15] J. C. Griess and R. E. Wacker, *HRP Quar. Prog. Rep. April 30, 1954*, ORNL-1753, p 78.

[16] J. C. Griess and R. S. Greeley, *HRP Quar. Prog. Rep. Jan. 31, 1955*, ORNL-1853, p 78.

cracking, but a longer run without oxygen might have produced cracks at the base of the pits.

3. One stress-corrosion crack occurred in 211 hr at 200°C in the presence of about 1000 ppm oxygen. The crack occurred in a crevice underneath a bolt where oxygen exhaustion apparently took place.

4. Numerous stress-corrosion cracks appeared in 200 hr at 200°C in the absence of oxygen.

5. In both these series no large effect of the added chloride was observed on standard annealed pins and coupons except for pitting as described in paragraph 2 above.

Thus it was shown that 50 ppm chloride need not produce stress-corrosion cracking in 0.17 *m* UO_2SO_4 if sufficient oxygen is present. However, loss of oxygen, either in a crevice or throughout the solution, can produce cracks at 200°C and pits that might develop into cracks at 250°C.

One other run with added chloride was attempted. In connection with another test, 0.05 *m* $CuCl_2$ (3500 ppm chloride) was added to 0.02 *m* UO_2SO_4 and circulated with about 1000 ppm oxygen at 250°C. After 22 hr a stress-corrosion crack developed in a ⅜-in. type 347 stainless steel pipe, and solution slowly leaked out, forcing termination of the run. Therefore, at high chloride concentration, cracking can occur even in the presence of oxygen.

11.2 LABORATORY CORROSION STUDIES

11.2.1 Stress-Corrosion Cracking

A continuation of tests during the past quarter to determine the susceptibility of type 347 stainless steel to stress-corrosion cracking by halide-containing uranyl sulfate solutions demonstrated that bromide ions, as well as chloride ions, are capable of inducing cracking in the stainless steel under the conditions of test. The environment consisted of boiling and aerated 0.04 *m* UO_2SO_4 solution containing 0.02 *m* H_2SO_4 and 0.005 *m* $CuSO_4$. Three levels of bromide concentration (added as KBr) were examined in the tests, 50, 100, and 200 ppm.

During the exposure period between 2000 and 2500 hr, a single crack developed on a simple beam-type specimen of type 347 stainless steel stressed at 15,000 psi and exposed in the solution containing 100 ppm bromide. A companion specimen stressed at 30,000 psi and exposed in the same environment showed no cracking during the 2500-hr period.

A second incidence of bromide-induced cracking occurred on two simple beam specimens of type 347 stainless steel exposed in the boiling uranyl sulfate solution containing 200 ppm bromide. One specimen was stressed at 15,000 psi and the other at 30,000 psi. Cracks developed on both specimens during the 1000- to 1500-hr exposure interval. Metallographic studies have been initiated to determine the nature of the cracks. (A preliminary metallographic examination, completed after the report period ended, indicates that the crack that occurred in the 100-ppm bromide solution is actually a break in the metal surface caused by severe subsurface attack and is not a typical stress-corrosion crack.)

It has been reported[17] that chloride concentrations of 25, 50, 200, and 500 ppm in boiling and aerated uranyl sulfate solution produce cracking in type 347 stainless steel stressed at 15,000 and 30,000 psi. In all cases, cracking occurred during the first 500 hr of exposure. Recently, cracking was also produced on stainless steel stressed at 15,000 psi and exposed in solution containing 100 ppm chloride. The time required for cracking to take place was considerably longer than has been experienced with the other crack-producing chloride-containing environments; cracking occurred in the 100-ppm chloride test during the exposure interval between 2000 and 2500 hr. A specimen stressed at 30,000 psi and exposed in the same environment showed no signs of cracking during the 2500-hr test.

A summary of the experience accumulated to date on the susceptibility of type 347 stainless steel to stress-corrosion cracking in boiling and aerated halide-containing uranyl sulfate solutions is included in Table 11.4. It should be noted that chloride concentrations even as low as 25 ppm, and perhaps lower, in the solution to be used in the HRT are capable of producing cracks in even moderately stressed type 347 stainless steel. Thus the necessity of keeping the chloride concentration in the HRT dump tanks very low is evident. While the cracking of stainless steel in the bromide-containing environment was unexpected,

[17] J. C. Griess *et al.*, *Quarterly Report of the Solution Corrosion Group Ending Jan. 31, 1957*, ORNL CF-57-1-144, p 27–30.

bromide ions are an unlikely contaminant, and the fission yield is very low; thus the control of bromide ions should present no problems. Similarly, the presence of an appreciable iodide concentration is not likely, since iodide ions are oxidized to iodine in the presence of uranyl sulfate and volatilized from the solution.

A number of tests to determine the effectiveness of the pertechnetate ion as an inhibitor of stress-corrosion cracking in type 347 stainless steel

Table 11.4. Testing of Stressed Type 347 Stainless Steel in Boiling and Aerated 0.04 *m* UO_2SO_4–0.02 *m* H_2SO_4–0.005 *m* $CuSO_4$ Solutions Containing Halide Ions

Number	Additive		Total Time (hr)	Applied Stress (psi)	Crack Incidence
	Species	Concentration (ppm)			
P-9	No additive		2500	15,000	No cracking
				30,000	No cracking
P-10	Cl^-	5	2500	15,000	No cracking
				30,000	No cracking
P-11	Cl^-	10	2500	15,000	No cracking
				30,000	No cracking
P-12	Cl^-	25	1000	15,000	Cracks; 100 to 200 hr exposure interval
				30,000	Cracks; 100 to 200 hr exposure interval
P-13	Cl^-	50	1000	15,000	Cracks; 100 to 200 hr exposure interval
				30,000	Cracks; 100 to 200 hr exposure interval
P-14	Cl^-	100	2500	15,000	Cracks; 2000 to 2500 hr exposure interval
				30,000	No cracking
S-25	Cl^-	200	1500	15,000	Cracks; 200 to 500 hr exposure interval
				30,000	Cracks; 200 to 500 hr exposure interval
S-26	Cl^-	500	1500	15,000	Crack; 200 to 500 hr exposure interval
				30,000	Cracks;* 200 to 500 hr exposure interval
S-27	Br^-	50	1500	15,000	No cracking
				30,000	No cracking
P-15	Br^-	100	2500	15,000	Cracks; 2000 to 2500 hr exposure interval
				30,000	No cracking
S-28	Br^-	200	1500	15,000	Crocks; 1000 to 1500 hr exposure interval
				30,000	Crocks; 1000 to 1500 hr exposure interval
P-16	I^-	100**	2500	15,000	No cracking
				30,000	No cracking

*No cracking on stress specimen; cracks occurred on "unstressed" specimen support plate.

**During 500-hr run, iodide concentration decreased to 5 to 10 ppm. The iodide concentration adjusted to 100 ppm at start of each 500-hr run.

have been completed. The test environment was oxygenated distilled water containing 100 ppm chloride (50-50 from NaCl-HCl) at a pH of 2.9; the temperature was 300°C. In the absence of pertechnetate ion this environment consistently produced cracks in stressed U-bends of type 347 stainless steel within periods of 100 to 340 hr (ref 18).

Pertechnetate concentrations of 6, 15, 30, 60, 510, and 825 ppm added as potassium pertechnetate were examined in the present tests, the results of which are summarized in Table 11.5. With the exception of the 6-ppm test, which was operated for a period of only 100 hr, pertechnetate concentrations of 60 ppm and less failed to inhibit stress-corrosion cracking of the solution-exposed stainless steel U-bends. Furthermore, a significant loss of the initial pertechnetate ion concentration occurred in every case during the 200-hr test. Microscopic examination of the specimen surfaces disclosed that in concentrations up to and including 60 ppm, the pertechnetate ion was not an effective inhibitor of pitting attack. Pitting was found to range from moderate to heavy in both frequency and intensity, with the most severe damage being along the edges of the specimens in the region of maximum applied stress. Most of the cracks appeared to originate in the pits.

At the higher pertechnetate levels, 510 and 825 ppm, no cracking was found on stressed stainless steel U-bends exposed in the solution after 100 hr in the 510-ppm test nor after 350 hr in the 825-ppm test. The nature of the corrosion attack was generalized, there being only one or two incidences of shallow pitting on edge surfaces. The analytical data indicated a possible loss of 30% of the initial pertechnetate concentration in the 825-ppm test during the 350-hr exposure but did not necessarily indicate that any loss had occurred in the 510-ppm test during the 100-hr exposure. Both solutions contained considerable

[18] J. C. Griess *et al.*, *Quarterly Report of the Solution Corrosion Group Ending Jan. 31, 1957*, ORNL CF-57-1-144, p 31–34.

Table 11.5. Effect of Pertechnetate Ion as an Inhibitor of Stress-Corrosion Cracking for Type 347 Stainless Steel U-Bends at 300°C in Oxygenated Distilled Water Containing 100 ppm Chloride Ion

Pertechnetate Concentration (ppm)[a]		Total Time (hr)	Specimen No.	Incidence of Cracking
Initial	Final			
6	1	100	1	No cracks in 100 hr
			2	No cracks in 100 hr
15	2	250	1	Cracked between 100 and 250 hr
			2	Cracked between 100 and 250 hr
30	2	250	1	Cracked between 100 and 250 hr
			2	Cracked between 100 and 250 hr
60	21[b]	200	1	Cracked before 100 hr
			2	Cracked between 100 and 200 hr
510	485	100	1	No cracks in 100 hr
			2	No cracks in 100 hr
825[c]	590	350	1	No cracks in 350 hr
			2	No cracks in 350 hr

[a] Solutions analyzed for pertechnetate ions polarographically.

[b] Pertechnetate content after 100 hr of test.

[c] Estimated initial concentration.

quantities of solid iron and chromium corrosion products, as identified by spectrographic analysis at the completion of the tests. Chemical analysis disclosed only trace amounts of technetium in the insoluble residues, however.

Intermediate pertechnetate concentrations of 100 and 250 ppm for possible inhibition of stress-corrosion cracking of type 347 stainless steel in the chloride-containing distilled water will be examined during the next quarter.

Although the data are not conclusive, it appears that relatively high concentrations of pertechnetate ions are capable of reducing the effectiveness of the chloride ion as a promoter of stress-corrosion cracking in the austenitic stainless steels. At low pertechnetate concentrations, loss of technetium from solution occurs, probably as a result of the reduction of pertechnetate ions followed by the hydrolytic precipitation of technetium dioxide. If the above postulate is correct, raising the pH of the solution should tend to stabilize the pertechnetate ion and thus allow an evaluation of its effectiveness at low concentration levels. Additional tests are now in progress to evaluate the effectiveness of pertechnetate ions in reducing the susceptibility of type 347 stainless steel to cracking in chloride environments and to determine its chemical stability in such near-neutral solutions. In the event that pertechnetate is stabilized and is an effective inhibitor at reasonable concentrations, it will be investigated under radiation and other conditions specifically involved in its use as an inhibitor in homogeneous reactor water systems (e.g., leak detection).

11.2.2 Corrosion Tests with Zirconium Alloys

The corrosion test program for the evaluation of zirconium-base alloys has continued.[19] The program is carried out in cooperation with the HRP metallurgy groups, and its purpose is to determine the corrosion behavior of a number of binary, ternary, and quaternary alloys of zirconium and to supply corrosion specimens for study of the oxide film structure. Corrosion results from the first group of alloys have been reported.[19]

The second group of alloys was tested in the same environment as the first: 0.04 *m* UO_2SO_4 containing 0.02 *m* H_2SO_4, 0.005 *m* $CuSO_4$, and oxygen. Each test was run for 1000 hr at 300°C. The following alloys were tested during the past quarter: Si-Zr, Cr-Zr, Mo-Zr, Mo-Nb-Zr, Ni-Nb-Zr, and V-Nb-Zr. The composition of the alloys and the corrosion data appear in Table 11.6. Unless otherwise noted, the alloys were prepared from high-purity iodide zirconium. Corrosion rates were determined from as-scrubbed weight losses; no attempt was made to defilm the specimens.

Of the entire group of alloys undergoing test, a 0.7% Cr–99.3% Zr alloy and an alloy containing 7% Mo–20% Nb–73% Zr showed the most promising corrosion behavior, which compared favorably with the excellent corrosion resistance exhibited by Zircaloy-2 exposed under similar conditions. The chromium-zirconium alloy was corroded at a near-negligible rate of 0.1 mpy during the 1000-hr test, whereas the molybdenum-niobium-zirconium alloy exhibited a slight weight gain of 0.1 mg/cm^2 during the same period. The alloys containing 1% Ni–20% Nb–79% Zr and 3% V–15% Nb–82% Zr also showed good corrosion resistance, although the specimens exhibited slightly higher weight gains than the 7% Mo–20% Nb–73% Zr alloy.

The 0.5% Si–99.5% Zr alloy showed a low corrosion rate, although the surface of the specimen was roughened. On the other hand, the 2% Si–98% Zr alloy corroded at rates ranging from 3 to 10 mpy. Thus increasing the silicon content seemed to have a detrimental effect on the corrosion resistance of the alloy. Mediocre corrosion resistance was exhibited also by a cold-rolled zirconium-base alloy containing 10 wt % molybdenum.

Additional zirconium-base alloys will be tested in high-temperature uranyl sulfate solutions during the next quarter. The alloying elements will include Fe, Nb, Cr, In, Mn, Ti, Pt, U, Sn, Ag, Pd, and Y.

11.2.3 Miscellaneous Tests

Laboratory tests were completed with different cast forms of Stellite 6, such as inert-arc deposits, weld rod, and ground valve seats, in a number of homogeneous-reactor-associated environments. The test program was initiated in an effort to determine the reasons for the generally unsatisfactory behavior of Stellite 6 valve seats and trim during water operation with fuel injection pumps and letdown-valve systems.

---

[19] J. C. Griess *et al.*, *Quarterly Report of the Solution Corrosion Group Ending Jan. 31, 1957*, ORNL CF-57-1-144, p 37–41.

Table 11.6. Corrosion of Zirconium-Base Alloys by Oxygenated 0.04 *m* UO_2SO_4–0.02 *m* H_2SO_4–0.005 *m* $CuSO_4$ Solution After 1000 hr at 300°C

Number	Material Identity	Alloy Composition (wt %)	Heat Treatment	Surface Condition	Specimen No.	Corrosion Rate (mpy)	Specimen Appearance
T-52	Zr-59	0.5 Si–99.5 Zr*	As cast	Abraded	1 2	0.5 0.3	Dull gray-brown mottled film; roughened surfaces
T-55	Zr-61	0.5 Si–99.5 Zr	As cast	Abraded	1	0.6	Dull uniform gray film; roughened surfaces
T-53	Zr-60	2 Si–98 Zr*	As cast	Abraded	1 2	10.1 8.9	Dull gray film with black stains; heavily roughened surfaces
T-54	Zr-62	2Si–98 Zr	As cast	Abraded	1	3.1	Dull gray with brown stains; moderately roughened surfaces
T-56	Zr-65	0.7 Cr–99.3 Zr	Cast; hot rolled at 700°C; ground; etched; filed to 0.093 in. thick	Abraded	1	0.1	Lustrous thin dark gray film
S-98	Zr-18	10 Mo–90 Zr	Cast; hot rolled at 700°C to 0.1 in.; cold rolled to 0.070 in.	Chemically polished	1 2	3.6 4.5	Mottled green-brown film; roughened surfaces
S-81	Zr-47	7 Mo–20 Nb–73 Zr	Cast; cold rolled	Chemically polished	1	(+0.1 mg/cm^2)	Lustrous metallic-gray film with yellow stains
S-82	Zr-48	1 Ni–20 Nb–79 Zr	Cast; cold rolled	Chemically polished	1	(+0.8 mg/cm^2)	Lustrous dark gray-brown film with small black deposits
S-83	Zr-68	3V–15 Nb–82 Zr	Cast; cold rolled	Chemically polished	1 2	(+1.1 mg/cm^2) (+1.1 mg/cm^2)	Lustrous dark black film with yellow streaks

*Alloy prepared directly from zirconium sponge.

Distilled water at 80°C with an oxygen overpressure of 150 psi was quite aggressive toward some specimens of Stellite 6, both inert-arc deposits and weld rod; other similar specimens were unaffected by the same environment. Evidently, nonhomogeneities in the metal were responsible for the irregular corrosion results that were obtained.

Inert-arc deposits of Stellite 6 were found to undergo appreciable corrosion attack in boiling 5 wt % HNO_3 solution. However, when the deposits were exposed initially in boiling 3 wt % Na_3PO_4 solution, the attack in the nitric acid solution was reduced from 11 mpy on untreated specimens to less than 4 mpy on the pretreated specimens.

As a possible substitute material for Stellite 6 in valve seats, hard-chrome plating on stainless steel received some consideration. The corrosion resistance of the chrome plate was found to be excellent in 0.04 *m* UO_2SO_4 solution containing 0.02 *m* H_2SO_4 and 0.005 *m* $CuSO_4$ at 80°C. No significant weight losses were observed on specimens after exposure periods of 400 hr. Similarly, no significant weight losses were observed on specimens exposed for 550 hr in distilled water at 80°C. In the latter case, however, the hard-chrome plate underwent appreciable staining and discoloration. Nevertheless, the corrosion resistance of the plate was quite acceptable in both media at 80°C. It should be noted that these tests were carried out in a static system; it is quite possible that mechanical action of an operating valve would cause the chromium to be removed from the surface.

The integrity of gold plate on type 347 stainless steel bellows was determined in boiling 10 wt % HCl solution. One bellows was plated with a few tenths of a mil of gold; the second was plated with 2-mil-thick gold. Within a short period of time after immersion in the hydrochloric acid solution, the gold plate on both bellows was badly blistered and cracked in numerous areas, allowing rapid attack of the underlying stainless steel. The results of the above tests and others carried out during the past few years show the impracticability of relying on noble electrodeposits for protection of the less-noble base metals.

The corrosion resistance of several grades of commercial sintered alumina and titania products was examined in oxygenated 1.33 *m* UO_2SO_4 solution at 250°C. The investigation was conducted to evaluate the behavior of possible replacement materials for the high-purity sintered aluminum oxide supplied by the Kearfott Mfg. Corp. and now used as a pump bearing material. Based upon observed weight losses after 1000-hr tests, AlSiMag 192 (TiO_2) and AlSiMag 652 (96 wt % Al_2O_3 minimum) exhibited a corrosion resistance twice as good as that of the Kearfott material. Apparent corrosion rates ranged from 15 to 17 mpy for the AlSiMags, as compared with rates of 28 to 30 mpy for the high-purity Kearfott aluminum oxide.

12. SLURRY CORROSION

E. L. Compere H. C. Savage
S. R. Buxton S. A. Reed
H. D. Cole J. A. Russell, Jr.
G. E. Moore R. M. Warner
W. C. Ulrich

12.1 PUMP LOOPS

12.1.1 Loop Engineering

(a) 100A Loop BS. – The assembly of a second thorium oxide slurry corrosion test facility, 100A pump loop BS, has been completed, and ten runs (BS-5 through BS-14), totaling 2010 hr of operation on slurry, have been completed since an engineering report was last made on the system.[1,2]

This second test facility has proved satisfactory from an operational standpoint. The use of the standard corrosion sample barrels[3] in loop BS eliminated plugging by thorium oxide slurry, which had occurred in the annular-flow sample barrels[4,5] previously used in loop CS.

Since two of the corrosion-specimen holders in loop BS are directly in series, having loop flow, and the third is in the return line which combines loop and pressurizer flows, the velocity range to which the corrosion specimens are exposed is adjusted by use of specimen holders with different cross-sectional-area flow channels. The bulk-flow rate of the system can be adjusted by means of orifice-type restrictor plates and/or by varying the speed of the circulating pump by means of a variable-frequency motor-generator set. Operation of the pump at reduced speeds has also helped reduce pump bearing wear, particularly when thorium oxide caking on the pump impeller caused dynamic unbalance.

After run BS-11, a capillary-tube letdown sampling unit was installed in the loop to facilitate sampling of the slurry. The sample unit consists of about 30 ft of 0.10-in.-OD stainless steel tubing coiled in a water-cooled jacket and arranged so that the tubing can be flushed with condensate before and after sampling to minimize the possibility of plugging and to ensure more representative loop slurry samples. Appropriate valving and the pressure drop through the capillary tubing allow slurry samples to be taken from the loop at operating temperature and pressure. This device has proved satisfactory in removing slurry samples from the loop. (This type of sampling unit has been previously used in the 200A pump loop.)

(b) 100A Loop CS. – Several changes were made to 100A pump loop CS during the period covered by this report. Figure 12.1 is a schematic drawing of loop CS, and Fig. 12.2 is a photograph of the loop.

The three parallel, vertical, annular-flow sample barrels previously used[4,5] have been replaced with three parallel, horizontal, standard 30-in. sample barrels like those used in solution corrosion loops.[3] The former arrangement was found to be unsatisfactory because of slurry buildup in the narrow ($\frac{1}{4}$-in.) flow annulus between the corrosion-specimen holder and barrel wall. This flow annulus is eliminated in the standard solution-corrosion sample barrels. The new barrel arrangement in loop CS allows corrosion-specimen holders to be used in parallel and series simultaneously, since each 30-in. sample barrel can accommodate two 15-in. specimen holders.

Three different bulk-flow rates can be maintained through the three parallel sample barrels, and relative velocity through each specimen holder can be adjusted by changes in the cross-sectional areas of the flow channels of the specimen holders. However, bulk-flow rates and velocities in the three parallel units are interdependent and require adjusting by means of appropriate restrictors to obtain the desired combinations of velocities. Flow rates in loop CS can also be controlled by

---

[1] E. L. Compere *et al.*, *HRP Dynamic Slurry Corrosion Studies: Quarter Ending April 30, 1956*, ORNL CF-56-4-139, p 10, Fig. 1.1.2.

[2] E. L. Compere *et al.*, *HRP Quar. Prog. Rep. April 30, 1956*, ORNL-2096, p 88.

[3] H. C. Savage *et al.*, *HRP Quar. Prog. Rep. March 15, 1952*, ORNL-1280, p 46, Fig. 16.

[4] J. C. Griess *et al.*, *HRP Quar. Prog. Rep. Oct. 31, 1954*, ORNL-1813, p 63.

[5] J. C. Griess *et al.*, *HRP Quar. Prog. Rep. July 31, 1955*, ORNL-1943, p 65, Fig. 8.3.

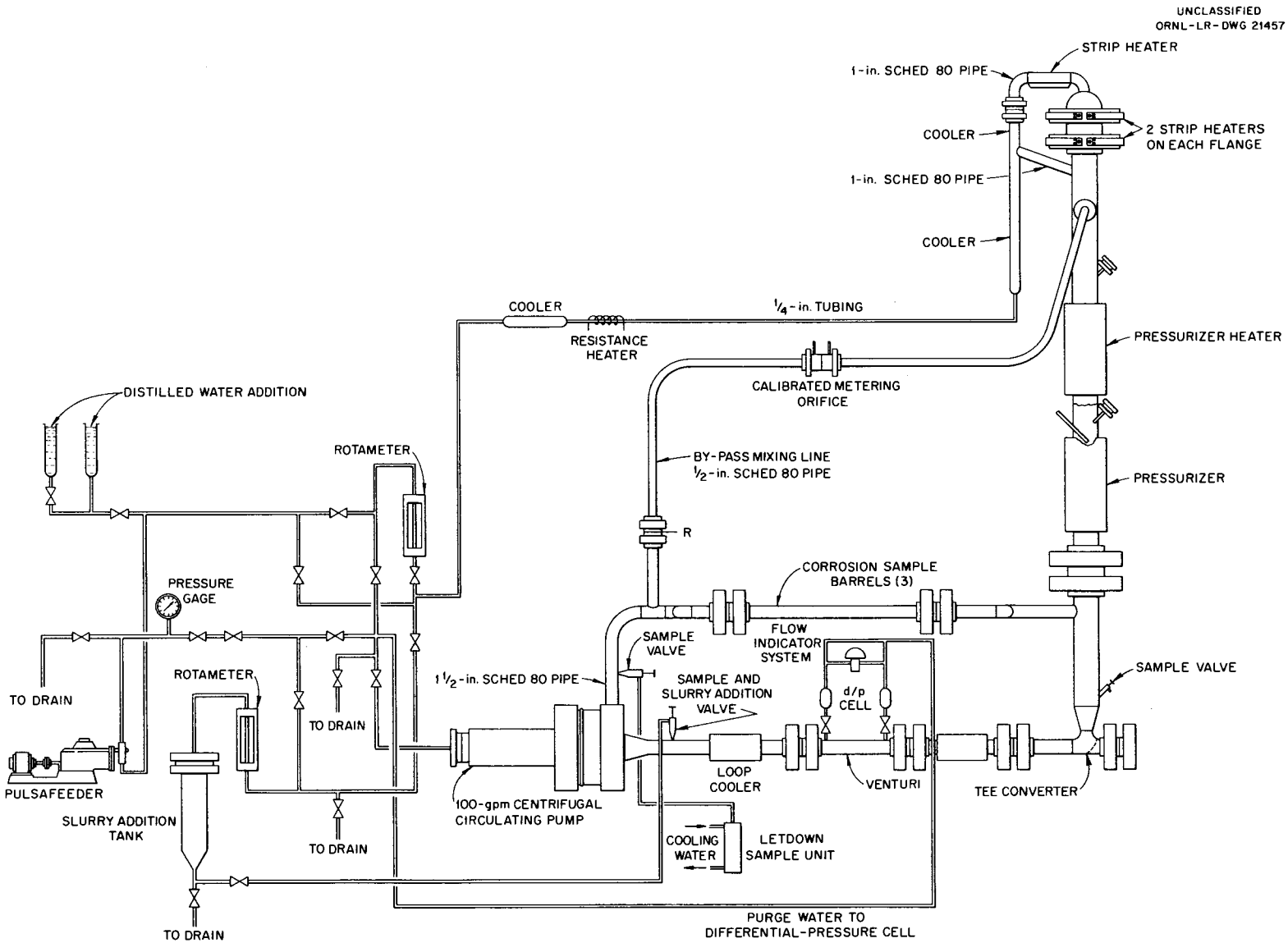

Fig. 12.1. Schematic Diagram of Loop CS.

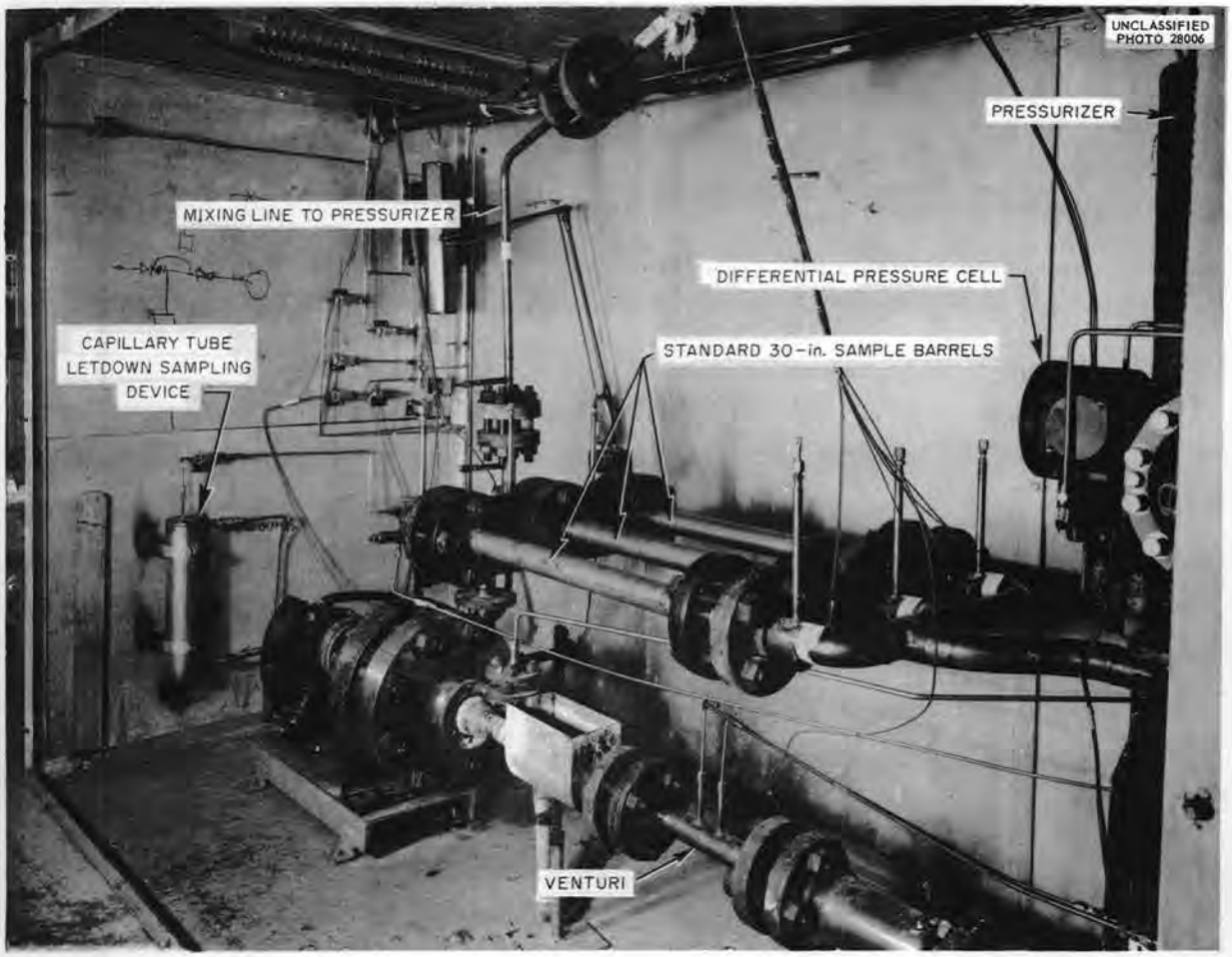

Fig. 12.2. Photograph of Loop CS Showing Venturi and Sample Barrel Arrangement.

changing the pump speed with a variable-frequency motor-generator set, as with loop BS, but the CS loop pump has not yet been operated at lower speeds.

Another component added to loop CS is a calibrated venturi installed in the pump suction line as an aid in monitoring the density and/or changes in flow rate of the circulating thorium oxide slurry. A comparison of pump amperes and venturi differential pressure with thorium oxide slurry concentration for run CS-34 is shown in Fig. 12.3. Load concentration was calculated from the amount of thorium oxide added to the loop, while sample concentration was obtained by analysis of samples taken from the loop at the operating times indicated. Where two or more samples were taken at the same time, the individual concentrations obtained are shown. However, a sample average value was used in constructing the graph. With the initial addition of thorium oxide to the loop at hour 64, pump amperes and venturi differential pressure both increased, but not proportionally either to each other or to the calculated slurry-density increase. At hour 280, water was added to the system, but the expected decrease in pump amperes and venturi differential pressure was not observed. At hour 304 (slurry circulation hour 240), more thorium oxide slurry was added. Pump amperes and differential-pressure readings both increased as expected with increased thorium oxide slurry concentration. Although pump amperes remained fairly constant from hour 304 until the end of the run, venturi differential pressure generally followed the decrease in thorium oxide slurry concentration in the loop as obtained from samples removed.

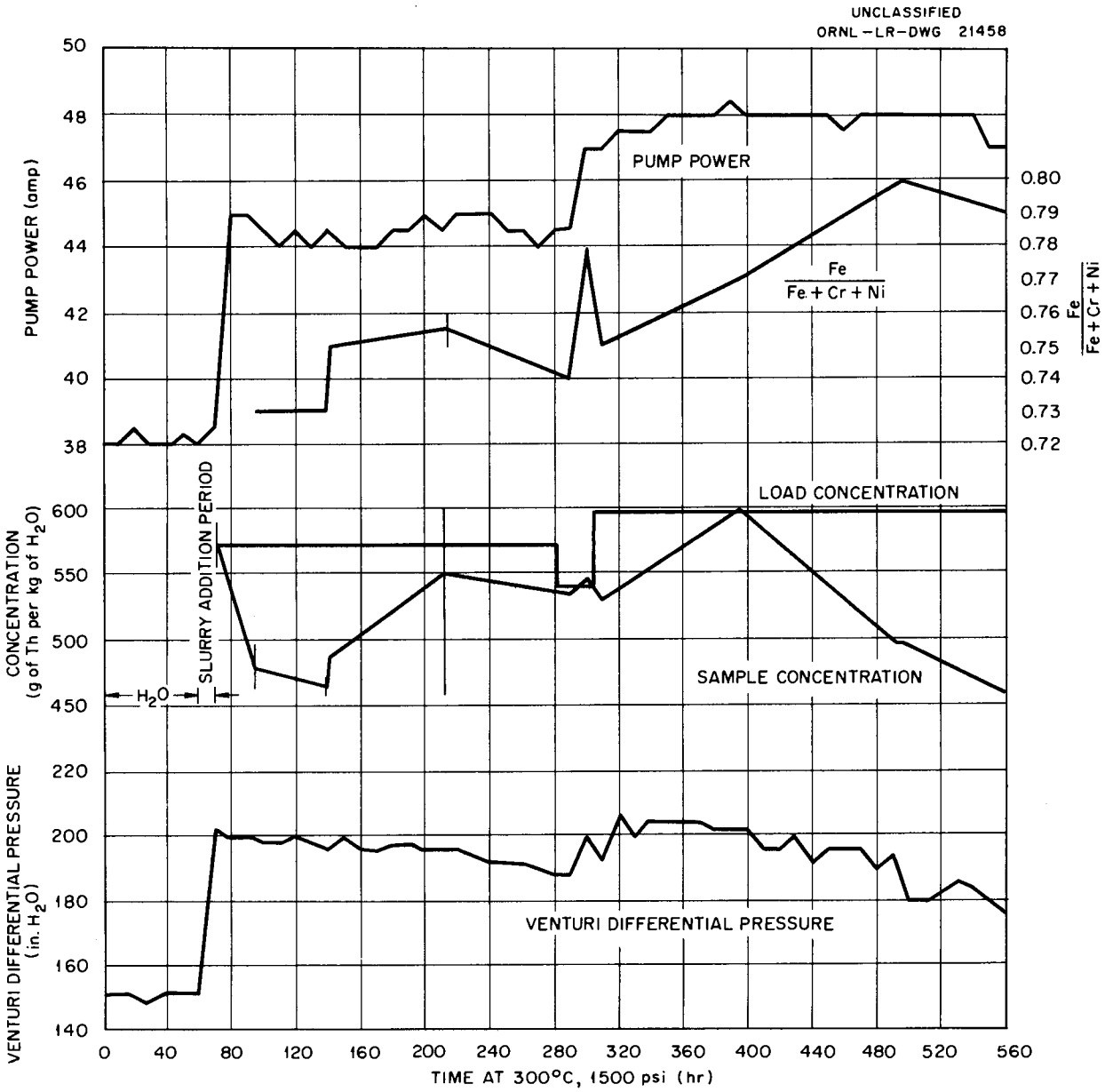

Fig. 12.3. Comparison of Pump Amperes and Venturi Differential Pressure with Thorium Oxide Concentration for Run CS-34.

When the pump was disassembled at the end of the run, a break about 1 in. long was found on the cylindrical surface of the stainless steel pump rotor can (Fig. 12.4). This break could account for the relatively large increase in pump amperes which occurred at hour 290. Another indication of the break in the pump rotor can is that after hour 290, the ratio of Fe/(Fe + Cr + Ni) corrosion products in the thorium oxide slurry increased more than could be expected from the corrosion of the 347 stainless steel loop components and corrosion specimens exposed to the slurry. [The ratio of Fe/(Fe + Cr + Ni) for type 347 stainless steel is 0.7.] The increased Fe concentration in the corrosion products probably was caused by the corrosion of the iron rotor core through the break in the rotor can, although there is no direct means of verifying this assumption. The rotor-can failure appeared to be mechanical, and not caused by chemical or corrosive action.

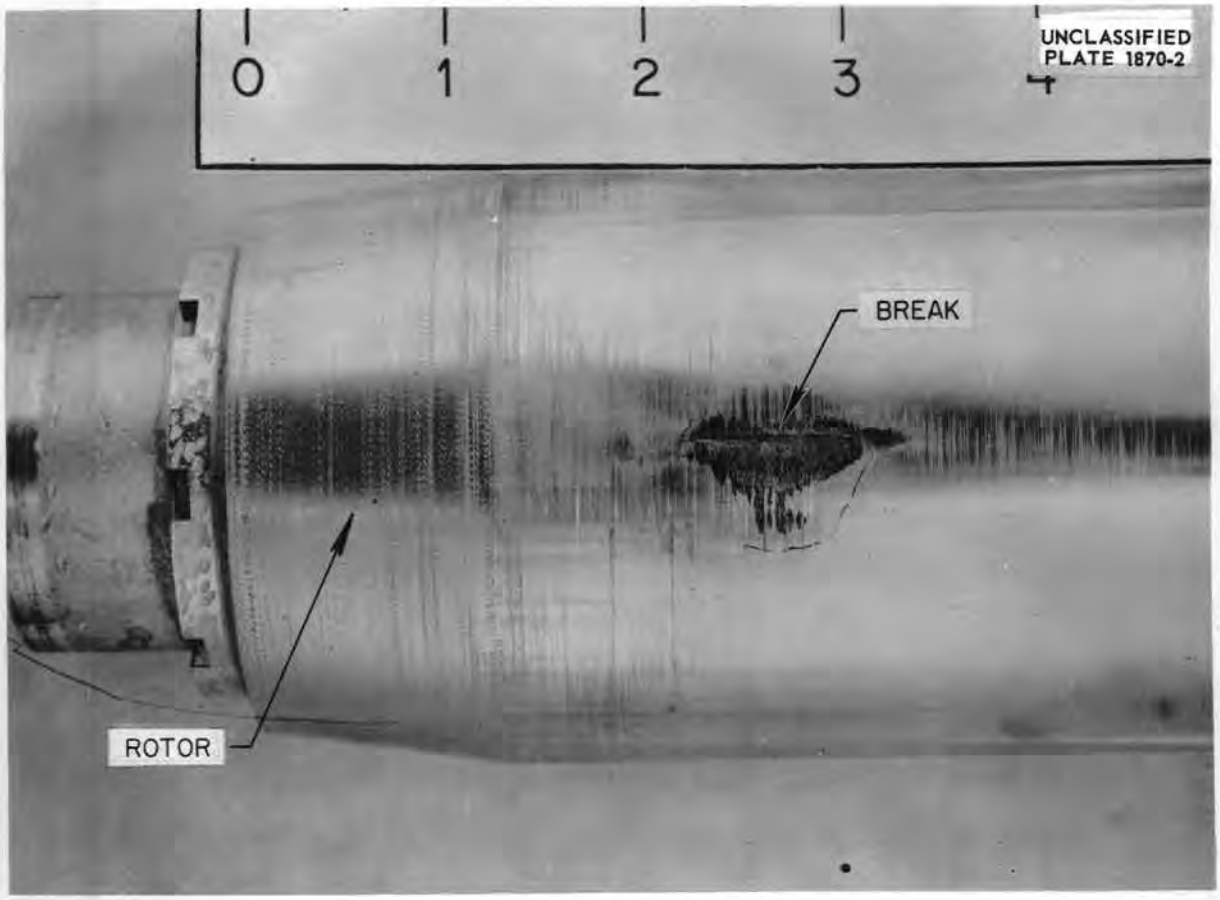

Fig. 12.4. Break in 100A Pump Rotor Can Found After Run CS-34.

The venturi pressure taps are connected directly to an 800-in. differential-pressure cell, which, in turn, transmits the pressure differential to a gage on the panel board. The venturi system was operated continuously, but readings were taken only every 4 hr.

In the event that the venturi pressure taps should become plugged with slurry, condensate can be flushed through the taps by means of the Pulsafeeder to remove the obstruction. Intermittent flushing with condensate, however, kept the lines free of slurry during run CS-34. The system was operated for 500 hr on slurry without plugging of the ¼-in.-OD × 0.035-in.-wall pressure lines.

A letdown capillary sampling device, identical with the one installed in loop BS, was also incorporated in loop CS.

12.1.2 100A Pump-Loop Tests

Five slurry-corrosion test runs were made in loop BS, and one was made in loop CS, during the quarter. Four of the tests in loop BS were made to complete a study of the effect of sulfate on the corrosivity of oxygenated aqueous thoria slurries at 300°C. The series of tests employed slurries at a charge concentration of approximately 500 g of thorium per kilogram of water to which was added ~3000 ppm sulfate (based on thoria) as sulfuric acid or 300 ppm sulfate as thorium sulfate. An 800°C-calcined thoria, batch LO-14, prepared at ORNL was used. The corrosivity of the slurries did not appear to be much changed by the addition of sulfate; however, the additives were observed to affect markedly the formation of slurry spheroids during circulation.

In the fifth test in loop BS, which circulated an ORNL-produced 650°C-calcined thoria at an average concentration of 478 g of thorium per kilogram of water at 300°C with oxygen, the thorium oxide was degraded to an average size of 0.5 μ with no spheroid formation. Corrosion rates closely

paralleled those obtained with slurries prepared from 800°C-calcined thoria.

The run in loop CS circulated slurry prepared from batch LO-2A, 800°C-calcined thoria, at 300°C for 501 hr at an average concentration of 516 g of thorium per kilogram of water. Corrosion rates were generally not excessive; however, pronounced erosive attack occurred in the circulating pump.

12.1.3 Tests with Sulfate Additives

In the four loop tests made to investigate the influence of sulfate ion on the corrosivity of thoria slurries, batch LO-14 thorium oxide was used. The particular spheroid-forming character of this thoria preparation and a summary of the loop test, run BS-8, which circulated it with sodium sulfate as an additive, have been described previously.[6,7]

For each test of the series, loop BS was operated isothermally at 300°C with oxygen overpressure. A bypass mixing line leading from the pump discharge line to the loop pressurizer was used in an attempt to maintain a uniform slurry concentration throughout the loop system. Flow through the mixing line was arbitrarily maintained at 12 to 13 gpm. As a result of favorable experience in previous tests with LO-14 slurry, the 100A centrifugal pump was operated at half of normal rotational speed, that is, at 1800 rpm, on 30-cycle current provided by a motor-generator set, to minimize bearing wear if caking occurred. The pump was equipped with Graphitar bearings and Stellite journals.

In each run the loop was loaded with three sets of pin-type corrosion specimens exposed to flow velocities, measured with water at room temperature, of approximately 10, 20, and 30 fps. When satisfactory operation on oxygenated water at 300°C was attained, slurry was charged to the system as a single batch addition. Each test was scheduled to run 300 hr.

In two tests, runs BS-9 and BS-10, the required quantity of sulfuric acid to provide ~3000 ppm SO_4^{--} (based on thoria) was injected into the loop immediately before adding the thoria. Heavy caking on the pump impeller and in the pump suction line necessitated stopping run BS-9 after 27 hr of circulation and run BS-10 after 123 hr of circulation. By chemical analysis, 14% of the thoria charged in run BS-9 was lost by deposition from the circulating stream during the 27-hr period. In run BS-10 the average circulating concentration was 615 g of thorium per kilogram of water, whereas the original charge concentration was only 533 g of thorium per kilogram of water. Slurry spheroids 15 to 40 μ in diameter were formed during each test.

In run BS-11, a 300-hr test, wide variations in circulating concentrations occurred; spheroid growth was pronounced; and hard, tenacious deposits of thoria were formed on the pump impeller and in the pump suction line. In this test the sulfuric acid was mixed with the slurry before charging of the system. During charging of the slurry, samples withdrawn from the loop main stream after 1.4 hr of circulation contained numerous 7- to 20-μ spheroids, as observed by using the microscope. After 100 hr of circulation, 95% of the slurry was composed of 40- to >120-μ spheroids.

Similar phenomena occurred in run BS-12, a 113-hr test in which thorium sulfate, to provide 300 ppm sulfate based on solids, was added to the slurry charged to the system. The use of 300 ppm sulfate rather than 3000 ppm was inadvertent. The average slurry concentration, by chemical analysis, for the 113-hr period was 558 g of thorium per kilogram of water. Slurry spheroids > 120 μ formed during circulation.

As in tests reported previously,[7] the marked increases in circulating concentration in runs BS-11 and BS-12 that occurred as the spheroids became larger resulted from a stripping action in the vertical loop pressurizer. A direct correlation was observed in these runs between the formation and growth of spheroids, the fluctuating concentration, and the corresponding drop or rise of the slurry meniscus in the pressurizer.

Data are presented in Table 12.1 which show the effects of circulation on LO-14 slurries with and without sulfate additives. For purposes of comparison, data from several earlier runs have also been included in the tabulation.

Similar trends occurred in all tests. A gradual increase in spheroid size occurred during about the first 50 hr of circulation, and after this period little measurable growth took place. After approximately 100 hr of circulation, the average size of

[6] E. L. Compere *et al.*, *HRP Quar. Prog. Rep. Oct. 31, 1956*, ORNL-2222, p 81.

[7] E. L. Compere *et al.*, *HRP Quar. Prog. Rep. Jan. 31, 1957*, ORNL-2272, p 90.

Table 12.1. Comparative Circulation and Corrosion Effects of Batch LO-14 and Batch LO-2 Slurries at 300°C

	Run BS-7 (ThO_2 Batch LO-14)			Run BS-8 (ThO_2 Batch LO-14)			Run BS-11 (ThO_2 Batch LO-14)			Run BS-12 (ThO_2 Batch LO-14)			Run CS-27 (ThO_2 Batch LO-2)		
Defilmed Corrosion Rate, mpy															
	10 fps	20 fps	30 fps	10 fps	20 fps	30 fps	10 fps	20 fps	30 fps	10 fps	20 fps	30 fps	10 fps	20 fps	30 fps
Austenitic SS	2	5	5	2	9	10	4	4.5	4.5	3	5	5	0.9	2	7
Titanium and alloys	1.6	0.9	4.5	5	7	9	0.3	0.7	0.8	0.1	1.5	1.2	0.2	2	6
Zircaloy-2	W.G.	1.0	1.5	0.2	1.1	1.4	0.3	0.8	1.4	0.0	0.0	0.6	0.0	0.1	2
Gold	1.3	1.6	2.5	0.7	1.8	2.1	0.1	1.2	2.5	0.1	2.5	3.0	0.05	0.10	0.60
Average loop corrosion rate, mpy		0.6			0.9			3.6			1.9			1.5	
Duration of test, hr		194.2			334.8			300.3			113.1			300.9	
Average circulating concentration (g of Th per kg of H_2O)		635			484			725			558			348	
Additives		O_2 (~1000 ppm)			O_2 (~1000 ppm) Na_2SO_4 0.02 *m*			O_2 (~1000 ppm) H_2SO_4 0.02 *m*			O_2 (~1000 ppm) $Th(SO_4)_2$ 0.001 *m*			O_2 (~1000 ppm)	
pH of slurry		8			7.5			6			7			7	

Nitrogen Adsorption Surface Area and Sedimentation Particle Size

Approximate Circulation Time (hr)	Surface Area (m^2/g)	Particle Size (wt %) >100 μ	10–50 μ	<10 μ	Surface Area (m^2/g)	Particle Size (wt %) >100 μ	10–50 μ	<10 μ	Surface Area (m^2/g)	Particle Size (wt %) >100 μ	10–50 μ	<10 μ	Surface Area (m^2/g)	Particle Size (wt %) >100 μ	10–50 μ	<10 μ	Surface Area (m^2/g)	Particle Size (wt %) >100 μ	10–50 μ	<10 μ
0	18.5	0	0	100	18.5	0	0	100	18.5	0	0	100	18.5	0	0	100	16.5	0	1	99
5	22.3	0	6	94	22.0	0	9	91	23.8	0	7	93	23.5	1	13	86	18.7			
20	24.2	0	39	61	25.9	0	11	89	26.9	0	28	72	28.7	16	37	47	21.9	No spheroids		
50					26.0	0	6	94					28.9	64	29	7	22.1	Degraded to av 0.7 μ		
100	26.7	0	36	64	27.5	0	85	15	26.7	0	68	32	26.7	51	42	7	21.9			
150	27.7	0	44	56	26.1	0	1	99	26.7	10	86	4	26.5	42	52	6	22.4			
200	26.5	0	43	57	26.3	0	3	97	25.2	7	83	4					22.5			
300					26.4	0	1	99	25.1	1	84	15					22.3			

the spheroids, measured by sedimentation, appeared to decrease. Actually, by microscopic examination, numerous large spheroids were still present, but many of them appeared to have been fractured or malformed during the latter stages of pumping. These changes are shown in the photomicrographs in Figs. 12.5–12.10.

Although the sulfate additives appeared to have little effect on spheroid growth rate in these tests, a marked difference in ultimate spheroid size was observed. Without sulfate additives, a maximum spheroid size of 20 μ was observed. In the run with sodium sulfate, spheroids of 5 to 16 μ were formed during 300 hr of circulation. Throughout the test, both sodium and sulfate ions were found to be in almost constant ratio between the slurry solids and the supernatant liquid. When sulfuric acid was used, spheroids 7 to 100 μ were present after 100 hr of circulation, but no apparent growth took place during the following 200 hr. In the test with thorium sulfate as an additive, spheroids ranged from 40 to >120 μ after only 30 hr of circulation. No further growth occurred during the remaining 83 hr of the test. In the sulfuric acid and thorium sulfate tests, the sulfate ions were found, by chemical analysis, to be associated solely with the slurry solids.

Nitrogen-adsorption surface-area data, included in Table 12.1, are also seen to follow a general trend with spheroid growth. While the significance of the surface-area measurements is not clear, the changes suggest that the spheroids or their surfaces are quite porous.

Comparative corrosion rates from loop runs with LO-14 slurry are shown in Table 12.1. Also included in the table are attack data obtained in a previously reported[8] run in which slurry prepared from batch LO-2 thorium oxide was circulated and in which no spheroid formation was observed. There are no known differences in the technique of preparation or firing of these batches. Neither the formation of spheroids nor the presence of sulfate additives appeared to affect the corrosivity of the slurries significantly.

12.1.4 Circulation of 650°C-calcined Thoria Slurry

The slurry circulated in run BS-13 was made from a new thorium oxide preparation designated as batch LO-18. The material was produced at ORNL by precipitation of thorium nitrate with oxalic acid at 70°C and final calcination at 650°C for 24 hr.

The conditions of operation and system flow velocities were the same as those described for runs BS-9 through BS-12. During operation at 300°C, sufficient slurry was charged to the system to provide a calculated circulating concentration of 636 g of thorium per kilogram of water. No additions, other than gaseous oxygen, were made to the loop. The loop was operated routinely for a period of 304.6 hr at an average concentration of 478 g of thorium per kilogram of water.

The run was terminated when a gasket ruptured in the high-pressure rotameter connected in the purge-water feed line to the circulating pump. The system, at 300°C, blew down in approximately 2 min from 1500 psi to atmospheric pressure.

After standing at room temperature for about 24 hr, the system was recharged with water. Without heating, the circulating pump was run for 30 min to resuspend the solids. The loop was then drained and rinsed, using the pump, in the usual manner. During disassembly, no deposits or accumulations of thoria were found in the system.

The rate of attrition of the LO-18, 650°C-calcined thoria was somewhat more rapid than that of other oxide preparations, fired at 800°C, which have been circulated in loop BS. The average particle size of the LO-18 material, measured by sedimentation analysis, before circulation in run BS-13, was 3.3 μ. After 2.9 hr of circulation at 300°C, the average size of the particles was 0.8 μ. After 22 hr of circulation, the average size had diminished to 0.6 μ, and after 70 hr of circulation, to 0.5 μ. No further degradation was detected after that time. No spheroids formed during the test.

Corrosion rates observed in run BS-13 with LO-18 thorium oxide slurry were moderate. Also, there was a negligible velocity effect between 20 and 30 fps. Defilmed rates at 10, 20, and 30 fps, respectively, were (in mpy) as follows: austenitic stainless steel, 4, 5, and 6; titanium and alloys, 2, 3, and 3.5; Zircaloy-2, 0.8, 2.0, and 3.2; and gold, 0.05, 0.4, and 0.4.

12.1.5 Wear of Pump Components

With the exception of the cast type 431 stainless steel impeller used in loop BS, the attack of pump components during runs BS-9 through BS-13 was

[8] E. L. Compere *et al.*, *HRP Quar. Prog. Rep. July 31, 1956*, ORNL-2148, p 83.

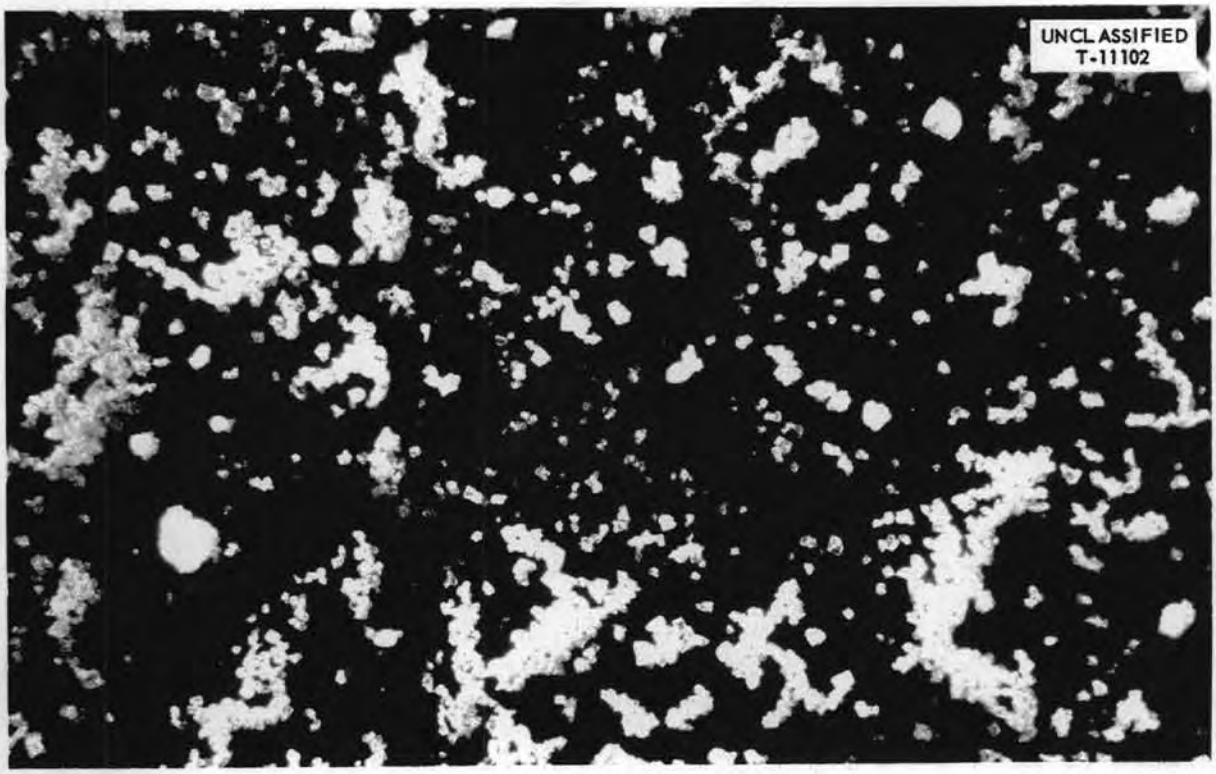

Fig. 12.5. LO-14 Slurry Before Circulation. 400X.

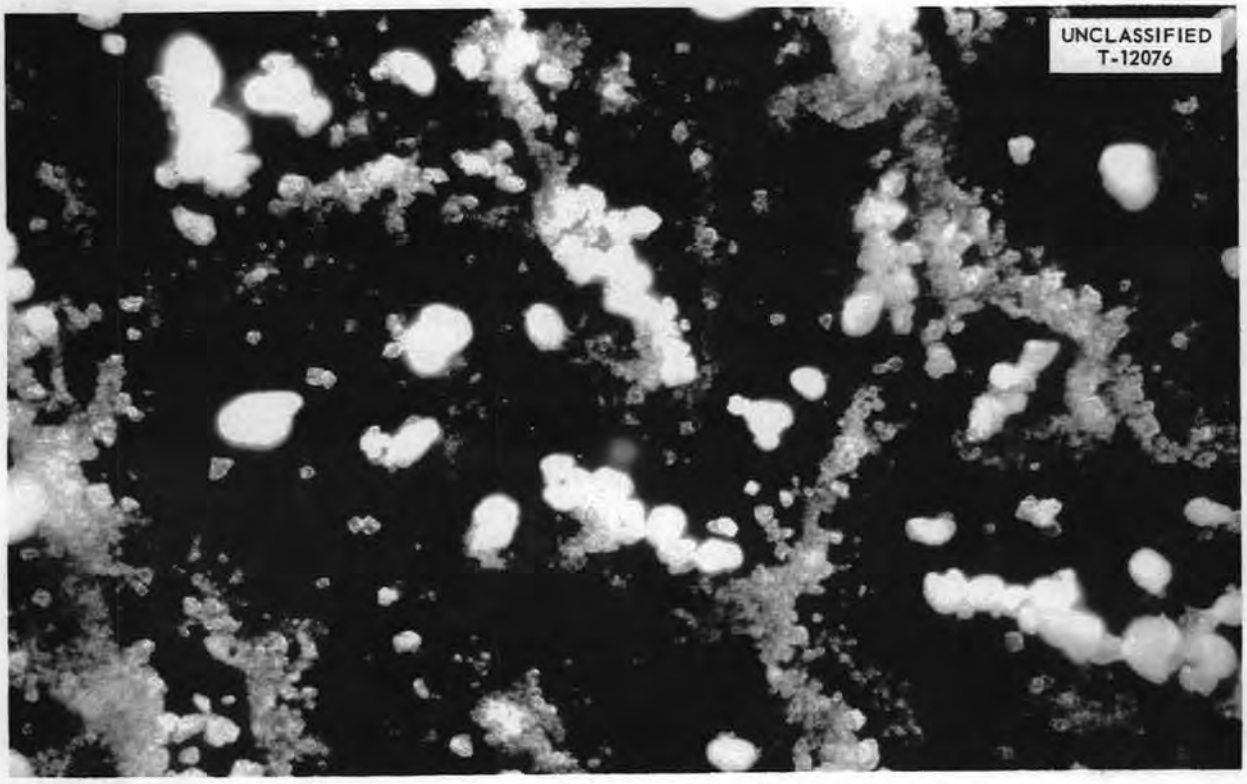

Fig. 12.6. LO-14 Slurry After 95 hr Circulation. 400X.

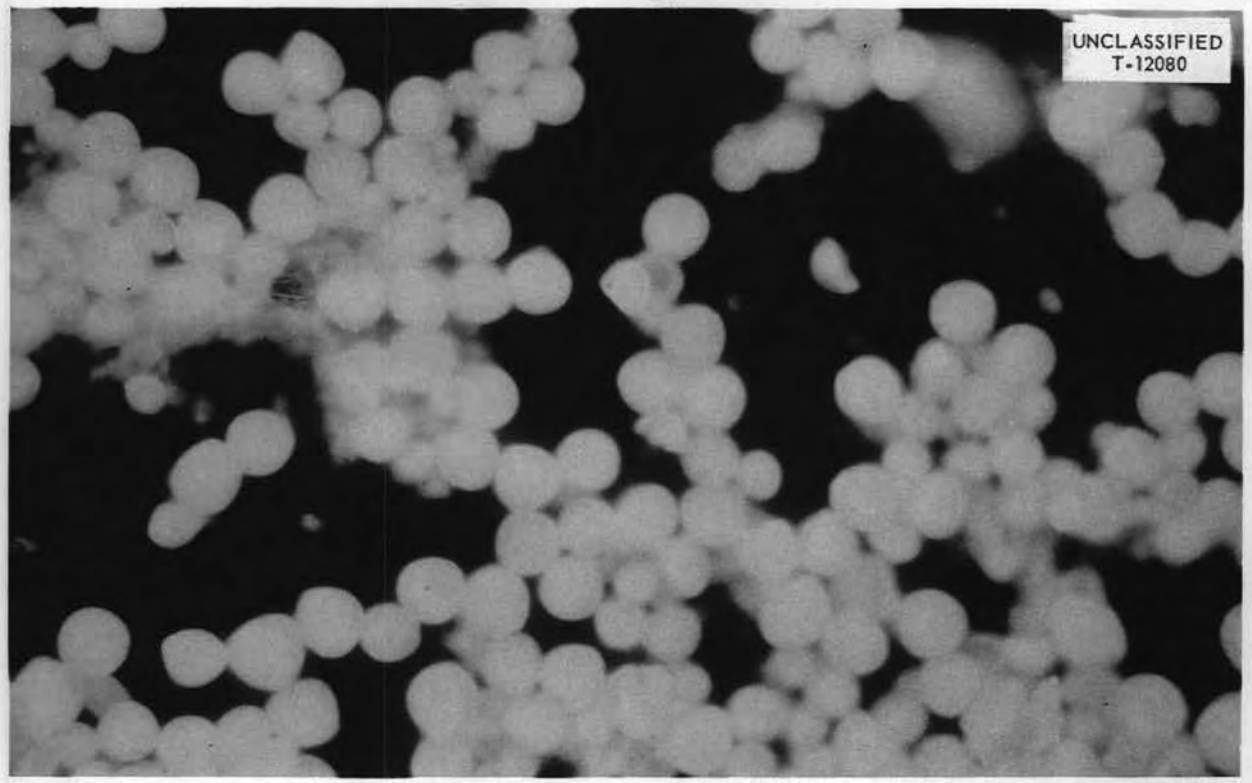

Fig. 12.7. LO-Slurry After 165 hr Circulation. 400X.

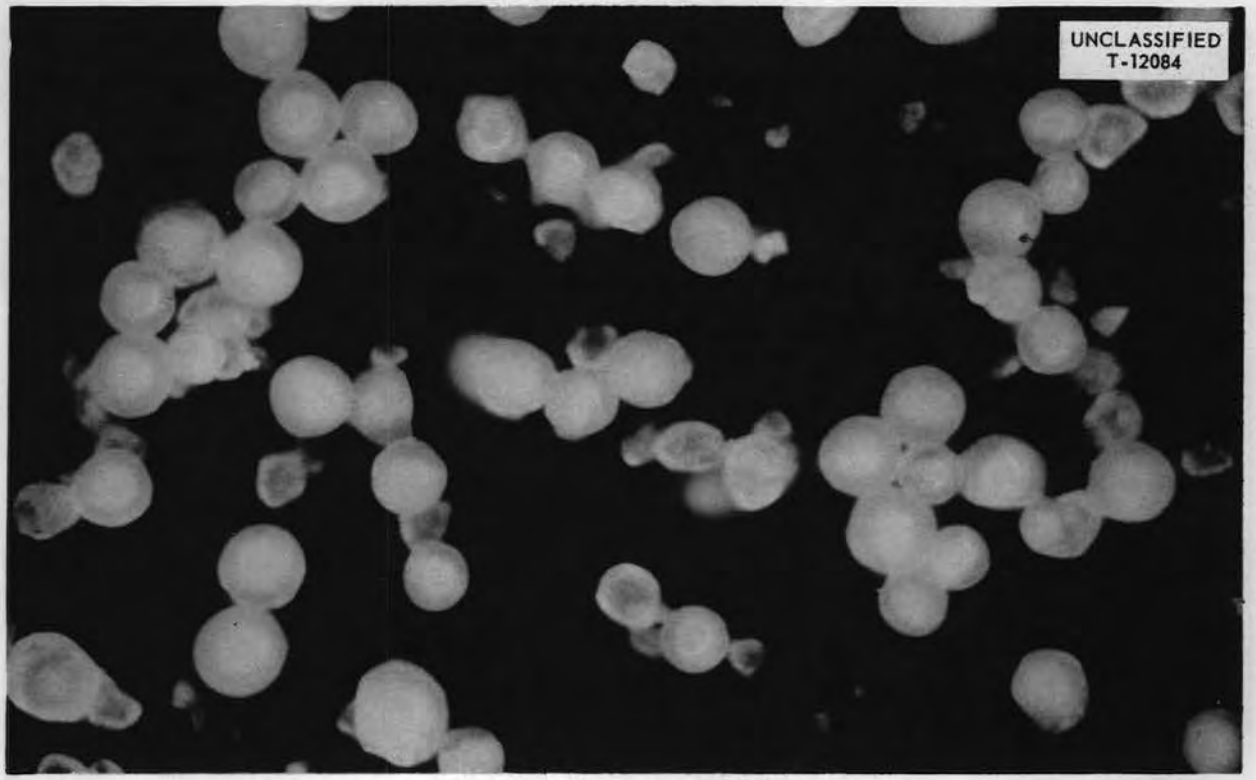

Fig. 12.8. LO-14 Slurry After 189 hr Circulation. 400X.

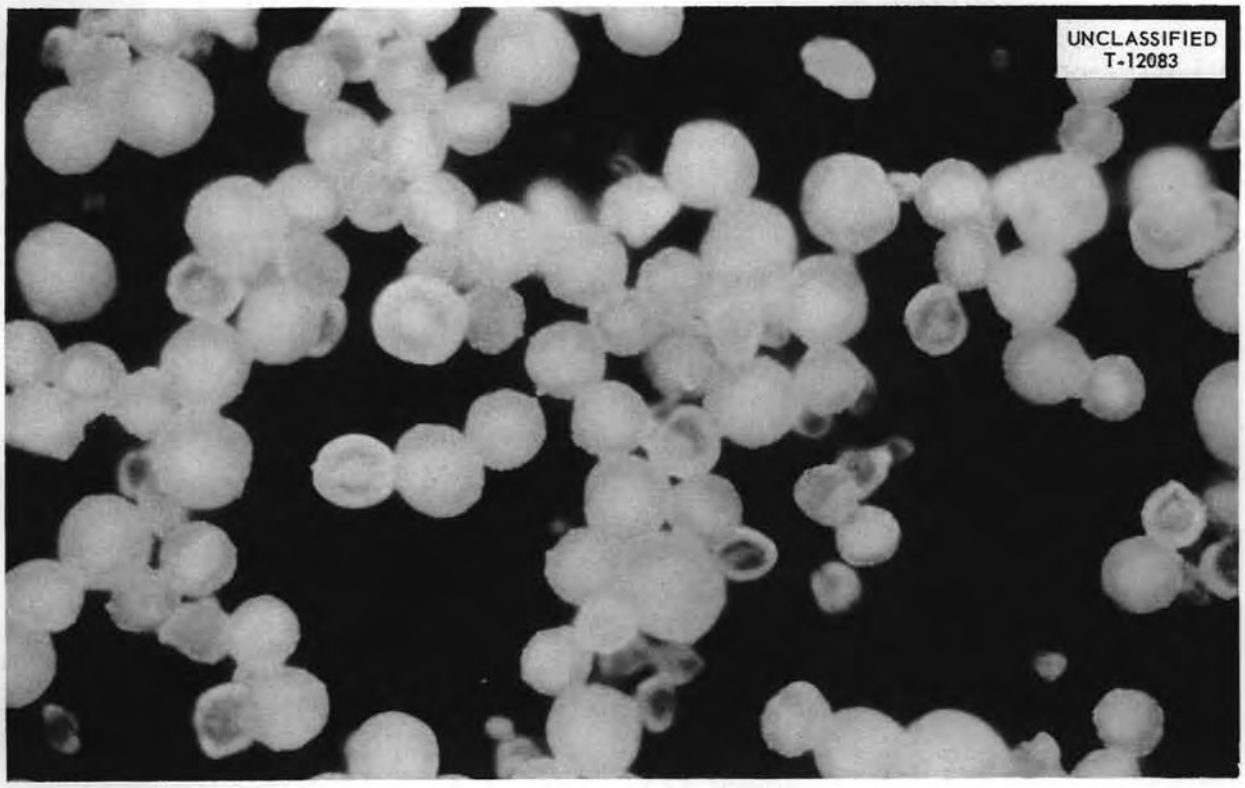

Fig. 12.9. LO-14 Slurry After 260 hr Circulation. 400X.

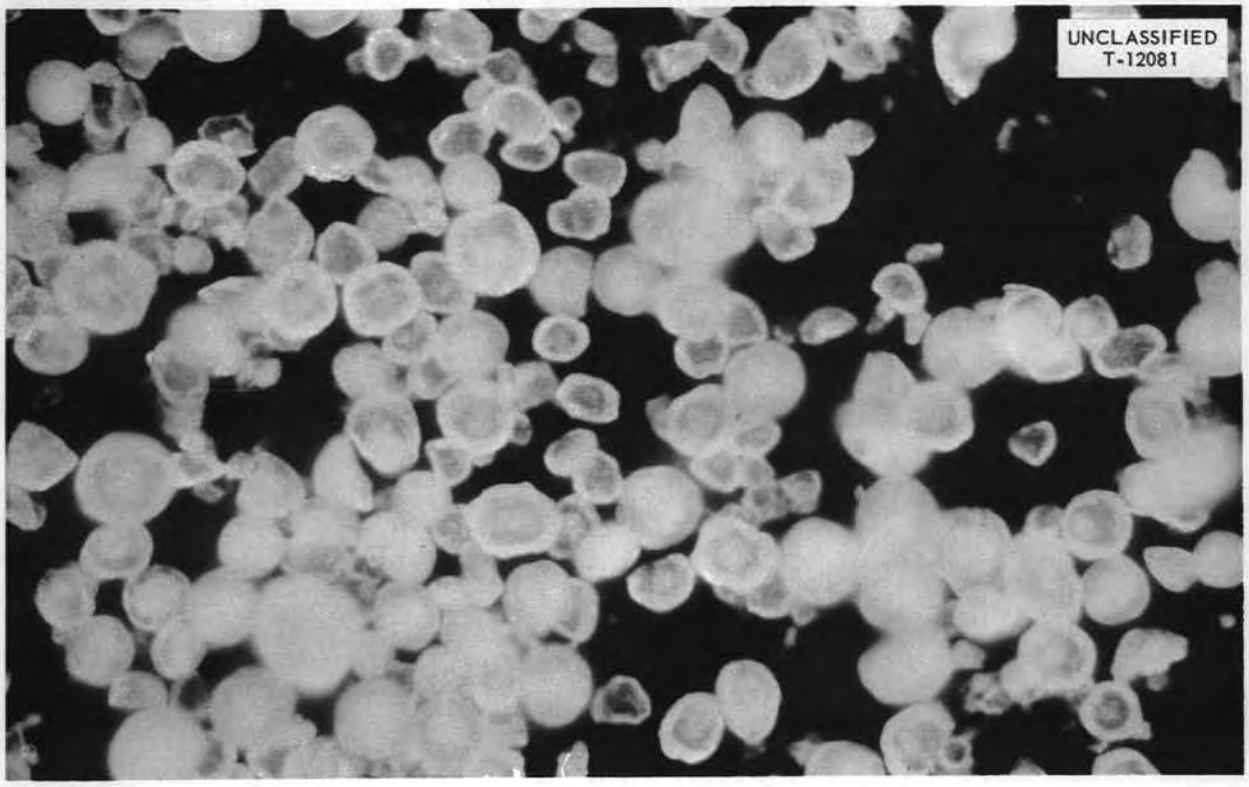

Fig. 12.10. LO-14 Slurry After 300 hr Circulation. 400X.

not excessive. The front Graphitar bearing, replaced after run BS-12, had worn only 0.0034 in. after 1169.7 hr service in slurry and 410.2 hr service in oxygenated water. There was no detectable wear on the rear Graphitar bearing after run BS-13. The bearing, which is still in use, had accumulated 1474.3 hr service in slurry and 441.3 hr service in oxygenated water when run BS-13 was completed. The same titanium wear rings were used in all tests through run BS-13.

The cast type 431 stainless steel impeller lost a total of 155 g through run BS-12, 128 g of which was lost during a 123-hr period in run BS-10 with sulfuric acid as additive. During run BS-10 most of the oxygen in the system was either consumed or lost through leakage.

12.1.6 Circulation Test in Revised Loop CS

After the revisions to loop CS were completed (see Sec 12.1.1*b*), run CS-34, a 501-hr test at 300°C with oxygenated slurry at an average circulating concentration of 516 g of thorium per kilogram of water was made. The slurry charge for the test was prepared from batch LO-2A thoria.

Bulk flows, measured on water at room temperature, through the three sample barrels were 6, 24, and 40 gpm, respectively. Flow through the bypass mixing line was 13 gpm. Each barrel was loaded with two sets of corrosion specimens in holders with different apertures to provide flow velocities ranging from 6 to 52 fps. A total of 76 specimens was exposed in the three loop barrels. In the loop pressurizer, six pin specimens were exposed to slurry at 0.1 fps, and four stress specimens were placed in the gas-vapor space above the mixing line.

After a 72-hr performance test at 300°C with oxygenated water, 10.6 kg of batch LO-2A was charged to the loop to provide a calculated circulating slurry concentration of 572 g of thorium per kilogram of water. Thereafter, the loop was operated and sampled in a routine manner for 501.2 hr.

One additional charge of slurry containing 1.15 kg of LO-2A thoria and 1.89 kg of water was added to the system after approximately 230 hr of operation as makeup for the volume of slurry withdrawn as samples.

Fifteen samples were taken during the test, most of them by means of the new letdown sampler. The average concentration of the samples, by chemical analysis, was 516 g of thorium per kilogram of water. Each 80-ml sample was preceded by two flush samples, of equal volume, for purging the sampler and associated tubing. No difficulty was experienced with the sampler during the test. When the run was completed, the system was cooled to room temperature, flushed with water (using the pump), and then disassembled for routine inspection.

There was only one area in the system where slurry had accumulated. A thin, hard deposit of thoria was found in the upstream header piping to the No. 3 sample barrel. Flow through this section was approximately 6 gpm ($\sim$1 fps). Also, both specimen holders in the No. 3 barrel were partially blocked with a soft deposit of slurry.

Pronounced erosion occurred in the pump. Areas adjacent to each weld pad on the pump head and on the thermal barrier were eroded to depths ranging from 0.030 to 0.115 in. Similar localized attack was found in the opening to the pump suction line. The pump head is type 347 stainless steel; the thermal barrier is type 75A titanium. The front hub of the titanium 75A impeller, shown in Fig. 12.11, was similarly eroded. Numerous pits 0.13 to 0.18 in. in depth were found.

All surfaces of the pump head and thermal barrier and the front surface of the impeller were highly polished. The back surface of the impeller, only slightly abraded, was covered with a thin corrosion film.

Differential corrosion rates for the run, calculated from chemical analysis of corrosion products in the slurry, began at 15 mpy for the first few hours, and successively became smaller, decreasing to a level somewhat below 1 mpy. No pronounced subsequent rise was noted. Average loop corrosion rate for the run was 1.0 mpy. Excess iron, above the stainless steel ratio, rose steadily, reaching a level of about 5 g after 250 hr, and 14 g after 500 hr. It is this iron which apparently came from within the cracked rotor can (see Fig. 12.4).

Corrosion rates calculated from defilmed weight losses of pin specimens exposed at 10, 30, and 40 fps were moderate. At 10 fps, austenitic stainless steel specimens corroded at an average rate of 0.3 mpy, mild steels at 23 mpy, and titanium alloys at 0.2 mpy. There were no detectable

UNCLASSIFIED
PHOTO 28544

Fig. 12.11. Localized Attack on Type 75A Titanium Pump Impeller After Run CS-34.

weight losses of gold, platinum, or Zircaloy-2 pin specimens at 10 fps. At 30 and 40 fps, respectively, the average rates (in mpy) were as follows: austenitic stainless steels, 1.5 and 12; mild steels, 24 and 31; titanium alloys, 2.4 and 9.4; Zircaloy-2, 0.6 and 3; and gold and platinum, 0.3 and 2.9.

At 46 fps, corrosion rates of pin specimens of the austenitic stainless steels ranged from 12 to 20 mpy; mild steel, 33 mpy; Zircaloy-2, 4 mpy; and titanium alloys, 12 to 13 mpy. Coupon specimens of the austenitic stainless steels exposed at 18 fps averaged 0.5 mpy; titanium 75A, 0.2 mpy; and mild steel, 12 mpy.

Type 347 stainless steel coupons contained in a variable-velocity specimen holder displayed rates from 0.2 to 17 mpy over the velocity range 6 to 52 fps. No critical velocity was noted. The last three specimens in the holder, at respective velocities of 33, 41, and 52 fps, showed marked localized attack. Irregular areas were attacked, apparently as a result of turbulence patterns, to a depth of 250 to 340 μ (0.010 to 0.015 in.).

No cracks were found in the four stress specimens exposed in the vapor space of the pressurizer. The four alloys, each stressed to approximately 80% of its yield value at temperature, were types 347 and AM 350 stainless steels, titanium-3Al-4V alloy, and Zircaloy-2.

12.2 TOROIDS

Tests were continued to study the corrosion effects of slurries prepared from thorium oxide calcined at different temperatures. Thoria prepared from thorium oxalate precipitated at 10°C was calcined at temperatures of 1000, 1200, 1400, and 1600°C. Average particle sizes, approximately 1 to 1.5 μ, were little changed in 314 hr of circulation in toroids.

In a 309-hr toroid run at 250°C, 26 fps, and 50 psi oxygen with slurries at 500 and 1000 g of thorium per kilogram of water using thorium oxides calcined at 550 and 650°C, corrosion rates were generally ordinary or slightly lower for type 347 stainless steel, titanium 75A, Zircaloy-2, or carbon steel SA 212 grade B. Final particle sizes were approximately 0.7 μ.

12.2.1 Effect of Calcination Temperature

Results of several runs, made to investigate the effect of calcination temperature on thorium oxide attrition and on metal attack rates during circulation in toroids, have been reported previously.[9] An additional test was made during the quarter with a new batch of ORNL-produced thoria, which was prepared by precipitation of thorium oxalate at 10°C and calcination at 1000°C. Portions of this preparation were subsequently recalcined at 1200, 1400, and 1600°C, respectively, for 4 hr in order to evaluate the most suitable temperature at which to calcine the entire batch for use in a proposed 100A loop run. Slurries prepared from each firing were circulated for 314 hr at 26 fps, 250°C, and with 50-psi oxygen at approximately 500 g of thorium per kilogram of water. Oxygen was provided by the thermal decomposition of hydrogen peroxide.

No apparent degradation occurred in any of the tests. The average sedimentation particle size of each thoria preparation before and after circulation was 1.2 $\pm$ 0.2 μ.

Corrosion rates of pin specimens (in mpy) were as follows: type 347 stainless steel, 1.4 to 0.4; titanium 75A, 0.9 to 0.0 and 0.7 to 0.0; and carbon steel SA212B, 1.6 to 0.8. In general, the lower rates were observed with slurries prepared from thoria calcined at the higher temperatures. Differences within the above ranges, however, are not regarded as significant. Consequently, it has appeared feasible to use any of these temperatures, including 1600°C, to calcine this material for loop use.

In another run, slurries made from three lots of ORNL-produced thoria which were prepared from thorium oxalate precipitated at 70°C and calcined at 550°C for 24 hr, 650°C for 4 hr, and 650°C for 24 hr, respectively, were circulated at 250°C for 309 hr at 26 fps with 50 psi of oxygen. The 550°C batch and the 650°C-calcined batch which was fired for 4 hr were circulated at a concentration of 500 g of thorium per kilogram of water. The 650°C-calcined batch which was fired for 24 hr was circulated at concentrations of 500 and 1000 g of thorium per kilogram of water.

Before circulation, the slurries were composed of particles whose average sizes were 2.6 to 4.6 μ. After circulation the average particle sizes ranged from 0.6 to 0.7 μ. Attack rates of the 500-g-of-thorium-per-kilogram-of-water slurries at 26 fps ranged from 0.9 to 1.1 mpy for type 347 stainless

[9] E. L. Compere, *Dynamic Slurry Corrosion Studies: Quarter Ending Jan. 31, 1956*, ORNL CF-56-1-168, p 33.

steel, 2 to 3 mpy for SA 212 grade B steel, and 0.0 to 0.1 mpy for Zircaloy-2. No significant difference in corrosivity between the above slurries was indicated.

At 1000 g of thorium per kilogram of water, using the 650°C-calcined oxide fired for 24 hr, corrosion rates (in mpy) were as follows: type 347 stainless steel, 1.2; titanium-75A, 1.0; Zircaloy-2, 1.0; and SA 212 grade B carbon steel, 4.7.

A loop test, run BS-13, which circulated this same preparation at 500 g of thorium per kilogram of water for 500 hr at 300°C is described in Sec 12.1.4.

12.3 IN-PILE SLURRY TOROID DEVELOPMENT

During the past quarter, test evaluation of the experimental model of an in-pile toroid rotator, described previously,[9,10] has continued. The primary mechanical difficulty encountered was the wearing of the rotator-arm bearings and rotator gears. Neither standard ball nor needle-type roller bearings have been satisfactory for this application. At present, a rotator arm which will employ double-row angular-contact ball bearings and case-hardened gears is being fabricated for test and evaluation.

A second experimental model of an in-pile toroid rotator has been designed and constructed (Fig. 12.12). Motion is applied to the toroids by an entirely different mechanism than in the first model. The air motor used in the first model is retained. However, the gear train is replaced by two rods with two gimbals and a universal

[10] E. L. Compere *et al.*, *HRP Quar. Prog. Rep. Jan. 31, 1957*, ORNL-2272, p 100–101.

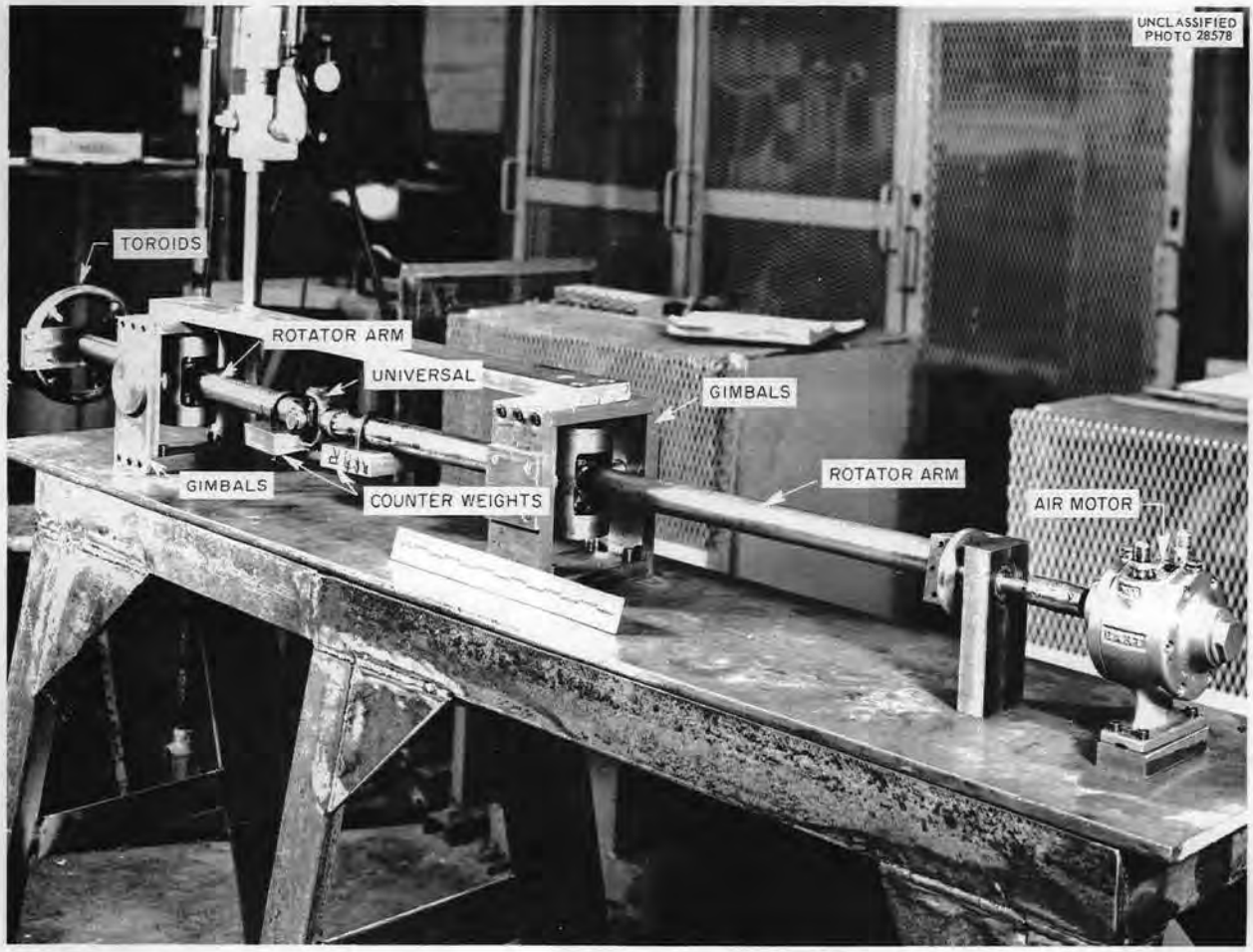

Fig. 12.12. Development Model of Rotator for In-Pile Slurry Toroid.

joint. The two gimbals prevent rotation of the toroids around their own axis, and the universal joint permits circular motion of the ends of the rotator arms. The double, instead of the single, rotator arms and gimbals have been used to attain dynamic balance of the rotating mechanism.

The advantages of this second model over the first are as follows: (1) the point where the rotator arm passes through the gimbals provides a null point of motion from which thermocouple, power, coolant, and pressure connection leads can be routed with minimum flexing during rotation, and (2) the toroids can be operated closer to the reactor lattice for maximum neutron-flux exposure, since operational clearance is not required for routing service lines at the forward or reactor side of the toroids. Dynamic balance of the second model appears to be a difficult problem and has not yet been demonstrated. Good dynamic balance is desirable during in-pile operation to prevent excessive vibration of the mechanism in the beam-hole liner. Development work will be continued on both the toroid-rotator models in an effort to obtain a satisfactory mechanism for in-pile operation.

Since controlled operating temperatures to 300°C will be required to obtain the in-pile slurry corrosion data, tests have been initiated to obtain the information necessary for the design of suitable service systems. A contained cooling system will be operated to remove the gamma heat generated in the toroids ($\frac{1}{2}$–4 w/g has been estimated) and portions of the rotator structure while the reactor is operating at power. However, heating facilities, probably consisting of resistance heating wire, will be required to maintain the experiment operating temperature when the reactor is down.

13. RADIATION CORROSION

G. H. Jenks H. C. Savage

A. L. Bacarella
J. E. Baker
S. E. Bolt
J. W. Brown
R. J. Davis
V. A. DeCarlo
D. T. Jones
R. A. Lorenz
T. H. Mauney
J. R. McWherter
A. R. Olsen
J. A. Russell
M. D. Silverman
K. S. Warren
S. H. Wheeler
L. F. Woo
W. C. Yee

13.1 IN-PILE LOOPS

13.1.1 Development and Construction

(a) HB-2 Loop Package. – The all-titanium loop,[1] L-2-14, and the stainless steel loop,[1] L-2-17, were completed, tested, and placed in operation in beam hole HB-2 of the LITR during the past quarter.

(b) HB-4 Loop Package. – Loop L-4-18, now being constructed, is a type 347 stainless steel loop containing coupon-type corrosion specimens and stressed specimens. Type 347 stainless steel tapered-channel coupon holders in the core and line contain Zircaloy-2, type 347 stainless steel, and type 430L (Croloy 16-1) stainless steel. The type 430L stainless steel has exhibited corrosion resistance comparable to that of type 347 stainless steel in preliminary out-of-pile corrosion tests in the dynamic corrosion test loops, and may be superior to type 347 in its resistance to chloride-induced stress-corrosion cracking. In addition to the coupon corrosion specimens in the tapered-channel holders, two ladder-type coupon holders[2] containing coupon corrosion specimens of types 347 and 430L stainless steel, Zircaloy-2, Zr–15% Nb, titanium-55AX, and Ti–3% Al are included in both the core and in-line positions. One Zircaloy-2 stressed specimen is installed in the core and line position.

(c) ORR Loop Package. – Development work on a dynamic loop for operation in the ORR to obtain corrosion data continued this past quarter. A layout of the loop is shown in Fig. 13.1. This design will be used for the assembly of an experimental test model of the ORR in-pile loop. Fabrication of component parts for this test model, designated 0-1-20, has begun.

Heaters and coolers to handle the fission and gamma heat during in-pile operation have been designed and constructed. As previously mentioned,[1] two types of a combination heater-cooler unit were under test. Test results obtained during the past quarter indicate that a heater-cooler unit consisting of four 1000-w Calrod-type electric heaters and $\frac{3}{8}$-in.-OD stainless steel tubing cooling coils cast in aluminum around the $\frac{3}{8}$-in.-IPS loop piping will provide sufficient heating and cooling. This heater-cooler unit is shown in Fig. 13.2. With air-water mixtures as the coolant media, heat-removal rates up to approximately 7 kw at a loop temperature of 250°C have been obtained. Figure 13.3 is a plot of some representative test data. Two of these heater-cooler assemblies, incorporated in the test model as shown in Fig. 13.1, will provide in the ORR loop up to 8 kw of heat, as compared with 3 kw in the present LITR loops, and up to 14 kw of cooling, as compared with ~3 kw in the present LITR loops. Although the 14 kw of cooling capacity is below the 20 kw which has been estimated as the maximum requirement for some in-pile operating conditions, it is deemed adequate for the initial ORR in-pile operating experiments. In addition to the loop coolers the core cooler is capable of removing 3 to 4 kw of gamma heat absorbed in the core wall. Space is available, with minor design changes in the loop package, for additional lengths of heater-cooler if they are required for future loops.

The LITR-type loop core is being modified for the ORR loop to provide a more uniform flow pattern and increased solution velocity in the annulus region. The irregular annulus flow pattern in the LITR-type loop core makes it almost impossible to calculate the temperature of corrosion specimens suspended in the annulus stream and subjected to gamma heating. In an ORR loop using an LITR-type core, the temperature of the forward annulus

[1] G. H. Jenks *et al.*, *HRP Quar. Prog. Rep. Jan. 31, 1957*, ORNL-2272, p 102–103.

[2] G. H. Jenks *et al.*, *HRP Quar. Prog. Rep. Oct. 31, 1956*, ORNL-2222, p 100.

UNCLASSIFIED
ORNL-LR-DWG 21459

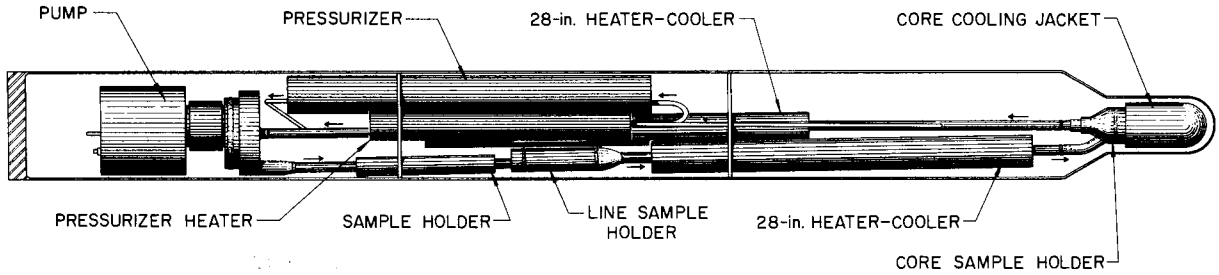

Fig. 13.1. ORR In-Pile Loop.

UNCLASSIFIED
ORNL-LR-DWG 21460

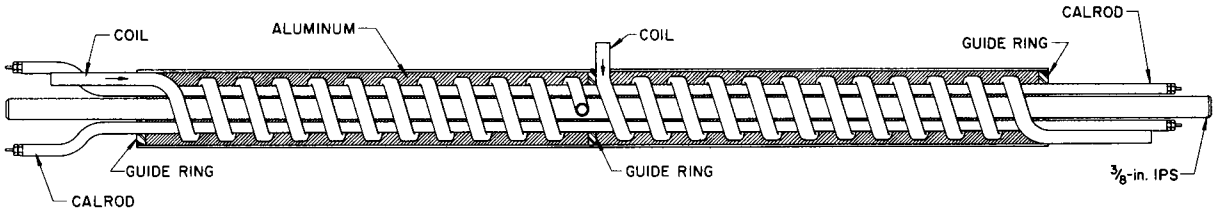

Fig. 13.2. Heater-Cooler for ORR Loop.

specimens would rise as much as 20°C above the average solution temperature. With the higher velocities and more uniform flow in the modified core, the temperature rise in specimens will be reduced and, in addition, it will be possible to make more reliable temperature calculations. The preliminary design of the ORR core employs the same shell as the LITR core; however, two tapered-channel coupon holders instead of one will be used. One holder will be in the inlet stream to the core and the other in the outlet stream. These, together with a lengthwise baffle plate which essentially splits the core in two halves, will cause the solution to make two lengthwise passes. This will give a velocity in an ORR core annulus approximately twice that in an LITR core annulus. Transparent models of the ORR loop core have been made and are being used to study flow patterns in the annulus.

Considerations of the gamma-ray intensity at the loop core position following reactor shutdown have led to the conclusion that provisions for retracting the loop should be included in the design. With the loop in the fully inserted position, reactor shutdown alone does not provide adequate safeguards against damage to the loop and specimens in the case of some of the loop malfunctions which must be anticipated.

A manually operated mechanism has been designed to permit an 18-in. retraction of the loop package during operation. A retraction of this distance effects a reduction of the neutron flux by a factor of about 100, and of the gamma-ray intensity by a factor of about 35. The expected effects of the full 18-in. retraction on the maximum power density and gamma heating in the experiment under typical operating conditions are summarized in Table 13.1.

13.1.2 General Description of In-Pile Loop Experiment L-4-13

Except for metallographic examination, the ninth in-pile loop experiment, L-4-13, has been completed. Details of this experiment and the results will be reported.[3] A summary is presented below.

[3] J. R. McWherter *et al.*, *HRP Radiation Corrosion Studies, In-Pile Loop L-4-13*, ORNL-2305 (in press).

For the first time, heavy water was used as the solvent in an in-pile loop experiment. Otherwise this experiment was operated under conditions similar to those for the previous HB-4 loops.[4] The temperature of the main stream was 250°C. The concentrations of UO_2SO_4 and $CuSO_4$ were 0.17 and 0.03 *M*, respectively (molarities are used here for ease in comparing heavy- with light-water solutions). The initial excess sulfuric acid concentration was 0.02 *M*. This acid concentration was employed in an effort to obtain information regarding the effect of acid concentration on steel corrosion under irradiation. Previous experiments in which the initial acid concentration was 0.04 *m* exhibited high over-all corrosion rates at the start of radiation and a marked decrease in rates at about the time that the calculated acid dropped below 0.03 *m* (ref 5). This drop in acidity is caused by the dissolution of nickel and manganese as corrosion proceeds. In the present experiment the excess acid ranged between 0.02 and 0.01 *M*, and the mean concentration was 0.015 *M*.

The loop body and the tapered-channel core and in-line coupon holders were fabricated from type 347 stainless steel. Loop L-2-10 was the only previous experiment with steel coupon holders. All other experiments, with the exception of L-4-12, had Zircaloy-2 holders; L-4-12 was equipped with titanium holders. Identical sets of corrosion coupons (24 each) were installed in the core and in-line holders and consisted of types 347 and 309 SCb stainless steel and crystal-bar zirconium. Six impact specimens were contained in both the core and the in-line positions. The specimens in both locations were of Zircaloy-3a and of a Zr–20% Nb alloy. In addition, there were two tensile specimens in the core position. These were made of Zircaloy-3a and of titanium A-40.

The structure of the loop was essentially the same as for the previous experiments.[4] The circulating pump was an ORNL 5-gpm pump of the outboard-bearing type with pure sintered aluminum oxide bearings and journal bushings.

No major operating difficulties were encountered; however, during operation of the loop the usual

[4]J. E. Baker *et al.*, *HRP Radiation Corrosion Studies (In-Pile Loop L-4-8)*, ORNL-2042 (Aug. 8, 1956).

[5]G. H. Jenks *et al.*, *HRP Quar. Prog. Rep. Oct. 31, 1956*, ORNL-2222, p 101–106.

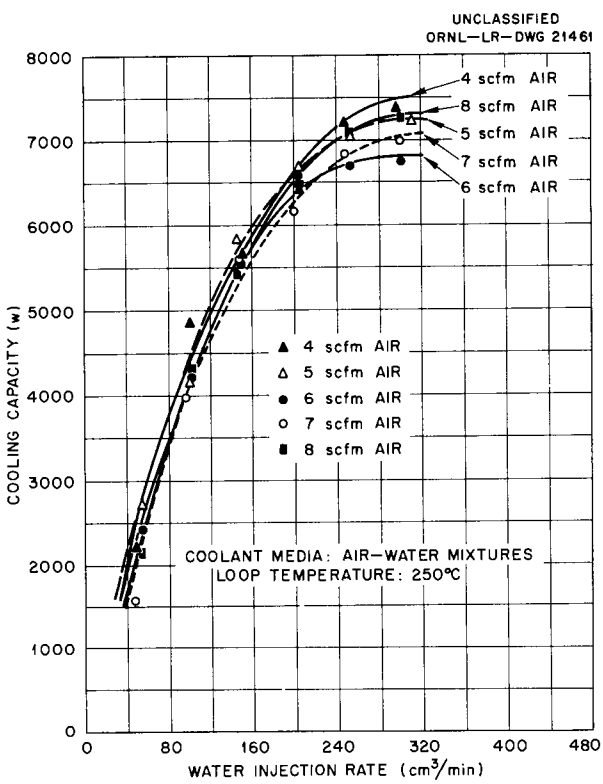

Fig. 13.3. Cooling Capacity of Heater-Cooler Unit for ORR In-Pile Loop Package.

Table 13.1. Expected Reductions of Radiation Intensities by Retraction of Loop

	Inserted		Retracted	
	Fission Heat (w/cc)	Gamma Heat (w/g)	Fission Heat (w/cc)	Gamma Heat (w/g)
Reactor at 30 Mw	100	5.5	1	0.16
10 min after reactor shutdown	0.01	0.5	~0	0.015

oxygen addition line appeared to be plugged, and additions had to be made through an alternate line. The experiment was terminated after 1042 hr of fuel circulation time, the first 73 hr of which were accumulated before the reactor went to power. The energy output of the LITR during the 969 hr of circulation after the reactor went to power was 2362 Mwhr. Essentially all the power was accumulated at the 3-Mw reactor level.

The average fission power during operation as determined from cesium analyses was 626 w. This is in reasonably good agreement with values observed in previous HB-4 experiments. The power density at a given position in the core was determined from measurements of the induced activities of types 347 and 309 SCb stainless steel core coupons. Measurements were also made of three pieces cut from the type 347 stainless steel core body. The core-body specimens gave flux values that averaged about 17% higher than those given by the core coupons. The power densities determined from induced activities of the core coupons ranged from 6.3 w/ml for the leading coupon to 1.1 w/ml for the rear coupon. The power density in solution at the nose of the core, calculated from induced activities, was 9.8 w/ml.

The average over-all corrosion rate of stainless steel, as calculated from the oxygen data, for the first 160 hr following the reactor startup was 2.5 mpy, and for the remaining 809 hr was 1.1 mpy. The over-all corrosion rates for the same periods, based on the amount of nickel in solution, were 2.5 and 0.7 mpy, respectively. The over-all rates for the total period of exposure to radiation were 1.3 mpy, based on oxygen-consumption data, and 1.0 mpy, based on the nickel data.

13.1.3 Qualitative Results of Inspection and Evaluation of Loop L-4-13

Minor difficulty in dismantling the loop was encountered when a repair sleeve on the cooling-water line would not clear the loop spacers. It was necessary to cut the cooling line near the core and remove the line with the loop. Components cut from the loop were the core, two in-line sample holders, the pressurizer, two sections from the pressurizer heater, a section of loop piping adjacent to the pump outlet, and the pump. The remainder of the loop package was buried. Several specimens of each material from the core and in-line coupon arrays, together with sections from the core cap, pressurizer heater, and main loop piping, were sent for hot metallographic examination.

All component surfaces outside the core were covered with scale. The scale was heavy, dark-brown, and rustlike in appearance except in the pressurizer. The scale in the liquid-phase portions of the pressurizer was heavy and black. In the vapor-phase region a thin dark-gray film was found on the surfaces. There was no evidence of localized attack on any of the components, including the pump impeller and volute. Further examination of the pressurizer revealed that the normal oxygen-addition port had been submerged in solution during operation and had become plugged with some of the heavy scale. This finding explains the oxygen-addition difficulties mentioned previously. The submersion was caused by a combination of factors: the capillary entrance was not on the vertical center line, the pressurizer was tilted from the horizontal, and the liquid level in the pressurizer was higher than usual.

All specimens outside the core were also uniformly coated with a heavy rustlike scale. As with all previous loops, cathodic defilming of the in-line coupons was only partially effective. All crystal-bar-zirconium in-line coupons, except one, showed weight increases following the final defilming. The in-line impact specimens were not defilmed but were transferred to the metallurgy group for inspection and evaluation.

The interior of the core body and the exterior of the core coupon holder, both type 347 stainless steel, were covered with scale. The scale at the forward or high-flux positions was soft and sooty-black in appearance, while the low-flux end was covered with a harder rustlike brown scale. The interior surfaces of the core coupon holder and all types 309 SCb and 347 stainless steel core coupons were covered with a dark-gray-to-black scale, the thickness of which increased from the high- to low-flux end of the holder. All the crystal-bar-zirconium core-holder coupons were free of scale but were covered with a thin iridescent film.

The single titanium A-40 tensile specimen in the core annulus was covered with a uniform gray film. The Zircaloy-3a core-annulus tensile and impact specimens were free from scale and were covered with a thin iridescent film, while the

Zr–20% Nb core-annulus impact specimens were covered with a uniform, tightly adherent, thin, dark scale.

13.1.4 Quantitative Results of Inspection and Evaluation of Loop L-4-13

All corrosion-rate values reported below were calculated from weight-loss data, with the exposed specimen area and total radiation time (equivalent to 787 hr of LITR operation at 3 Mw) used as the bases for the calculations. Average solution velocities across the coupons contained in the tapered type 347 stainless steel core and in-line holders were from 9.4 to 44.4 fps. As mentioned previously, power-density values were calculated on the basis of the thermal-neutron fluxes in the core-holder coupon positions.

(a) Crystal-Bar Zirconium. – This was the first loop experiment to contain full sets of crystal-bar-zirconium specimens. The only previous loop[6] with crystal-bar-zirconium specimens was L-4-11, which contained one core-holder coupon and three core-rod coupons of this material. Corrosion rates for the eight crystal-bar-zirconium core-holder coupons in the present experiment were power-density dependent. Observed rates were from 2.0 mpy at 1.4 w/ml to 3.9 mpy at 5.8 w/ml. Seven of the in-line crystal-bar-zirconium coupons showed weight increases. The eighth, located in position 23 in the holder, exhibited a rate of 1.6 mpy. As yet it has not been determined where the corrosion occurred on this specimen. It is possible that it occurred at the holder contact surface as a result of fretting, as was observed[5] in L-4-12. Final determination will await metallographic examination of the specimen. Solution velocities across the core and in-line zirconium holder coupons varied from 10.1 to 44.4 fps.

(b) Type 347 Stainless Steel. – Eight type 347 stainless steel coupons were contained in the core coupon holder. Corrosion rates for these specimens varied from 0.1 mpy at 1.1 w/ml to 7.2 mpy at 4.8 w/ml. The solution velocity across the specimens varied from 9.9 to 40.1 fps and produced no apparent effect on the relative corrosion rates. An identical in-line-holder coupon array exhibited corrosion rates from 0.6 to 0.1 mpy and averaged 0.3 mpy.

(c) Type 309 SCb Stainless Steel. – Eight type 309 SCb stainless steel coupons were contained in the core coupon holder. Corrosion rates for these specimens varied from 0.1 mpy at 1.7 w/ml to 147 mpy at 6.3 w/ml. Seven in-line-holder coupons of type 309 SCb stainless steel showed corrosion rates from 0.2 to 0.9 mpy. The eighth coupon, located in position 16 in the in-line holder, showed a weight increase after defilming. The average rate for the seven coupons was 0.41 mpy. Solution velocities across both sets of specimens were the same and varied from 9.4 to 37.0 fps.

13.1.5 Discussion of Results from Loop L-4-13

In a previous discussion of Zircaloy-2 in-pile corrosion data,[7] the relationship between corrosion rate and power density over the range studied was shown to be expressed by equations of the general form:

$$CR = APD(1 - e^{-B/CR^{1.5}}) , \quad (1)$$

where

CR = corrosion rate, mpy,

PD = power density, w/ml,

A = constant depending on solution composition and temperature,

B = constant depending on temperature.

Values for the constants A and B were previously established at 1.25 and 8.3, respectively, from in-pile autoclave and loop experiments conducted at 250°C and utilizing 0.17 m UO_2SO_4 solutions. These data plus more recent autoclave data were re-evaluated, and the resulting constants A and B have been changed to 1.25 and 6.5, respectively.

Loop L-4-13 contained a number of crystal-bar-zirconium specimens but no Zircaloy-2. The radiation-corrosion behavior of crystal-bar zirconium in this experiment is also reasonably well described by Eq. 1, with the constants 1.25 and 6.5. Similarity in the radiation-corrosion behavior of crystal-bar zirconium and Zircaloy-2 has been noted previously[6] in loop L-4-11. Consequently, the results of this experiment may be considered as indicating that the corrosion of crystal-bar zirconium in a heavy-water solution under the

[6] J. R. McWherter *et al.*, *HRP Quar. Prog. Rep. July 31, 1956*, ORNL-2148, p 93–97.

[7] G. H. Jenks *et,al.*, *HRP Quar. Prog. Rep. Jan. 31, 1957*, ORNL-2272, p 107–110.

conditions of this experiment is not significantly different from that in a normal-water solution under otherwise similar conditions.

In contrast, a bomb test,[8] Z-20, of the effect on the corrosion of Zircaloy-2 of the substitution of D_2O for light water indicated that the rate in the D_2O solution was 30% greater than that in a light-water solution under otherwise similar conditions. The conditions for the autoclave test were similar to those for the present loop experiment, except that the autoclave solution was 0.04 *M* in excess H_2SO_4 and the fission power densities were higher than those in the loop.

The explanation of the difference between these various D_2O results is uncertain. However, it is considered unlikely that the substitution of D_2O for H_2O affects the corrosion of Zircaloy-2 but does not affect that of crystal-bar zirconium. It is considered more likely that the higher rate in the D_2O bomb experiment was a result of the same type of effect that is observed in bomb experiments when excess acid is omitted from the solution. Observed rates in the absence of excess acid are about 30% greater than in the presence[8] of 0.04 *m* excess H_2SO_4. No significant effect of acid concentration has been detected in the results of the various 250°C loop experiments.[9] It is true that none of these loop solutions were entirely free of excess acid, but the concentration in one experiment, EE, was held between calculated concentrations of 0.008 to 0.004 *m*, with a mean concentration of 0.006 *m*. In another, L-4-12, the calculated acid concentration ranged between the initial 0.04 *m* and a final 0.025 *m*, with a mean concentration of 0.03 *m*. If small differences are considered significant, the rates observed in the solution of lower acidity fall below those observed in the solutions of higher acidity.

The corrosion data for the steel specimens which were located in the core holder are shown in Fig. 13.4, with the logarithm of the corrosion rate plotted against the fission power density which prevailed in solution adjacent to a given specimen. On the basis of this correlation, the results for the type 309 SCb stainless steel specimens agree reasonably well with those for the type 347 steel.

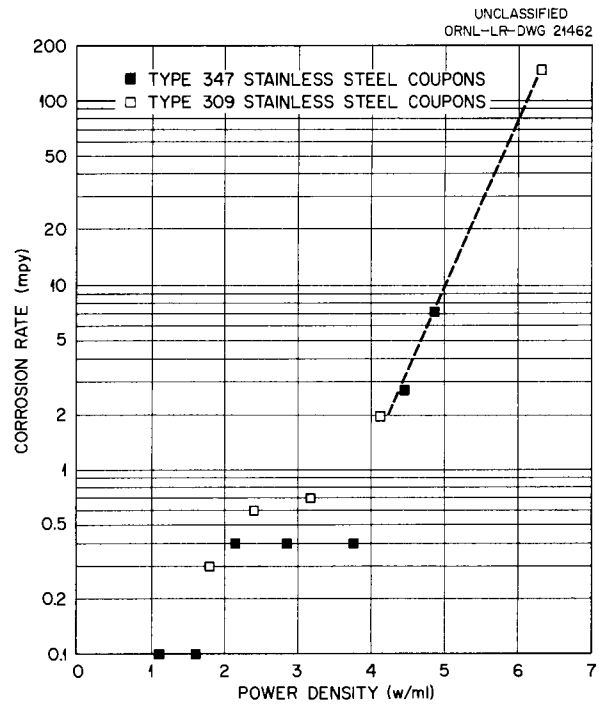

Fig. 13.4. Stainless Steel Corrosion Rate vs Power Density in Experiment L-4-13.

A similar plot for previous loops has been reported.[10] Rates for the type 347 steel in the present experiment are significantly lower than those observed for similarly located specimens at similar power densities in previous experiments. Other evidence that the corrosion rate of steel in the core was less in this loop than in some previous experiments was provided by the results of the over-all rate measurements. The initial over-all rate of 2.5 mpy is a factor of 3 to 4 lower than that observed in previous loops with steel cores when the initial excess acid concentration[11] is 0.04 *m*. As discussed in a previous report,[11] there is evidence that the high initial over-all rates which have been observed are representative of high corrosion rates in the core during the initial period. There is also evidence that the high rates are associated with acid concentrations greater than about 0.03 *m*.

[8] G. H. Jenks *et al.*, *HRP Quar. Prog. Rep. Oct. 31, 1956*, ORNL-2222, p 109–111.

[9] G. H. Jenks *et al.*, *HRP Quar. Prog. Rep. Oct. 31, 1956*, ORNL-2222, p 104, Fig. 13.2.

[10] J. E. Baker *et al.*, *HRP Radiation Corrosion Studies (In-Pile Loop L-4-8)*, ORNL-2042 (Aug. 8, 1956).

[11] G. H. Jenks *et al.*, *HRP Quar. Prog. Rep. Oct. 31, 1956*, ORNL-2222, p 101–106.

On the basis of the above consideration it can be speculated that the results of this experiment indicate that corrosion of steel in a fissioning solution is less when the acid concentration is in the range 0.02 to 0.01 *m* than when the concentration range is 0.04 to 0.02 *m*. It should also be noted that the rates for the core-holder specimens in this loop are less than those observed in the loop experiment, EE, for which the concentration of excess acid was maintained between 0.008 and 0.004 *m*. However, these speculations regarding the beneficial effects of the particular acid concentration employed in this experiment cannot be regarded very seriously at this time. The D_2O solution employed in this loop may have a different effect on steel corrosion than does a light-water solution. Also, a given holder material may have an effect on corrosion under radiation which is different from the effect of some other material. Steel holders were employed in this loop, whereas previous loops were equipped with Zircaloy-2 or, in one experiment, titanium holders. Additional experiments will be required to resolve the effects of these various factors.

13.1.6 In-Pile Loop L-4-16

Stainless steel loop L-4-16 has been exposed in beam hole HB-4 at the LITR. Total circulation time for the experiment was 1032 hr, of which 135 hr were accumulated outside the reactor. The energy output of the LITR during in-pile operation was 2325 Mwhr. Almost all this energy was liberated at the 3-Mw level. Operation of the loop was halted by failure of the fuel circulation pump. Disassembly and examination of the loop and specimens are in progress.

The operating conditions and contents of loop L-4-16 were reported previously.[7] The initial solution was 0.17 *m* UO_2SO_4 (enriched), 0.015 *m* $CuSO_4$, and 0.025 *m* H_2SO_4. The calculated free-acid concentration was maintained reasonably constant during the run, and the mean acid concentration was 0.024 *m*. The main-stream operating temperature was 280°C; the pressurizer temperature was 296°C.

No evidence of solution instability was observed at these operating conditions. The over-all stainless steel corrosion rate was 0.5 mpy based on both the nickel-in-solution and oxygen-consumption data.

13.1.7 In-Pile Loop L-2-14

Experiment L-2-14 was the first all-titanium loop. It was also the first loop experiment to employ a solution 0.4 *m* in excess H_2SO_4. The objective of this experiment was to determine the effect of a solution of this high acidity on the radiation corrosion of Zircaloy-2 and titanium. Tapered-channel coupon holders of titanium 75A in the core and in-line positions initially contained coupon specimens of titanium alloys, zirconium alloys, and stainless steel. Prior to placing the loop in the reactor, the steel was probably dissolved in on out-of-pile run with a normal-uranium solution with 0.4 *m* H_2SO_4.

The solution charged to loop L-2-14 for in-pile operation was 0.17 *m* UO_2SO_4 (enriched), 0.15 *m* $CuSO_4$, and 0.4 *m* H_2SO_4. The uranyl sulfate solution used as makeup to replace samples withdrawn from the loop was only 0.07 *m* H_2SO_4 and contained 100 ppm added chromium to minimize the attack on the valve stems during solution addition. The calculated free-acid concentration decreased during operation from 0.42 to 0.38 *m*. The mean free-acid concentration was 0.39 *m*. The main-stream operating temperature was 280°C, and the pressurizer temperature was 300°C. Total circulation time for the experiment was 663 hr, of which 46 hr were accumulated outside the reactor. The energy output of the LITR during in-pile operation was 1530 Mwhr. Almost all this energy was liberated at the 3-Mw level. Operation of the loop was halted by failure of the fuel circulation pump. Disassembly and examination of the loop and specimens are in progress. The over-all titanium corrosion rate based on oxygen consumption was 2.7 mpy.

Appreciable quantities of aluminum were detected in solution samples withdrawn from the loop during pretreatment operations and also during operation with enriched solution. In addition, analysis of a precipitate found in the final enriched-solution sample, withdrawn before the pump failed, showed aluminum to be present.

13.1.8 In-Pile Loop L-2-17

Stainless steel loop L-2-17 is now being exposed in beam hole HB-2 at the LITR. The core and in-line coupon holders are tapered-channel holders

fabricated of Zircaloy-2 and contain coupon specimens of type 347 stainless steel, titanium-55AX, and Zircaloy-2.

The solution composition for L-2-17 is 0.04 *m* UO_2SO_4 (enriched), 0.005 *m* $CuSO_4$, and 0.025 *m* H_2SO_4 in a light-water solvent. With the exception of the light-water solvent, this solution is similar to the proposed HRT solution. The solution used as makeup solution to replace samples withdrawn from the loop is the same as that above, except that it contains 0.06 *m* H_2SO_4 to replace acid consumed in corrosion and 100 ppm chromium to minimize attack on the valve stems during solution addition.

Operating temperatures for this loop are 300°C in the main stream and 315°C in the pressurizer. The purpose of this experiment is to determine the effect of the higher operating temperature on the corrosion rate of the specimens. Experiment L-2-10 (ref 12), which was otherwise similar, had a main-stream temperature of 280°C.

13.2 IN-PILE AUTOCLAVE TESTS, LITR

13.2.1 Development and Construction

Operational testing of the new in-pile autoclave mockup test facility, previously described,[13] has been completed. During the initial testing it became apparent that certain revisions to the autoclave assembly were necessary in order to maintain close control of temperature and pressure during operation. For example, it was observed that the operating temperature of the autoclave fluctuated excessively when the heating or cooling rates were varied in a manner which simulated the expected in-pile operating conditions. The temperature of the autoclave is maintained by an aluminum heater-cooler assembly[14] which surrounds the autoclave. The assembly is wound alternately with electrical resistance wire and aluminum cooling coils. The cooling-to-heating-capacity ratio of this assembly was found to be 6 to 1, with an air-water mixture being used as the coolant and with the heater wire operating at its maximum temperature. To reduce the temperature fluctuations this ratio was decreased by substituting stainless steel for the aluminum cooling coils, which reduced the cooling, and by doubling the windings of the heater wire, which increased the heating capacity. These changes reduced the cooling-to-heating-capacity ratio to 2 to 1 and decreased the temperature fluctuations to an acceptable value. Another reason for substituting stainless steel for aluminum in the cooling coils was the danger of high-temperature corrosion of the aluminum when air-water mixtures are used as the coolant media. Temperatures in excess of 250°C may be attained in the exit coolant line.

It was also noted that the temperature of the rear or low-flux end of the autoclave wall was as much as 20°C lower than that of the middle or front end. This resulted from the fact that the coolant entered the heater-cooler assembly at the rear end of the autoclave. In the reactor this wall-temperature gradient would be increased by the neutron-flux gradient. In an attempt to reduce this temperature gradient, an experiment was conducted in which the coolant inlet was moved to the front end of the heater-cooler assembly. No appreciable temperature gradient from front to rear of the autoclave was observed during this experiment.

In an attempt to obtain a more reliable measure of the true solution temperature in the autoclave, a thermocouple well was installed in the autoclave. After comparing the temperatures observed in the well with those of the outside wall of the autoclave, it was concluded that the well temperatures were more reliable points from which to control and measure the operating temperature of the experiment during reactor exposure.

To obtain the neutron-flux gradient to which the bomb is exposed, during in-pile operation, a canned Al-Co alloy wire will be included in the bomb as a flux monitor.

The revisions described above, as well as other minor modifications, have been incorporated into the design of this new experiment to facilitate assembly and to eliminate operational difficulties. The first experiment, L51Z-105, for operation in the new multibomb radiation-corrosion facility has been assembled and pretreated at the Y-12 site and is ready for in-pile operation.

---

[12] G. H. Jenks *et al.*, *HRP Quar. Prog. Rep. Jan. 31, 1957*, ORNL-2272, p 104–108.

[13] G. H. Jenks *et al.*, *HRP Quar. Prog. Rep. Jan. 31, 1957*, ORNL-2272, p 110.

[14] G. H. Jenks *et al.*, *HRP Quar. Prog. Rep. Jan. 31, 1957*, ORNL-2272, p 112.

13.2.2 In-Pile Tests

Four rocking-autoclave experiments have been performed in the LITR during the past quarter – two Zircaloy-2 experiments in the HB-5 facility and one Zircaloy-2 and one type 347 stainless steel experiment in HB-6. The data for each experiment are in Table 13.2. Atmospheric nitrogen was excluded from all runs reported.

(a) Experiment Z-22. – Experiment Z-22 was the second LITR exposure of a system employing a depleted-fuel solution. The earlier, similar experiment,[15] Z-13 (see Table 13.2), was filled in such a way as to include about 600 ppm of nitrogen as N_2. In comparison, Z-22 was filled in an oxygen atmosphere in order to exclude nitrogen. Some of the pressure data obtained in each experiment are plotted in Fig. 13.5. Both Z-13 and Z-22 demonstrated a phenomenon which has been apparent only with these two depleted-uranium experiments. A relation to a pressure-excursion phenomenon observed in experiments of appreciable fission power density, described by Day,[16] is, however, possible. During the initial portion of both experiments Z-13 and Z-22, the pressure increased appreciably, reached a maximum, and then decreased to somewhat less than the original pressure. Following this pressure excursion in each case, the pressure decreased slowly and constantly with continued exposure. In each case an extrapolation of a line through the later points intersects the zero time axis at a pressure value which is in near agreement with the initial pressure. This agreement may indicate that the corrosion was proceeding at the constant rate from the start, and that some other phenomenon affecting the gas pressure was superimposed on the effect due to corrosion.

The total penetration measured by pin weight losses in both Z-13 and Z-22 is considerably lower than that measured from oxygen consumption. This is probably due to incomplete defilming, since the film in these depleted runs seems to be more tenacious and more difficult to remove than films exposed even to as little as 2 w/ml of fission power. Hence the oxygen data are considered more reliable than the weight data.

In the present experiment the rate at 250°C following the pressure excursion was 0.78 mpy as determined from oxygen-depletion measurements. The rate at 280°C in the subsequent exposure was 1.4 mpy. In the previous experiment, Z-13, the indicated rate during the initial exposure at 250°C was 1.8 mpy, and the rate in the subsequent 280°C exposure was 0.75 mpy. A second exposure at 250°C was made following the exposures at 280 and 300°C, and the rate observed in this case was 0.39 mpy. If the initial Z-13 data at 250°C are neglected, the remaining data indicate that the rates at 250 and 280°C in Z-13 were about one-half those observed in Z-22. However, in view of the pressure-excursion phenomenon, which may have influenced all the oxygen data for both experiments, and the discrepancies between pin and oxygen data, the differences in corrosion rates between Z-13 and Z-22 are not considered significant.

In considering possible causes of the pressure excursion, it must be assumed that the gas which supports the increase in pressure is oxygen. Each bomb contained excess oxygen at the start, and each solution was 0.02 *m* in $CuSO_4$. At the low fission power densities which prevailed, molecular hydrogen was produced at a very low rate, and a negligible steady-state radiolytic-gas pressure would be expected. Furthermore, many of the pressure readings were taken after the reactor had been at zero power for times sufficient to permit the recombination of any radiolytic gas which may have been present.

If it is assumed that the increase in pressure represents an increase in oxygen pressure, then it appears that hydrogen was lost from the bomb in some manner during the initial exposure. This loss would leave uncombined oxygen gas within the bomb. Since the excess pressure did not persist, the majority of the lost hydrogen was eventually recovered within the system. No mechanism is pictured for this process at this time other than that of the metal first absorbing hydrogen and later releasing it.

(b) Experiment Z-23. – Experiment Z-23 employed a solution of 1.3 *m* UO_2SO_4, 93% enriched, and was carried out in an attempt to gain information regarding the radiation effect on Zircaloy-2 at very high power densities. The very high rate of heat

[15] G. H. Jenks *et al.*, *HRP Quar. Prog. Rep. July 31, 1955*, ORNL-1943, p 129.

[16] H. O. Day, *The Anomalous Decrease of Radiolytic Gas Pressure in In-Pile Corrosion Studies. The Possible Importance to the Homogeneous Reactor Project*, ORNL CF-56-9-26 (Sept. 11, 1956).

Table 13.2. LITR In-Pile Bomb Data

Bomb No.	LITR Beam Hole	Bomb Material	Solution Composition (m)			Enrichment (% U^{235})	Exposure Temperature (°C)	Fission Power Density (w/ml)	Irradiation Time (hr) (1 hr = 3 Mwhr)	Penetration (mils)		Corrosion Rate, O_2 Data (mpy)
			UO_2SO_4	$CuSO_4$	H_2SO_4					O_2 Data	Pin Weight Data	
Z-22	HB-5	Zr-2	0.170	0.02	0	0.054	250	0.01	514.8	0.059	0.019	0.78[a]
							280	0.009	131.9			1.4
Z-23	HB-5	Zr-2	1.274	0.04	0.04	93.2	280	109	20.5	0.024	0.055	23[b]
L6Z-102	HB-6	Zr-2	0.169	0.04	0	12.0	250	1.2	350.3	0.309	0.266	2.0
							280	1.2	733.2			2.3
L6S-103	HB-6	347 SS	0.174	0.01	0	93.2	250	6.3	897.1	0.062	0.066	0 (380 hr)
												2.4 (150 hr)
												0.30 (370 hr)
Z-13	HB-5	Zr-2	0.168	0.02	0	0.054	250	0.01	579	0.212	0.123	1.8[c]
							280	0.01	265			0.75
							300	0.009	302			1.3
							250	0.01	442			0.39

[a]During the initial 100 hr of exposure, the pressure went through a maximum as described in the text. The rate reported corresponds to the oxygen consumption after the initial 100-hr period.

[b]This rate is probably erroneous; see text.

[c]Rate calculated from pin weight loss.

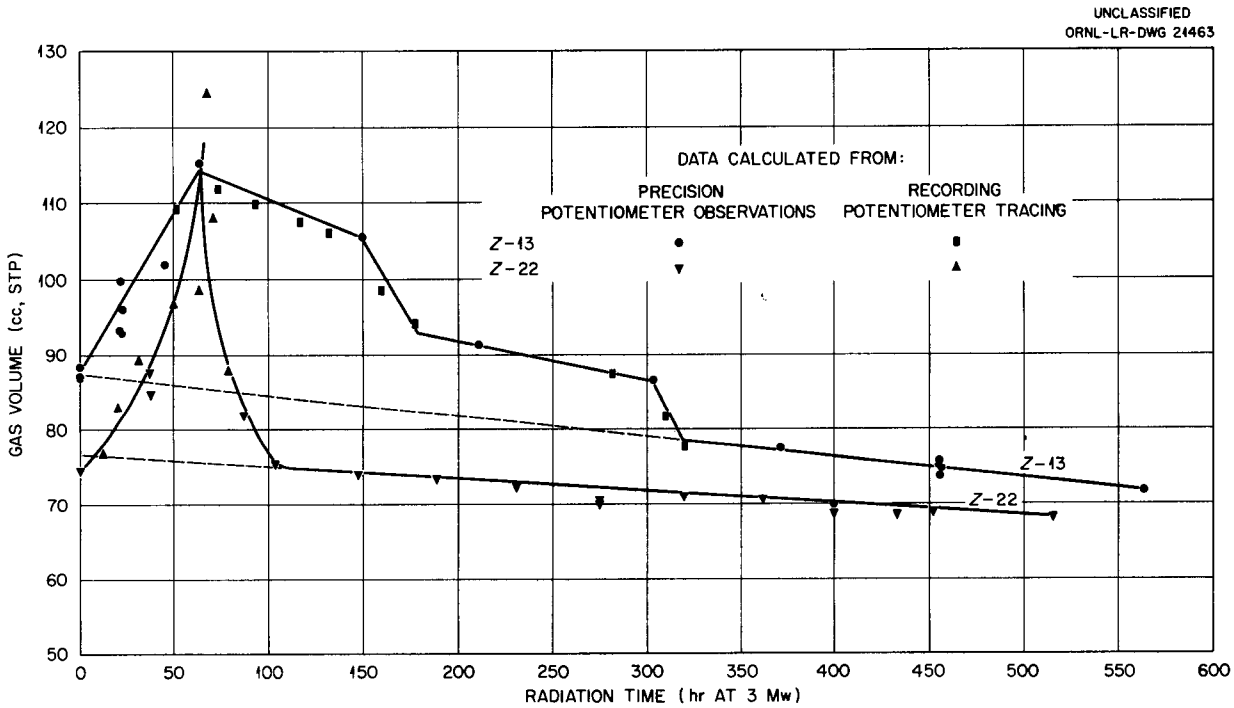

Fig. 13.5. Calculated Gas Volume in Z-13 and Z-22 During Initial Portion of Experiments.

generation in the bomb (~500 w) and the probable shadowing of neutrons at the high concentration of U^{235} introduced difficulties which make the results less precise than usual. The experiment was terminated at the end of 20.5 hr of radiation exposure because of a stoppage in the capillary connection.

The neutron flux prevailing in the bomb during exposure was determined as usual from measurements of the induced Zr^{95} activity in the pin specimens. Each of the six specimens was measured, and the values for the neutron flux determined are listed in Table 13.3. The corresponding power densities as well as corrosion penetration from pin weight losses are included in the table. The data from two pins are out of line; the flux values for these are higher, and the corrosion penetrations are lower than the average of the others. The neutron-flux values are considerably higher than the (0.9 to 1.6) $\times 10^{13}$ neutrons·cm^{-2}·sec^{-1} previously measured in HB-5 of the LITR. For these reasons, only the data from the four pins, L′, M′, S′, and L, have been averaged and reported in Table 13.2.

The corrosion rate indicated by pin results (23 mpy) is in near agreement with the rate of 21 mpy predicted by use of the equation

$$CR = APD(1 - e^{-B/CR^{1.5}}) ,$$

where $A = 0.318$ and $B = 95$. The constants were evaluated from observations from lower-power-density experiments. Constant B, which is considered to be temperature dependent only, was evaluated from essentially all previous 280°C corrosion data. The equations have been discussed by Jenks *et al.*,[17] although the value of constant B reported for 280°C data has since been revised due to the inclusion of more data. Constant A is dependent on the nature of the solution, as well as temperature, and was evaluated by substitution of the corrosion rate and power density observed[18] at 280°C in experiment Z-16 (1.355 *m* UO_2SO_4, 0.043 *m* $CuSO_4$, 0.043 *m* H_2SO_4, 23.6 w/ml, 7.5 mpy). It is interesting to note that linear extrapolation of the Z-16 result predicts a corrosion rate of 34.7 mpy at 109 w/ml.

Considerable uranium was found in the corrosion film of the Z-23 experiment. Of the 1135 mg of uranium put into the bomb, about 14 mg (calculated from analysis of film on the pins) was found in the film. This is a small fraction of the total uranium, but it constitutes nearly 17% of the film.

The corrosion rate reported was calculated from pin weight-loss data. The oxygen consumption indicates 21 mpy, which is in close agreement with the weight-loss data. However, in view of heat flux (~12 w/cm^2), which presumably caused

[17] G. H. Jenks *et al.*, *HRP Quar. Prog. Rep. Oct. 31, 1956*, ORNL-2222, p 111.

[18] G. H. Jenks *et al.*, *HRP Quar. Prog. Rep. July 31, 1956*, ORNL-2148, p 99.

Table 13.3. Power-Density Data for Z-23

Pin Identification	Slow-Neutron Flux (neutrons·cm^{-2}·sec^{-1})	Power Density (w/ml)	Corrosion Penetration from Weight Loss (mils)
L′	0.99×10^{13}	107	0.056
M′	1.01×10^{13}	109	0.056
S′	1.03×10^{13}	112	0.058
L	1.00×10^{13}	108	0.049
Av (above pins)	1.01×10^{13}	109	0.055
M	1.76×10^{13}	191	0.039
S	2.08×10^{13}	226	0.029

the temperature of the bomb wall to run considerably lower than the solution temperature, the pin weight-loss data are considered to more reliably show the 280°C corrosion rate.

(c) Experiment L6Z-102. – This Zircaloy-2 experiment was run to establish the nature of the relationship of corrosion rate vs power density at a low power density in the 0.17 *m* UO_2SO_4 system without excess acid. The rate observed at 250°C agrees fairly well with that predicted by previously reported correlations,[17] but the very slight increase in rate in raising the temperature to 280°C disagrees with the predicted increase of a factor of 2. The results of this experiment, together with preliminary data from in-pile loops L-2-15 and L-4-16, indicate that the constants in the equation[17] for corrosion rate vs power density for 280°C and the solution used in L6Z-102 have the values $A = 2.45$ and $B = 95$, rather than $A = 3.8$ and $B = 40$, as reported earlier.

(d) Experiment L6S-103. – This type 347 stainless steel experiment was carefully assembled in a way to exclude atmospheric nitrogen. Otherwise L6S-103 was similar to H-49 and H-51 (ref 19); H-96 (refs 20 and 21) was also similar except for the 0.0011 *m* $KTcO_4$ contained in that solution. All three of these earlier experiments (H-49, H-51, and H-96) showed similar corrosion, that is, 0.5 to 1 mpy for 200 to 250 hr, followed by a sharp break to a rate of 5 to 6 mpy for 75 to 125 hr. Experiment H-96 was run longer than the others, and from 350 hr to the end of the experiment the rate was 2.6 mpy.

Corrosion in L6S-103 was much less than in earlier experiments. In fact, for 380 hr (Table 13.2), no corrosion was detected by oxygen consumption. At the end of this time corrosion definitely started and continued quite linearly at 2.4 mpy for 150 hr. Then the rate again changed sharply, to 0.30 mpy, and this rate persisted for the remainder of the experiment. This behavior is qualitatively similar to that of H-96, in that two rather sharp breaks and three different rates were exhibited.

It is noteworthy that analysis of the solution for NO_3^- following irradiation indicated that this ion was present at a concentration of 327 ppm. Because of insufficient solution, no analysis for total nitrogen was carried out. In a previous bomb test in which atmospheric nitrogen was included in the charge,[22] the analyses of the final solution indicated much smaller amounts of NO_3^- but about 900 ppm of nitrogen in a total nitrogen analysis. Hence it seems likely that the total nitrogen in the present solution was greater than that indicated by the NO_3^- analysis. The source of this nitrogen is unknown, although it probably was not contamination in the bomb charge. The recent Zircaloy-2 bomb, L6Z-102 (described above), which was charged in a similar manner, exhibited only 8 ppm nitrogen in a total nitrogen analysis.

---

[19] S. F. Clark *et al.*, *HRP Quar. Prog. Rep. July 31, 1954*, ORNL-1772, p 162.

[20] G. H. Jenks *et al.*, *HRP Quar. Prog. Rep. Oct. 31, 1956*, ORNL-2222, p 107.

[21] G. H. Jenks *et al.*, *HRP Quar. Prog. Rep. April 30, 1956*, ORNL-2096, p 93.

[22] G. H. Jenks *et al.*, *HRP Quar. Prog. Rep. Jan. 31, 1957*, ORNL-2272, p 110.

14. METALLURGY

G. M. Adamson

R. G. Berggren
J. P. Hammond
T. M. Kegley
W. J. Leonard
M. L. Picklesimer
J. J. Prislinger
P. L. Rittenhouse
R. L. Stephenson
J. K. White
J. C. Wilson

14.1 PHYSICAL METALLURGY

14.1.1 Zirconium-Alloy Development

Zirconium-niobium alloys, which have shown an in-pile corrosion resistance superior to that of Zircaloy-2, are being studied in the alloy development program. Improvement of the corrosion resistance of the Zr-Nb alloys and a determination of the transformation kinetics and mechanisms of the alloys are major objectives of the program. Most of the work has been and will continue to be concentrated on the Zr–15% Nb base alloys, with minor additions of ternary elements. The earlier work on the Zr–15% Nb base systems was reported previously,[1,2] where some micrographs and age-hardening curves were presented in interpretation of the transformation kinetics and products of the system. It was concluded that the major hardening observed on subcritical heat treatment of the eutectoidal alloys was caused by the formation of the transition phase "omega," quite like that formed in the alpha-beta titanium alloys. Overaging of the alloys was observed only at 500 and 600°C and in about two weeks.

Recently, studies of the quench-and-reheat type have been made on the Zr–15% Nb, sponge Zr–15% Nb, Zr–15% Nb–1% Fe, and Zr–15% Nb–2% Pd alloys in the isothermal transformation machine at temperatures from 400 to 600°C for times from 2 min to 1 hr. The specimens are immersed bare for the desired time interval in a constant-temperature lead bath, where they are heated very quickly to bath temperature (less than 5 sec to within 1°C of bath temperature), in contrast with the much slower heating rates in the prior studies, where the specimens were capsulated in quartz in vacuum and plunged into a hot furnace (about 7 to 8 min to within 5°C of furnace temperature). The time-temperature-hardness curves are presented in Figs. 14.1(*a–d*). The data agree reasonably well with those for the capsulated specimens,[2] with the exception of the as-quenched hardnesses. It is believed that there was a small amount of cold work present in the last series of specimens, since they were sheared to approximate size after beta quenching. Consequently, specimens which have not been sheared are now being tested. There is also a possibility of a difference in composition, because the specimens were taken from a different ingot. The data from the transformation-machine specimens do indicate the same trend as that in the capsulated specimens; that is, the addition of 1% Fe and 2% Pd slows down the rate of precipitation of the omega phase appreciably, but not so much as had been hoped.

A difference in the microstructure of the specimens processed by the two methods has been observed and is shown for the 30-min and 1-hr specimens at 600°C in Fig. 14.2 and for various periods of time and at various temperatures in Fig. 14.3. Specimens have been run ot 500, 550, and 600°C in the transformation machine, but the grain-boundary transformation observed in the capsulated specimens at 600°C has not been seen except for a very small amount in the 500°C specimens. Specimens will now be run at 525 and 575°C to determine whether the grain-boundary transformation occurs at these temperatures. It is now believed, because of the transformation-machine data, that the grain-boundary transformation observed in the 600°C capsulated specimens forms during the heating of the specimens to temperature, and that the reason for the differences in the character of the transformation product in the 30-min and 1-hr (600°C) specimens of the Zr–15% Nb alloy is that the transformation to this product does not occur at 600°C but at a lower temperature;

[1] G. M. Adamson *et al.*, *HRP Quar. Prog. Rep. Oct. 31, 1956*, ORNL-2222, p 114–116.

[2] G. M. Adamson *et al.*, *HRP Quar. Prog. Rep. Jan. 31, 1957*, ORNL-2272, p 119–123.

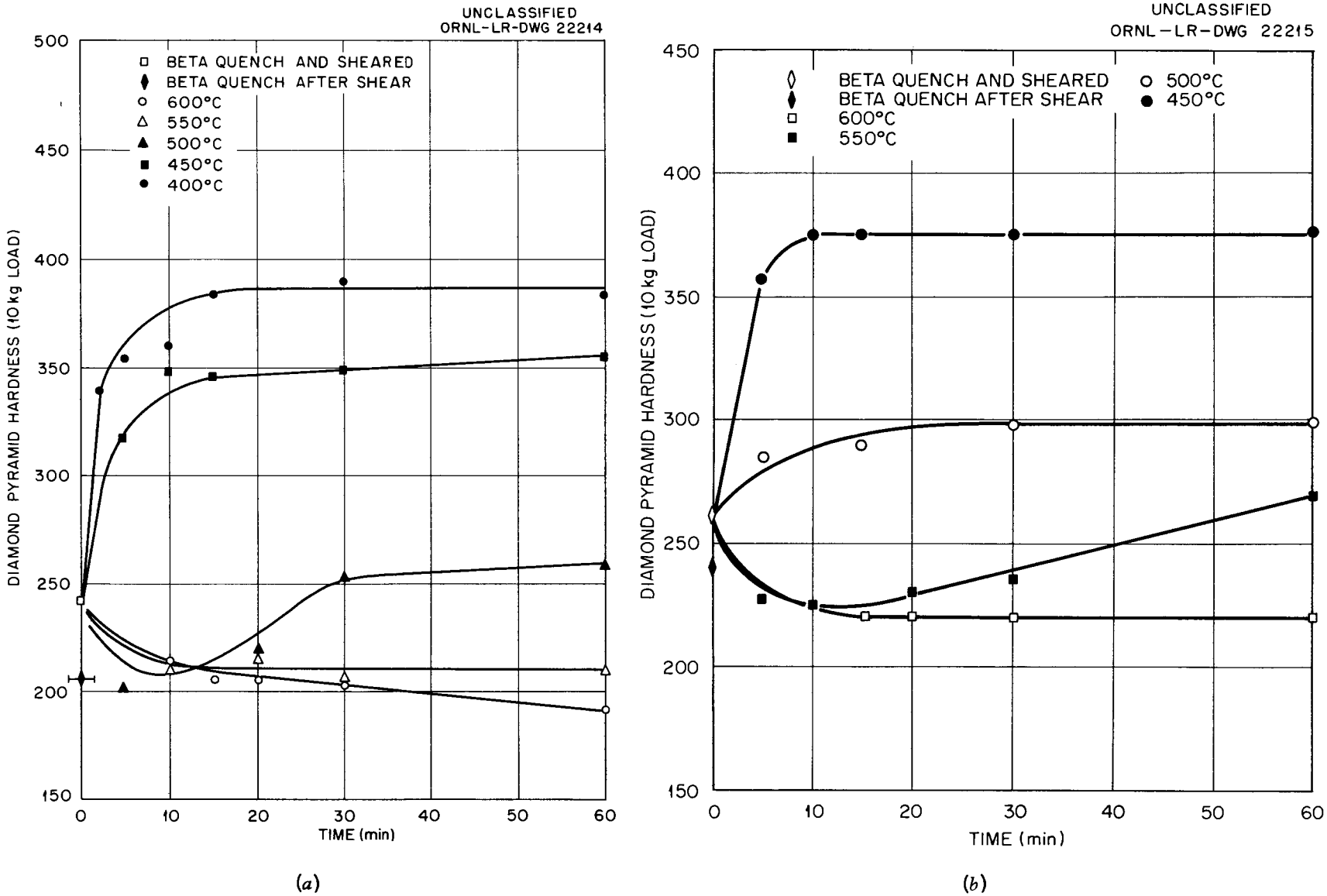

Fig. 14.1. (*a*) **Quench-and-Reheat Time, Temperature, Hardness Curves for Zr–15% Nb Aged in the Transformation Machine.** (*b*) **Quench-and-Reheat Time, Temperature, Hardness Curves for Sponge Zr–15% Nb Aged in the Transformation Machine.**

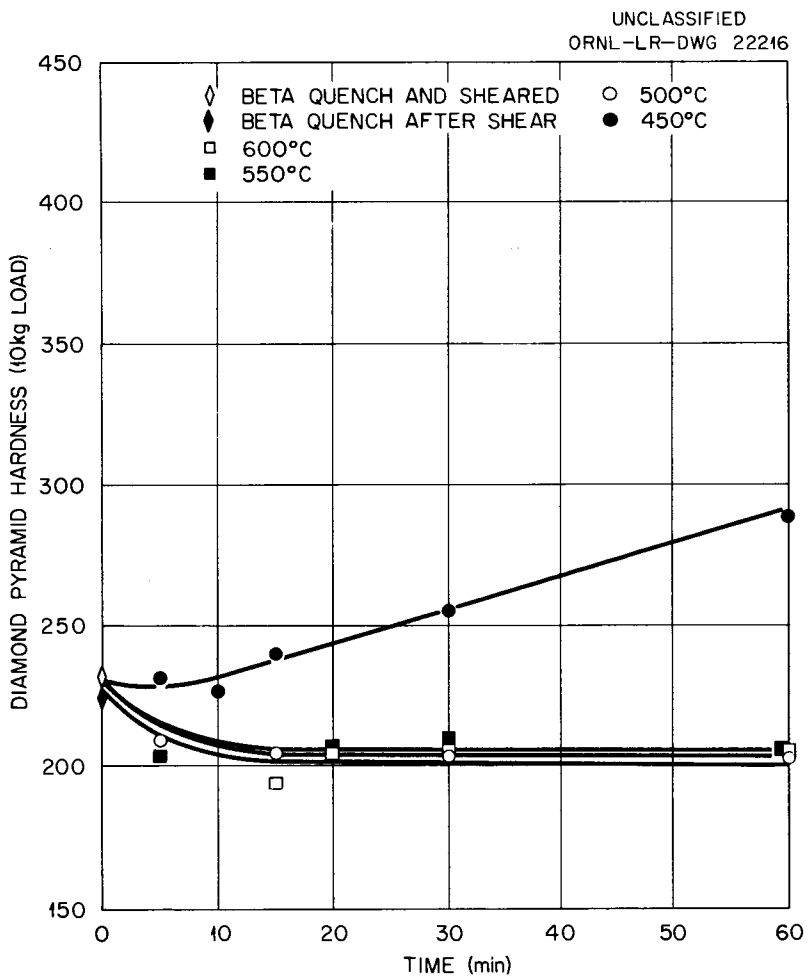

(c)

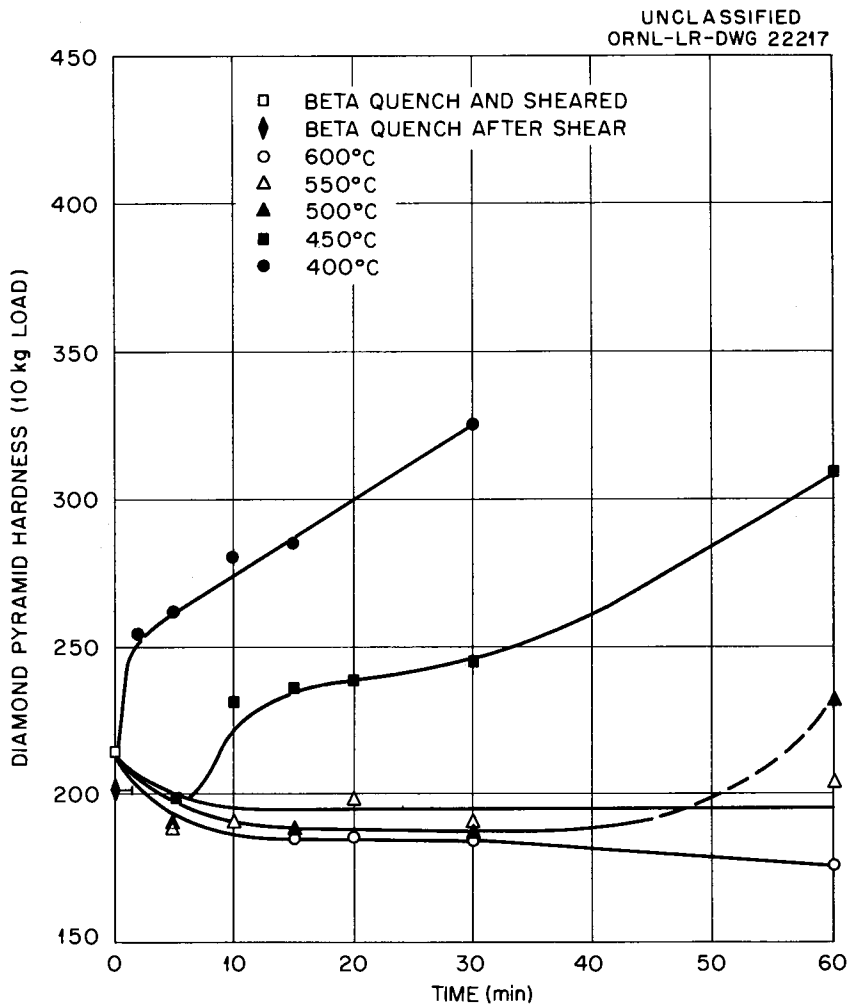

(d)

Fig. 14.1. (*c*) Quench-and-Reheat Time, Temperature, Hardness Curves for Sponge Zr–15% Nb–1% Fe. (*d*) Quench-and-Reheat Time, Temperature, Hardness Curves for Sponge Zr–15% Nb–2% Pd.

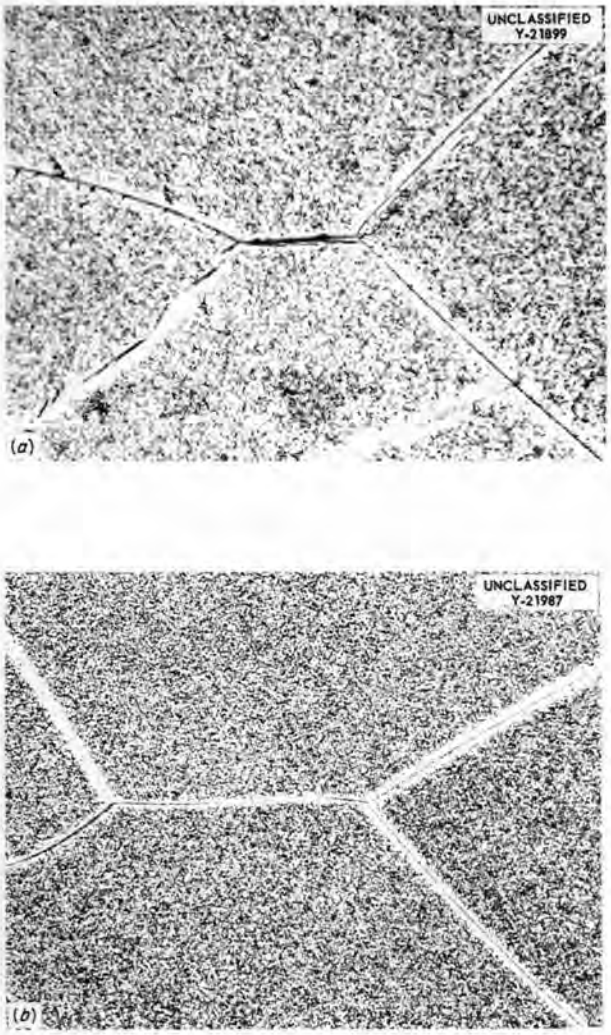

Fig. 14.2. Microstructures of Aged Quench-and-Reheat Specimens of Zr–15% Nb Alloy Aged at 600°C in the Transformation Machine. (*a*) Aged for 30 min and mercury quenched; (*b*) aged for 1 hr and mercury quenched. Bright field. 750X. Reduced 31%.

consequently, the transformation does not proceed at 600°C, and the character of the product changes with time at 600°C (somewhat similar to spheroidization).

The microstructures of the capsulated quench-and-reheat specimens of Zr–15% Nb, Zr–15% Nb–1% Fe, and Zr–15% Nb–2% Pd are shown in Figs. 14.3, 14.4, and 14.5, respectively, at 300, 400, and 600°C. The microstructures of the Zr–15% Nb–2% Pd alloy (Fig. 14.5) indicate the possibility of yet a third transition transformation product occurring in the decomposition of the retained beta in these alloys. The structure shown in 24 hr at 400°C and in 1 week at 300°C has also been seen in 20 min at 500°C in this alloy. The structure has not yet been observed in any of the other alloys, but, since it appears and then disappears, the times selected for transformation in the other alloys may not have been such as to have permitted observation of the structure. No detectable change in hardnesses has resulted from the formation of this third "transition" product.

Two extrusions have been made from an arc-cast 25-lb ingot of sponge Zr–15% Nb. The extrusion billets were saw-cut from the cast ingot with no further conditioning. The billets were extruded bare from a salt bath at 950°C through a shear die with a glass lining in the extrusion-press container. The 3½-in.-dia by 4½-in.-long billets were upset in the press to the 4-in. container diameter and extruded to 1⅛-in.-dia rounds, one 25 in. long and the other 31 in. long after removal of the extrusion defects. The maximum capacity of the press was used. Photographs of the extrusions are shown in Fig. 14.6, as are some of the representative surface defects due to galling in the die. The surface defects will not prevent the rod from being made into in-pile corrosion bombs, since it will be machined to 0.900 in., which will remove the defects. If further fabrication were planned, the rod would not be satisfactory without considerable surface conditioning to remove the galling tears. The next extrusions will be made with the billets canned in iron jackets and with a cone die in the extrusion press.

14.1.2 Zirconium-Hydrogen System

The design of the modified Sievert's apparatus has been altered so as to include new-type valves requiring no grease and completely enclosed in glass.[3] The metal parts of the valves have been made, and the glass parts are now under construction.

Cold-worked iodide Zr and Ti specimens have been observed to recrystallize at reported temperatures of 230 to 240°C in the vapor flow (H_2, O_2, H_2O) from the generating cell of a recombiner loop.[4] The experiment has been performed twice,

[3] G. M. Adamson *et al.*, *HRP Quar. Prog. Rep. Jan. 31, 1957*, ORNL-2272, p 124.

[4] G. M. Adamson *et al.*, *HRP Quar. Prog. Rep. July 31, 1956*, ORNL-2148, p 107–112.

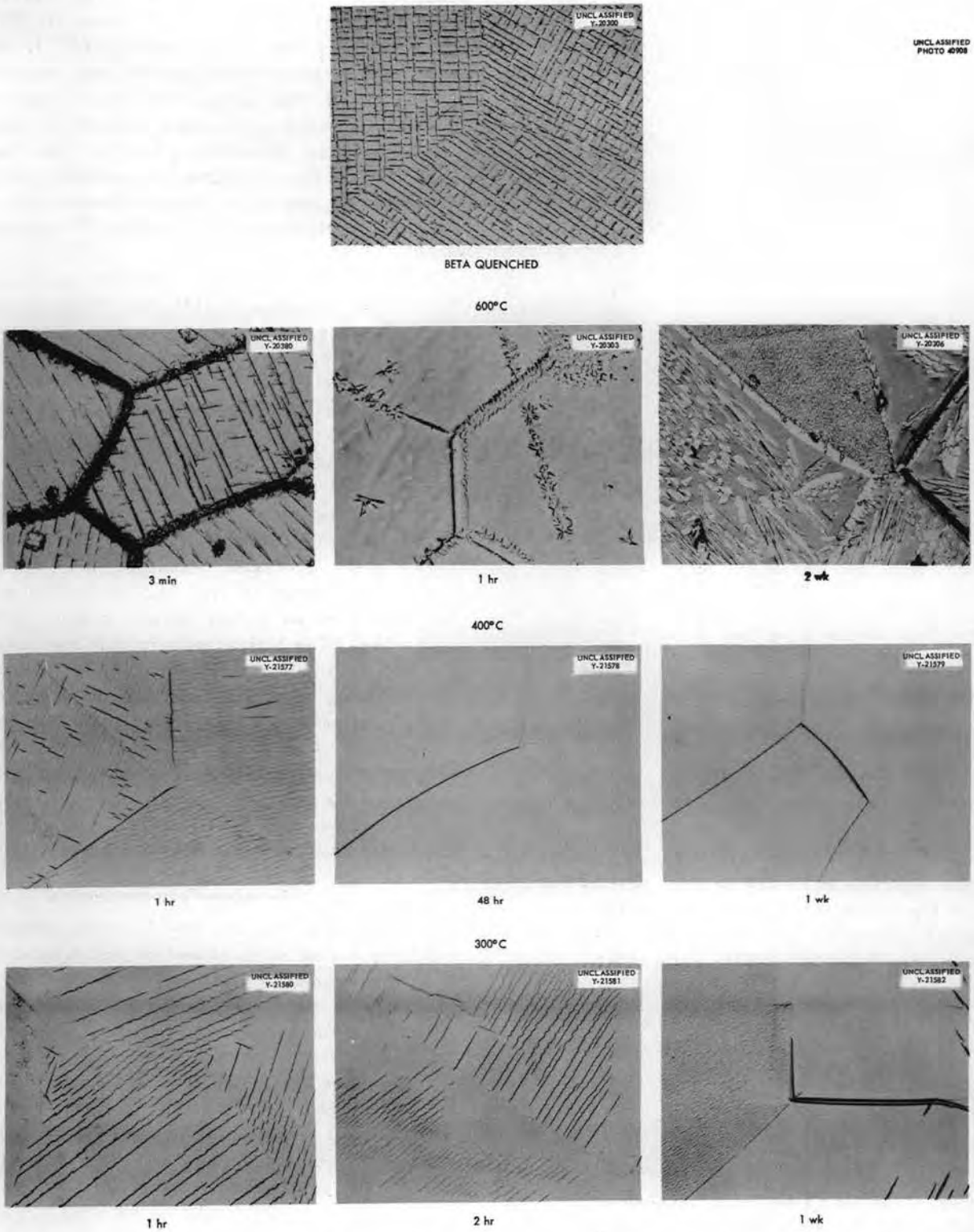

Fig. 14.3. Microstructures of Aged Quench-and-Reheat Specimens of Zr–15% Nb Alloy, Capsulated. 750X. Reduced 52%.

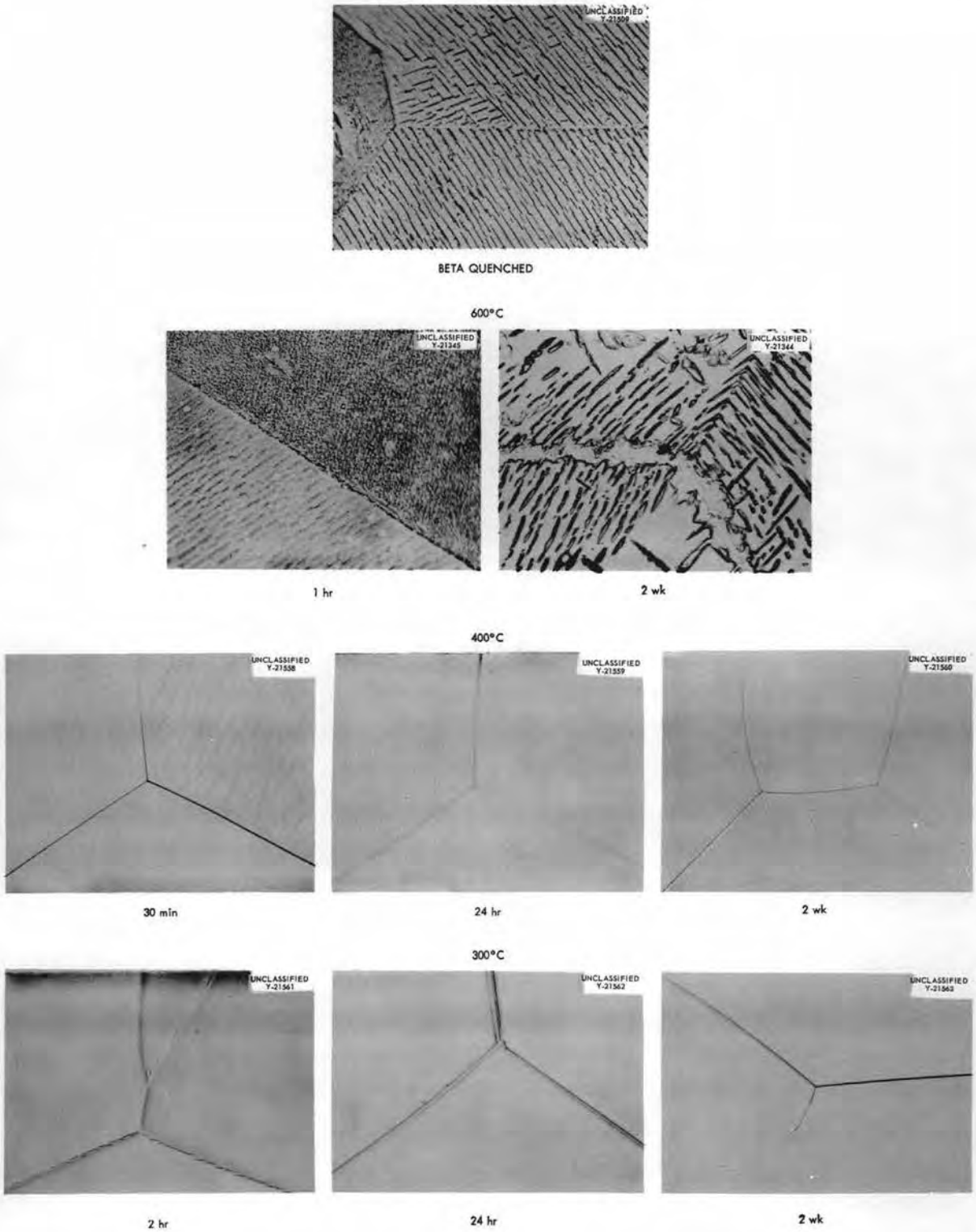

Fig. 14.4. Microstructures of Aged Quench-and-Reheat Specimens of Zr–15% Nb–1% Fe Alloy, Capsulated. 750 X. Reduced 52%.

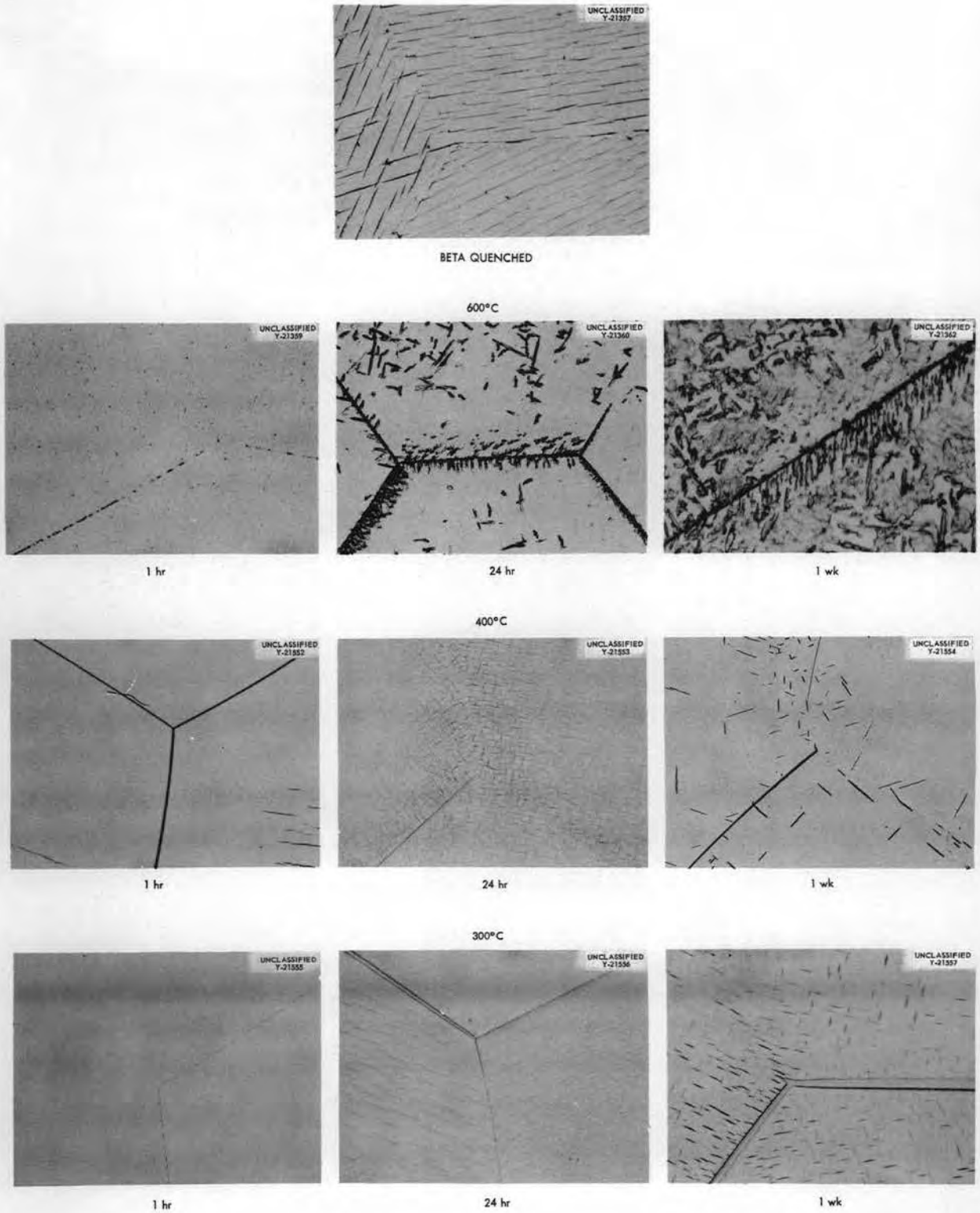

Fig. 14.5. Microstructures of Aged Quench-and-Reheat Specimens of Zr–15% Nb–2% Pd alloy, Capsulated. 750X. Reduced 52.5%.

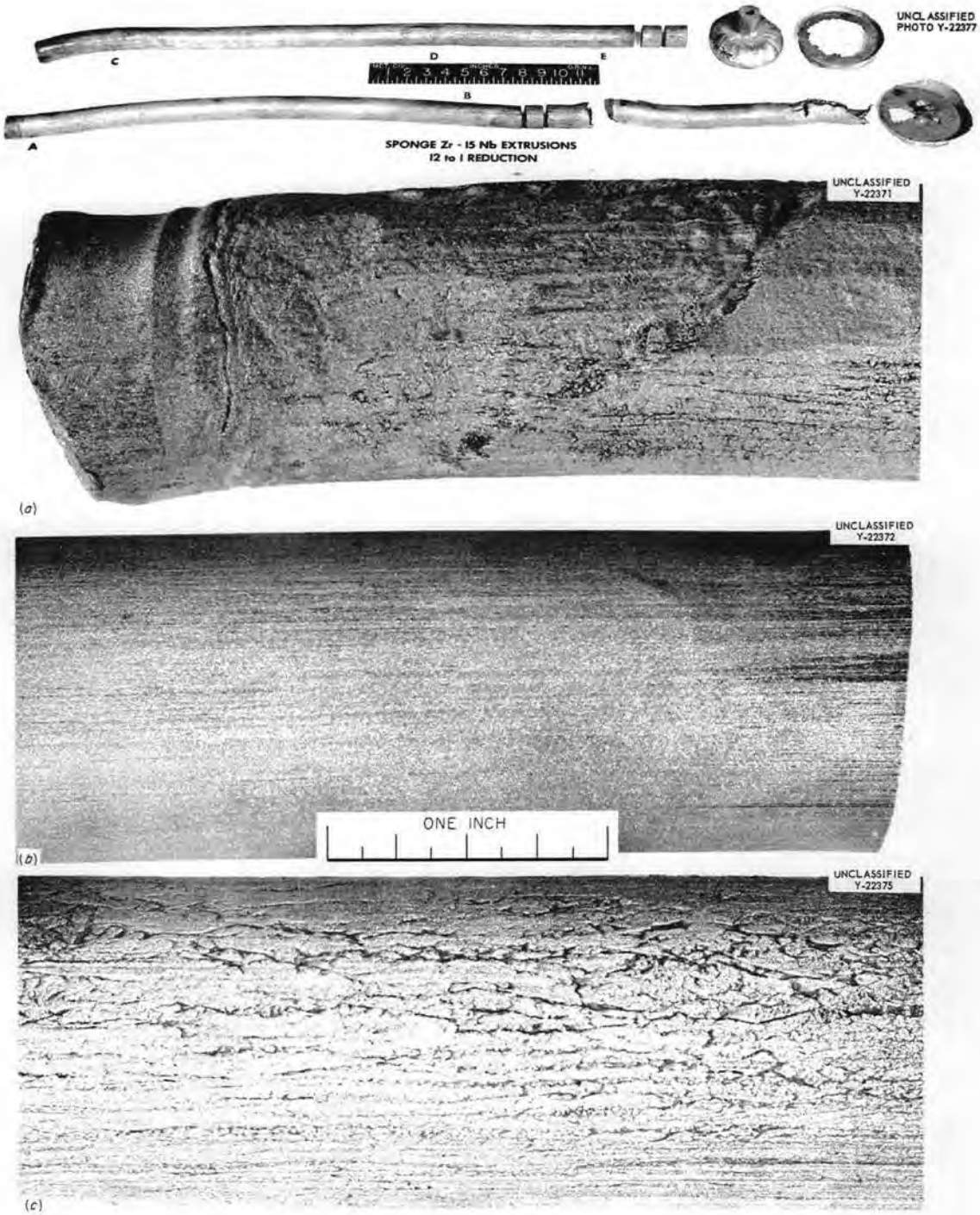

Fig. 14.6. Sectioned Extrusions of Sponge Zr–15% Nb Alloy Showing Limit of Internal Extrusion Defects in $1\frac{1}{8}$-in. Rod. (*a*) Surface defects at point A; (*b*) surface defects at point B; (*c*) surface defects at point E.

with conditions reproduced as nearly as possible, and the results of both runs are in essential agreement. In all cases where recrystallization of the cold-worked specimens was observed, the specimens had picked up H_2, in some cases as much as 1500 ppm. Since the normal recrystallization temperature for iodide Zr and Ti is 550°C or above, the phenomenon of recrystallization occurring at 230 to 240°C cannot be explained. Control experiments have been performed out of the loop, in the Sievert's apparatus, with H_2 atmospheres sufficient for additions up to 2000 ppm H_2, with temperatures up to 400°C, for times up to one week. In no case has H_2 been absorbed nor has recrystallization been observed. The specimens were severely cold-worked and thoroughly cleaned before installation in the system. However, the very thin oxide layer that is always on the surface of the specimens exposed to air could not be absorbed by the specimen, to clean up the surface, without raising the temperature of the specimen above the normal recrystallization temperature and thereby destroying one of the necessary conditions for the experiment. One run, with an atmosphere of H_2 sufficient to put 1000 ppm H_2 into the specimen at 400°C, was made with a spark-coil vacuum leak detector held against the quartz specimen tube near the specimen so as to cause a glow discharge in the system. This should have formed a considerable amount of nascent hydrogen near the specimen. Four 1-hr periods of glow discharge were used before the specimen was removed from the system. No hydrogen was absorbed and no recrystallization of the specimen occurred. Wet tank hydrogen will be used in another attempt, to determine whether the presence of water vapor will affect the conditions of operation and cause some H_2 pickup by the specimens.

14.1.3 Special Zirconium Alloys – Mechanical Properties

The Armour Research Foundation of the Illinois Institute of Technology during the past year has been investigating, under a research contract, the stability of all-beta and all-alpha zirconium-base alloys for applications under stress at temperatures[5] up to approximately 300°C. In coordination with the HRP physical-metallurgy group, a series of Zr–15% Nb binary and ternary alloys was selected for further studies, and their heat treatments were outlined from the aging studies performed and reported. The alloys have been cast and are now being fabricated and machined into specimens for the desired study.

14.2 MECHANICAL METALLURGY

14.2.1 Zirconium Alloys

As might be expected in a hexagonal metal, Zircaloy-2 reacts in a strongly anisotropic manner in Charpy V-notch impact-energy tests. Radically different curves were obtained for similar specimens cut from the same plate but with their notches at right angles to each other. As shown in Fig. 14.7, very low energies were required to fracture specimens with the notch cut in the plane of the plate, and if a transition region was present it occurred at very high temperatures. When the notch was cut through the plate, a transition region was found. At low temperatures, or in the brittle region, orientation does not seem to have an effect. This is also confirmed by the drop-weight test, the results of which did not show any orientation effects.

14.2.2 Titanium Alloys

While any failure in a reactor system may be serious, a brittle-type failure in which a sudden complete fracture occurs is much more serious than a slow leak. A study of the possibility of this type of failure in the materials of interest to the HRP is being carried out with Charpy V-notch and Izod-type impact tests and with drop-weight tests.[6]

A Charpy V-notch impact curve for high-purity commercial titanium is shown in Fig. 14.8. This curve has a shape similar to one reported for A-40 titanium;[7] however, some differences were found in the location of the peaks. The decrease in energy values at elevated temperatures will receive additional study but is not thought to be serious. The lowest energy required for a fracture in this temperature range is still higher than would be expected from a brittle failure.

---

[5] G. M. Adamson *et al.*, *HRP Quar. Prog. Rep. Jan. 31, 1957*, ORNL-2272, p 123–124.

[6] G. M. Adamson *et al.*, *HRP Quar. Prog. Rep. Oct. 31, 1956*, ORNL-2222, p 114–116.

[7] Rem-Cru Titanium, Inc., Data Sheet A40, A55, and A70, Feb. 1956.

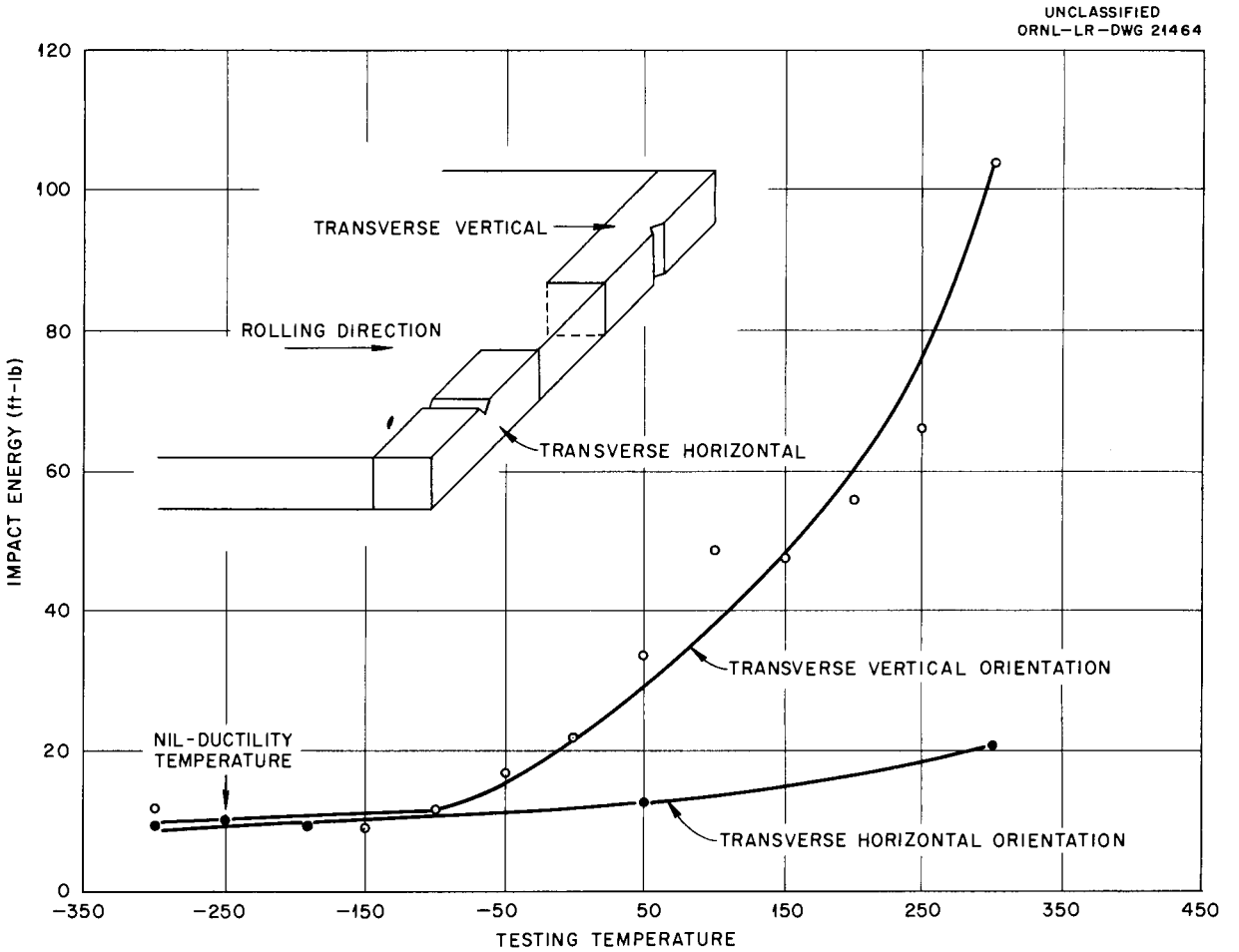

Fig. 14.7. Orientation Effect on Charpy V-Notch Impact Strength of Zircaloy-2.

The lower curve in Fig. 14.8 shows the variation in per cent lateral expansion, as measured on the side opposite the notch, with temperature. This measurement, while not a standard test, should be another way of determining changes in ductility. No explanation is available for the apparent increase in ductility at 500°F by this method without a similar increase in the impact curve.

Both longitudinal and transverse drop-weight tests conducted on this material showed no fractures at −320°F or above. It was noted that in all specimens tested (room temperature was the highest) a crack propagated through the heat-affected zone of the base metal. Additional tests will be conducted to determine if this fracture is a result of contamination or of changes in metal structure.

As a part of the study of the effects of impurities on brittle failure of titanium, drop-weight tests were run with A-75 material that had been on hand for several years. By ORNL analyses the material was shown to contain 400 ppm hydrogen. The nil ductility temperature for this material was greater than 200°F, or more than 500°F higher than was found for A-55 material.

A preliminary thermal-cycling study was conducted in an attempt to simulate the heating and cooling that might occur if high-purity commercial titanium was used as a heat-exchanger tubing material. The impact curve in Fig. 14.9 indicates that there is no impairment of ductility, as measured by impact strength, upon thermal cycling between 575°F and room temperature for ten cycles. An electric furnace operating at 575°F without any protective atmosphere was used as the heating unit. A thermal cycle consisted in heating the specimens for 1 hr and then removing them from the furnace and air-cooling them under atmospheric conditions for 1 hr.

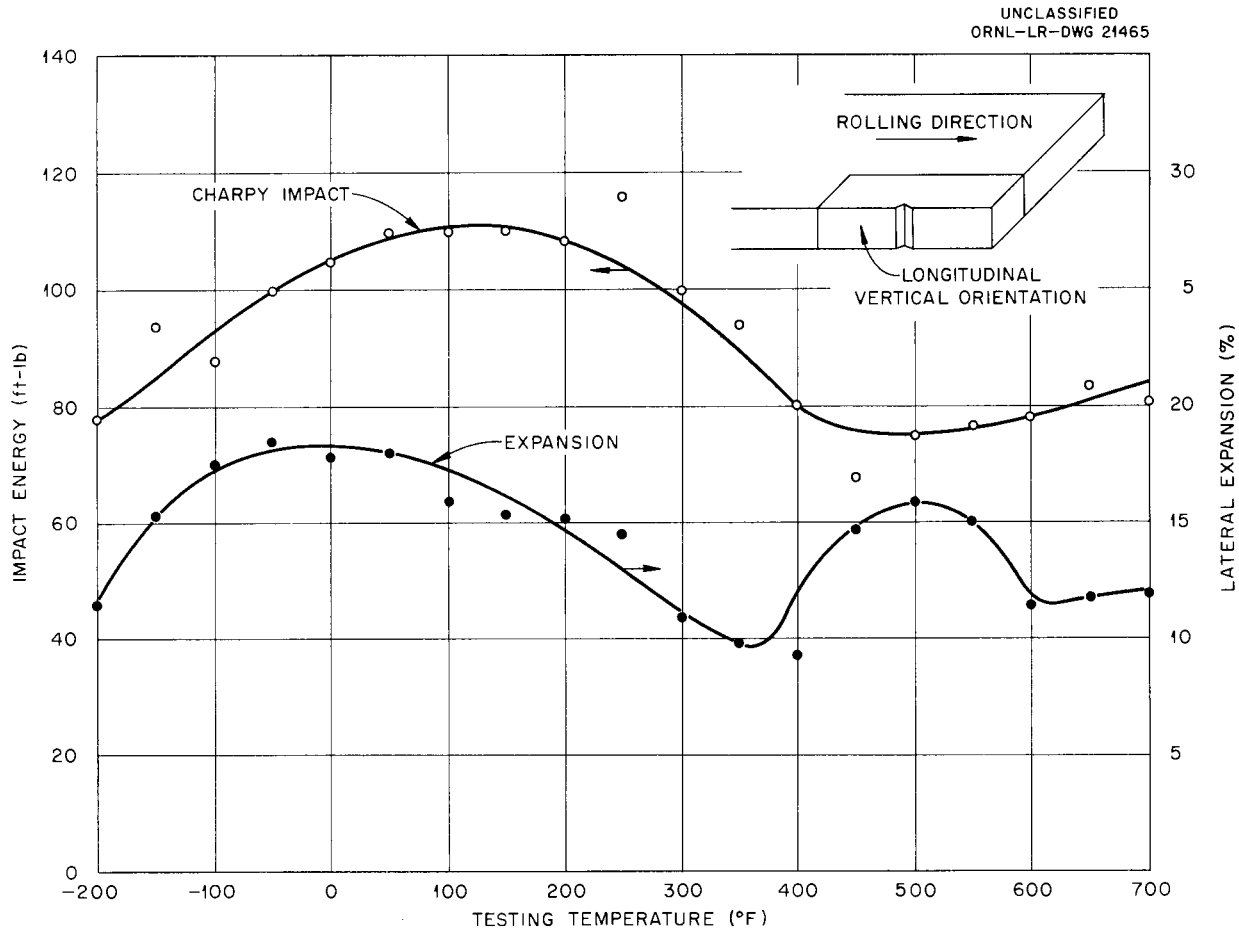

Fig. 14.8. Charpy V-Notch Impact Strength of High-Purity Commercial Titanium, in Which Nil-Ductility Transition Temperature Is Below −320°F.

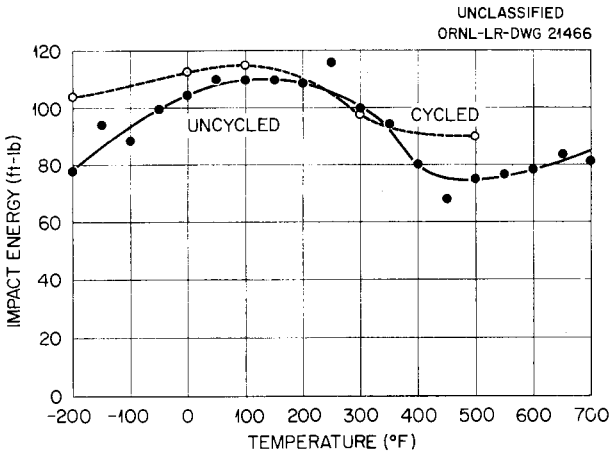

Fig. 14.9. Effect of Thermal Cycling upon the Charpy V-Notch Impact Strength of High-Purity Commercial Titanium, in Which Nil-Ductility Temperature Is Below −320°F.

14.3 METALLURGICAL DEVELOPMENT AND SERVICE

14.3.1 Bolt Failures in HRP Flange Test Loop

In early March widespread breakage occurred to bolts as well as to ferrules and nuts which had been in service in the flange test loop. This hardware is of the same lots which were earlier shown to have numerous incidents of quench cracking.[8] An investigation, which is still in progress, has already shown that the latest failures resulted from cadmium embrittlement. The nuts and ferrules, fabricated from heat-treated AISI 1040 and 4140 steel, respectively, had been cadmium-plated, whereas the bolts, made from heat-treated AISI 4140 steel, had been zinc-plated. Of the

[8] G. M. Adamson *et al.*, *HRP Quar. Prog. Rep. Jan. 31, 1957*, ORNL-2272, p 119–123.

48 bolts, nuts, and ferrules installed in the loop, 14 bolts and nuts and 13 ferrules showed defects on examination by Magnaflux. All these are believed to be cracks resulting from cadmium embrittlement, except for a few indications on the bolt heads which are seams or quench cracks. The cracks produced by the cadmium embrittlement in the bolts, as well as the conditions which produced the failures, are described below.

The bolts, inclusive of ferrules and nuts, had been installed in type 347 stainless steel flanges and tightened to a tensile stress of 30,000 psi. As a result of the difference in coefficient of thermal expansion between bolt and flange, heating up to operating temperature increased this stress to 35,000 to 40,000 psi. Bending moments stemming from flange flexing and misalignment conceivably superimposed stresses in certain segments of the threaded portion of the bolts, near or in excess of the yield point. The test loop had undergone 43 cycles of heating-up over a period of four months before the failures were observed. A cycle consisted in pumping hot solution through the loop for a 12-hr period, producing an estimated temperature of 500°F in the bolts.

Figure 14.10 is a macrograph showing a fracture through a bolt and a photomicrograph showing the structure along an internal crack. The breaks in all parts were intergranular and brittle and occurred through transverse sections in the bolts and predominantly along longitudinal planes in the nuts and ferrules. The fractures in the bolts invariably occurred in the regions where the threading engaged the nuts and usually intersected the pitch diameter, where the nut mates with greatest pressure. This conforms to the findings relative to the cause for the failures – that the cadmium from the plated nuts diffused intergranularly into the bolts and caused embrittlement.

Cadmium and sometimes a trace amount of zinc were detected on the bolt fracture interfaces both by spectrographic and chemical means. Also, an indication of $CdFe_2O_4$ was found on one of the faces by electron diffraction.

Since the hardware in the HRT is similarly plated and has been exposed to like conditions, it was recommended that it be replaced during the scheduled shutdown. The same alloys were recommended for replacement bolts and nuts, whereas the ferrules were changed from AISI 4140 to 4135 to better enable spot welding of the part in place.

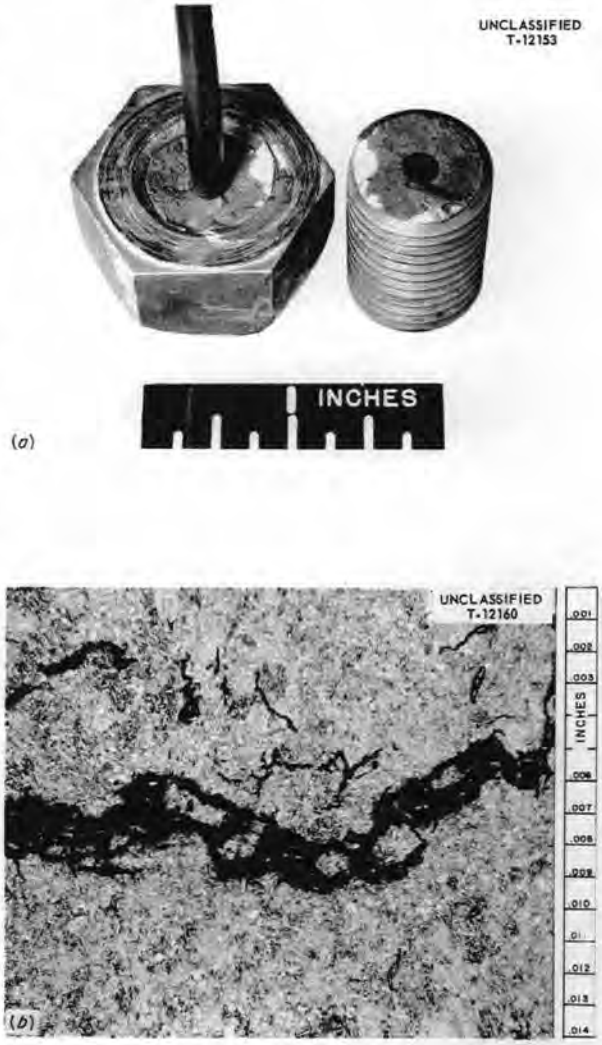

Fig. 14.10. Cracks in a Bolt from HRT Flange Test Loop. (*a*) Macrograph showing nature and location of fractures; (*b*) micrograph showing intergranular character of crack. Longitudinal section. 250X. Reduced 32%.

Also, it was recommended that the parts be treated to give greater toughness. A hardness range of Rockwell C 24 to 30 has been prescribed instead of RH_C 24 to 38. The last bolts were RH_C 37, and the ferrules and nuts were even harder. One of the black oxide coatings with a heat-resisting silicone grease is being considered as a protective finish.

HRT flanges are being examined for damage from cadmium. The cadmium-plated nuts had been fastened to the flanges by spot welding.

14.4 INSPECTION DEVELOPMENT

14.4.1 Eddy-Current Testing of ¼-in. Type 347 Stainless Steel Tubing

Development work by the American Testing and Control Company in the field of eddy-current testing of heat exchanger tubing has been previously reported.[8] This contract was completed February 11, 1957, with the receipt of a supplementary report describing results of tests with ID probe coils.

Eddy-current testing involves measuring some component of the impedance of a coil which is in close proximity to the test piece. Impedance of the coil is affected by the following variables: permeability, conductivity, coil coupling or coil-to-work distance, dimensions of the work piece, flaws in the work piece, characteristics of the coil itself, and various secondary effects such as the metallurgical history of the work piece. Thus, if other factors are known or controlled, the method may be used for flaw detection.

Minimum requirements for a successful test were listed in the contract proposal as follows:

1. sensitivity – satisfactory detection, on both the inside and the outside of the tube wall, of No. 80 drill holes and of square longitudinal grooves 3% of the tube wall thickness in width and depth;
2. inspection speed – equipment must be capable of completely inspecting 100 or more feet of tubing per minute;
3. versatility – equipment must be capable of inspecting ⅜-in.-OD by 0.065-in.-wall, and also 0.049-in.-minimum-wall, type 347 stainless steel tubing in lengths up to 32 ft;
4. rejection indication – equipment is to have a suitable visual alarm and a recording device and is to automatically mark defective portions of the tubing inspected.

All these requirements were met by the American Testing and Control Company's Metron V, with the exception of the one considered most important – the reproducible detection of 3% grooves. They tried to remedy this shortcoming by building another instrument, but have not yet perfected it.

The confidence in the use of eddy currents as a prime test method for the type 347 leak-detector tubing (¼-in. dia., 0.065-in. wall) suffered when it was found that a large percentage of the most recent order had a magnetic iron oxide on the inside surface, causing a large impedance effect on any eddy-current test. Fortunately, the routine immersed ultrasonic inspection method proved even better than had been expected.[9] Preliminary trials showed that surface treatment was necessary to remove scratches, since it is almost impossible to distinguish a surface scratch from an internal defect with small-diameter tubing. Once the outside surface was given a light grinding, the immersed ultrasonic method was able to readily detect inside and outside defects of from 3 to 5% of wall thickness in depth, as shown in Fig. 14.11. The specifications proposed for the tubing allowed defects up to 5% of wall thickness; therefore the immersed ultrasonic method is being used as the primary test method. Due to its rapidity, the Cyclograph type of eddy-current test is being used, but only as an adjunct to the ultrasonic inspection.

14.5 WELDING DEVELOPMENT

Welding techniques were developed and qualified for the inert-gas tungsten arc welding of type 347 stainless steel pipe and tubing by use of a preplaced insert for making the root pass. These procedures made use of the Electric Boat (EB) type of insert.[10] This work has now been extended and the complicated EB-type insert replaced with a simple round-wire insert. Pipe sizes from ¼ to 8 in. in diameter, with wall thicknesses from 0.065 to 0.375 in., have been welded successfully by using a 3/32- to 5/32-in. wire insert. Figure 14.12 is a photograph of the root face of such a weld.

During the development of the round-wire inserts, welds were made by using a flattened-wire or washer-type insert. While successful welds were made, they were not so uniform as those with the round-wire inserts. If it should be desirable to use this type of insert, it is quite likely that uniform and satisfactory welds could be obtained with variations in the height-to-width ratio of the insert. A washer-type insert technique has been developed for welding the ¼- by 0.065-in. type 347 leak-detector tubing in the reactor. The insert being used has a cross section of 0.048 in.^{2} and an ID 0.008 in. smaller than the ID of the tubing. One difficulty in using both the washer and round-wire type of inserts is the positioning of the insert.

---

[9] G. M. Adamson *et al.*, *HRP Quar. Prog. Rep. Oct. 31, 1956*, ORNL-2222, p 114–116.

[10] HRP Welding Specification No. 9 – Inert Gas-Shielded Arc Welding of Chromium Nickel Stainless Steels Using Pre-Placed Root Insert Rings.

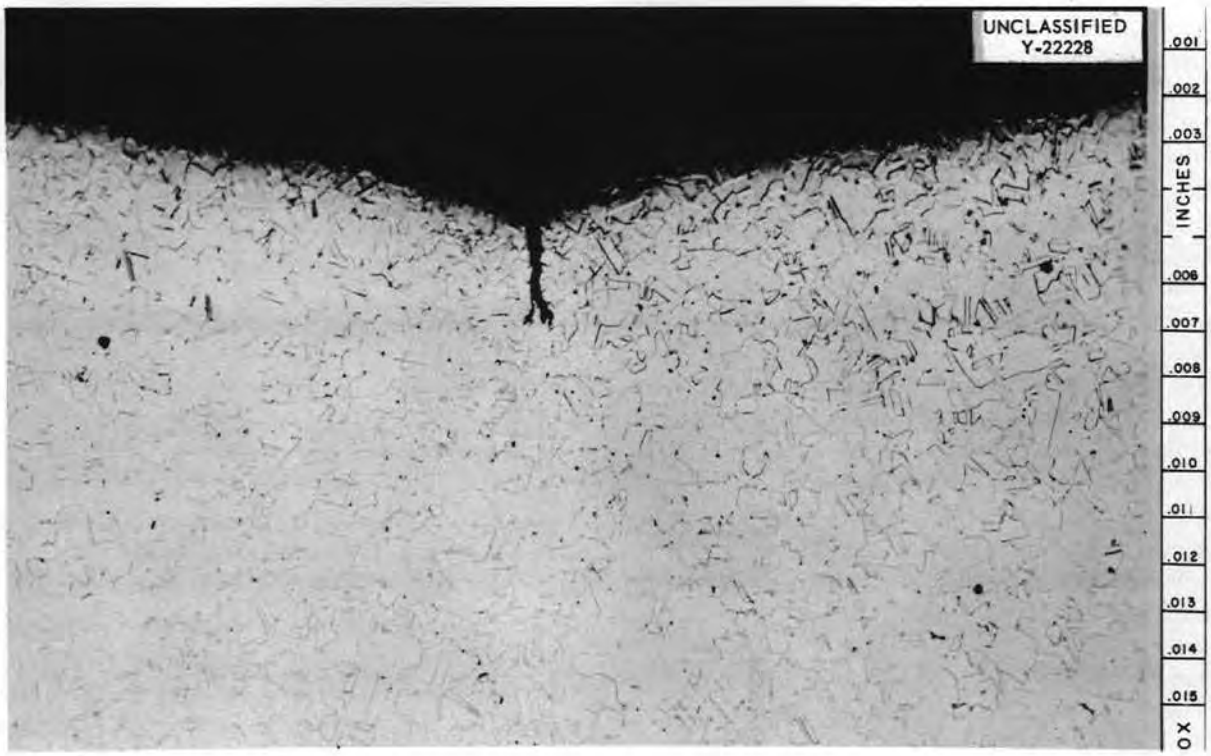

Fig. 14.11. Micrograph of 5% Crack in Leak-Detector Tubing. 250X. Reduced 1%.

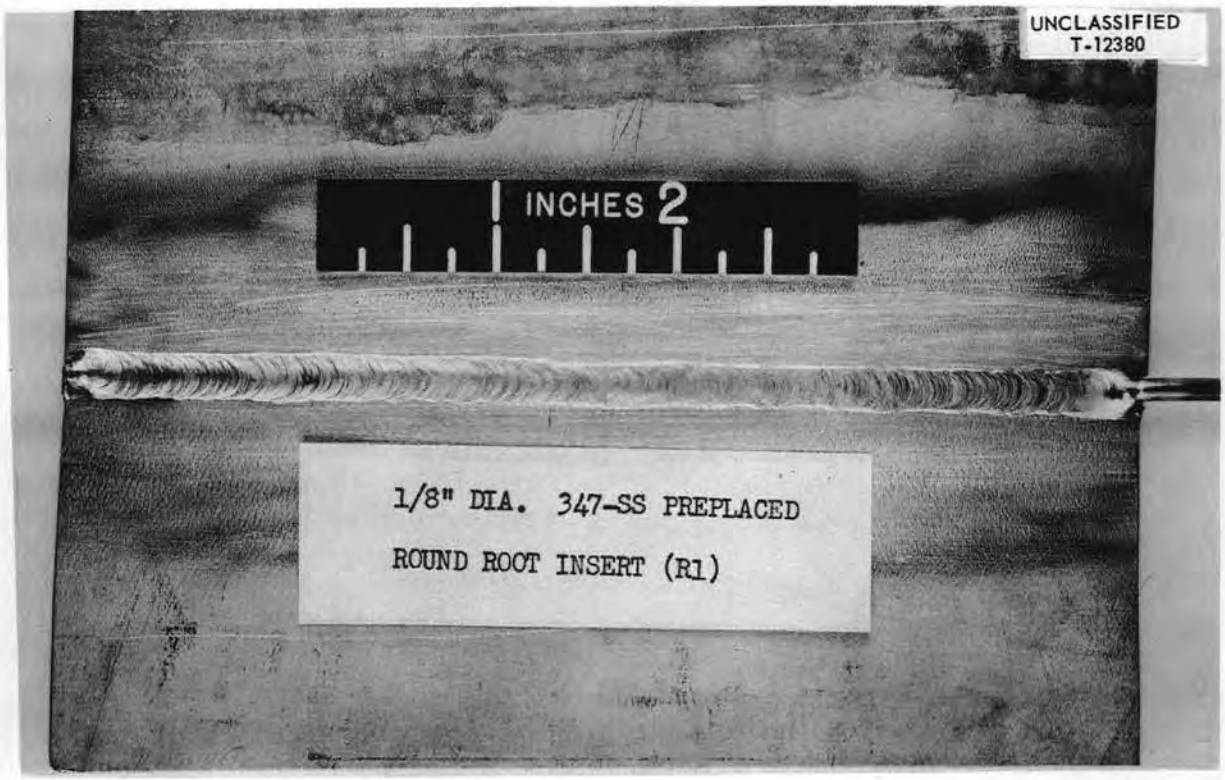

Fig. 14.12. Appearance of Root Face of a Type 347 Stainless Steel Weld with Round Insert.

Figure 14.13 shows the simple jig developed for positioning the insert in this job.

The same techniques used in stainless steel pipe welding have been adapted for titanium welding. Figure 14.14 is a photograph of the root face of a titanium weld made by using a $\frac{3}{32}$-in.-dia round-wire insert. This type of weld requires approximately the same heat input (40 to 60 amp) as the welds made by using the hand-fed technique. The penetration and the root reinforcement are much more uniform than they are with the latter type. Both flat-washer type and EB inserts were investigated for root-pass welding of titanium. Welding currents of 60 to 80 amp were required for proper fusion of the washers, and even greater ones were required for the EB type, thus increasing the welding contamination problem. The root reinforcement was less uniform, and proper penetration of the base metal on each side of the inserts was difficult to maintain without exceedingly close fitups.

The preparation of subsize tensile and impact specimens of the same metallurgical structure as that existing at various points in the heat-affected zone of the base metal of weldments has been completed by Rensselaer Polytechnic Institute

UNCLASSIFIED
T-12379

Fig. 14.13. Jig Developed for Positioning Preplaced Insert.

Fig. 14.14. Appearance of Root Face of Titanium Weld Made by Using Round Preplaced Insert.

under a research contract. Corrosion specimens of the same type are to be completed in the next quarter. Materials to be evaluated in these conditions are titanium RS-55A, titanium 110AT, and Zircaloy-2, which are to be tested in both the irradiated and unirradiated condition.

14.6 EFFECTS OF RADIATION ON STRUCTURAL METALS AND ALLOYS

An elevated-temperature irradiation of impact and tensile test specimens in the HB-3 facility of the MTR was completed, and the specimen chamber is being returned to ORNL for removal and testing of the specimens.

Assembly of an ambient-temperature (<200°F) irradiation experiment containing tensile, subsize Izod, and full-size Charpy impact specimens was completed and the experiment shipped to the MTR for insertion in the HB-3 facility.

A comparison study of subsize Izod, standard V-notch Charpy, and drop-weight tests is being conducted in cooperation with the Naval Research Laboratory. The specimens include samples from ruptured steel hulls of ships and from other origins. Drop-weight and Charpy test characteristics of these steels had been determined by NRL, and during this quarter subsize Izod tests were conducted on these same steels (in the unirradiated condition). It is hoped that comparison of results from these various tests will establish a correlation between the tests and aid in the interpretation of data from subsize tests on irradiated metals.

Part V

CHEMICAL ENGINEERING DEVELOPMENT

D. E. Ferguson

15. URANYL SULFATE FUEL PROCESSING

R. A. McNees E. O. Nurmi
S. Peterson R. W. Horton

15.1 PROPERTIES OF SIMULATED REACTOR SOLIDS

Some of the physical properties of simulated reactor solids are being measured, and the effects on these properties of possible variables in reactor operation are being studied. These studies, by contributing to the knowledge of the behavior of simulated reactor solids in various pieces of test and experimental equipment, should aid in the prediction of the behavior of fission- and corrosion-product solids produced in a homogeneous reactor.

Several lots of simulated solids were prepared.[1] The composition of the various batches is shown in Table 15.1 and the subsequent autoclave treatment of each in Table 15.2. The particle sizes, determined by Leddicotte's activation technique,[2] are shown in Figs. 15.1, 15.2, and 15.3. Electron photomicrographs of the same materials are shown in Figs. 15.4, 15.5, and 15.6. Both activation-analysis and electron-diffraction data indicate that in the case of the solids containing 40 to 45% each of Fe_2O_3 and ZrO_2, the ZrO_2 is present as a discrete phase and is contained in the small particles, while the mixed Fe_2O_3-Cr_2O_3 phase is segregated as the matrix material in the larger particles. Examination of the photomicrographs shows that, in the case of the batch 3 materials, particle growth is favored by increasing either the temperature or the time of autoclaving.

Hindered-settling data for the various batches of synthetic solids are shown in Table 15.3 as a function of solids concentration and temperature. These data indicated a strong tendency of particles containing large amounts of iron to grow during heating at the higher temperatures. This characteristic was not evident in the behavior of the samples containing high concentrations of zirconium and was not so pronounced in the case of the mixed iron and zirconium oxide particles. Studies made of the effect of time of heating on settling rate showed that at 250°C no gross agglomeration of particles occurred (Fig. 15.7). At 275°C, during an induction period of 2.7 hr, the settling rate increased only moderately, but then the characteristics of the system changed abruptly. In an x-ray photograph of the settling system taken at 2.7 hr, immediately before the transformation, a normal settling interface is seen; at 3.2 hr, immediately after the transformation, a rapidly settling interface characteristic of large flocs is shown,

[1] *Chem. Tech. Monthly Prog. Rep. Feb. 1957*, ORNL-2270 (in press) (Classified).

[2] G. W. Leddicotte *et al.*, *Particle Size Analysis by Radioactivation*, ORNL-2160 (in preparation).

Table 15.1. Chemical Composition of Simulated Reactor Solids

Batch No.	Composition of Solids (%)		
	ZrO_2	Fe_2O_3	Cr_2O_3
1	15	65	20
2	85	11	4
3	46	41	13

Table 15.2. Autoclave Treatment of Simulated Reactor Solids

Lot No.	Batch No. 1		Batch No. 2		Batch No. 3	
	Time (hr)	Temperature (°C)	Time (hr)	Temperature (°C)	Time (hr)	Temperature (°C)
1	62	264	62	302	13	252
2	62	312	13	250	13	305
3	13	246	13	300	62	250
4	13	300	46	250	62	300

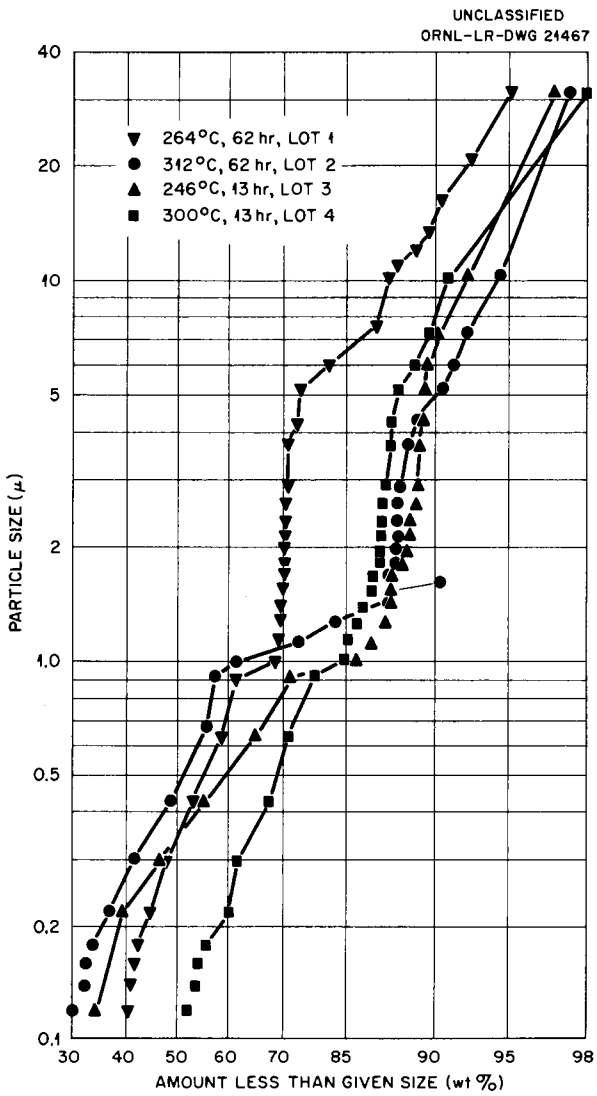

Fig. 15.1. Particle-Size Distribution in Simulated Reactor Solids, Batch 1.

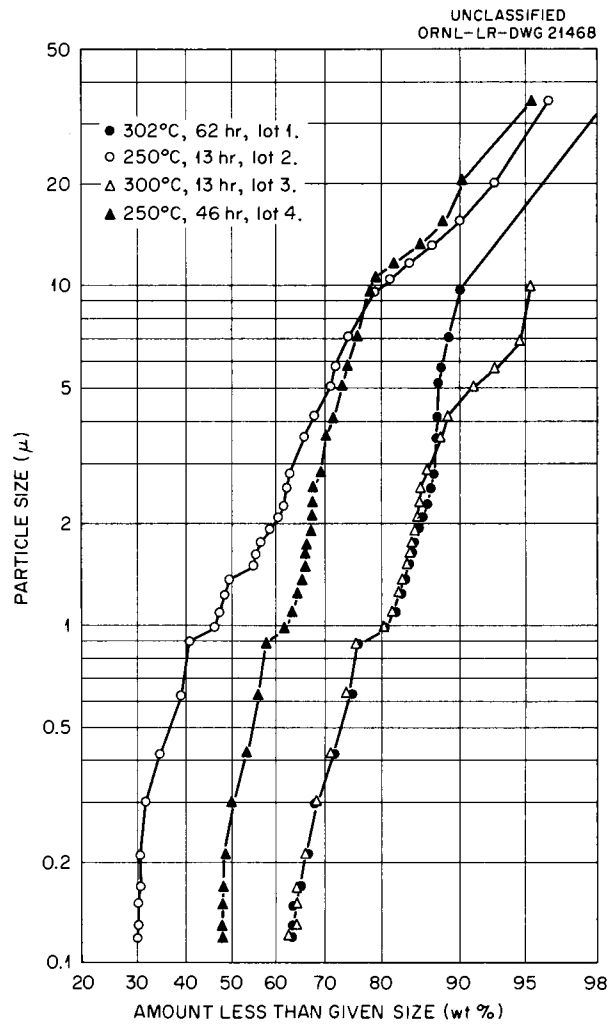

Fig. 15.2. Particle-Size Distribution in Simulated Reactor Solids, Batch 2.

as is a deposit of solids on the bottom of the shaker bomb (Fig. 15.8). At 300°C, flocculation of the mixed oxide particles was very rapid except in the case of those with high ZrO_2 content (Fig. 15.7).

15.2 IODINE CHEMISTRY

Investigation of the oxidation-reduction behavior of iodine under gamma irradiation in simulated fuel solution has been extended to a solution with a uranium concentration approximating that of HRT fuel. In previous experiments[3] with a simulated fuel solution (0.02 *m* UO_2SO_4, 0.005 *m* H_2SO_4, 0.005 *m* $CuSO_4$, 10^{-6} or 10^{-5} *m* HIO_3), under irradiation at 2 w/liter, a balance between iodate and reduced iodine (elemental iodine plus a trace of iodide) was reached. At 100 to 110°C the iodate content decreased with increasing H_2/O_2 ratio in the atmosphere above the solution, with a sharp break at the stoichiometric ratio.

In solutions containing more uranium (0.04 *m* UO_2SO_4, 0.01 *m* H_2SO_4, 0.005 *m* $CuSO_4$, 10^{-5} *m*

[3] D. E. Ferguson *et al.*, *HRP Quar. Prog. Rep. Jan. 31, 1957*, ORNL-2272, p 133–135.

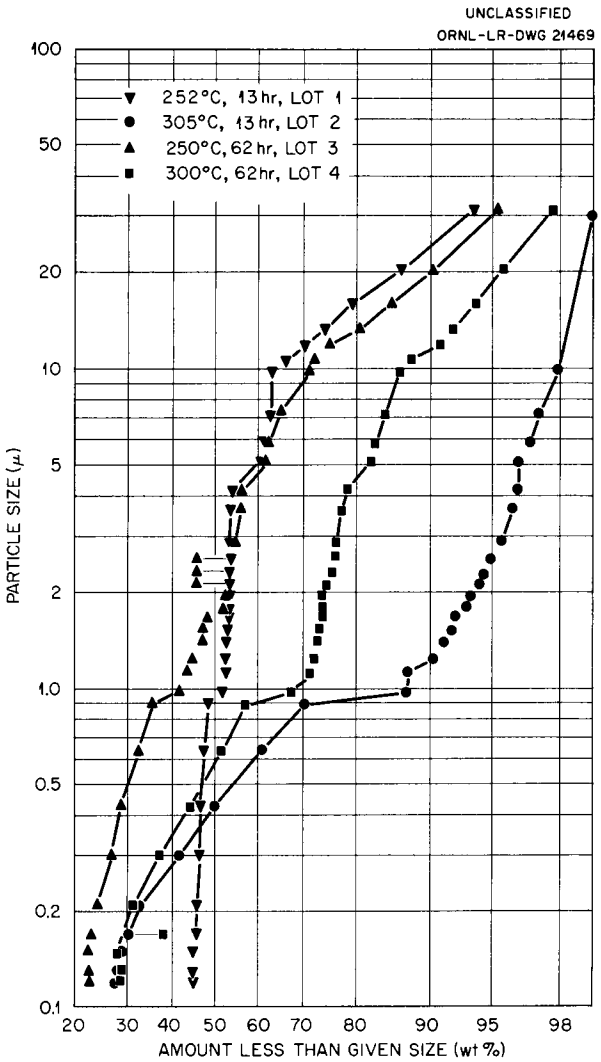

Fig. 15.3. Particle-Size Distribution in Simulated Reactor Solids, Batch 3.

HIO_3), the effect of gas composition was similar (curves 1, 2, and 3 of Fig. 15.9), but the iodate stability was greater. Since steady state was apparently far from reached with the high H_2/O_2 ratio (curve 3), additional experiments were made with iodine introduced as KI. Steady state was still not reached (curves 1 and 2, Fig. 15.10), but even at high H_2/O_2 ratios the iodate stability was considerably greater than in 0.02 *m* UO_2SO_4. In Table 15.4 the steady-state information for the 0.04 *m* UO_2SO_4 is compared with that for the same gas ratios read from the smooth graph[4] for the more dilute solution. Just as in the more dilute solutions, the stability of iodate in 0.04 *m* UO_2SO_4 was markedly decreased by raising the temperature from 100°C to 120°C (curve 5 in Fig. 15.9 and curve 3 in Fig. 15.10).

The iodate stability increased with increasing radiation intensity (curves 1 and 4 in Fig. 15.9). This is to be contrasted with the observation[5] that in 0.02 *m* UO_2SO_4 in the absence of hydrogen, increasing radiation intensity decreased the iodate stability.

When uranyl sulfate solutions containing iodine are exposed to gamma radiation at 100°C, the usual behavior has been an immediate reduction of iodate, reaching a minimum iodate content after 1 to 3 hr, followed by a reoxidation approaching a steady state in which the iodate content may be higher or lower than in the starting solution. This suggests that the free radicals produced by the radiation have a reducing effect on iodate, but prolonged irradiation builds up an oxidizing substance which favors oxidation of iodine. This substance is probably hydrogen peroxide, which is known to build up slowly to a steady state in gamma-irradiated water. Since the stability of peroxide decreases above 100°C, iodate stability should be markedly reduced at 120°C. To test this hypothesis, irradiations were performed with the fuel solution made 0.001 *m* in ferric ion, which is a good catalyst for peroxide decomposition, particularly in combination with copper ion. The results of these experiments (Fig. 15.11) showed that the ferric ion does eliminate the reversal of reaction direction. With H_2/O_2 ratios higher than stoichiometric, a monotonic decrease in iodate content was observed. Comparison with the behavior in the absence of ferric ion, but with otherwise the same conditions, shows that the iodate stability is definitely diminished in the presence of ferric ion. Also, the initial rate of reduction is slowed down, showing that ferric ion competes with iodate for the reducing radicals. With oxygen in excess of stoichiometric, iodate stability was high in the presence of ferric ion.

---

[4] *Ibid.*, p 134.

[5] D. E. Ferguson *et al.*, *HRP Quar. Prog. Rep. Oct. 31, 1956*, ORNL-2222, p 137.

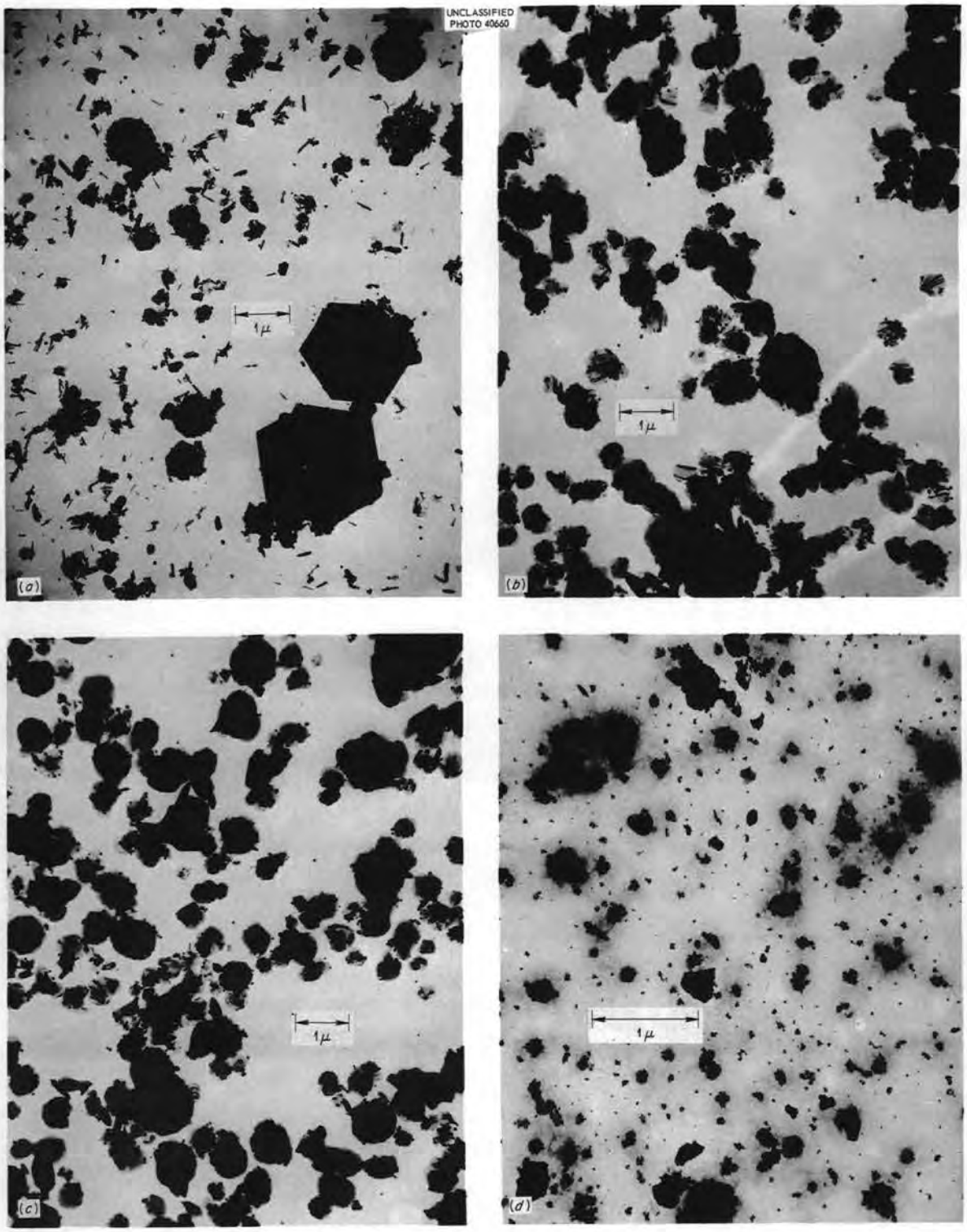

Fig. 15.4. Electron Photomicrographs (Reduced 55%) of Simulated Reactor Solids. (*a*) Batch 1, Lot 1 sample, autoclaved at 264°C for 62 hr. 20,000X. (*b*) Batch 1, Lot 2 sample, autoclaved at 312°C for 62 hr. 20,000X. (*c*) Batch 1, Lot 3 sample autoclaved at 246°C for 13 hr. 20,000X. (*d*) Batch 1, Lot 4 sample, autoclaved at 300°C for 13 hr. 40,000X.

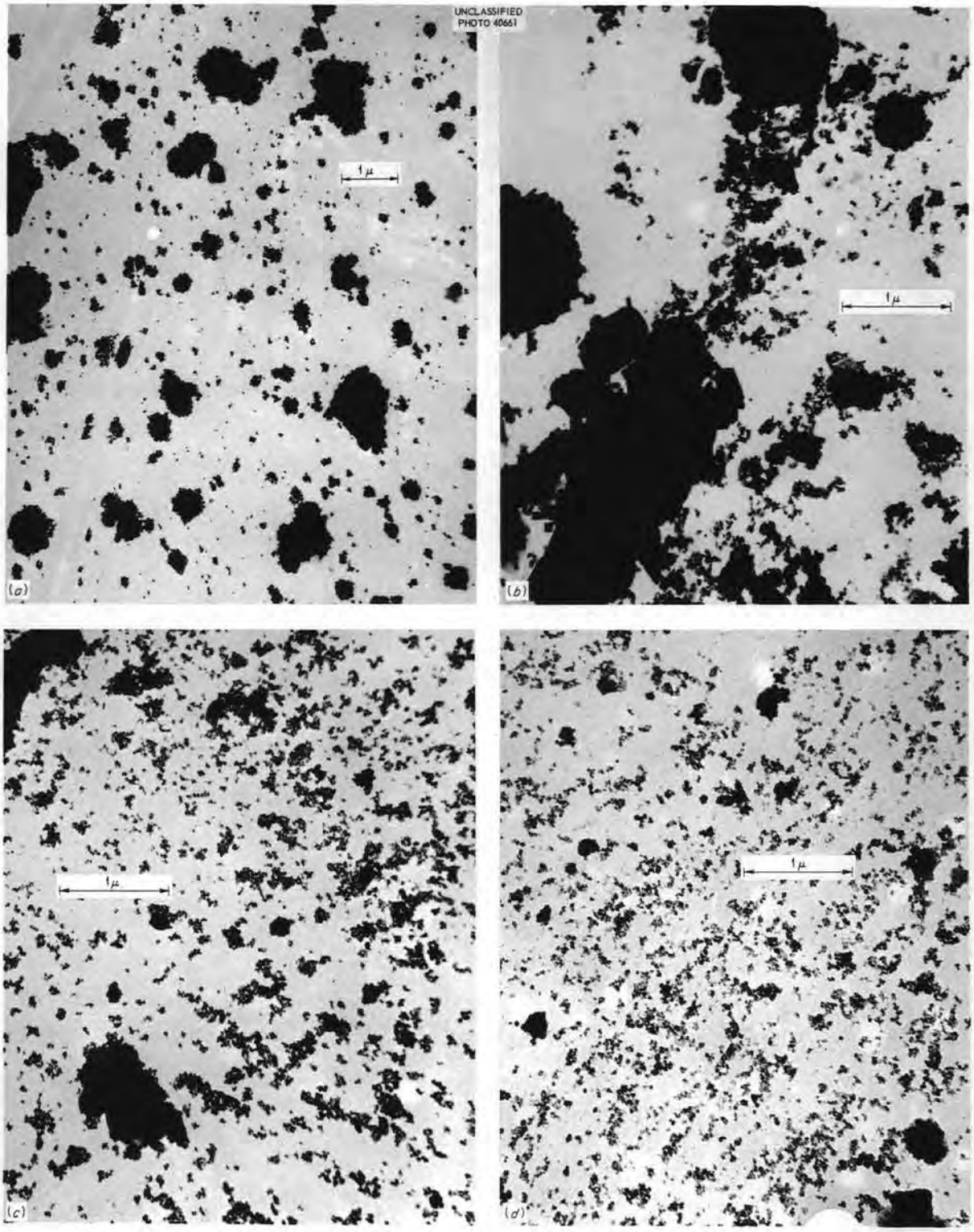

Fig. 15.5. Electron Photomicrographs (Reduced 54%) of Simulated Reactor Solids. (*a*) Batch 2, Lot 1 sample, autoclaved at 302°C for 62 hr. 20,000X. (*b*) Batch 2, Lot 2 sample, autoclaved at 250°C for 13 hr. 40,000X. (*c*) Batch 2, Lot 3 sample, autoclaved at 300°C for 13 hr. 40,000X. (*d*) Batch 2, Lot 4 sample, autoclaved at 250°C for 46 hr. 40,000X.

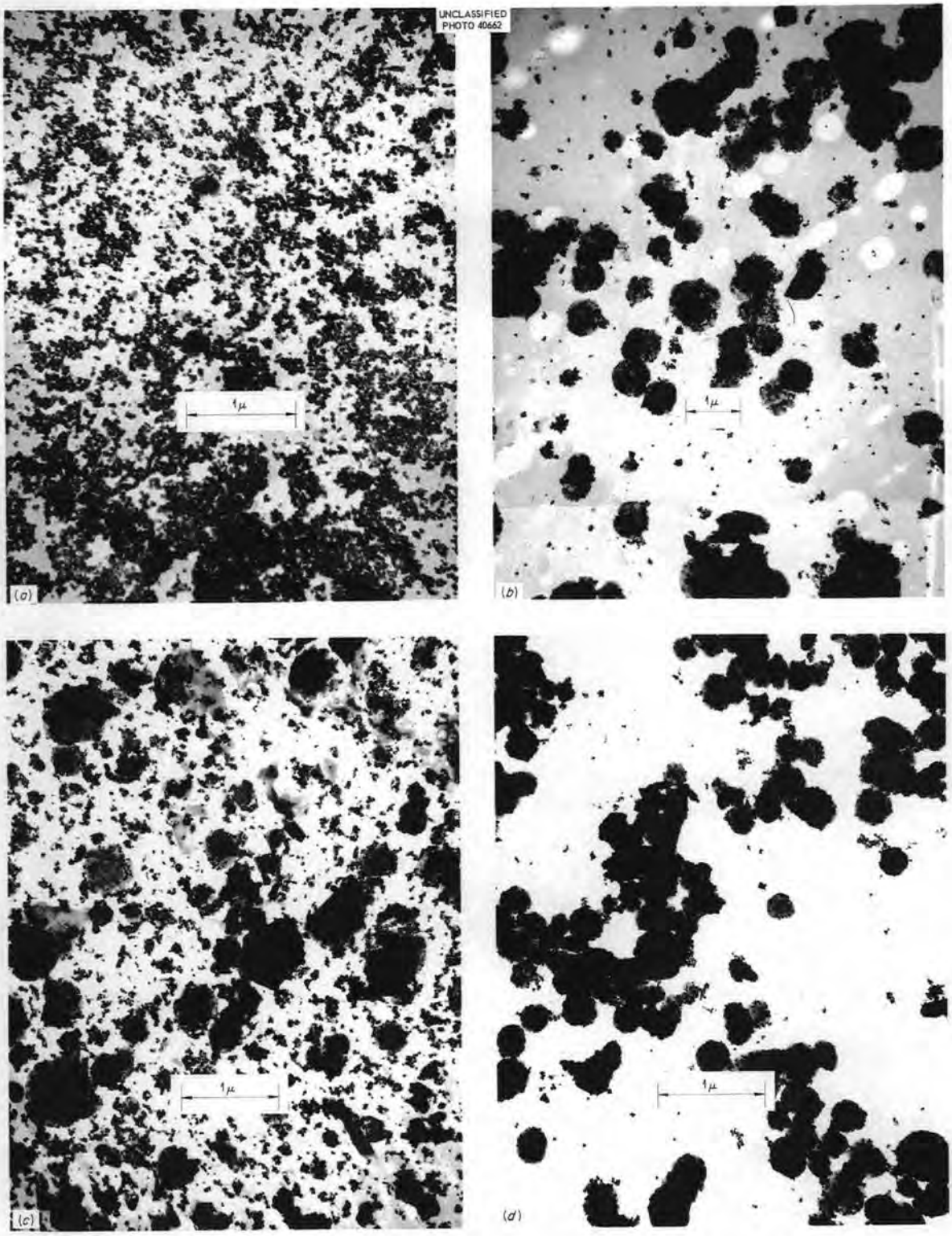

Fig. 15.6. Electron Photomicrographs (Reduced 54%) of Simulated Reactor Solids. (*a*) Batch 3, Lot 1 sample, autoclaved at 252°C for 13 hr. 40,000X. (*b*) Batch 3, Lot 2 sample, autoclaved at 305°C for 13 hr. 20,000X. (*c*) Batch 3, Lot 3 sample, autoclaved at 250°C for 62 hr. 36,000X. (*d*) Batch 3, Lot 4 sample, autoclaved at 300°C for 62 hr. 40,000X.

Table 15.3. Hindered-settling Rates of Simulated Reactor Solids

Sample No.	Solids Concentration (g/liter)	Hindered-settling Rate (cm/sec)			
		225°C	250°C	275°C	300°C
B-1-L-1	50	0.019	0.043	N.S.*	N.S.
-2	50	0.029		0.183	N.S.
-3	50	0.033	0.082	N.S.	N.S.
-4	50		0.148	N.S.	N.S.
-4	100		0.062	0.119	0.247
B-2-L-1	50		0.084	N.S.	N.S.
-1	100		0.050	0.079	0.169
-2	50		0.049	0.081	0.141
-2	100		0.026	0.056	0.087
-3	50		0.098	0.141	0.193
-3	100		0.021	0.052	0.115
-4	50		0.069	0.119	0.173
-4	100		0.050	0.166	0.105
B-3-L-1	50		0.010	0.035	0.075
-1	100		0.014	0.017	0.023
-2	50		0.155	0.183	0.242
-2	100		0.037	0.110	0.167
-3	50		0.134	0.182	0.223
-3	100		0.035	0.102	0.187
-4	50		0.168	0.221	0.289
-4	100		0.077	0.145	0.198

*N.S. = solids could not be suspended by shaking.

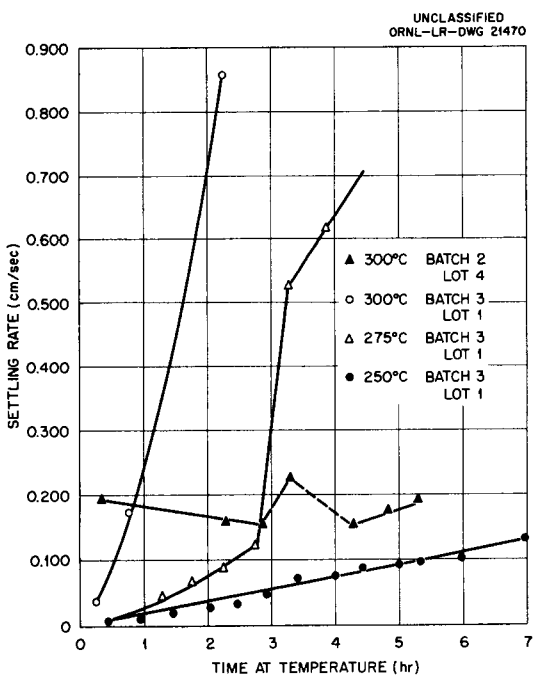

Fig. 15.7. Hindered-Settling Rates as a Function of Heating Time.

15.3 VOLATILITY OF IODINE UNDER REACTOR CONDITIONS[6]

Previous work[7] had indicated that iodine adsorption on platinized alundum was increased at 350°C by the presence of hydrogen in the gas stream and that platinum loaded with iodine from an H_2-O_2 gas mixture would liberate iodine if the gas stream contained only oxygen. In a series of tests in which iodine-saturated platinized alundum pellets were subjected to a hydrogen-oxygen-steam atmosphere at 350°C, iodine transfer to the vapor phase was significant. When the hydrogen flow was stopped, the vapor (O_2 + steam) leaving the pellet bed was colored violet, indicating an immediate wholesale desorption of iodine. This indicates that if, during reactor operation, hydrogen flow to the recombiner was

[6] This work was done by Vitro Laboratories; for greater detail, see R. A. Keeler *et al.*, *Fission Product Separations Study (Quar. Prog. Rep. Sept. 27–Nov. 30, 1956, Vitro Job 2077)*, KLX-10067.

[7] D. E. Ferguson *et al.*, *HRP Quar. Prog. Rep. Jan. 31, 1957*, ORNL-2272, pp 135, 136.

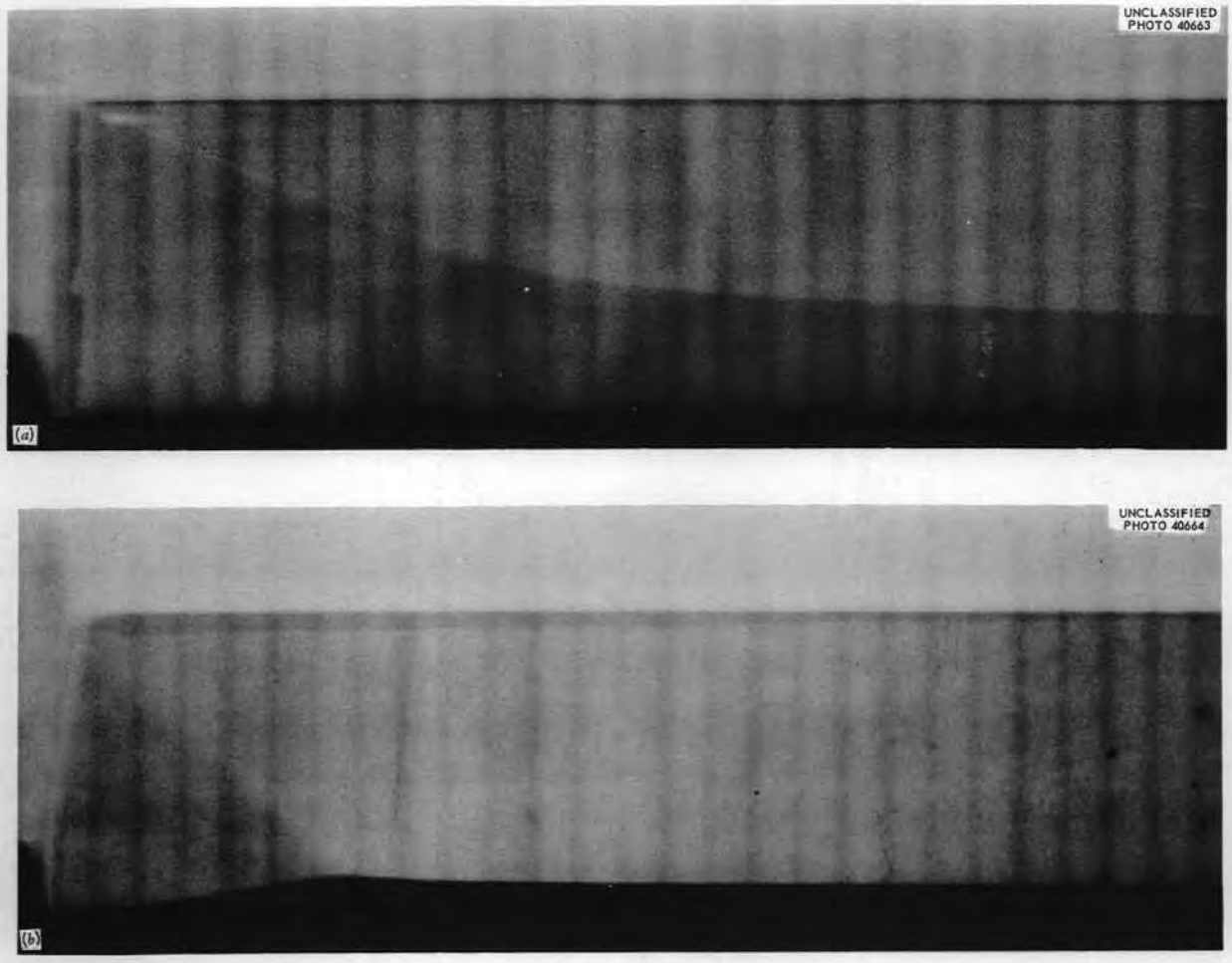

Fig. 15.8. X-Ray Photograph of B-3-L-1 Solids Settling (*a*) After 2.7 hr at 275°C and (*b*) After 3.2 hr at 275°C.

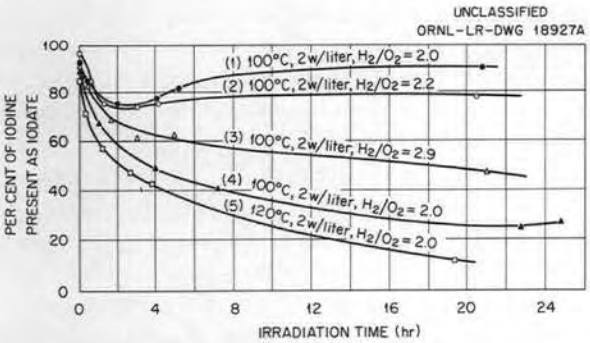

Fig. 15.9. Behavior of Iodine in Co^{60} Irradiation of 10 g of Uranium Fuel Solution.

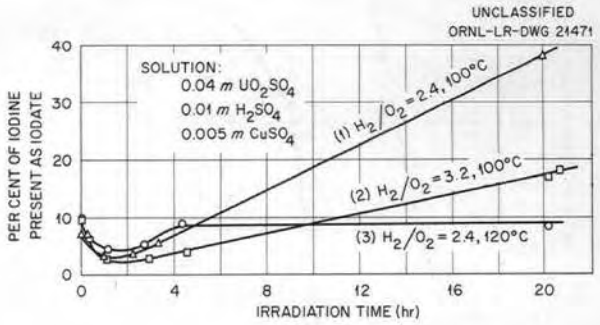

Fig. 15.10. Irradiation of Simulated Fuel Solutions with Co^{60} Gamma Rays at an Energy Level of 2 w/liter.

Table 15.4. Iodine Steady-State Valence in Solutions Irradiated at 2 w/liter at 100°C

H_2/O_2 Mole Ratio	IO_3^- at Steady State (% of total iodine)	
	Solution A*	Solution B**
2.0	92	60
2.2	79	38
2.4	>38	22
2.9	<47	8
3.2	≧18	4

*Solution A: 0.04 *m* UO_2SO_4, 0.01 *m* H_2SO_4, 0.005 *m* $CuSO_4$.

**Solution B: 0.02 *m* UO_2SO_4, 0.005 *m* H_2SO_4, 0.005 *m* $CuSO_4$.

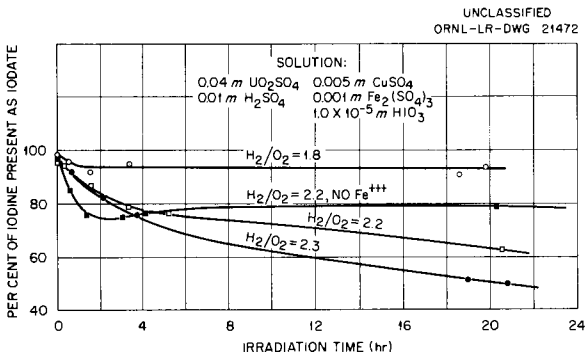

Fig. 15.11. Gamma Irradiation of Simulated Fuel Solution Containing Ferric Ion.

interrupted, iodine would be immediately liberated from a saturated platinized alundum bed.

15.4 RARE-GAS SOLUBILITY[6]

The solubility of krypton in water and in 0.02 *m* UO_2SO_4 was measured as a function of temperature and krypton partial pressure. The temperature range was 100 to 300°C for the water study and 250 to 300°C for the uranyl sulfate solution. The krypton partial pressures approximated those expected in HRT operation and were in the range 3.3×10^{-4} to 55.8×10^{-4} psi. The Henry's law constant for krypton in both H_2O and 0.02 *m* UO_2SO_4 solution was a linear function of temperature and was independent of the krypton partial pressure. The constants are described by

$$K_{(0.02\ m\ UO_2SO_4)} = 10^5 \left[9.233 - 0.0265T \pm \sqrt{0.0588 + \frac{(T-275)^2}{7500}} \right],$$

$$K_{(H_2O)} = 10^5 \left[9.09 - 0.026T \pm \sqrt{0.0625 + \frac{(T-205)^2}{77{,}500}} \right],$$

where K is Henry's law constant in psi/mole fraction and T is the centigrade temperature. In 0.02 *m* UO_2SO_4 solution the constant varies from $(2.60 \pm 0.15) \times 10^5$ psi/mole fraction at 250°C to $(1.28 \pm 0.15) \times 10^5$ at 300°C. For water the constant changes from $(6.39 \pm 0.26) \times 10^5$ psi/mole fraction at 100°C to $(1.29 \pm 0.25) \times 10^5$ at 300°C. Thus the solubility of krypton in dilute uranyl sulfate solutions increases with temperature, and the effect of the solute is negligible at this low concentration. A plot of the oxygen constants, obtained simultaneously with the krypton data, gives a line parallel to, but slightly higher than, the average line reported by Battelle.[8] There was also no significant difference in the oxygen constants for water and for 0.02 *m* UO_2SO_4 solutions.

15.5 URANIUM PROCESSING[6]

Continuation of the studies on decontamination of uranyl sulfate solution showed that decontamination from cesium by UO_4 precipitation was adequate. Decontamination factors were 52.6, 8.7, 3.5, and 2.0 with uranyl sulfate solutions containing, respectively, 5, 50, 100, and 150 g of uranium per liter. The Cs/U ratio in all cases was 12 mg of cesium per gram of uranium. A material balance showed 99.7% recovery of uranium from the solution containing 50 g of uranium per liter, with only 2.5% of the total loss accounted for by three washes.

Air-dried UO_4 dissolved completely and decomposed in 0.04 *m* H_2SO_4–0.005 *m* $CuSO_4$, to yield a solution containing 5 g of uranium per liter, in less than 30 min at 85°C; at 70°C, 195 min was required.

[8] E. S. Stephan *et al.*, *Solubility of Gases in Uranyl Sulfate Solutions*, BMI-1067 (Jan. 23, 1956).

Increasing the concentrations of all reactants tenfold gave a solution containing 50 g of uranium per liter in 188 min at 70°C.

The UO_4 precipitate obtained by adding MgO_2 either as a solid or a slurry to uranyl sulfate solutions could not be handled satisfactorily. However, MgO_2 may serve as a desirable starting material for the preparation of D_2O_2. Precipitates of UO_4 obtained by using solid Na_2O_2 also had undesirable handling characteristics, but a 2% solution of Na_2O_2 in water at room temperature was satisfactory for precipitation use. At 85°C, peroxide decomposition was sufficiently rapid to prevent formation of a permanent precipitate.

15.6 BEHAVIOR OF DILUTE ZrO_2 SUSPENSIONS IN CIRCULATING FUEL SOLUTION

A series of test runs in loop A was made to determine the rate at which typical homogeneous-reactor corrosion-product solids settle out from fuel solutions in a circulating system and to study the effect of temperature, concentration, and circulation velocity on the settling rate. The characteristics of the zirconium oxide solids used in these tests were described previously.[9]

[9] *Chem. Tech. Monthly Prog. Rep. March 1957*, ORNL-2307 (in press) (Classified).

Apparently, equilibrium concentration is approached over a period of about 10 hr (Table 15.5). The data indicate that the deposition rate has a first-order dependence on the instantaneous concentration of the suspended material in excess of the equilibrium concentration over most of the run time; that is, the concentration would follow an equation of the type

$$\frac{dC}{dt} = k(C - C_\infty) ,$$

where C_∞ is the equilibrium concentration and C is the sample concentration at time t. A plot of log $(C - C_\infty)$ vs time shows the rate constant, k, to be larger during the first 60 min of any run. The effect of the independent variables cannot be presented quantitatively, since the value of k is a sensitive function of the equilibrium concentration, which was not measured accurately. However, the trend of values of C at 600 min showed that C_∞ did increase as the initial concentration of solids increased. The first sample concentration was always larger than the calculated, possibly because of erosion of previously deposited solids. A glass loop is under construction which will be used to study the mechanism of solids deposition in a dynamic system.

Table 15.5. Solids Deposition Rate Data

Run No.	Temperature (°C)	Flow Rate (fps)	Concentration (ppm)		Suspended Solids (% of initial)									
			Calcd Initial	1st Sample	0 min	20 min	40 min	60 min	100 min	200 min	300 min	400 min	500 min	600 min
S-15	260	4	250	342	100	73	63	53	43	30	23	19	16	14
S-17	115	4	250	375	100	80	69	61	51	38	30	24	21	19
S-19	115	3	250	385	100	85	76	69	58	41	30	23	18	15
S-22	115	4	375	820	100	67	53	48	41	32	26	22	18	16
S-23	115	4	500	944	100	69	58	53	47	39	34	31	29	27
S-29*	115	4	625	N.D.**	100	74	63	58	51	39	34	31	29	29
S-30*	115	3	625	N.D.	100	77	68	62	53	42	35	30	27	25
S-31*	115	4	1320	N.D.	100	70	61	55	50	43	39	37	35	33

*Samples analyzed by gamma count.

**Not determined.

16. URANYL SULFATE BLANKET PROCESSING

R. E. Leuze
J. M. Chilton
S. S. Kirslis
E. O. Nurmi
P. A. Haas
S. D. Clinton

The study of plutonium chemistry in uranyl sulfate solutions included investigation of plutonium behavior in stainless steel equipment, solubility of Pu(VI), variables affecting plutonium valence, and plutonium behavior in the presence of radiation. The solution used in the HRT mockup was analyzed and inspected for solids.

16.1 SOLUBILITY OF Pu(VI) IN URANYL SULFATE SOLUTIONS

When 1.4 *m* UO_2SO_4 containing less than 300 mg of Pu(VI) per kilogram of H_2O was heated to 250°C in pyrex tubes under 200 psi of O_2, essentially all the plutonium stayed in the hexavalent state, and there was no precipitation. However, solutions containing more than this amount lost plutonium from solution, leaving about 215 mg per kilogram of H_2O in solution. Excess sulfuric acid increased the solubility. A sample containing no uranium but 0.15 *m* H_2SO_4 showed a solubility greater than 820 mg per kilogram of H_2O, and a sample in 1.4 *m* uranyl sulfate with 0.014 *m* H_2SO_4 showed a solubility of 620 mg per kilogram of H_2O. Since this solubility value is much lower than would be predicted by comparison with the solubility of U(VI), these experiments probably are a measure of the equilibrium between Pu(IV) and Pu(VI) in solution. If this is true, the total amount remaining in solution is controlled by the solubility of Pu(IV) and the ratio of Pu(VI) to Pu(IV) in solution.

16.2 PLUTONIUM VALENCE IN URANYL SULFATE SOLUTIONS

It has been previously reported[1] that after 1.4 *m* UO_2SO_4 containing plutonium has been heated to 250°C under stoichiometric hydrogen and oxygen, plutonium is predominantly in the tetravalent state. However, dissolved chromium acts as a catalyst for oxidation of plutonium to the hexavalent state. At room temperature the addition of an equivalent amount of Cr(VI) to a solution of Pu(IV) in 1.4 *m* UO_2SO_4 oxidizes approximately half the plutonium to Pu(VI). This indicates that the Cr(III)-Cr(VI) potential is approximately equal to the Pu(IV)-Pu(VI) potential under these conditions. Experiments were carried out to determine the effect of various gas overpressures on the behavior of dissolved chromium. When 1.4 *m* UO_2SO_4 containing Cr(III) was heated to 250°C under 200 psi of O_2, essentially all the chromium was oxidized to Cr(VI). When the O_2 overpressure was 100 psi and the H_2 overpressure was 200 psi, 80 to 90% of the chromium was present as Cr(VI). When the O_2 overpressure was 80 psi and the H_2 overpressure was 240 psi, 35 to 40% of the chromium was present as Cr(VI). Under these conditions essentially all the plutonium was oxidized to Pu(VI).

When 1.4 *m* UO_2SO_4 containing plutonium and chromium was heated to 250°C under 200 psi of O_2 and simultaneously irradiated in the Co^{60} source to 2 w/liter, chromium was present as Cr(III), and 80% of the plutonium was Pu(IV). The solution was prepared by adding 17 mg of Pu(IV) per kilogram of H_2O, and the chromium in solution resulted from slight corrosion of the stainless steel bomb. From these results it appears that plutonium in the presence of radiation will be reduced even if the overpressure is due to essentially pure oxygen.

16.3 PLUTONIUM BEHAVIOR IN 1.4 *m* UO_2SO_4 CONTAINED IN STAINLESS STEEL

A series of experiments was carried out to simulate the gradual buildup of plutonium in a reactor blanket solution. Plutonium was added batchwise to 1.4 *m* UO_2SO_4 at the rate of about 6 mg per kilogram of H_2O per day. The solution was heated overnight at 250°C under 200 psi of hydrogen and 100 psi of oxygen. The solution was cooled to room temperature for analysis and for adding more plutonium. This was repeated until a total of 140 mg of plutonium per kilogram of water was added. The behavior of plutonium for a ratio of 0.6 cm^2/ml for a stainless steel surface area to solution volume is shown in

[1] D. E. Ferguson *et al.*, *HRP Quar. Prog. Rep. Oct. 31, 1956*, ORNL-2222, p 143.

Fig. 16.1. As the plutonium concentration was gradually increased to 45 mg per kilogram of H_2O, essentially all the plutonium remained in solution as Pu(VI). There was a small amount of adsorption, but no plutonium precipitated. During the next few additions the amount of plutonium in solution decreased rapidly to about 5 mg per kilogram of H_2O. At the same time there was a rapid increase in plutonium adsorption and in the formation of a loose PuO_2 precipitate. All plutonium added after this was either adsorbed or precipitated.

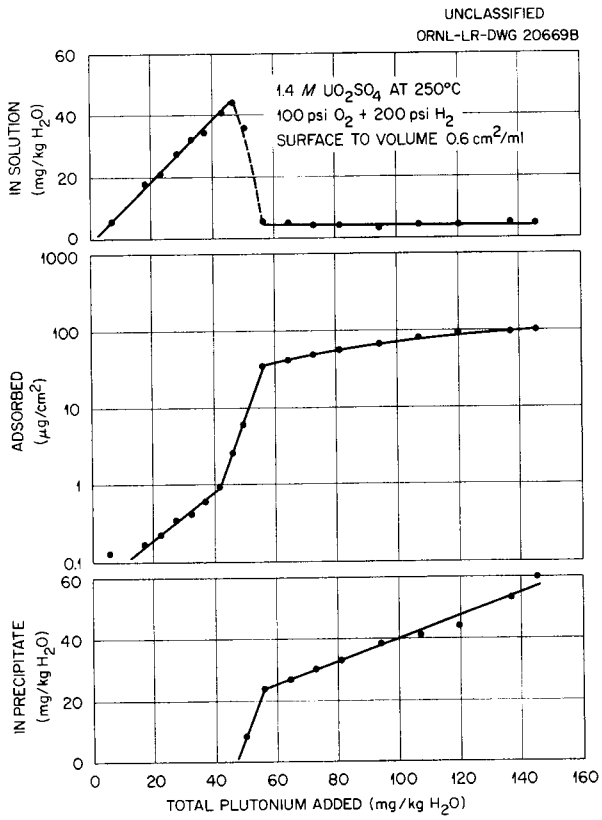

Fig. 16.1. Behavior of Plutonium Contained in Stainless Steel.

Other experiments were made with surface/volume ratios of 0.2 and 0.4 cm^2/ml. In all cases the plutonium remaining in solution and the plutonium adsorption per square centimeter were essentially the same as shown in Fig. 16.1. By decreasing the surface-to-volume ratio, it is thus possible to increase the amount of plutonium in the loose precipitate. For example, when the total plutonium addition was 130 mg per kilogram of H_2O, 40% of the plutonium was as a loose precipitate for a surface/volume ratio of 0.6 cm^2/ml, 60% for a ratio of 0.4 cm^2/ml, and 68% for a ratio of 0.2 cm^2/ml. A full-scale reactor may have a surface/volume ratio of about 0.4 cm^2/ml. However, results of these static experiments cannot be extrapolated to reactor conditions, since plutonium behavior may be different in dynamic systems and in the presence of radiation.

16.4 IN-PILE EXPERIMENT

To determine the behavior of plutonium and neptunium produced in a uranium solution under reactor conditions, a few milliliters of 1.4 *m* UO_2SO_4 solution were irradiated in the LITR for 10.9 days in a titanium bomb at 250°C under an oxygen overpressure. The bomb was opened 4 hr after reactor shutdown, and its contents were analyzed. The results are summarized in Table 16.1. It can be seen that 57% of the plutonium

Table 16.1. Plutonium and Neptunium Distribution* in Irradiated UO_2SO_4

1.4 *m* UO_2SO_4 in titanium irradiated 10.9 days in the LITR under oxygen at 250°C

Location	Total Pu (μg)	Pu Concentration	Total Np (μg)	Np Concentration
Solution	108.7	26 mg per kg of H_2O	79.6	18 mg per kg of H_2O
Precipitate	1.9		1.4	
Adsorbed	80.2	2.4 μg/cm²	62.3	1.8 μg/cm²
Total	190.8		143.3	

*Corrected to time of removal from LITR.

was in solution, 42% was adsorbed, and only 1% was in the precipitate. Neptunium behavior was similar, with 56% in solution, 43% adsorbed, and 1% in the precipitate. The amount of plutonium in solution, 26 mg per kilogram of H_2O, agrees fairly well with that in out-of-pile experiments. However, this solubility would be expected to decrease as more plutonium is formed. Neptunium adsorption was not expected to be as great as the plutonium adsorption, although there are no data available for neptunium adsorption in out-of-pile experiments. Analysis made several hours after the solution was removed from the LITR indicated that less than 0.1% of the plutonium was in the reduced states, Pu(III) and Pu(IV). When heated under oxygen, plutonium is oxidized; however, the presence of radiation was expected to cause reduction of the plutonium (Sec 16.3).

On the basis of the total quantity of Np^{239} at the end of the irradiation and the thermal-neutron flux, the capture cross section of U^{238} in this experiment was calculated to be approximately 13 barns. The large amount of resonance capture makes the value reasonable. If it is correct, 340 μg of plutonium would have been produced. However, only 191 μg of plutonium was found by analysis. The reason for this discrepancy is not known. It may be due to analytical difficulties, or there is a possibility that all the plutonium was not removed from the titanium bomb walls. Additional treatment of the titanium bomb will be made to make certain that all the plutonium has been removed.

In-pile experiments will be continued in an effort to better understand plutonium chemistry in the presence of radiation.

16.5 URANYL SULFATE SOLUTION FROM THE HRT MOCKUP

Solution drained from the HRT mockup was examined for solid particles. This solution was approximately 1 *m* UO_2SO_4 with a slight excess of acid. The quantity of solids in the solution was low, only 1.21 g total. This material was approximately 60% iron oxide, 25% uranium oxide, and 10% titanium oxide. The uranium oxide tended to be concentrated in the large particles (those held on a 40-μ filter), and the titanium oxide was practically colloidal and had to be coagulated before it could be removed by filtration. After a second similar run (see Sec 3.4), the mockup was drained, and a large amount of solid material, more than 100 g, was removed from the horizontal header between the main loop and the pressurizer. A sample of this material showed that it was of two distinct types. One part was typical iron oxide scale containing some chromium and nickel, and the other was essentially pure $UO_3 \cdot 0.5H_2O$.

16.6 LABORATORY SUPPORT FOR LOOP P-1 PROGRAM

Since it is desirable to obtain as much information as possible on the chemistry of plutonium in concentrated uranyl sulfate from the operation of the stainless steel P-1 loop, operational procedures were developed for preparation of feed samples and handling of product samples containing plutonium. In order to insert plutonium into the uranyl sulfate solution without addition of excess acid, 10 g of plutonium was prepared as crystalline $Pu(SO_4)_2$ from a solution of $Pu(NO_3)_4$. The molecular weight, based on chemical analysis of the plutonium content, was 462. An x-ray diffraction pattern of the material showed only faint traces, if any, of PuO_2. No standard pattern of $Pu(SO_4)_2$ is available for direct comparison.

Since the usual method for separation of PuO_2 from supernatant solutions, centrifugation with a clinical centrifuge, is not adaptable to large volumes of solution, the efficiency of a filtration technique was investigated. A 1.4 *m* UO_2SO_4 solution containing precipitated PuO_2 was filtered through an ultrafine fritted-glass filter, nominal pore size 1.5 μ. The filtrate was then centrifuged in the usual way. Samples of the filtrate taken before and after centrifugation showed no change in plutonium concentration, indicating that filtration is at least as efficient as centrifugation.

16.7 LOOP P-1 STUDIES

After operation of loop P-1 (Fig. 16.2) for a cumulative time of 43 hr with H_2O and O_2 overpressure at approximately 220°C and 950 psi, the A-150-D Westinghouse pump had to be disassembled and the upper and lower Graphitar bearings and corresponding Stellite journals replaced. The inner surfaces of the Graphitar radial bearings were deeply scored, and the Stellite journals were discolored and contained several axial stress cracks ranging from ½ to ¾ in. in length. During operation there was no evidence

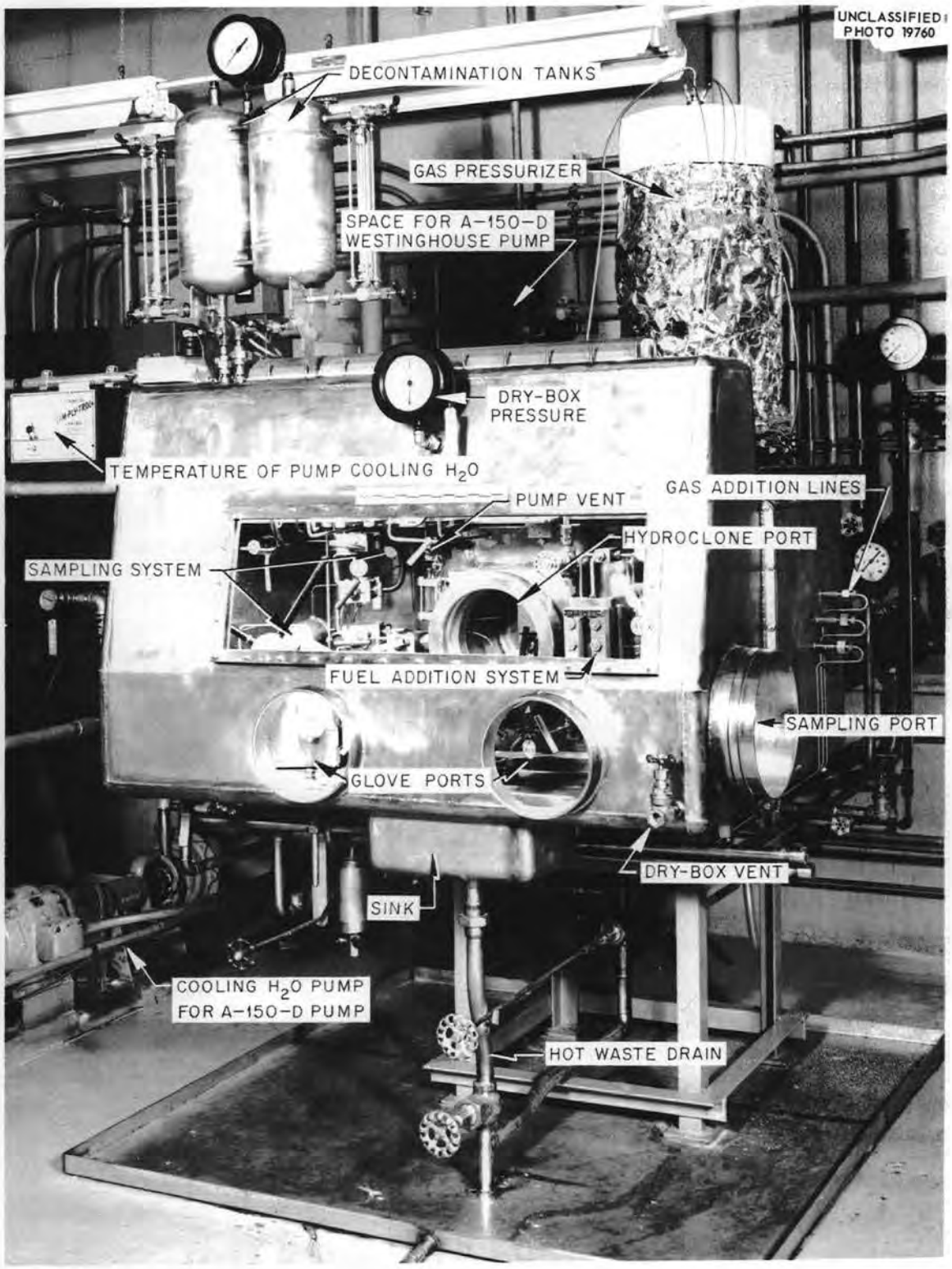

Fig. 16.2. Loop P-1 with Accessory Equipment.

of any damage to the pump bearings except for the presence of finely divided graphite particles in the solution bled from the back of the pump.

The reason for the early bearing failure in the pump was attributed to gas formation because of the temperature, pressure, and gas concentration in the loop. With a partial-gas-pressurization system, oxygen gas was believed to have been released in the pump bearing region because of the differences in the equilibrium solubility of oxygen at the loop temperature and an estimated pump temperature of 50 to 100°C.

The pump was reassembled with a titanium impeller and thermal barrier and was installed along with a titanium wear ring and a gold-plated stainless steel gasket in the pump scroll. While the pump was being repaired, a solids-addition and sampling bomb and a deposition coupon holder were installed in the loop. Nine runs have now been made with the reassembled pump, for a cumulative operating time of approximately 175 hr with no apparent damage to the bearings. One run of 46 hr was made with a 5 wt % HNO_3 solution at a temperature not exceeding 85°C. Five thermal cycles were made with water at loop temperatures ranging between 220 and 240°C, for a total operating time of 60 hr. Three runs were made with uranyl sulfate (10 g of uranium per kilogram of H_2O) at loop temperatures of 220 to 230°C. All runs were made with an initial oxygen overpressure of 50 psi.

Results of the nitric acid run showed that all corrosion occurred during the first 2 hr of operation, in which 5 g of iron and 1 g of nickel were dissolved. Samples taken during the uranyl sulfate runs indicated that the uranium remained in solution and that none was adsorbed on the loop surfaces. No corrosion was apparent during the uranyl sulfate runs, since the nickel content of the solution remained below 20 ppm.

The biggest problem encountered in the thermal cycling was leakage around autoclave valve glands and fittings upon cooling the loop after a run. Attempts are still being made to tighten these connections. After the pump-scroll case bolts were cleaned, relubricated, and tightened to a torque of 300 ft-lb, the gold-plated stainless steel gasket between the pump housing and scroll continued to hold 1000 psi of nitrogen after five thermal cycles.

17. THORIUM OXIDE BLANKET PROCESSING

R. E. Leuze
R. D. Baybarz

Simple methods of processing thorium oxide for removal of fission-product poisons are being investigated. Since calculations show that the recoil energy of fission fragments is sufficient to eject most of the fission products into the aqueous phase of a slurry, it may be possible to develop a process to remove these poisons without destroying the ThO_2 particle. Scouting studies were made to investigate this possibility.

17.1 CATION ADSORPTION ON ThO_2

The cation adsorption properties that ThO_2 exhibits at 250°C in an aqueous slurry were investigated by using uranium adsorption from a dilute uranyl sulfate solution. It was found that ThO_2 adsorbed considerable amounts of uranium and held it in such a fashion as to necessitate dissolution of the thoria before any leaching occurred.[1]

Since the thoria adsorbed the uranium from solution and held it irreversibly, various additives and pretreating methods were tried in an attempt to diminish the adsorption. Adsorption was greater at 250°C than at 23°C (Table 17.1), the adsorption varying at 250°C from 15,000 to 56,000 ppm on untreated ThO_2. Pretreatment [with sulfur-saturated alcohol, dilute H_2SO_4, or dilute $Th(SO_4)_2$] reduced this by a factor of about 10. Although this reduction in adsorption is in the right direction, it appears that a more drastic treatment is needed to reduce the adsorption still further.

The effect of calcining temperatures on the cation adsorption properties of thorium oxide was investigated. Increasing the calcining temperature of the thoria from 650 to 1100°C decreased the uranium adsorption (Table 17.2). It is believed that calcination at a high temperature, possibly 1600°C, will practically eliminate the adsorption. This will solve part of the problem by keeping the fission products from being adsorbed irreversibly on thoria. However, it may be assumed that the fission and corrosion products will hydrolyze and precipitate and exist intermixed with ThO_2 so as to make separation difficult. Various inorganic exchangers that may be coslurried with the thoria to sorb the fission products are being investigated. Preliminary scouting studies indicate that colloidal silica, magnesium silicate, and bismuth oxide may be useful.

Future work will involve a closer look at possible inorganic exchangers and the adsorption characteristics of highly calcined ThO_2.

Table 17.1. Uranium Adsorption on ThO_2

Thorium oxide with surface area of 35 m^2/g, prepared by thermal decomposition of thorium oxalate at 600°C

Oxide Pretreatment[a]	Adsorption from 0.01 *m* UO_2SO_4 (parts per 1000 parts Th)[b]	
	23°C	250°C
Untreated	2–5	15–56
S[c]	0.02–0.05	2.0–3.7
H_2SO_4	0.40	2.1–3.4
$Th(SO_4)_2$	0.45	4.3

[a] ThO_2 was contacted with dilute solutions of these materials prior to contacting with UO_2SO_4.

[b] Single numbers represent data from single experiments. In other cases the range for several experiments is given.

[c] ThO_2 was contacted with absolute alcohol saturated with sulfur.

Table 17.2. Effect of ThO_2 Calcination Temperature on Uranium Adsorption

Calcination Temperature (°C)	Uranium Adsorption (parts per 1000 parts Th)
650	3.3–4.4
850	1.9–2.4
1000	0.72–1.10
1100	0.08–0.19

[1] D. E. Ferguson, R. E. Leuze, and R. D. Baybarz, *HRP Quar. Prog. Rep. Jan. 31, 1957*, ORNL-2272, p 159.

18. THORIUM OXIDE SLURRY DEVELOPMENT

J. P. McBride

E. V. Jones
N. A. Krohn
L. E. Morse
R. L. Pearson
C. E. Schilling
W. M. Woods

18.1 SLURRY IRRADIATION STUDIES

18.1.1 Slurry Irradiations in the LITR

The new diagonal-tube irradiation facility (C-43) was put into operation. The neutron flux, measured with a cobalt-aluminum alloy, is 2.9×10^{13} neutrons·cm^{-2}·sec^{-1}. A projected three-month irradiation of a settled slurry of 800°C-calcined micropulverized thorium oxide was initiated.

18.1.2 Postirradiation Examination of Slurries

(a) Chemical and Radiochemical Analyses. – Nine thorium oxide slurries – seven containing enriched uranium – that had been irradiated in the LITR[1] were analyzed to determine uranium, thorium, the corrosion-product pickup, and the fission-product, protactinium, and U^{233} distribution. Uranium/thorium ratios were as expected (Table 18.1). Corrosion-product pickup in the irradiated slurries agreed well with data from out-of-pile control experiments (Table 18.1). The bulk of the radioactive materials was associated with the solids, only cesium appearing in the supernatant in significant amounts (Table 18.2). The ruthenium analyses were erratic, probably because of the perchloric acid dissolution procedure used on the slurry solids.

(b) Particle-Size Analyses. – The particle-size distributions of the irradiated slurries were determined by sedimentation[2] (Table 18.3). The marked increase in the number of large particles in several of the irradiated slurries is contrary to previous experience. Microscopic examination showed the large particles to be irregular in shape. The long cooling period may have allowed formation of hard agglomerates, which were not

[1] D. E. Ferguson *et al.*, *HRP Quar. Prog. Rep. Jan. 31, 1957*, ORNL-2272, p 144.

[2] G. W. Leddicotte *et al.*, *Particle Size Analysis by Radioactivation*, ORNL-2160 (in preparation).

Table 18.1. Chemical Analyses of Irradiated Slurries

Slurry composition: 750 to 1000 g of thorium and 5 g of U^{235} per kilogram of H_2O

Code	Preparation	U/Th Ratio	Corrosion Products (ppm)					
			Control			Irradiated		
			Fe	Ni	Cr	Fe[a]	Ni[b]	Cr[c]
LITR-17	900°C calcination[d] of autoclaved mixture	56.6	4,140	554	856	5,100	949	1930
LITR-18	Same	56.2				3,600	458	911
LITR-25	900°C calcination[e] of coprecipitated oxalates	59.6	15,600			18,900		
LITR-28	800°C calcination[e] of coprecipitated oxalates	46.4	21,300	2900	3500	22,200		

[a] All the iron associated with the slurry solids.
[b] Nickel in supernatant: LITR-17, 8.2%; LITR-18, 22.1%.
[c] Chromium in supernatant: LITR-17, 2.1%; LITR-18, 15.3%.
[d] 1000 ppm PdO added as gas recombination catalyst.
[e] 20,000 ppm MoO_3 added as gas recombination catalyst.

Table 18.2. Radiochemical Analyses of Irradiated Slurries

Slurry composition: 750 to 1000 g of thorium per kilogram of H_2O

Code	Material	Preparation	Activity in Supernatant (% of total)									
			Gross β	Gross γ	Total Rare-Earth β	Sr β	Ru γ	Cs γ	Zr-Nb γ	Nb γ	Pa γ	U
LITR-19	ThO_2–0.5% enriched U	900°C calcination[a] of coprecipitated oxalates	0.6	0.4	0.3	0.6	4.0	5.3	0.1	0.004	0.2	0.003
LITR-21	Same	Same	1.0	1.8	0.1	0.1	82.5	63.0	0.52	0.03	0.5	0
LITR-29	Same	800°C calcination[b] of coprecipitated oxalates	1.0	0.2	0.4	19.2	<0.001	13.4	<0.002		0.004	
LITR-26	ThO_2 (TO-10-900-24)	Precipitated at 10°C as oxalate; calcined at 900°C	0.08	0.01	0.01	0.3	0.3	0.6	0.03	0.02	0.002	0.1[c]
LITR-27	ThO_2 (200A-6)	Pilot-plant oxide pumped 100 hr	0.15	0.15	13.8	0.4	0.02	0.5	0.9	0.03	0.12	0.1[c]

[a] 1000 ppm PdO added as gas recombination catalyst.
[b] 20,000 ppm MoO_3 added as gas recombination catalyst.
[c] U^{233} analyses by alpha counting.

Table 18.3. Particle-Size Distribution of Irradiated Slurries

Code[a]	Irradiation Time (hr)	Cooling Time (months)	Particle-Size Distribution (% in size range)							
			Control				Irradiated			
			<1 μ	1–3 μ	3–10 μ	>10 μ	<1 μ	1–3 μ	3–10 μ	>10 μ
LITR-17	90	12	49	27	17	7	56	15	13	16
LITR-18	20	11	25	35	25	15	11	3	17	69
LITR-19	251	10	49	26	21	4	15	9	11	65
LITR-21	160	9	53	36	7	4	35	30	26	9
LITR-25	192	7	53	36	7	4[b]	57	10	9	24
LITR-28	136	4.5	52	46	2		39	19	34	8
LITR-29	314	4	52	46	2		61	16	18	5
LITR-26	198	6	78	19	2	1[c]	57	13	17	13
LITR-27	344	5.5	24	12	57	7	25	23	29	23

[a]For slurry concentration, material, and preparation, see Tables 18.1 and 18.2.
[b]Control from LITR-21.
[c]Particle-size distribution of original charge.

broken up during the brief shaking prior to opening of the in-pile autoclaves.

18.2 GAS RECOMBINATION STUDIES

18.2.1 Effect of Sulfate

The effect of sulfate on the combination of stoichiometric mixtures of hydrogen and oxygen by an aqueous mixed ThO_2-UO_3 slurry containing sulfate was investigated for sulfate concentrations of 2300 to 9600 ppm, based on ThO_2. While the hydrogen-oxygen combination rates with the hydrogen-activated slurry varied somewhat with increasing sulfate concentration, they were in all cases but one in excess of 10 moles of H_2 per hour per liter of slurry and more than sufficient for the use of such a slurry in a TBR type blanket (Table 18.4). The lower combination rate in the one exception appeared to be associated with corrosion-product pickup, and reactivation with hydrogen restored its activity.

The initial slurry containing 2300 ppm sulfate was prepared by tumbling the dry ThO_2, $UO_3 \cdot H_2O$, MoO_3, and $Th(SO_4)_2 \cdot xH_2O$ solids for 1 hr and then heating the mixture in water at 280°C for 3 hr with a small oxygen overpressure. After the combination rate had been determined, the slurry was activated by heating with hydrogen (1000 psi at 25°C) for 1.1 hr at 285°C. The sulfate concentration was increased by adding thorium sulfate and heating for 1 hr at 280°C under oxygen after each sulfate addition. A total of 11,600 ppm sulfate was added to the slurry, but the maximum amount on the recovered solids was 9600 ppm. The solids were reslurried in fresh water after the completion of the experiments at each sulfate concentration or when heating the slurry with hydrogen and oxygen. Hence some of the sulfate remained in the supernatant or was leached from the solids during the experiments. The sulfate concentrations listed in Table 18.4 were determined by analyses of the recovered solids.

From the data of Table 18.4 the gas combination rates with the activated slurry were highest at sulfate concentrations of 2300 and 8750 ppm. Treatment of the slurry containing 9600 ppm sulfate with oxygen at 274°C markedly decreased its catalytic activity. Reactivation with hydrogen gave an extremely active slurry, with an actual increase in activity on subsequent heating with oxygen.

The decrease in gas reaction rate with the slurry containing 9600 ppm sulfate and treated with oxygen appeared to be associated with enhanced

Table 18.4. Effect of $Th(SO_4)_2 \cdot xH_2O$ Additions on the Reaction Rates of Stoichiometric H_2-O_2 Mixtures in Aqueous Mixed ThO_2-UO_3 Slurries

Slurry composition: 1000 g of thorium (as 900°C-fired ThO_2) and 5 g of uranium (as $UO_3 \cdot H_2O$) per kilogram of H_2O; heated with oxygen (300 psi, 25°C) 3 hr at 280°C; sulfate added as $Th(SO_4)_2 \cdot xH_2O$

Sulfate Concentration[a] (ppm, based on ThO_2)	Slurry Preparation	Temperature (°C)	Combination Rate, P_{H_2} = 500 psi (moles H_2 per hr per liter)
2300	As prepared	277	1.8
2300	Activated with hydrogen[b]	167	37.4
4500	Heated with oxygen[c]	167	27.7
6650	Same	167	30.3
8750	Same	167	38.9
9600	Same	167	22.5
8350	Same	204	2.1
7400	Reactivated with hydrogen[b]	159	57.5
6850	Reheated with oxygen[d]	160	71.4

[a]Solids reslurried in fresh water after completion of experiments at each sulfate concentration or when treating the slurry with oxygen or hydrogen.

[b]Slurry heated with hydrogen (1000 psi, 25°C) at 285°C for 1.1 hr.

[c]Slurry heated with oxygen (300 psi, 25°C) at 280°C for 1 hr.

[d]Slurry heated with oxygen (500 psi, 25°C) at 274°C for 3.0 hr.

corrosion of the bomb and the resultant deposition of iron oxide on the slurry solids. The red color of the slurry after the first oxygen treatment suggested the presence of Fe_2O_3, and 1580 ppm iron, based on ThO_2, was found in the slurry at the end of the experiments. After the slurry had been treated with hydrogen at 285°C for 1.1 hr, its normal light tan color was restored, and the gas reaction rate was double that obtained previous to oxygen treatment. The further increase in reaction rate on treatment with oxygen at elevated temperature a second time suggests that the system may have been slow in approaching equilibrium.

18.2.2 Effect of Calcination Temperature

Catalysis of the reaction of hydrogen and oxygen by thorium-uranium oxide slurries (500 g of thorium per kilogram of H_2O) containing 0.05 *m* MoO_3 is being studied as a function of the calcination temperature of the oxide. The study is being carried out in support of a projected gas recombination study in loop 100A at Y-12 by the slurry corrosion group. The mixed oxide for these studies has a U/Th mole ratio of 0.005/1 and was prepared by thermal decomposition of the coprecipitated oxalates. Gas reaction rates were satisfactory only with the slurry prepared from the coprecipitated oxide calcined at 1000°C for 24 hr. The rates at 224°C for this slurry as prepared and after activation by heating at 270°C for 2 hr with hydrogen (250 psi at room temperature) were 38 and 45 moles of H_2 per hour per liter of slurry, respectively. Both rates were calculated for a hydrogen partial pressure of 500 psi.

The aqueous slurry of the mixed oxide calcined at 650°C showed only negligible combination activity (0.05 *m* MoO_3 concentration) even after activation by heating with hydrogen. The 800°C-calcined mixed oxide was also inactive (Table 18.5).

The slurries were prepared for the combination studies by tumbling the dry solids (i.e., thorium-uranium oxide and MoO_3) for 1 hr, dispersing in water, and heating 1 hr at 280°C under an oxygen overpressure (300 psi at room temperature).

18.3 THORIUM-URANIUM MIXED-OXIDE STUDIES

18.3.1 Effect of Firing Temperature on Characteristic Properties

The effect of firing temperature for 24-hr firings on the properties of a thorium-uranium mixed oxide (MSO-CG-10-650-2) with a U/Th mole ratio of 0.005/1 and prepared from the coprecipitated oxalates was determined. Data included the uranium content, average sedimentation particle size, x-ray crystallite size, and specific surface area. The results (Table 18.6) were similar to those obtained with pure oxide prepared under similar conditions.

The mixed oxide was prepared by coprecipitating thorium and uranous oxalates at 10°C and decomposing by a two-stage calcination (400 and 600°C), ending with a 650°C firing for 2 hr.

Table 18.5. Effect of Oxide Calcination Temperature on the Combination Rate of Hydrogen-Oxygen Mixture in Aqueous Slurries of Thorium-Uranium Oxide Prepared from the Coprecipitated Oxalates

Slurry composition: 500 g of thorium and 5 g of uranium per kilogram of H_2O, 0.05 m MoO_3; heated at 280°C for 3 hr with O_2 (300 psi at room temperature)

Calcination Condition	Reaction Temperature (°C)	Combination Rate, P_{H_2} = 500 psi (moles H_2 per hr per liter)	
		As Prepared	After Activation*
650°C, 2 hr	280	0.02	0.02
800°C, 24 hr	285	0.12	
1000°C, 24 hr	224	38	45

*Heated for 2 hr at 270°C under hydrogen (250 psi at room temperature).

Table 18.6. Effect of Firing Temperature on Thorium-Uranium Oxide Properties

U/Th ratio of slurry: 0.005/1
Initial decomposition of 10°C-coprecipitated oxalates: 650°C, 2 hr
Firing time: 24 hr

Firing Temperature (°C)	Uranium Content (g/100 g Th)	Average Particle Size (μ)	Geometric Mean Deviation, σ	X-Ray Crystallite Size (Å)	Specific Surface Area (m^2/g)	Relative Surface Available for N_2 Adsorption, S/θ
650	0.41	0.68	1.3	137	20.1	0.46
800	0.59	0.71	1.6	235	11.7	0.46
900	0.59	0.75	1.4	360	9.15	0.55
1000	0.55	0.74	1.4	580	6.16	0.60
1170	0.60	0.78	1.5	1657	2.31	0.64
1400	0.46			2950*	1.04	0.52
1600	0.45			7480*	0.84	1.05

*Sieved through 200-mesh screen prior to x-ray diffraction measurement.

(a) Uranium Content. – The possibility of uranium losses at the higher firing temperatures was suggested by members of the Ceramics Laboratory, whose experience has been that such losses do occur. As can be seen from Table 18.6, no uranium loss occurred up to 1170°C firing temperature. Samples fired in the oxyacetylene furnace at 1400 and 1600°C may have suffered very slight uranium losses.

(b) Average Particle Size. – Particle size did not increase significantly with firing temperatures up to 1170°C. However, material fired at 1400 and 1600°C, for which data are not yet available, showed definite sintering effects, the products resembling sand in appearance.

(c) X-Ray Crystallite Size and Specific Surface Area. – The usual increase in x-ray crystallite size and the accompanying decrease in specific surface area with increasing firing temperature were noted. The data were used to calculate a relative surface available for nitrogen adsorption (S/θ). This ratio changed very little with increasing firing temperature up to 1400°C. However, the ratio was 0.5/1 to 0.6/1 rather than the 0.2/1 to 0.3/1 previously observed for mixed oxides prepared from the coprecipitated oxalates.[3] At 1600°C the ratio was 1.05/1.

18.3.2 Hindered-settling Rates at Elevated Temperatures

Hindered-settling rates were determined for slurries of the above mixed oxides, 250 g of thorium per kilogram of H_2O, from 100 to 300°C by the x-ray absorption technique.[4] The settling rates of the slurry of mixed oxide fired at 900°C were about twice those of a similar preparation of pure oxide (TO-10-900-24, Table 18.7). The mixed oxide handled easily, but there was some foaming at the higher temperatures, and several times at 300°C striations and solid-phase separations were observed, indicative of the formation of large agglomerates.

The hindered-settling rates, in general, increased slightly with increasing firing temperature up to 1170°C, except for the slurry of mixed oxide fired at 1000°C. With the 1170°C material the settling rate and critical concentration increased markedly (Table 18.7; Fig. 18.1).

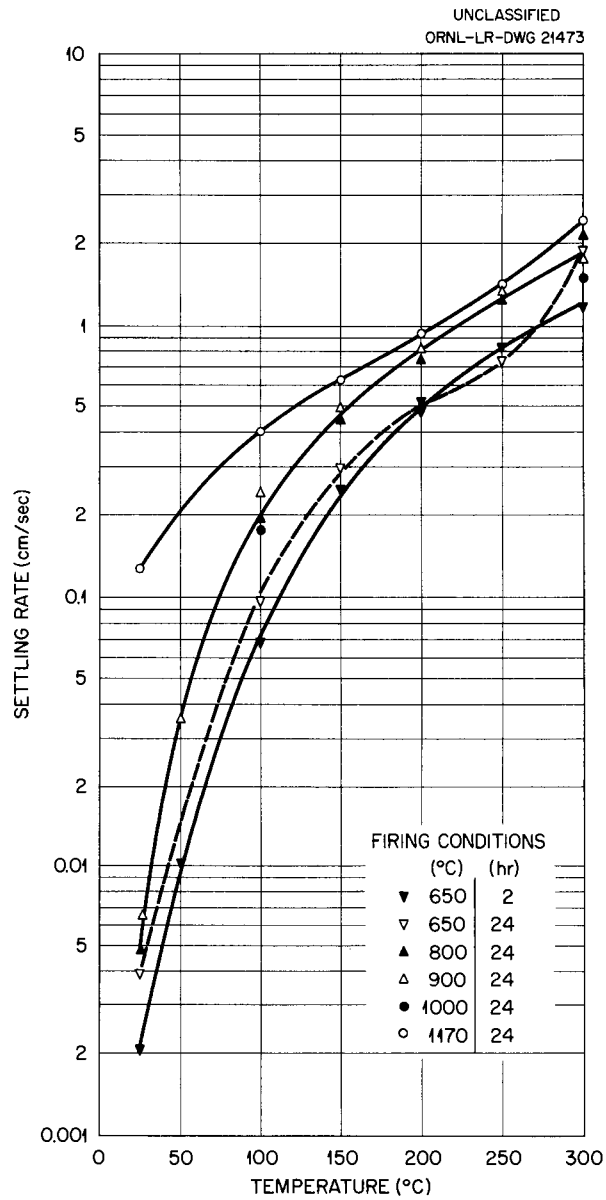

Fig. 18.1. Effect of Oxide Firing Temperature on the Settling Rates of Thorium-Uranium Oxide Slurries: 250 g Th per kg of H_2O; U/Th = 0.005.

[3] D. E. Ferguson *et al.*, *HRP Quar. Prog. Rep. Jan. 31, 1957*, ORNL-2272, p 144.

[4] V. D. Allred, E. V. Jones, and J. P. McBride, *HRP Quar. Prog. Rep. April 30, 1956*, ORNL-2096, p 112.

Table 18.7. Effect of Oxide Firing Temperature on the Sedimentation Properties of Thorium-Uranium Oxide Slurries

Slurry composition: 250 g of thorium per kilogram of H_2O, U/Th ratio of 0.005/1; thorium oxide prepared from 10°C-coprecipitated oxalates, MSO-CG-650-2

Firing Conditions		Slurry Temperature (°C)	U_0, Hindered-settling Rate (cm/sec)	Concentration (g of Th per liter)		Average Sedimentation Particle Size (μ)
Temperature (°C)	Time (hr)			Critical*	Settled**	
650	2	100	0.068	308	652	0.66
		150	0.250	381		
		200	0.480	398		
		250	0.740	433		
		300	1.19	490		
650	24	100	0.096	349	750	0.68
		150	0.300	392		
		200	0.520	450		
		250	0.820	408		
		300	1.86	676		
800	24	100	0.195	406	---	0.71
		150	0.450	468		
		200	0.750	474		
		250	1.20	507		
		300	2.14	553		
900	24	100	0.240	414	732	0.75
		150	0.500	459		
		200	0.820	507		
		250	1.32	529		
		300	1.78	652		
1000	24	100	0.167	341	---	0.74
		150	0.500	441		
		200	0.785	492		
		250	1.23	509		
		300	1.46	565		
1170	24	100	0.401	780	1256	0.78
		150	0.628	616		
		200	0.928	751		
		250	1.41	681		
		300	2.41	1128		
TO-10-900-24		110	0.169	655	760	0.8
		155	0.281	580		
		205	0.335	545		
		265	0.663	520		

*Concentration at which slurry enters compaction zone of settling.

**After settling 15 min.

18.4 SILICATE ADDITION STUDIES

18.4.1 Room-Temperature Sedimentation Studies

The effects of the addition of hydrogen bentonite and various silicon compounds on the room-temperature sedimentation properties of 800°C-calcined thorium oxide slurries (250 g of thorium per kilogram of H_2O) autoclaved at 300°C were studied.

Concentrations of hydrogen bentonite greater than 5000 ppm, based on ThO_2, lowered the settling rates and increased the settled densities. At hydrogen bentonite concentrations greater than 13,000 ppm the settling rates were much too slow for practical measurement, and the settled concentrations after prolonged settling were 2400 to 2500 g of thorium per liter (Table 18.8).

The effects of silicon added as sodium metasilicate, silicic acid, or silica were much more pronounced, dispersion effects being observed at concentrations as low as 2500 ppm SiO_2, based on ThO_2. The dispersion effects with the three forms of silica were very similar, despite the fact that the final pH's were 10 to 12 in the case of the sodium metasilicate and 5 to 7 for the silicic acid and silica additions (Table 18.9). Dispersion was maximum (settling rates lowest) for the sodium metasilicate at 2500 to 5000 ppm SiO_2, based on ThO_2. At 20,000 ppm SiO_2 the settling rate was the same as that at 1000 ppm.

Both the hydrogen bentonite and the sodium metasilicate systems were at apparent equilibrium after 22 hr of autoclaving at 300°C. The silica-containing slurry may not have been at chemical equilibrium even after 44 hr of autoclaving at 300°C, but, nonetheless, dispersion effects were pronounced for all silicon-containing compounds at 5000 ppm.

18.4.2 Settling Rates at Elevated Temperatures

The effects of $Na_2O{\cdot}SiO_2$ (1000 to 30,000 ppm SiO_2, based on ThO_2) on slurry settling rates at elevated temperatures were determined with aqueous slurries (250 g of thorium per kilogram of H_2O) of an 800°C-fired pilot-plant oxide (ACDC-13) as

Table 18.8. Effects of Hydrogen Bentonite Additions on Room-Temperature Sedimentation Properties of Thorium Oxide Slurries

Slurry composition: 250 g of thorium per kilogram of H_2O, 800°C-fired oxide, autoclaved 22 hr at 300°C

Bentonite Concentration (ppm, based on ThO_2)	Supernatant pH	Settling Rate (cm/sec)	Concentration (g of Th per liter)	
			Critical[a]	Settled
0	6.6	0.0630	900	1400
268	6.5	0.0615	900	1600
1,060	6.6	0.0550	900	1400
2,120	6.7	0.0610	900	1500
3,180	6.9	0.0715	900	1600
4,770	6.7	0.0615	900	1500
6,360	6.3	0.0495	900	1600
9,540	6.3	0.0495	1000	1700
12,725	5.9	0.0300	700	1800
15,900[b]	6.0	c		2500
25,450	5.6	c		2400

[a]Concentration at which slurry enters compaction zone of settling.
[b]Per cent concentration based on H_2O: 0.4.
[c]Too slow to read.

Table 18.9. Effect of the Addition of Sodium Metasilicate, Silicic Acid, and Silica on the Room-Temperature Sedimentation Properties of Thorium Oxide Slurries

Slurry composition: 250 g of thorium per kilogram of H_2O, 800°C-fired oxide, autoclaved at 300°C

SiO_2 Concentration (ppm, based on ThO_2)	Supernatant pH	Settling Rate (cm/sec)	Concentration (g of Th per liter)	
			Critical*	Settled
		Sodium Metasilicate, Autoclaved 22 hr		
200	10.4	0.0810	900	1500
500	10.8	0.0730	900	1700
1,000	11.0	0.0350		1900
2,500	11.6	**		2400
5,000	11.8	**		2400
5,000	11.7	**		2400
10,000	12.0	0.0040		2200
20,000	12.1	0.0305	800	1900
		Solid SiO_2, Autoclaved 44 hr		
500	6.4	0.0595	800	1400
1,000	6.5	0.0645	800	1400
2,500	6.8	0.0465	800	1500
5,000	6.8	**		2400
10,000	5.0	**		2200
20,000	5.0	**		2200
		Solid H_2SiO_3, Autoclaved 22 hr		
500	6.1	0.0740	800	1200
1,000	7.6	0.0540	900	1400
2,500	6.8	0.0476	900	1500
5,000 (20 hr)	6.8	0.0370	800	1700
5,000 (44 hr)	7.2	0.0385	900	1800
10,000	6.9	**		2100
20,000	6.3	**		2300

*Concentration at which slurry enters compaction zone of settling.

**Too slow to read.

received and after micropulverizing. All slurries were heated at 300°C prior to the settling studies.

With the slurry of the oxide as received (not pulverized), the addition of 1000 ppm SiO_2, based on ThO_2, markedly decreased the settling rate below 100°C but above this temperature did not change the settling rate from that observed in the absence of silicate. At silica concentrations of 5000 to 20,000 ppm, the settling rates were greatly reduced at all temperatures below 275°C, but there was no change above this temperature (Fig. 18.2). Maximum dispersion (minimum settling rates) was obtained with the 10,000-ppm SiO_2/ThO_2 concentration.

Slurries of the micropulverized oxide settled more slowly at all temperatures and for all silica concentrations than slurries of the oxide as received (Fig. 18.3). The slurry of micropulverized oxide containing 1000 ppm SiO_2, based on ThO_2, appeared to settle faster at 100 and 150°C than the same slurry containing no silicate. At silica concentrations of 5000 to 30,000 ppm the settling

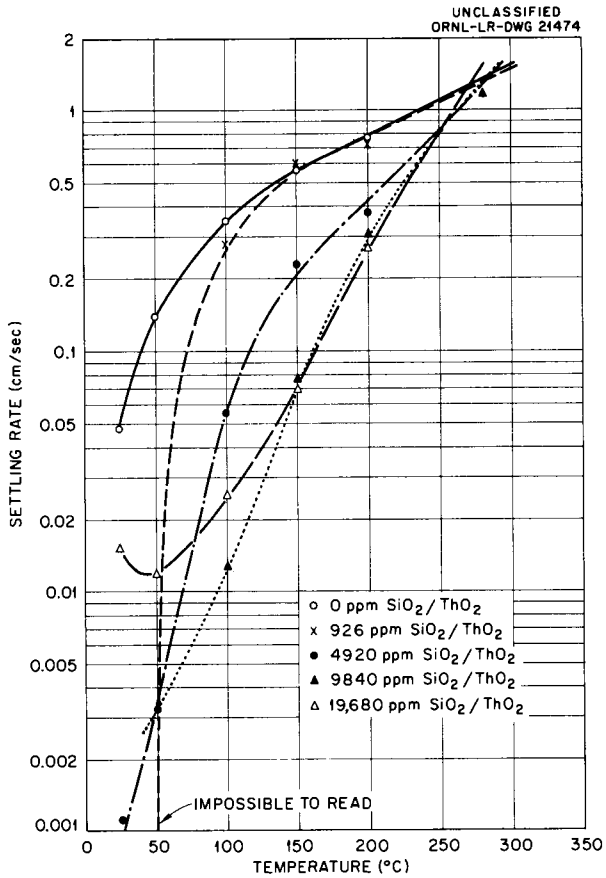

Fig. 18.2. Effect of $Na_2O \cdot SiO_2$ Additions on the Settling Rates of Aqueous Slurries of ACDC-13. Thorium oxide: 250 g of Th per kg of H_2O; average particle size of oxide, 2.6 μ.

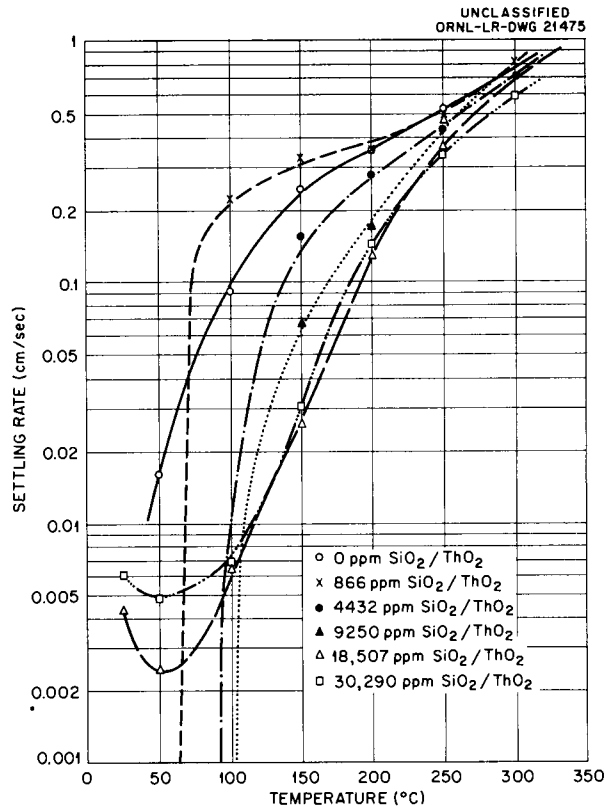

Fig. 18.3. Effect of $Na_2O \cdot SiO_2$ Additions on the Settling Rates of Aqueous Slurries of Micropulverized ACDC-13. Thorium oxide: 250 g of Th per kg of H_2O; average particle size of oxide, 1 μ.

rates were decreased below those of the pure slurry at all temperatures through 300°C, but the effect was more pronounced below 225°C. Dispersion effects were maximum with 20,000 ppm SiO_2.

Three passes through the micropulverizer degraded the ACDC-13 oxide from an average particle size of 2.6 μ to 1.0 μ. With the lower average particle size the settling rate at 300°C decreased threefold.

18.4.3 Equilibrium Studies

Settling rates were determined at 100°C to find the rate of approach to equilibrium in the thorium oxide slurry containing sodium metasilicate. The study was carried out with a slurry containing 250 g of 800°C-fired oxide (ACDC-13) and containing 10,000 ppm SiO_2, based on ThO_2. Twenty minutes after the preparation of the slurry at room temperature, the first settling rate, equal to 0.005 cm/sec, was determined at 100°C. Essentially no change was observed in the settling rate on subsequent heating for 16 hr at 100°C (Table 18.10).

To determine the effect of preheating the slurry at 300°C, the above slurry was heated overnight at 300°C. The temperature was then lowered to 100°C, and a second series of settling studies was initiated. The initial settling rate was approximately twice that observed above, but after 45 min of heating it approached the above value. Hence it appears that equilibrium is attained at 100°C in at least 1 hr, the time depending somewhat on the previous heat treatment of the slurry.

Table 18.10. Equilibrium Studies in Thorium Oxide Slurries Containing Silicate

Slurry composition: 250 g of thorium (800°C-fired oxide) per kilogram of H_2O, 10,000 ppm SiO_2 ($Na_2O \cdot SiO_2$), based on ThO_2
Temperature: 100°C

Time of Heating at 100°C (min)	Settling Rate (cm/sec)
0 (90°C)	0.006
6 (97°C)	0.005
12	0.005
22	0.005
62	0.006
957	0.005
After Heating at 300°C	
8	0.011
13	0.009
45	0.0075

18.4.4 Studies with Mixed Thorium-Silicon Oxide

Mixtures of thorium oxide and solid silicic acid containing 0.5 and 1 mole % SiO_2 were tumbled for 26 hr and then fired at 1000°C for 24 hr. These solids were dispersed as aqueous slurries (250 g of thorium per kilogram of H_2O) for studies on the effect of silicate additions on slurry behavior. The objective was to determine the effect of such an oxide preparation method on the dispersing action of silicates. In general, the silicates were somewhat more effective as dispersing agents for this material than for the pure thorium oxide.

Silicate was added to the aqueous dispersions in the form of sodium metasilicate (Na_2SiO_3) and silicic acid (H_2SiO_3) at concentrations from 1000 to 10,000 ppm SiO_2, based on ThO_2. The slurries were autoclaved at 300°C for 22 hr and, after cooling, their room-temperature sedimentation characteristics were determined (Tables 18.11 and 18.12). All silicate concentrations markedly decreased the settling rates and increased the

Table 18.11. Effect of Na_2SiO_3 Additions on the Room-Temperature Sedimentation Properties of Thorium-Silicon Oxide Slurries

Slurry composition: 250 g of thorium per kilogram of H_2O, prepared by firing the mixed thorium-silicon oxides at 1000°C for 24 hr; autoclaved 22 hr at 300°C

Slurry Solid	Na_2SiO_3 Concentration (ppm SiO_2, based on ThO_2)	pH	Hindered-settling Rate (cm/sec)	Settled Concentration (g of Th per liter)
D-16 ThO_2, 1000°C fired	None	7.1	0.0820	1730
	10,000		0.0043	
ThO_2–0.5 mole % SiO_2	None	7.0	0.0695	1630
	1,000	10.3	*	2710
	2,500	11.1	*	2420
	5,000	11.6	*	2615
	10,000	12.4	0.0037	2420
ThO_2–1 mole % SiO_2	None	6.5	0.0580	2185
	1,000	9.8	*	2645
	2,500	11.3	*	2370
	5,000	10.6	*	2370
	10,000	11.7	0.0035	2500

*Settled too slowly to read conveniently.

Table 18.12. Effect of H_2SiO_3 Additions on the Room-Temperature Sedimentation Properties of Thorium-Silicon Oxide Slurries

Slurry composition: 250 g of thorium per kilogram of H_2O, prepared by firing the mixed thorium-silicon oxides at 1000°C for 24 hr; autoclaved 22 hr at 300°C

Solid	H_2SiO_3 Concentration (ppm SiO_2, based on ThO_2)	pH	Hindered-settling Rate (cm/sec)	Settled Concentration (g of Th per liter)
D-16 ThO_2, fired at 1000°C	None	7.1	0.0820	1730
	10,000	6.8	*	2585
ThO_2–0.5 mole % SiO_2	None	7.0	0.0695	1630
	2,500	6.0	*	2250
	5,000	6.0	*	2585
	10,000	6.1	*	2810
ThO_2–1 mole % SiO_2	None	6.5	0.0580	2185
	2,500	7.0	*	2500
	5,000	6.2	*	2615
	10,000	5.8	*	2645

*Settled too slowly to read conveniently.

settled concentrations when compared with those of the pure oxide and the mixed thorium-silicon oxides in the absence of silicate.

18.5 DEEP-BED SETTLING EXPERIMENTS

Local concentrations (1100 g of thorium per kilogram of H_2O) of ThO_2 have been found at the bottom of the blanket in the slurry blanket mockup which were considerably higher than the average concentration charged and also higher than the settled concentrations, 700 g of thorium per kilogram of H_2O, obtained with the same slurry and at comparable temperatures in the x-ray settling apparatus. Accordingly, a series of settling experiments was carried out with pilot-plant oxide to determine the effect of slurry concentration and bed height on the concentration of ThO_2 at the bottom of a settling column of slurry. It was concluded from these experiments that the difference in bed height (between the slurry in the blanket and that in the autoclave used in the settling studies) does not of itself account for the observed discrepancy.

The settling tests were carried out with 40-in.-deep beds of ThO_2 slurries (800°C-fired pilot-plant oxide) in a 3-in.-ID glass column arranged for sampling the slurry at the bottom. Parallel settling tests were made for a small graduate similar in geometry to the autoclave used in the x-ray studies.

The slurry containing 1000 g of thorium per kilogram of H_2O in the deep bed was in compaction, and the concentration at the bottom was equal to the average concentration during the entire time of settling (Fig. 18.4). For lower slurry concentrations (250, 500, and 750 g of thorium per kilogram of H_2O), the concentration at the bottom was greater than the average concentration until the slurry entered the compaction region of settling, when it became equal to the average concentration (Figs. 18.5, 18.6, and 18.7).

At equal concentrations, settling rates were faster in the 3-in.-dia glass column than in the graduate: 2.5 times at 250 g of thorium per kilogram of H_2O and 23 times at 1000 g of thorium per kilogram of H_2O. Settled concentrations in the graduate were, however, only 10 to 25% less than those in the deep-bed studies (Fig. 18.8).

18.6 PREPARATION OF THORIA SOLS AND GELS[5]

Thoria sols were not stabilized by nitrate ion under reactor conditions. A sample of the best nitrate-stabilized thoria sol is being prepared for toroid tests to determine the behavior of the flocculated suspension resulting from thermal deterioration of the sols.

Pilot-scale apparatus for the production of thorium oxide microspheres has been assembled and tested. Silica-gel beads ranging in size from 10 to 70 μ (wet) were produced. Modifications in the pilot-plant apparatus to make it more easily operable are nearly complete. Small-scale experiments with the same jet velocities showed that thoria gels form smaller beads than does silica gel. Preliminary washing and drying experiments indicate that thoria beads are easily handled. Figure 18.9 is a photomicrograph of thoria beads dried at 105°C. These beads remained discrete spheres when fired at 1400°C.

[5]Work done by Houdry Process Corp.

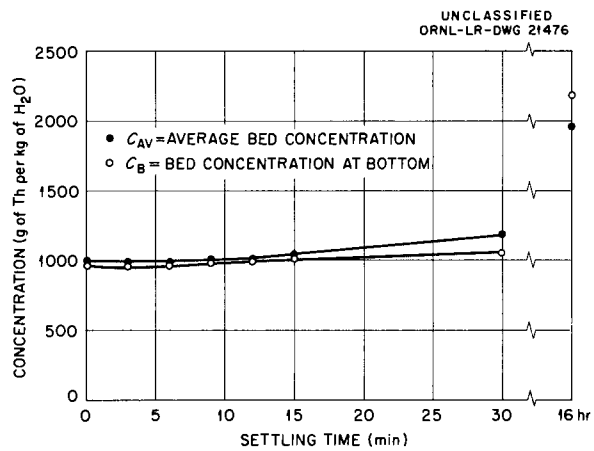

Fig. 18.4. Bottom and Average Settled Bed Concentration vs Settling Time in 40-In.-Deep Bed. Slurry concentration at room temperature = 1000 g of Th per kg of H_2O; thorium oxide prepared by precipitation of the oxalate at 70°C and firing at 800°C.

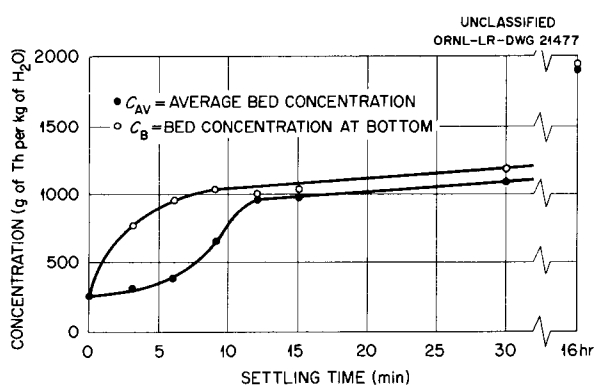

Fig. 18.5. Bottom Concentration and Average Settled Bed Concentration vs Settling Time in Deep Bed. Slurry concentration at room temperature = 250 g of Th per kg of H2O; thorium oxide prepared by precipitation of the oxalate at 70°C and Firing at 800°C.

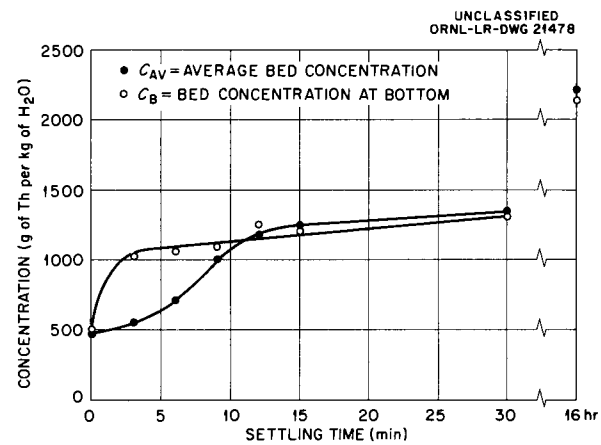

Fig. 18.6. Bottom and Average Settled Bed Concentration vs Settling Time in Deep Bed. Slurry concentration at room temperature = 500 g of Th per kg of H_2O; thorium oxide prepared by precipitation of the oxalate at 70°C and firing at 800°C.

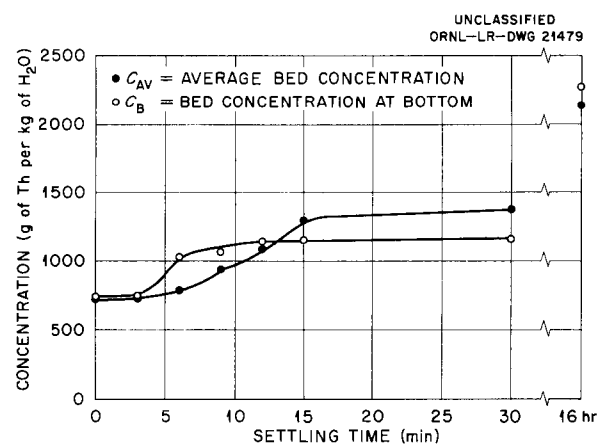

Fig. 18.7. Bottom and Average Settled Bed Concentration vs Settling Time in Deep Bed. Slurry concentration at room temperature = 750 g of Th per kg of H_2O; thorium oxide prepared by precipitation of the oxalate at 70°C and firing at 800°C.

The prototype ultrasonic interface follower is in the last stages of construction. Measurements of the attenuation of ultrasound by thoria slurries have shown that, at frequencies below 1 Mc/sec, it will be possible to correlate attenuation with thoria concentration.

Calculations were made of the heat necessary for flame-spraying thoria sols to prepare thoria beads. The heat demand was found to be a minimum of 3000 kcal per kilogram of thoria produced at the relatively low calcination temperature of 1727°C.

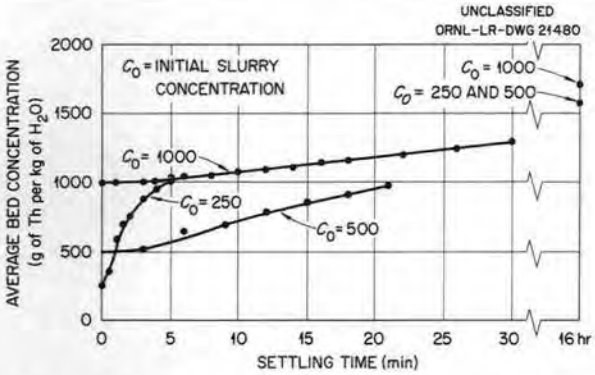

Fig. 18.8. Average Settled Bed Concentration in Small Graduate vs Settling Time. Graduate diameter = 0.75 in.; room temperature; thorium oxide prepared by precipitation of the oxalate at 70°C and firing at 800°C.

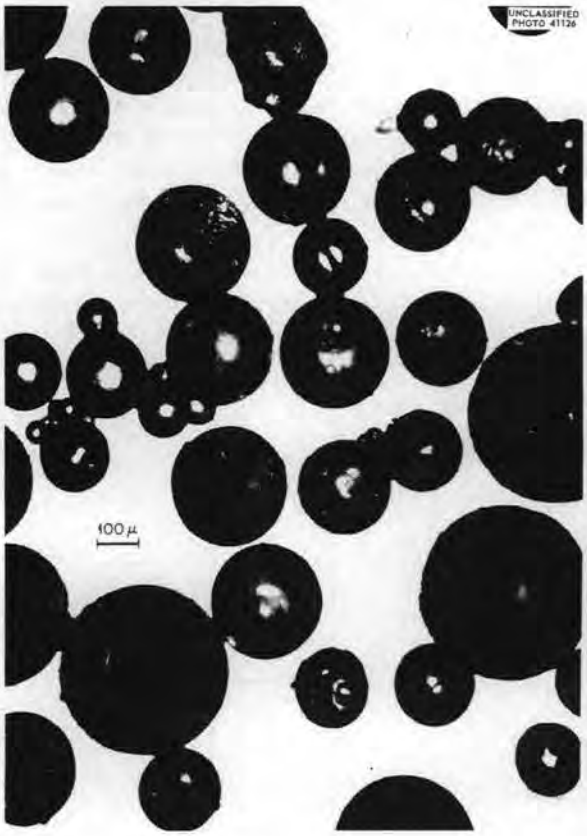

Fig. 18.9. Thoria Spheres Dried at 105°C. Average particle size, 120 μ.

Part VI

SUPPORTING CHEMICAL RESEARCH

E. H. Taylor

19. AQUEOUS SYSTEMS AT ELEVATED TEMPERATURES

C. H. Secoy

H. F. McDuffie H. H. Stone

F. H. Sweeton

19.1 CHARACTERIZATION OF SLURRY FLOCCULATION BY pH

When an acid such as H_2SO_4 is added to a ThO_2 slurry to control its peptization state, knowledge of the pH of the slurry appears to be a convenient aid in evaluating the effectiveness of the acid. This effectiveness can be expected to depend on the acid left free in solution after an equilibrium has been established with the ThO_2 surface. The value of the pH measurement is that it corresponds to this free acid rather than to the total acid.

The measurement of the pH of a slurry appears to be difficult. In order to avoid liquid-junction errors associated with the calomel electrode, it is necessary to make the measurements on some supernatant that has been separated from the slurry rather than on the slurry itself. When the acid concentration approaches zero, the supernatant becomes essentially distilled H_2O, and its pH can be expected to change appreciably with very small amounts of impurities; for example, the CO_2 in only one volume of air should lower the pH of 100 volumes of pure H_2O by about 0.2 unit.

Experimental work on the measurement of the pH of distilled water was undertaken to develop techniques adequate for measuring the pH of slurries containing very small concentrations of electrolytes. Much of the problem has been the preparation of the water.

Water, purified in a two-stage still, was made to flow through a Teflon cell for the determination of its pH. The still was constructed entirely of pyrex except for a platinum condenser in the second stage. The two stages were charged with alkaline $KMnO_4$ and with H_3PO_4, respectively. The cold joints in the still system were sealed with Apiezon N stopcock grease; the hot joints were unsealed except for distillate. The gas inside the still and in the collection flask was air that had been passed over $Mg(ClO_4)_2$ and Ascarite. The pH cell held small glass and calomel electrodes sealed from atmospheric CO_2.

The pH of the H_2O delivered by the still ranged from 6.2 to 6.5. The fact that bubbling of purified air through the distillate raised the reading toward 7.0 indicated that CO_2 was probably the impurity. In the last two runs the final pH readings after bubbling were 6.9 and 7.0; these results were regarded as satisfactory.

19.2 HOMOGENEOUS CATALYSIS OF THE HYDROGEN-OXYGEN REACTION IN AQUEOUS SOLUTIONS

During the past quarter, additional[1] studies of the sulfate system (cupric sulfate–sulfuric acid) were performed at 200 and at 175°C in order to determine the effects of changes in temperature, acidity, and copper concentration upon the catalytic activity of the solution. Further attempts were made to reconcile the data with the mechanism proposed by Halpern *et al.*[2] for the perchlorate system at 110°C. This mechanism would require that the data conform to the equation

$$\frac{1}{R} = \frac{1}{k_1[Cu^{++}][H_2]}\left[1 + \frac{k_{-1}[H^+]}{k_2[Cu^{++}]}\right].$$

Figures 19.1 and 19.2 are plots of experimentally determined inverse rates, corrected for differences

[1] C. H. Secoy *et al.*, *HRP Quar. Prog. Rep. Jan. 31, 1957*, ORNL-2272, p 163.

[2] J. Halpern, E. R. Macgregor, and E. Peters, *J. Phys. Chem.* **60**, 1455 (1956).

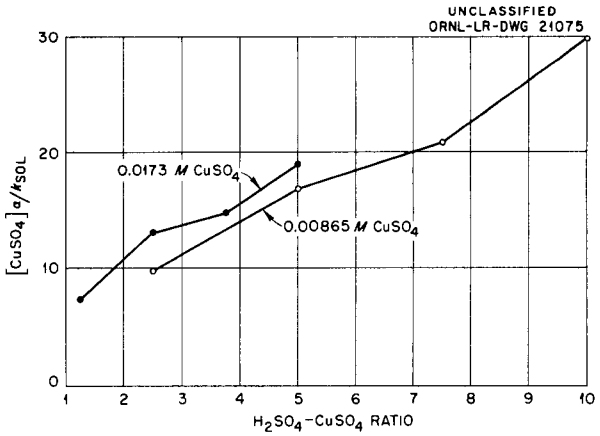

Fig. 19.1. Effect of Acid-to-Copper Ratio upon Inverse Recombination Rate at 200°C.

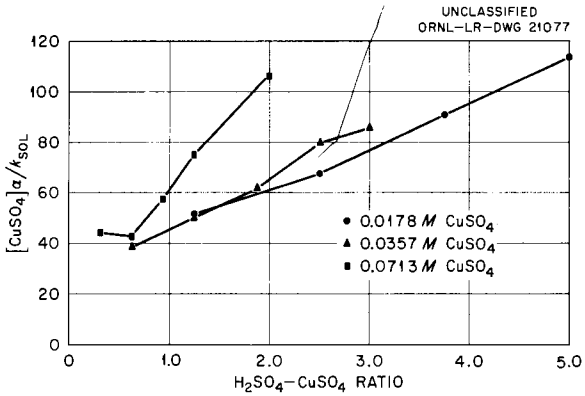

Fig. 19.2. Effect of Acid-to-Copper Ratio upon Inverse Recombination Rate at 175°C.

in copper concentration, vs the acid-to-copper ratio. It is obvious from the systematic bias introduced as the copper concentration is increased, especially at 175°C, that the data are not consistent with the Halpern mechanism.

Since the so-called geometry factor used in our earlier studies of homogeneous recombination[3] makes it possible, theoretically, to separate effects due to gas solubility from those due to the catalytic activity of the solution, an attempt was made to realize this separation. Figure 19.3 presents the values for k_{sol}, the catalytic activity of the solution determined experimentally, plotted vs the copper concentration of the solution for different acidities at 175°C. It is obvious that increasing the acidity from 0.0223 *M* to 0.0446 *M* was associated with a substantial decrease in catalytic activity, but additional increases in acidity were without effect. Also, the activity appeared to increase linearly with the copper concentration at all acidities, although there was a slight systematic trend to lower activity at the highest copper concentration. At this stage the relationship between activity and concentration can well be taken as linear, and, above 0.04 *M* acidity, the rate may be expressed by the product of the concentration of copper and a single specific reaction-rate constant, k_{Cu}. The average value of k_{Cu} for this set of data is 36.8 $M^{-1}\cdot hr^{-1}$.

The experimentally determined values for the solubility coefficient, α, reveal a dependence on

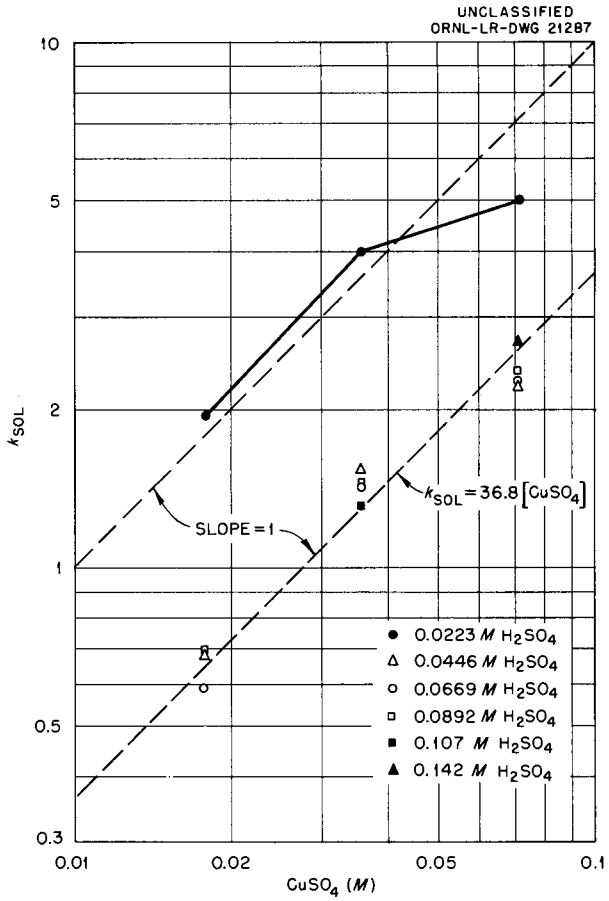

Fig. 19.3. Effect of Copper Concentration on Catalytic Activity at 175°C.

copper concentration and on acidity. Figure 19.4 presents the variation of the solubility, as $10^4/\alpha$ (so that positive values represent high solubility), vs copper concentration for different acidities. It is obvious that the solubility follows the square root of the copper concentration at all acidities but that increasing the acidity has a double effect; at first the solubility increases, but raising the acidity above 0.04 *M* is associated with a decrease in the solubility. Figure 19.5, a plot of the solubility function vs acidity (after correcting for the square root of the copper concentration), suggests that, above 0.04 *M*, the solubility is inversely proportional to the acidity. Thus, over the range of copper concentration from 0.0178 to 0.0713 *M* cupric sulfate and over the range of acidity from 0.04 to 0.142 *M* sulfuric acid, our experimental data are all well fitted by a two-parameter equation, one parameter associated with the solubility function and the other with the

[3]H. F. McDuffie *et al.*, *The Radiation Chemistry of Homogeneous Reactor Systems. III. Homogeneous Catalysis of the Hydrogen–Oxygen Reaction*, ORNL CF-54-1-122 (Jan. 26, 1954).

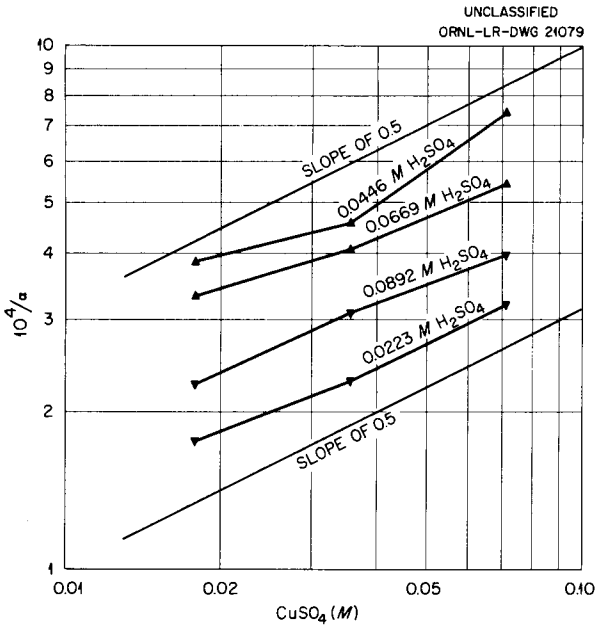

Fig. 19.4. Effect of $CuSO_4$ Concentration on Hydrogen Solubility at 175°C.

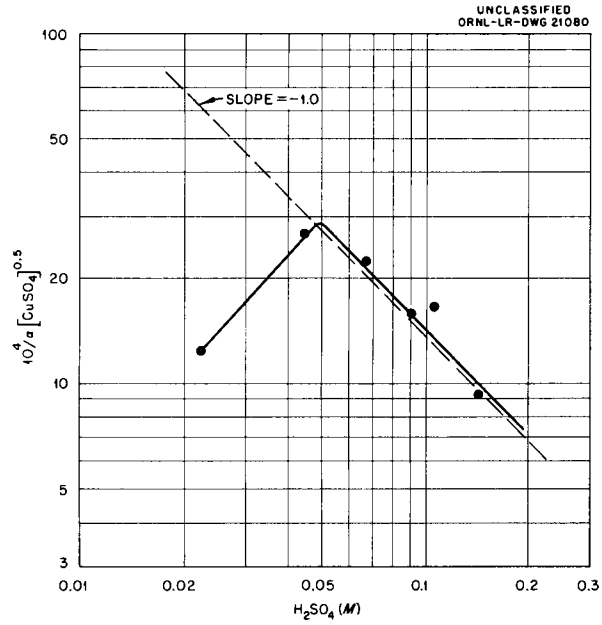

Fig. 19.5. Effect of Acidity on Hydrogen Solubility.

catalytic activity of the copper solution in the final step of the reaction:

$$k_\pi \equiv \frac{dP}{dt} \cdot \frac{1}{P} = \frac{36.8\,[CuSO_4]^1}{\left[\dfrac{V_g}{V_l} \cdot \dfrac{\left(\dfrac{[H_2SO_4]}{1.41 \times 10^{-4}\,[CuSO_4]^{0.5}}\right)}{RT} + 1\right]} .$$

Attempts are being made to develop a mechanism for the reaction which is consistent with the observed experimental relationships, and it appears possible that the solubility function may be consistent with an equilibrium in which two molecules of dissolved hydrogen react with one molecule of a dimerized copper species to liberate one molecule of acid.

It is planned that a similar systematic examination of the perchlorate system be made, covering the same ranges of temperature, concentration, and acidity as those tested with the sulfate system. It is expected that the solubility function may be less complex in the perchlorate system than in the sulfate system, since the perchlorate ion is less susceptible to complex formation.

Additional studies in the sulfate system, and in the mixed sulfate and perchlorate system, will be performed to extend the ranges over which the two-parameter equation has been tested and to provide information as to the nature of the participation of sulfate in the solubility function.

It is also planned that studies with deuterium and heavy water be made in parallel with studies on hydrogen and light water in order to provide comparison between the two hydrogen isotopes and because of reactor interest in the heavy-water systems.

20. RADIATION CHEMISTRY

J. W. Boyle H. A. Mahlman

20.1 FUNDAMENTAL PROCESSES IN THE RADIATION CHEMISTRY OF HEAVY WATER

The decomposition induced by Co^{60} radiation in a 0.4 *M* sulfuric acid solution in heavy water has been assumed to proceed in a manner similar to that in light water. The free-radical and molecular product yields may be defined by reference to three systems, each in 0.4 *M* sulfuric acid: D_2 formation in a degassed dilute bromide solution, deuterium peroxide formation in an aerated solution, and ferrous oxidation in an aerated solution. The product yields predicted from the reaction mechanisms are

$$G(D_2) = G_{D_2} ,$$

$$G(D_2O_2)_{air} = G_{D_2O_2} + \tfrac{1}{2}(G_D - G_{OD}) ,$$

$$G(Fe^{+++}) = 3G_D + 2G_{D_2O_2} + G_{OD} .$$

The 100-ev yield of final product is denoted by *G*(product), while the 100-ev yields of D, OD, D_2O_2, and D_2 (assumed to be the initial products of aqueous Co^{60} radiolysis) are denoted by G_D, G_{OD}, $G_{D_2O_2}$, and G_{D_2}.

It was assumed in the preliminary work previously reported[1] that the molar extinction coefficient of Fe^{+++} ions determined in 0.4 *M* sulfuric acid solution at 3050 Å was the same in light and heavy water. Critical experimental evaluation showed that the molar extinction coefficient of Fe^{+++} ions in heavy-water solution was 7.1% higher than in the light-water acid solution. With this molar extinction coefficient, the oxidation rate of ferrous ions in 0.4 *M* sulfuric acid heavy-water solution was recalculated to be 16.57 molecules per 100 ev of absorbed energy. The $G(D_2)$ and $G(D_2O_2)_{air}$ were determined to be 0.39 and 1.26, respectively. From these data the free-radical and molecular product yields were calculated to be $G_{D_2} = 0.39$, $G_{D_2O_2} = 0.83$, $G_D = 3.95$, and $G_{OD} = 3.08$. The corresponding values for light water[2] are $G_{H_2} = 0.39$, $G_{H_2O_2} = 0.78$, $G_H = 3.70$, and $G_{OH} = 2.92$.

[1] J. W. Boyle and H. A. Mahlman, *HRP Quar. Prog. Rep. Jan. 31, 1957*, ORNL-2272, p 172.

[2] T. J. Sworski, *J. Am. Chem. Soc.* 76, 4687 (1952).

[redacted]

OAK RIDGE NATIONAL LABORATORY
HOMOGENEOUS REACTOR PROJECT

MAY 1, 1957

PROJECT DIRECTOR
R. B. BRIGGS D

ASSOCIATE PROJECT DIRECTOR
C. E. WINTERS** D
A. L. GUNNELS, SEC. D

PROJECT EDITOR
W. D. REEL TI

DESIGN AND ENGINEERING
J. A. LANE, DIRECTOR REE
R. N. LYON, ASSISTANT DIRECTOR REE
T. K. CARLSMITH, SEC. REE

DESIGN
W. R. GALL, SECTION CHIEF REE
M. I. LUNDIN,* ASSISTANT SECTION CHIEF REE

MECHANICAL DESIGN
F. C. ZAPP, GROUP LEADER REE
F. C. BOWEN VITRO
C. A. BURCHSTED REE
C. J. CLAFFEY REE
C. W. COLLINS REE
E. M. GUGLIELMO VITRO
R. C. MOREN WESTINGHOUSE
R. G. PITKIN VITRO
R. E. SCHAPPEL REE
D. O. TARR VITRO

HRE-2 CONCEPTUAL DESIGN
M. I. LUNDIN,* ACTING GROUP LEADER REE
J. C. BOLGER REE
E. H. GIFT REE
R. D. MAAK FOSTER-WHEELER
E. A. MASON REE

PLANT LAYOUT AND DRAFTING
C. L. SEGASER, GROUP LEADER REE
W. ROBINSON REE
W. TERRY* REE
H. H. BRADFORD REE
R. L. CAUBLE REE
C. W. DAY REE
J. P. DILORENZO REE
W. B. KRICK REE
A. S. LUDLOW REE
C. A. ROBERTS REE
R. D. SATTERFIELD REE
R. H. SIGLER REE
W. G. STERLING REE

PROCESS DESIGN
R. C. ROBERTSON, GROUP LEADER REE
H. A. MCLAIN REE

EXPERIMENTAL STRESS ANALYSIS
R. D. CHEVERTON, GROUP LEADER REE
J. N. ROBINSON REE

ENGINEERING DEVELOPMENT
I. SPIEWAK, SECTION CHIEF REE

HEAT EXCHANGER, TITANIUM PROGRAM, MISCELLANEOUS EQUIPMENT
J. S. CULVER, GROUP LEADER REE
B. D. DRAPER TVA
P. P. HOLZ* REE
I. K. NAMBA REE
D. L. SNYDER REE

PUMPS
C. H. GABBARD, GROUP LEADER REE
J. M. BAKER REE
R. BLUMBERG REE
E. C. HISE REE
J. C. MOYERS REE
J. P. HURST REE
C. C. HURTT REE
R. J. LOCKETT REE

HRT MOCKUP, RECOMBINERS
P. H. HARLEY, GROUP LEADER REE
B. A. HANNAFORD REE
H. C. ROLLER REE
D. E. WILLIS REE
T. L. CASTILE REE
A. B. DAFFRON REE
R. GOODMAN REE
W. M. PARKS REE

SPECIAL ASSIGNMENT
P. P. HOLZ* REE
T. M. CATE REE
L. E. PENTON REE
S. R. WEST REE
T. R. WILSON REE

ENGINEERING RESEARCH
R. B. KORSMEYER, SECTION CHIEF REE

SLURRY SYSTEM DEVELOPMENT
L. F. PARSLY, GROUP LEADER REE
I. M. MILLER REE

SLURRY PROPERTIES
D. G. THOMAS, GROUP LEADER REE
R. B. GALLAHER REE
D. H. GIBSON REE
C. S. MORGAN REE
R. H. NIMKO REE
R. P. WICHNER REE

SPECIAL ASSIGNMENT
H. L. FALKENBERRY TVA
M. RICHARDSON REE
C. F. VANDEN BULCK UCNC

SERVICES
A. N. SMITH REE
T. L. BOSWELL REE
R. E. CARNES REE
B. R. CHILCOAT REE
J. T. DICKIE REE
C. M. FITZPATRICK REE
C. A. GIFFORD REE
P. H. HAYES REE
C. A. MCLAUGHLIN REE
H. G. MOORE REE
R. E. POTTER REE
R. M. SUMMERS REE
B. J. SUTTON REE
D. H. WALLACE REE

INSTRUMENTATION AND CONTROLS
O. S. TOOMB, SECTION CHIEF I&C

HRT AND INSTRUMENT DEVELOPMENT
R. L. MOORE, GROUP LEADER I&C
J. C. GUNDLACH** I&C
R. M. PIERCE* TVA
H. D. WILLS I&C
R. W. BORGERS I&C

HRP SUPPORTING FACILITIES
D. G. DAVIS, GROUP LEADER I&C
G. W. GREENE I&C
J. D. GRIMES TVA
P. G. HERNDON I&C
J. A. RUSSELL I&C
R. M. BURNETT I&C
M. A. MEACHAM I&C
P. E. SMITH I&C

VALVES AND ACTUATORS
A. M. BILLINGS, GROUP LEADER I&C
E. H. BELL I&C
P. F. HURAY I&C
B. J. JONES I&C
A. J. SHARONBERGER* I&C

REACTOR ANALYSIS
P. R. KASTEN, SECTION CHIEF REE

REACTOR PHYSICS
T. B. FOWLER REE
C. W. NESTOR, JR. REE
M. W. ROSENTHAL REE
M. TOBIAS REE

LONG RANGE STUDIES
S. JAYE REE
M. P. LIETZKE REE
B. E. PRINCE REE

SPECIAL ASSIGNMENT
H. C. CLAIBORNE REE

REACTOR MATERIALS RESEARCH
E. G. BOHLMANN, ASSISTANT DIRECTOR REE
T. F. KELLY, SEC. REE
D. P. MALENFANT, STENO. REE
R. E. WACKER, RECORDS REE

SOLUTIONS
J. C. GRIESS, ASSISTANT SECTION CHIEF REE

LOOPS
R. S. GREELEY REE
S. R. BUXTON REE
J. E. EVE REE
W. H. HINDS REE

LABORATORY STUDIES
J. L. ENGLISH, GROUP LEADER REE
D. N. HESS REE
P. D. NEUMANN REE
L. L. FAIRCHILD, LEADER REE
H. L. BARKER REE
P. B. DAVIS REE
H. R. TINCH REE
J. L. UNDERWOOD REE

E. L. COMPERE, ASSISTANT SECTION CHIEF REE

LOOPS
S. A. REEO* REE

TOROIDS
S. A. REEO* REE
R. F. BENSON REE
F. E. MCDANIEL REE

HRT LIAISON
O. M. RICHARDSON* C
H. D. COLE REE

H. C. SAVAGE, ASSISTANT SECTION CHIEF REE

SOLUTIONS
W. C. ULRICH REE
J. F. WINESETTE, LEADER REE
L. L. ALLEN REE
C. R. BENSON REE
C. M. BURCHELL REE
C. L. FRANCIS REE
J. B. FRENCH REE
D. G. GATES REE
J. W. GOOCH REE
J. E. JACKSON REE
B. L. JOHNSON REE
G. A. MOORE REE
L. G. PHELPS REE
A. E. PUGH REE
T. R. RAYBURN REE
W. H. WAGNER REE

SLURRIES
R. M. WARNER REE
J. D. BARNES REE

RADIATION
S. E. BOLT REE
V. A. DECARLO REE
T. H. MAUNEY REE
C. H. BURBAGE REE
J. R. HART REE
H. F. HENDERSON REE
B. H. PARKS REE
R. W. RAY REE
B. W. SCOTT REE

G. M. JENKS, SECTION CHIEF REE
D. T. JONES, ENGRG. COORDINATOR REE
V. R. BULLINGTON REE

RADIATION
G. M. JENKS, SECTION CHIEF REE
D. T. JONES, ENGRG. COORDINATOR REE
V. R. BULLINGTON REE

IN-PILE LOOPS
J. R. MCWHERTER, GROUP LEADER REE
J. E. BAKER REE
J. W. BROWN REE
R. A. LORENZ REE
F. J. WALTER* REE
S. H. WHEELER REE
W. E. TEICHERT, A SHIFT LEADER REE
K. G. CHANDLER REE
C. E. ROBERTS REE
E. H. GUINN, B SHIFT LEADER REE
J. P. GORDON REE
D. M. SMITH REE
A. L. SUTTON, C SHIFT LEADER REE
R. A. JONES REE
R. M. WALLER REE
J. W. MYERS, D SHIFT LEADER REE
J. W. MOSIER REE
R. G. ROSS REE

IN-PILE BOMBS
R. J. DAVIS, GROUP LEADER C
F. J. WALTER* REE
K. S. WARREN C
J. L. RUTHERFORD REE
R. L. PLEMONS REE

SUPPORTING RESEARCH
A. L. BACARELLA C
M. D. SILVERMAN C
W. C. YEE C

REMOTE EVALUATION
A. R. OLSEN REE
B. W. MCCOLLUM, SHIFT LEADER REE
W. J. SCHILL REE
W. H. SMITH, JR. REE
J. C. THOMPSON REE

METALLURGY
G. M. ADAMSON, SECTION CHIEF M

METALLURGICAL RESEARCH
M. L. PICKLESIMER, LEADER M
P. L. RITTENHOUSE M
R. L. STEPHENSON M
P. J. JONES M
G. C. NELSON M
M. A. WHEELER M

METALLURGICAL ENGINEERING
J. P. HAMMOND, LEADER M
W. J. LEONARD M
J. J. PRISLINGER M
J. K. WHITE M
C. M. SMITH M
J. J. WOODHOUSE M

METALLOGRAPHY
R. S. CROUSE,** LEADER M
T. M. KEGLEY, JR. M
E. R. BOYD M
B. F. DAY** M
T. J. HENSON** M
L. G. SHRADER** M

RADIATION DAMAGE
R. G. BERGGREN SS
A. E. RICHT SS
D. D. THOMPSON SS
J. C. WILSON** SS
F. M. GRIZZEL SS

PERSONNEL SUMMARY

	FULL TIME	PART TIME	INDUSTRIAL PARTICIPANTS
ADMINISTRATION	7	4	
ANALYTICAL CHEMISTRY	41		
CHEMICAL RESEARCH	8	10	
CHEMICAL TECHNOLOGY	55		
DESIGN AND ENGINEERING	105	1	7
HOMOGENEOUS REACTOR TEST	39		6
REACTOR MATERIALS RESEARCH	99	5	
TOTAL	354	20	13

CHEMICAL TECHNOLOGY
D. E. FERGUSON,* PROGRAM LEADER CT
I. LOOPE, SEC CT

CHEMICAL DEVELOPMENT
D. E. FERGUSON,* SECTION CHIEF CT

BLANKET PROCESSING
R. E. LEUZE, PROBLEM LEADER CT
R. D. BAYBARZ CT
J. M. CHILTON CT
S. S. KIRSLIS CT
J. M. DELOZIER CT
R. L. HICKEY CT
O. K. TALLENT CT

CORE PROCESSING
R. A. MCNEES, PROBLEM LEADER CT
M. H. LLOYD CT
S. PETERSON CT
J. E. DAVIDSON CO-OP, UNIV. OF TENN.
W. B. HOWERTON CT

THORIUM BLANKET STUDIES
J. P. MCBRIDE, PROBLEM LEADER CT
E. V. JONES C
N. A. KROHN CT
L. E. MORSE CT
R. L. PEARSON CT
C. E. SCHILLING CT
W. M. WOODS CT
C. W. GREENE CT
P. P. HAYDON CT
W. L. PATTISON CT
H. F. SOARD CT

DESIGN
W. E. UNGER, ASSISTANT SECTION CHIEF CT

PROCESS DESIGN
H. O. WEEREN CT
B. F. BOTTENFIELD CT

PROJECT DESIGN
A. M. ROM, PROBLEM LEADER CT
G. B. BERRY E&M
F. C. MCCLUDDUGH CT
E. B. BRIDGES E&M
J. D. CUPP E&M
H. W. FALLON CATALYTIC CONSTRUCTION CO.
P. P. FEBBO CATALYTIC CONSTRUCTION CO.
W. J. LEE COOP, GA. TECH.
J. H. MANNEY E&M
F. L. PEISEL E&M
J. PHILLIPS CATALYTIC CONSTRUCTION CO.
K. F. STOOKSBURY CT
J. N. WHEELER E&M

LOOP DESIGN
T. A. AREHART CT
W. F. SCHAFFER CT

INSTRUMENTATION
C. S. LISSER I&C

PILOT PLANT
R. B. LINDAUER,** SECTION CHIEF CT

SLURRY PREPARATION
E. M. SHANK,** PROBLEM LEADER CT
C. V. ELLISON** CT
J. R. PARROTT** CT

UNIT OPERATIONS
P. A. HAAS, GROUP LEADER CT

CORE PROCESSING
R. W. HORTON CT
J. W. SNYDER CT
R. D. ARTHUR CT
F. N. MCLAIN CT

SLURRY PROCESSING
C. C. HAWS CT
W. J. CLOSSEY CATALYTIC CONSTRUCTION CO.
R. C. EARLY CT

BLANKET PROCESSING
S. D. CLINTON CT
G. E. WOODALL CT
D. A. MCWHERTER CT

CHEMICAL RESEARCH
E. H. TAYLOR,** DIRECTOR C
E. SCHAPPEL, SEC. C

FUEL SOLUTION CHEMISTRY
C. H. SECOY, GROUP LEADER C
F. E. CLARK C
J. S. GILL C
G. M. HEBERT C
H. F. MCDUFFIE C
R. SLUSHER C
H. H. STONE C
F. H. SWEETON C

RADIATION CHEMISTRY
C. J. HOCHANADEL,** GROUP LEADER C
J. W. BOYLE** C
H. A. MAHLMAN** C

HEAVY ELEMENT CHEMISTRY
R. W. STOUGHTON,** GROUP LEADER C
J. HALPERIN** C
M. H. LIETZKE** C
W. C. WAGGENER** C

INORGANIC SOLUTION CHEMISTRY
K. A. KRAUS,** GROUP LEADER C
T. A. CARLSON** C
H. O. PHILLIPS** C

ANALYTICAL CHEMISTRY
MYRON T. KELLEY,** DIRECTOR
C. D. SUSANO,** ASSOCIATE DIRECTOR

K. OOOM, SEC. AC

CORROSION ANALYTICAL LABORATORY
O. MENIS,* SUPERVISOR AC
H. P. HOUSE, ASSISTANT SUPERVISOR AC

RESEARCH
O. MENIS,* GROUP LEADER AC
R. G. BALL AC
C. M. BOYD AC
G. GOLDSTEIN AC
D. L. MANNING AC
R. H. POWELL AC
T. C. RAINS AC
I. B. RUBIN AC

SERVICES
C. K. TALBOTT, GROUP LEADER AC
N. M. FERGUSON AC
F. L. LAYTON AC
T. P. BACON AC
W. D. CLAPP, JR. AC
C. A. CLARK AC
C. G. FUSON AC
P. S. GOODWIN AC
B. D. HICKS AC
T. G. MILLER AC
V. S. NORMAN AC
E. ONKST AC

HRT AND IN-PILE LOOP ANALYSES
U. KOSKELA, SUPERVISOR AC
L. G. FARRAR, ASSISTANT SUPERVISOR AC
J. E. ATTRILL AC
C. P. BAKER AC
R. E. CORCORAN AC
S. R. DINSMORE AC
J. L. MOTTERN AC
G. M. CAMPBELL AC
G. I. GAULT AC
M. H. MCCORQUODALE AC
J. SLESSINGER, JR. AC
W. R. WARREN AC
H. L. WEBB AC
H. L. WHITTINGTON AC

HRT DEVELOPMENT
P. F. THOMASON, GROUP LEADER AC
R. E. BIGGERS AC
F. J. MILLER AC
S. A. REYNOLDS, GROUP LEADER AC
T. H. HANOLEY AC

HIGH RADIATION LABORATORY
C. L. BURROS AC

HOMOGENEOUS REACTOR TEST
S. E. BEALL, PROJECT ENGINEER REE
B. ELBANK, SEC. REE
M. SWANK, SEC. CT

OPERATIONS PLANNING
S. I. KAPLAN REE

SPECIAL ASSIGNMENT
H. M. MCLEOD CT

REACTOR TEST PROGRAM
J. W. HILL, JR., CHIEF REE
R. SMITH, JR. REE
J. R. ENGEL, SUPERVISOR CT
J. R. BUCHANAN CT
H. K. SEARCH PA. POWER AND LIGHT CO.
D. T. GODWIN REE
A. L. JOHNSON REE
J. D. FLYNN, SUPERVISOR REE
H. F. BAUMAN CT
R. J. HARVEY REE
W. T. BOSTIC CT
E. W. BROWN CT
T. G. HILL REE
J. G. KOLB, SUPERVISOR REE
N. A. BROWN TVA
D. F. FRECH REE
H. D. CURTIS REE
R. J. SHANNON CT
J. E. WOLFE REE
G. W. RIVENBARK, SUPERVISOR REE
T. H. GLADNEY TVA
R. H. GUYMON CT
R. J. HUNTER REE
L. J. SHERSKY CT
J. L. STEPP REE

CHEMICAL PLANT COORDINATION
W. D. BURCH, PROBLEM LEADER CT
W. L. ALBRECHT TVA
N. C. BRADLEY CT
R. H. WINGET CT
W. A. LINDSEY CT

REACTOR COORDINATION
R. VAN WINKLE, GROUP LEADER REE
R. R. WIETHAUP CT
J. A. WATTS REE

REACTOR ANALYSIS
P. N. HAUBENREICH, GROUP LEADER REE

MAINTENANCE PLANNING
W. TERRY,* SUPERVISOR REE
R. W. JURGENSEN AM. GAS AND ELEC. CO.
H. L. BROWN REE
T. E. HAYNES REE
G. H. JOHNSTONE REE

REACTOR MATERIALS AND CHEMISTRY
D. M. RICHARDSON,* GROUP LEADER C
J. D. JONES REE

INSTRUMENTATION
K. W. WEST, GROUP LEADER I&C
R. M. PIERCE* TVA
A. J. SHARONBERGER* I&C

SUBCONTRACTS
AEROJET-GENERAL CORPORATION
ARMOUR RESEARCH FOUNDATION
FLORIDA UNIVERSITY
HOUDRY PROCESS CORPORATION
OHIO STATE UNIVERSITY
RENSSELAER POLYTECHNIC INSTITUTE
STANFORD RESEARCH INSTITUTE
STANFORD UNIVERSITY
SYRACUSE UNIVERSITY
TULANE UNIVERSITY
UNIVERSITY OF TENNESSEE
UNIVERSITY OF UTAH
UNIVERSITY OF VIRGINIA
VITRO CORPORATION OF AMERICA

INDUSTRIAL PARTICIPATION
AMERICAN GAS AND ELECTRIC COMPANY
FOSTER WHEELER
PENNSYLVANIA POWER AND LIGHT COMPANY
TENNESSEE VALLEY AUTHORITY
UNION CARBIDE NUCLEAR COMPANY, NEW YORK
WESTINGHOUSE ELECTRIC CORPORATION

AC ANALYTICAL CHEMISTRY DIVISION
C CHEMISTRY DIVISION
CT CHEMICAL TECHNOLOGY DIVISION
D DIRECTOR'S DIVISION
E&M ENGINEERING AND MECHANICAL DIVISION
I&C INSTRUMENTATION AND CONTROLS DIVISION
M METALLURGY DIVISION
REE REACTOR EXPERIMENTAL ENGINEERING DIVISION
SS SOLID STATE DIVISION
TI TECHNICAL INFORMATION DIVISION
* DUAL CAPACITY
** PART TIME ON PROJECT